OZONE AND SECONDARY ORGANIC AEROSOL FORMATION FROM ORGANIC PRECURSORS

Thesis by
Frank M. Bowman

In Partial Fulfillment of the Requirements
for the Degree of
Doctor of Philosophy

California Institute of Technology
Pasadena, California

1997
(Submitted February 27, 1997)

ACKNOWLEDGMENTS

I would like to thank my advisor John Seinfeld for his support and guidance and for allowing me the flexibility to work on a variety of projects.

I also express my appreciation to Rick Flagan for teaching me (both in and out of class) what I know about aerosols.

Thanks to Jay Odum, Thorsten Hoffmann, Hali Forstner, Richard McClurg, Don Collins and many others no less important. I have had the privilege to work with many fine people while doing this research and they deserve much of the credit for the ideas and results presented here. Beyond the realm of science I am also grateful for their friendship which has made my time at Caltech all the more enjoyable.

A particular acknowledgment is due to Dan Millward, Aaron Hawkins, and Justin Lawyer among others, for sharing with me the unique life of Caltech undergrads.

A special debt of gratitude is owed to my father and mother who have provided me with a rich heritage of learning and whose continued love and support has helped me to achieve this goal.

Finally, and most significantly, I thank my dear wife Alisa for her patience, love and abiding confidence in my abilities.

ABSTRACT

A technique was developed to determine the amount of ozone and other secondary pollutants generated by individual organic components of atmospheric VOC/NO_x mixtures. This technique was used to investigate the chemical interactions associated with incremental reactivity calculations. It was shown that the incremental reactivity of an individual organic species is a result of changes in the ozone generated by each of the organics present. Incremental reactivities, therefore, are dependent on the nature of the VOC/NO_x mixture. Aldehydes, alkenes and reactive aromatics were found to have the highest incremental reactivities due to their behavior as radical sources, thereby increasing the rate of reaction of all available organics. Ozone and secondary aerosol formation within the South Coast Air Basin of California during the Southern California Air Quality Study (SCAQS) air pollution episode of August 27-28, 1987 were also analyzed and again the same species were shown to be the most productive compounds in the organic mixture. Less productive compounds, such as CO and alkanes, were also found to be major contributors to ozone concentrations due to their relative abundance. Eight reformulated fuel components were investigated to determine their ozone-forming potential. Most of the fuel oxygenates were found to have relatively low incremental reactivities due to their slow reaction rates and to the formation of relatively unreactive formate and acetate products.

Secondary organic aerosol formation was studied in the Caltech outdoor smog chamber and a model was developed to describe the gas-particle absorptive partitioning of semi-volatile organics. Particle deposition, nucleation and vapor transport to aerosol particles, chamber walls and deposited particles are accounted for by the model. Simulations of a pair of *m*-xylene/NO_x experiments were performed to investigate the nature of aerosol growth. Characteristic transport times indicate that gas-particle equilibrium will typically be established quite rapidly. Additional delays in aerosol formation were shown to result when the condensing semi-volatile products are second-generation, rather than first-generation, products of a parent hydrocarbon. Within a smog chamber, partitioning to chamber walls and deposited particles are shown to be negligible due to unfavorable equilibrium and transport conditions.

TABLE OF CONTENTS

LIST OF TABLES

Chapter 2

Chapter 3

Chapter 4

Chapter 5

Chapter 6

Chapter 7

Appendix A

LIST OF FIGURES

Chapter 2

Chapter 3

Chapter 4

Chapter 5

Chapter 6

Chapter 7

Chapter 8

CHAPTER 1:

INTRODUCTION

Ground-level ozone and particulate matter continue to be among the most difficult air pollutants to control. In order to design the most effective control measures, a correct understanding of how these pollutants are formed is needed. Atmospheric ozone formation is the result of a complex series of photochemical reactions involving volatile organic compounds (VOCs) and oxides of nitrogen (NO_x). Individual VOCs differ widely in their ozone-forming capability (Carter and Atkinson, 1987; Derwent and Jenkin, 1991; McNair *et al.*, 1992) and the total amount of ozone formed will depend on the mixture of VOCs that is present and on the VOC/NO_x ratio. A significant contributor to particulate matter in urban atmospheres, particularly in the fine particle size range (D_p < 2.5 μm), is secondary organic material (Pandis *et al.*, 1993). Secondary organic aerosol is formed when VOCs react to produce semi-volatile vapors which can undergo gas-to-particle conversion.

Chapters 2-5 center on determining the ozone-forming potential of individual VOC species and analyzing the chemical interactions that lead to ozone formation, while Chapter 6 describes a model for the gas/particle partitioning of secondary organic aerosols. The focus of my work has been to investigate the ozone- and particulate-forming capabilities of VOCs and to understand how individual VOCs within a mixture contribute to total ozone and secondary organic aerosol concentrations.

Chapter 2 outlines a technique for determining the amount of ozone and other secondary products generated by the individual organic components of an atmospheric VOC/NO_x mixture. The basic concept of the assignment method is to follow the reaction pathways of a mechanism and trace the ozone formed back to the original organic precursors. The assignment method was used to examine the SAPRC chemical mechanism (Carter, 1990) in a box model simulation of summertime Los Angeles at various VOC/NO_x ratios. A measure of the ozone-forming potential of each organic, termed productivity, was defined as the total amount of ozone produced due to an individual VOC per amount of that VOC emitted. The assignment method also allows the reactions of radical species to be traced so that radical sources, sinks and conversion between radical types can be determined.

The assignment method was used to investigate the chemical interactions of incremental reactivity in Chapter 3. Incremental reactivity is a measure of the additional amount of ozone generated when a small amount of an individual organic is added to a VOC/NO_x mixture. Due to the complex nature of the VOC/NO_x photochemistry, adding an increment of organic affects the entire mixture. Not only is there an additional amount of organic available for reaction, but the rates of reaction for and the efficiencies with which ozone is produced by the other organics in the mixture will also be affected. The amount of additional ozone formed is a result of all of these changes. The mathematical relation between incremental reactivity and productivity was described and kinetic and mechanistic factors were defined. These factors were used to analyze the various

contributions to incremental reactivity for a box model simulation with the SAPRC mechanism.

Chapter 4 applied the assignment method to a trajectory model and represented an extension of the technique to include deposition of chemical species and continuous emissions of organic species and NO_x. This study also incorporated secondary organic aerosol formation from parent VOCs using the Size Resolved Secondary Organic Aerosol Model (SRSOAM) (Pandis *et al.*, 1992). In SRSOAM the gas-phase chemistry of the SAPRC mechanism is modified to include production of condensable organic vapors which condense to the aerosol phase upon exceeding their saturation concentrations. Using the assignment method the contributions of individual VOCs to ozone and aerosol formation were determined for two trajectories from the Southern California Air Quality Study (SCAQS). The influence of individual VOCs on aerosol formation through radical concentrations was also explored with those VOCs that act as radical sources found to enhance aerosol formation.

One element of air quality control efforts has been the use of reformulated gasolines containing oxygenates such as methyl *tert*-butyl ether (MTBE). Chapter 5 contains a review of relevant motor vehicle emissions and reformulated fuel regulations as well as a description of the assignment method, productivity and the factors contributing to incremental reactivity. The ozone-forming potential of eight oxygenated fuel components is studied and they are shown to have low incremental reactivities due to both kinetic and mechanistic factors.

Chapter 6 marks a transition in research from applications of the assignment method to a more focused investigation of secondary organic aerosol formation. During 1995 a series of smog chamber experiments was performed to study the secondary organic aerosol formation rates of several aromatic and biogenic hydrocarbons (Odum *et al.*, 1996; Hoffmann *et al.*, 1997). The results of these experiments can be described with absorption partitioning theory (Pankow, 1994*ab*; Odum *et al.*, 1996). The mathematical model described in Chapter 6 implements absorption partitioning theory into a dynamic model that describes secondary organic aerosol formation and growth. The model was used to simulate a pair of *m*-xylene smog chamber experiments and those results were used to explain the nature of gas-particle partitioning.

REFERENCES

Carter W. P. L. (1990) A detailed mechanism for the gas-phase atmospheric reactions of organic compounds. *Atmos. Environ.* **24**, 481-518.

Carter W. P. L. and Atkinson R. J. (1987) An experimental study of incremental hydrocarbon reactivity. *Environ. Sci. Technol.* **21**, 670-679.

Derwent R. G. And Jenkin M. E. (1991) Hydrocarbons and the long-range transport of ozone and PAN across Europe. *Atmos. Environ.* **25**, 1661-1678.

Hoffmann T., Odum J. R., Bowman F., Collins D., Klockow D., Flagan R. C. and Seinfeld J. H. (1997) Formation of organic aerosols from the oxidation of biogenic hydrocarbons. *J. Atmos. Chem.* (in press).

McNair L., Russell A. and Odman M. T. (1992) Airshed calculation of the sensitivity of pollutant formation to organic compound classes and oxygenates associated with alternative fuels. *J. Air Waste Manage. Assoc.* **42**, 174-178.

Odum J. R., Hoffmann T., Bowman F., Collins D., Flagan R. C. and Seinfeld J. H. (1996) Gas/particle partitioning and secondary organic aerosol yields. *Environ. Sci. Technol.* **30**, 2580-2585.

Pandis S. N., Harley R. A., Cass G. R. and Seinfeld J. H. (1992) Secondary organic aerosol formation and transport. *Atmos. Environ.* **26**, 2269-2282.

Pandis S. N., Wexler A. S. and Seinfeld J. H. (1993) Secondary organic aerosol formation and transport-II. Predicting the ambient secondary organic aerosol size distribution. *Atmos. Environ.* **27**, 2403-2416.

Pankow J. F. (1994*a*) An absorption model of gas/particle partitioning of organic compounds in the atmosphere. *Atmos. Environ.* **28**, 185-188.

Pankow J. F. (1994*b*) An absorption model of gas/aerosol partitioning involved in the formation of secondary organic aerosol. *Atmos. Environ.* **28**, 189-193.

CHAPTER 2:

OZONE PRODUCTIVITY OF ATMOSPHERIC ORGANICS

Published in *J. Geophys. Res.*, **99**, 5309 (1994).

ABSTRACT

A technique is developed to determine the amount of ozone and other products, such as nitric acid and PAN, generated by the individual organic components of a complex atmospheric organic/NO_x mixture. The technique is applied to the SAPRC 90 photochemical mechanism to study the individual contributions of carbonyls, aromatics, alkanes, alkenes, and carbon monoxide to ozone, nitric acid, PAN, and free radical production at varying organic to NO_x ratios typical of atmospheric conditions.

INTRODUCTION

Ozone formation in the troposphere results from complex interactions among nitrogen oxides (NO and NO_2, with the sum denoted as NO_x) and volatile organic compounds (VOCs) (Seinfeld, 1986; National Research Council, 1991). Apart from remote regions, where the in situ tropospheric chemical generation of ozone is driven essentially by methane (Logan *et al.*, 1981), a relatively large number of VOCs participate in ozone generation. Measurements of non-methane organic compounds in the South Coast Air Basin of California during the 1987 Southern California Air Quality Study, for example, revealed over 280 hydrocarbon and oxygenated organic species, many of which contribute to some degree to ozone generation (Lurmann and Main, 1992).

It has been recognized for some time that VOCs differ in their ozone-forming capability. Smog chamber experiments carried out with a series of single hydrocarbons irradiated in the presence of NO_x provide a measure of the relative amount of ozone formed by individual hydrocarbons, leading to reactivity scales. Hydrocarbons do not occur singly in the atmosphere, however, and the ozone-forming potential of an individual VOC will depend on the characteristics of the complex mixture of which it is a part, including the NO_x level and the other VOCs that are present. It has long been of interest to be able to determine, for any given VOC/NO_x mixture, the contribution of each individual organic species to the total amount of ozone generated in that mixture. That

determination has important implications to the relative control of different hydrocarbon emissions in ozone abatement.

Over the past 20 years or so there has been a significant effort devoted to developing chemical reaction mechanisms for atmospheric VOC/NO_x chemistry (Lurmann *et al.*, 1986; Gery *et al.*, 1989; Atkinson, 1990; Carter, 1990; Stockwell *et al.*, 1990; Carter and Lurmann, 1991). Such mechanisms form a core around which atmospheric models describing urban and regional ozone formation are constructed (Lamb, 1983; Chang *et al.*, 1987; Liu *et al.*, 1987; Morris and Myers, 1990; Sillman *et al.*, 1990*a*; McKeen *et al.*, 1991*a*; Harley *et al.*, 1993). Decisions concerning the relative amounts of VOC versus NO_x control to achieve ozone air quality standards (Milford *et al.*, 1989; Sillman *et al.*, 1990*b*; McKeen *et al.*, 1991*b*; Rao and Sistla, 1993; Possiel and Cox, 1993), as well as the relative controls of different VOCs (Dunker *et al.*, 1992; Auto/Oil, 1993*a*), are being made by employing these comprehensive atmospheric models. The question of how much of the total amount of ozone generated under a particular set of conditions is attributable to each of the individual constituents of the VOC mixture is, therefore, appropriately addressed by analysis of the atmospheric VOC/NO_x reaction mechanism.

Ozone production in a VOC/NO_x system is usually initiated by hydroxyl (OH) radical attack on a hydrocarbon molecule to produce a peroxyalkyl radical, RO_2,

$$RH + OH \xrightarrow{O_2} RO_2 + H_2O \qquad \text{R1}$$

followed by reactions of RO_2 with NO,

$$RO_2 + NO \xrightarrow{O_2} R'CHO + HO_2 + NO_2 \qquad R2$$

$$HO_2 + NO \longrightarrow OH + NO_2 \qquad R3$$

Photolysis of the NO_2 formed from NO then leads to ozone through the photochemical cycle,

$$NO_2 + h\nu \longrightarrow NO + O \qquad R4$$

$$O + O_2 + M \longrightarrow O_3 + M \qquad R5$$

$$NO + O_3 \longrightarrow NO_2 + O_2 \qquad R6$$

Ozone formation is governed by the efficiency of reactions R2 and R3 relative to R6, since R6 requires the consumption of a molecule of ozone, while R2 and R3 do not. The cycling of a particular nitrogen atom through reactions R2-R6 can be terminated by reactions that convert NO_2, either permanently or temporarily, into inorganic (e.g., nitric acid, HNO_3) and organic nitrogen (e.g., PAN, $CH_3C(O)OO\ NO_2$) products. At moderately high NO_x concentrations ($NO_x > 0.3$ ppb), particularly under urban conditions, reactions R2 and R3 represent the dominant reaction pathway for RO_2 and HO_2 radicals. In the remote troposphere ($NO_x < 0.1$ ppb) reactions R2 and R3 are no longer the dominant reactions of the peroxy radicals. Radical-radical, ($RO_2 + RO_2$, $RO_2 + HO_2$, and $HO_2 + HO_2$), and other reactions such as $HO_2 + O_3$, become important in NO_x

-limited conditions (Madronich and Calvert, 1990; Trainer *et al.*, 1987). With a mixture of hydrocarbons present, the peroxy radical pool that drives ozone formation consists of a constantly varying mixture with species that originated from all the VOCs present. Also, species like the aldehyde R'CHO, formed in reaction R2, can be present initially or, as indicated in R2, can be formed as a product of the oxidation of one or more of the hydrocarbons present. The aldehyde, whether present initially or produced in the photooxidation of hydrocarbons, will itself proceed to be oxidized and make its own contribution to overall ozone formation. If the aldehyde resulted from the oxidation of a hydrocarbon, then the ozone contributed by the aldehyde is ultimately attributable to its hydrocarbon precursor. The same aldehyde may have also been present in the initial mixture, or been emitted, and it may be desirable to be able to differentiate between the ozone formed from the initially present aldehyde and that attributable to the aldehyde formed photochemically during the course of oxidation of hydrocarbons.

The key oxidizing species in the chemistry of the troposphere is the OH radical. Hydroxyl radicals are formed from ozone photolysis,

$$O_3 + h\nu \longrightarrow O_2 + O(^1D) \qquad \text{R7}$$

$$O(^1D) + H_2O \longrightarrow 2\,OH \qquad \text{R8}$$

They are also formed in reaction R3, and as a product of ozone-olefin reactions (Paulson *et al.*, 1992; Paulson and Seinfeld, 1992). The OH formed as a result of reactions R7 and R8 can be considered as "new" OH, as opposed to that formed in reaction R3, which is

the result of radical propagation originally initiated by an OH in reaction R1. As noted above, radical termination reactions such as $HO_2 + HO_2$, or

$$OH + NO_2 \longrightarrow HNO_3 \qquad R9$$

compete with radical propagation reactions such as R2 and R3. Under conditions where sufficient NO_x is present, a new OH that participates in R1 is more likely to emerge as reformed OH, say in reaction R3, and therefore be available to participate again in R1, than to be terminated, say, by R9. Each VOC photooxidation mechanism has its own radical propagation/termination character. One would like to be able to determine at any time the fraction of the radical pool that is "new" radicals and also to determine the contributions to the radical pool from each of the initially present and photochemically formed VOCs.

In this paper we present a method for determining the contributions of each individual VOC in a complex VOC/NO_x mixture to ozone, radical, and product formation. In so doing we will be able to answer questions such as: (1) How much of the total ozone formed during a given photooxidation is attributable to each initially present VOC; (2) What is the individual contribution of each VOC to the radical pool at any time; (3) What are the contributions of each VOC to products such as PAN and nitric acid; and (4) For a compound such as formaldehyde (HCHO) that generally occurs both in the initial VOC mixture and is produced by the photooxidation of other VOCs, what

are the contributions to ozone and other product formation from that initially present, or emitted from sources, and that produced by in situ chemistry.

OZONE ASSIGNMENT METHOD

Hydrocarbon reactivity in atmospheric VOC/NO_x systems can be judged on the basis of ozone-forming capability (Carter and Atkinson, 1989; Chang and Rudy, 1990; Carter, 1991; Auto/Oil, 1993b). Recent efforts have been directed toward evaluating the so-called incremental reactivity of VOCs, the incremental change in peak ozone generated resulting from addition of a small amount of an individual VOC to a VOC/NO_x mixture (Carter and Atkinson, 1987). The question underlying studies of hydrocarbon reactivity is that of the individual contribution of each VOC to ozone formation. We present in this section a method to accomplish this assignment of ozone for any atmospheric VOC/NO_x chemical mechanism.

The basic concept of this method is to follow the reaction pathways of a mechanism and trace the ozone, or other product species, formed back to the original organic precursors. As an organic species reacts, the RO_2 radicals and all other product species that are formed are assigned to that initial organic. When these species in turn react, the resultant ozone, PAN, or other products are assigned back to the original organic from which the RO_2 radical was created. In this way, the total amount of ozone

attributable to an individual VOC may be calculated. It should be noted that this method deals with the total amount of ozone produced during a simulation, in contrast to the incremental reactivity approach which analyzes changes in peak ozone - changes that occur upon adding an individual VOC and include changes to the ozone production from all VOCs in the mixture.

The technique we will present actually represents a continuation and extension of ideas previously in the literature (Leone and Seinfeld, 1984; Leone and Seinfeld, 1985; Jeffries, 1993). The essential concept is to track the progress of each reaction in the chemical mechanism through the use of dummy products added to each reaction, termed counter species (since they "count" the number of times a particular reaction occurs), and then, by appropriate stoichiometric manipulations of these products, to unravel the complex chemistry.

Given a mechanism with N species, A_i, i=1,2,...,N, and M reactions, a generalized reaction using the species, A_i, and the stoichiometric coefficients, s_{ij}, can be written

$$(-s_{1j})A_1 + (-s_{2j})A_2 \xrightarrow{j} s_{3j}A_3 + s_{4j}A_4 + \ldots + s_{Nj}A_N, \qquad j=1,2,\ldots,M$$

where the stoichiometric coefficient s_{ij} is, by convention, negative for reactants and positive for products. As noted, a counter species, C_j, is added to each reaction,

$$(-s_{1j})A_1 + (-s_{2j})A_2 \xrightarrow{j} s_{3j}A_3 + s_{4j}A_4 + \ldots + s_{Nj}A_N + C_j$$

The concentrations of the chemical species, A_i, and the counter species, C_j, at any time can be represented by the vectors, $\mathbf{x}(t)$ and $\mathbf{f}(t)$, the elements of which are $x_i(t)$, the concentration of species A_i at time t, i=1,2,...,N, and $f_j(t)$, the concentration of the counter species C_j for reaction j at time t, j=1,2,...,M.

This technique for following the reaction pathways of a mechanism, which we call the Ozone Assignment Method, requires that one reactant in each reaction be selected as the "dominant" or controlling reactant. The dominant reactant for a given reaction will be the precursor to which the product species formed in the reaction will be assigned. Thus for the reaction

$$A_1 + A_2 \longrightarrow A_3 + A_4$$

the product species A_3 and A_4 can be "assigned" to either A_1 or A_2 depending on which species is specified as the dominant reactant. The selection of dominant reactants is based upon the information sought from the mechanism. The selection process is straightforward for reactions that have essentially only one reactant. Examples are photolysis reactions and those involving a constant species such as O_2 or H_2O. Since the main goal of the Ozone Assignment Method is to assign ozone back to the emitted organics, for our calculations when more than one reactant was present, these organics were given priority for selection as dominant reactant followed by organic radical species and, lastly, the nitrogen oxides. When, for example, an organic reacts with the OH radical, the organic species will be designated the dominant reactant. For the case of

peroxy-peroxy reactions, the larger radical is selected as the dominant reactant such that a peroxyalkyl radical has preference over an HO_2 radical which itself takes priority over an OH radical. In this way the organics and their more immediate products are selected as dominant reactants. Dominant reactant information can be placed in a vector **d**, composed of the elements d_j, where d_j is the index number of the species selected as the dominant reactant for reaction j, j=1,2,...,M. Thus for the reaction above, if A_2 is selected as the dominant reactant, the vector element d_j for this reaction will be 2. In this way the dominant reactant for any reaction j will be the species A_{d_j}.

Using the concentration vectors, $\mathbf{x}(t)$ and $\mathbf{f}(t)$, together with the stoichiometric coefficient matrix **S**, with elements s_{ij}, i=1,2,...,N, j=1,2,...,M, and the above vector **d**, all the necessary manipulations to trace the mechanism pathways may be performed. The first step is to determine the fraction, $h_j(t)$, of the dominant reactant A_{d_j} that passes through each reaction j. This fraction can be expressed in the following form,

$$h_j(t) = \frac{\Delta f_j(t)}{x_{d_j}(t-\Delta t) + \sum_{\substack{k=1 \\ s_{d_j k}>0}}^{M} s_{d_j k}\Delta f_k(t) + e_{d_j}(t)}$$

$$= \frac{\text{amount of reactant passing through reaction } j \text{ during time step } \Delta t \text{ ending at } t}{\text{amount of reactant available during time step } \Delta t \text{ ending at } t}$$

where $\Delta f_j(t)$ is the change in counter species j during the time step ending at t, $x_{d_j}(t-\Delta t)$ is the concentration at the beginning of the time step of species A_{d_j} (the dominant reactant for reaction j), $s_{d_j k}$ is the stoichiometric coefficient of A_{d_j} in reaction k, and $e_{d_j}(t)$, an

element of the vector **e**(t), is the concentration of species A_{d_j} emitted during the time step ending at t. The summation in the above expression is over all reactions k, k=1,2,...,M, in which species A_{d_j} is produced (that is, when $s_{d_j k} > 0$). The variables $h_j(t)$, j=1,2,...,M, constitute the elements of a vector $\mathbf{h}(t)$.

To illustrate this consider the following three reactions, with counter species C_1, C_2, and C_3 added, that occur in all VOC/NO_x mechanisms:

$$\mathrm{HCHO} + h\nu \xrightarrow{1} 2\,\mathrm{HO_2} + \mathrm{CO} + \mathrm{C_1}$$
$$\mathrm{CO} + \mathrm{OH} \xrightarrow{2} \mathrm{HO_2} + \mathrm{CO_2} + \mathrm{C_2}$$
$$\mathrm{HO_2} + \mathrm{NO} \xrightarrow{3} \mathrm{OH} + \mathrm{NO_2} + \mathrm{C_3}$$

For the reactions above, the fraction of HO_2, the dominant reactant in reaction (3), reacting via reaction (3) is obtained by calculating $h_3(t)$,

$$h_3(t) = \frac{\Delta[\mathrm{C_3}]}{[\mathrm{HO_2}]_{t-\Delta t} + 2\,\Delta[\mathrm{C_1}] + \Delta[\mathrm{C_2}]}$$

The numerator of the above expression is the amount of HO_2 that has passed through reaction (3) during the time step from t-Δt to t. The denominator is the total amount of HO_2 available for reaction during the time step, being composed of the HO_2 present at the beginning of the time step as well as any HO_2 produced during the time step by reactions (1) and (2), with, in this case, no HO_2 emitted.

The next quantities to be calculated are termed production factors, and can be placed in an N x N matrix, $\mathbf{G}(t)$, composed of the elements $g_{ik}(t)$, defined such that

$$g_{ik}(t) = \frac{\text{net amount of species } k \text{ produced or destroyed attributable to the reactions of species } i \text{ and its products during the time step ending at } t}{\text{amount of reactant species } i \text{ available during the time step ending at } t}$$

That is, g_{ik} is the amount of species k attributable to species i that is produced per amount of species i available for reaction. The production factor, $g_{ik}(t)$, when multiplied by a species concentration $x_i(t-\Delta t)$, will give the net amount of species k produced (or destroyed) by species i during the time step Δt ending at time t. It is in defining the production factors that the degradation pathways of the mechanism are traced. The production of species k due to species i is not merely the amount of species k formed or destroyed directly by reactions of species i, but includes also any amount of species k that is formed or destroyed by the reaction products of species i. Using the simple three-reaction mechanism from above, with HO_2 as the assigned species k, the following production factors can be written

$$\begin{aligned} g_{HCHO,HO_2}(t) &= h_1(t)\,[2 + 2g_{HO_2,HO_2}(t) + g_{CO,HO_2}(t)] \\ g_{CO,HO_2}(t) &= h_2(t)\,[1 + g_{HO_2,HO_2}(t) + g_{CO_2,HO_2}(t)] \\ g_{HO_2,HO_2}(t) &= h_3(t)\,[-1 + g_{OH,HO_2}(t) + g_{NO_2,HO_2}(t)] \end{aligned}$$

Production factors are obtained by multiplying the reaction probability, $h_j(t)$, for each reaction j in which species i is the dominant reactant, by the production factor of each product species in reaction j. When the assigned species k is formed, as is the case for HO_2 in reactions (1) and (2), a factor of +1 is included for each molecule of species k

created; when species k is destroyed, as occurs for HO_2 in reaction (3), a factor of -1 is included. For more complicated mechanisms each production factor will contain several terms corresponding to each reaction in which species i is the dominant reactant. Production factors are, therefore, interdependent and can be determined by solving the system of linear equations for $\mathbf{G}(t)$,

$$\mathbf{A}(t)\,\mathbf{G}(t) = \mathbf{B}(t)$$

where the $N \times N$ matrices $\mathbf{A}(t)$ and $\mathbf{B}(t)$ are formed according to

$$\mathbf{A}(t) = \mathbf{S''}\,\mathbf{h}(t)$$

$$\mathbf{B}(t) = \mathbf{S'}\,\mathbf{h}(t)$$

where the $N \times N \times M$ matrices $\mathbf{S'}$ and $\mathbf{S''}$ are composed of the elements s'_{ikj} and s''_{ikj}, i=1,2,...,N, k=1,2,...,N, j=1,2,...,M, with

$$s'_{ikj} = 0 \quad \text{for } i \neq d_j \qquad\qquad s''_{ikj} = 0 \quad \text{for } i \neq d_j$$

$$s'_{ikj} = -s_{kj} \quad \text{for } i = d_j \qquad\qquad s''_{ikj} = s_{kj} \quad \text{for } i = d_j,\ s_{kj} > 0$$

$$s''_{ikj} = 0 \quad \text{for } i = d_j,\ s_{kj} \leq 0$$

such that

$$a_{ik}(t) = \frac{\text{amount of species } k \text{ formed as a product in reactions of species } i \text{ during the time step ending at } t}{\text{amount of reactant species } i \text{ available during the time step ending at } t}$$

$$b_{ik}(t) = \frac{\text{net amount of species } k \text{ produced (amount formed as product minus amount destroyed as reactant) in reactions of species } i \text{ during the time step ending at } t}{\text{amount of reactant species } i \text{ available during the time step ending at } t}$$

Once the matrices $\mathbf{A}(t)$ and $\mathbf{B}(t)$ are calculated, the system of equations is solved for the matrix $\mathbf{G}(t)$. $\mathbf{A}(t)$, $\mathbf{B}(t)$, and $\mathbf{G}(t)$ are all square $N \times N$, non-singular matrices, thus permitting a variety of methods for solving the equations. The computer code we used for our calculations employed simple Gauss-Jordan reduction. The set of production factors, $\mathbf{G}(t)$, once calculated, may then be used to create a matrix of assigned species, $\mathbf{X'}(t)$, composed of the elements $x'_{ik}(t)$, the concentration of species i attributable to species k at time t, i=1,2,...,N, k=1,2,...,N. At time $t = 0$, the initially present hydrocarbons will be assigned to themselves such that

$$x'_{ik}(t) = x_i(t) \qquad \text{for } i = k$$

$$x'_{ik}(t) = 0 \qquad \text{for } i \neq k$$

Similarly, emitted species, whose concentrations are listed in $\mathbf{e}(t)$, are also assigned to themselves by forming a diagonal $N \times N$ matrix, $\mathbf{E'}(t)$, composed of the elements $e'_{ik}(t)$, i=1,2,...,N, k=1,2,...,N, where

$$e'_{ik}(t) = e'_i(t) \quad \text{for } i = k$$

$$e'_{ik}(t) = 0 \qquad \text{for } i \neq k$$

The matrix $\mathbf{X'}(t)$ is then calculated as follows

$$\mathbf{X'}(t) = \mathbf{X'}(t\text{-}\Delta t) + \mathbf{X'}(t\text{-}\Delta t)\,\mathbf{G}(t) + \mathbf{E'}(t)\,\mathbf{G}(t)$$

The concentration of a species *i*, attributable to species *k*, at a given time is, therefore, the sum of the concentration at the previous time step plus any change in the concentration of species *i* during the time step due to the reactions of all the species attributable to species *k*, including emissions of species *k* during the time step. Once calculations are completed for all time steps, the matrix $\mathbf{X'}(t)$ will contain full information assigning all species within the mechanism back to the initially present or emitted hydrocarbons.

The Ozone Assignment Method as presented in this section is applicable in principle to any chemical reaction mechanism. With slight modification, the above analysis can be applied to multiple cell models in which the chemical mechanism is being solved simultaneously in each grid cell. For mechanisms of atmospheric chemistry, with the addition of counter species to the mechanism reactions, the theory developed above will enable identification of the individual contributions of each VOC to the formation of ozone, radicals, and all other photochemical products. This information can then be used to analyze the complex chemistry of a large VOC/NO_x system. The following sections illustrate analysis possible using the Ozone Assignment Method.

Similar techniques have been developed by Jeffries and co-workers to assess individual VOC contributions to ozone formation (Jeffries and Crouse, 1990; Jeffries, 1993). Both methods follow the reaction pathways of a mechanism; in the Jeffries approach, ozone production is apparently determined by explicitly calculating various

ratios of radicals and NO to NO_2 conversions. The methodology presented here is universally applicable to any given chemical reaction mechanism and can be used to determine VOC contributions not only to ozone, but to all other product species as well.

APPLICATION TO EVALUATE OZONE PRODUCTIVITY

Ozone Assignment was used to investigate the reaction pathways of the condensed SAPRC 90 VOC/NO_x mechanism (Carter and Lurmann, 1990). The version of the mechanism we used contained methane, two lumped higher alkanes, termed ALK1 and ALK2, two lumped aromatics, termed ARO1 and ARO2, ethene, three lumped higher alkenes, designated OLE1, OLE2, and OLE3, and four carbonyls, HCHO, CCHO, RCHO, and MEK. The lumped species in the mechanism represent a composite of the individual species present in the organic mixture, with species assigned to the lumped groups based on their OH radical rate constants. The species ALK1 represents alkanes with $k_{OH} < 10^4$ $ppm^{-1}min^{-1}$, and contains approximately 4 carbons per molecule. Alkanes with $k_{OH} \geq 10^4$ $ppm^{-1}min^{-1}$ are assigned to ALK2 and contain on average 8 carbons per molecule. The lumped aromatic species ARO1 represents all aromatics with $k_{OH} < 2x10^4$ $ppm^{-1}min^{-1}$ and is composed mostly of toluene. ARO2 represents the aromatics with $k_{OH} \geq 2x10^4$ $ppm^{-1}min^{-1}$ and contains mostly xylene. Alkenes with $k_{OH} < 7.5x10^4$ $ppm^{-1}min^{-1}$ are assigned to OLE1 which are in general terminal olefins with 4 carbons per molecule.

OLE2 represents the alkenes with $k_{OH} \geq 7.5x10^4$ $ppm^{-1}min^{-1}$ which are mostly internal olefins of approximately 5 carbons. Biogenic alkenes and isoprene are used to form the lumped group OLE3 which has on average 7 carbons per molecule. The carbonyls are modeled after formaldehyde (HCHO), acetaldehyde (CCHO), propionaldehyde (RCHO), and methyl ethyl ketone (MEK).

A photochemical box model, from the Carter mechanism preparation program (Carter, 1988), was used to implement the mechanism for simulations designed to represent summertime conditions in Los Angeles. All reactants were present initially, with no additional emissions or dilution occurring over the course of the simulation. Organic reactant concentrations were determined using the August 21, 1987, California Air Resources Board (ARB) inventory for the South Coast Air Basin of California (ARB, 1987), from which concentrations for all VOCs except CO were obtained, together with the EPA EKMA scenario for Los Angeles (EPA, 1988), which contains CO levels. The EKMA scenario was also used to select a representative base case VOC/NO_x ratio of 8.2. The initial reaction mixture contained 1230 ppbC of NMHC, 1700 ppb CH_4, 1500 ppb CO, 120 ppb NO, and 30 ppb NO_2. (See Table 1.) Kinetic parameters for the lumped species in the SAPRC 90 mechanism were calculated from the Carter emissions processing program (Carter, 1988) using the initial organic reactant concentrations. Chemical reactions occurred under the influence of time-varying solar irradiation, corresponding to June 21, and were followed for 15 hours, from 6 am to 9 pm.

Calculations were performed at the base case VOC/NO_x ratio of 8.2 as well as VOC/NO_x ratios of 4 and 20, representing high and low NO_x conditions.

General results of the analysis of the SAPRC 90 mechanism by the Ozone Assignment Method are shown in Figures 1-3. Figure 1 shows ozone concentration over the course of the 15 hour run, with a breakdown of the ozone due to each emitted hydrocarbon. A summary of the relative contribution to peak ozone levels of each species for the three VOC/NO_x ratios investigated is given in Table 2. The base case NO_x conditions lead to ozone levels very close to the maximum obtained for the given VOC concentrations. The base case can, therefore, be viewed as representing maximum ozone production near the ridge line on an ozone isopleth diagram, while the high and low VOC/NO_x conditions will fall on either side of the ridge line and produce relatively lower ozone levels. For each of these VOC/NO_x conditions, the alkenes, alkanes, and aromatics produce the majority of the ozone. CO also produces a significant amount of O_3 at the higher VOC/NO_x ratios due to its relatively high concentration. Methane and the higher aldehydes, at the given concentration levels, however, are responsible for only a small fraction of the total ozone produced.

The total O_3 attributable to each organic is influenced greatly by the relative concentrations of each species. A measure of the relative ozone forming potential of each organic, its ozone productivity, normalizes the ozone produced from an organic in a particular situation by the amount of that organic, both initially present and emitted, available for reaction.

$$P_{O_3,VOC_i} = \frac{[O_3]_{VOC_i}}{[VOC_i]}$$

$$= \frac{\text{ppb } O_3 \text{ produced due to VOC}_i}{\text{ppbC VOC}_i \text{ initially present} + \text{ppbC VOC}_i \text{ emitted}}$$

Figure 2 compares the ozone productivity of the organics present at VOC/NO_x ratios of 4, 8.2 and 20. In all cases, the aldehydes, alkenes, and the xylene class aromatics, ARO2, exhibit the highest productivity of ozone. The alkanes, ketones, and lower molecular weight aromatics show much lower productivity, and CO and CH_4 produce only small amounts of ozone on a per carbon basis. The highest ozone productivities occur in the base case. Productivity will also vary with the VOC mixture composition since ozone production by each organic is affected by the other species present. The relative productivity of the various organics also varies significantly with the NO_x conditions. This behavior is notable, for example, with the higher aldehydes, where RCHO is the most productive at low VOC/NO_x, but at high VOC/NO_x, CCHO is more productive.

An alternative measure of ozone production is the amount of ozone formed per "molecule" of NO_x, as shown in Figure 3. The alkanes, olefins, aromatics, and CO account for the majority of the ozone produced. This measure is greatly influenced by the relative abundance of the various organic species, as evidenced by the large ozone contribution from the alkanes and CO, which is more a reflection of their high initial concentrations than their relatively small ozone productivities. The shape of the curve is different for each species as a result of varying relative productivities. The variability of

ozone production by the individual organics points once again to the complex behavior of the VOC/NO_x mixture.

ORIGIN AND EVOLUTION OF THE RADICAL POOL

The Ozone Assignment Method was also used to track the formation of radical species. Through photolysis of O_3, aldehydes, and other species, substantial amounts of radical species are created; however, their production is offset by equally large losses due to HNO_3 and PAN formation and radical-radical loss reactions. In order to accurately track radical species, both radical-creating reactions and radical-destroying reactions were identified for OH, HO_2, and RO_2 radicals. The SAPRC 90 mechanism represents OH and HO_2 radicals explicitly and employs several other radical species to represent the various peroxy radicals. For our purposes all of these higher peroxy radicals were defined as RO_2 radicals. A radical-creating reaction is one in which more radicals are created than destroyed, and, likewise, a radical-destroying reaction is one where more radicals are destroyed than created. Propagation reactions which involve conversions between RO_2, HO_2, and OH radicals are also identified, but those propagation reactions where one type of RO_2 radical is converted into another type of RO_2 radical were not considered since no net change to the RO_2 pool occurs.

The interrelation between these various radical flows for the entire VOC mixture at each of the three VOC/NO_x ratios is shown in Figures 4-6, where the numbers by each arrow indicate the amount of radicals, in units of ppb, that follow each pathway over the entire time of the simulation. Sources of radical creation are identified by lightly shaded ovals, and radical-destroying sinks are denoted by more heavily shaded ovals. Conversion flows between the three radical types and the species that cause the conversion are listed within rounded rectangles.

New OH production increases dramatically with increasing VOC/NO_x ratios and is a result of two main processes. Ozone photolysis accounts for virtually all of the new OH radicals at low VOC/NO_x, and the majority of new OH production at high VOC/NO_x. At the high VOC/NO_x ratio, peroxide concentrations become large enough to result in significant new OH formation through photolysis. The increase in new OH as VOC/NO_x increases is a result of increased ozone concentrations. Although the peak ozone concentration for VOC/NO_x = 20 is lower than for VOC/NO_x = 8.2 (see Table 2), the amount of ozone photolysis is greater at the higher VOC/NO_x ratios since in that scenario, ozone concentrations build up more quickly, resulting in a higher average ozone level.

The production of new HO_2 and RO_2 radicals also increases with increasing VOC/NO_x and is primarily a result of the photolysis of aldehydes and, in the case of RO_2 radicals, other species, such as aromatic fragmentation products and cresols. While a small fraction of these species are present initially, the majority are produced from reactions of the larger lumped species. As VOC/NO_x increases, more of these organics

react, causing the amount of new HO_2 and RO_2 radicals to increase. Both HO_2 and RO_2 creation are major sources of new radicals at all three VOC/NO_x ratios, while OH creation is important for all but the low VOC/NO_x condition.

The loss reactions of OH, HO_2, and RO_2 when taken together, match the creation reactions of new OH, new HO_2, and new RO_2 radicals, indicating that all of the radicals created are destroyed with no net buildup of radical species. Creation and loss flows for the individual radicals, however, are not equal, as a result of interconversion between the three radical types. In fact, it can be seen from Figures 4-6, that propagation, the arrows between the OH, HO_2, and RO_2 boxes, occurs much more often than termination as new radicals cycle between the radical types several times before being destroyed. While the overall amount of radical termination increases with VOC/NO_x to match radical creation flows, OH losses decrease at high VOC/NO_x and RO_2 and HO_2 losses increase.

OH losses occur almost exclusively via reaction with NO_2 to form HNO_3 . Between VOC/NO_x =4 and 8.2, an increase in OH concentration is sufficient to offset the decrease in the amount of NO_2 present causing nitric acid formation to remain relatively constant, but at high VOC/NO_x, the drop in NO_2 levels causes the OH - NO_2 reaction rate to decrease. Since most of the radicals at low VOC/NO_x are removed as OH via HNO_3 formation, the RO_2 loss pathway is quite small, and HO_2 losses are negligible. As the NO_x level decreases and radical levels increase, however, HO_2 and RO_2 destruction become important. The majority of RO_2 radical losses occur through reaction with NO_x, forming PAN or causing NO to NO_2 conversions without radical propagation. Radical

destruction via these pathways peaks at the intermediate VOC/NO_x ratio when both NO_x and RO_2 are present at appreciable levels, but drops off at both low VOC/NO_x, due to a lack of RO_2 radicals, and high VOC/NO_x, due to an absence of NO_x. Additional losses of RO_2, and the only losses of HO_2, result from radical-radical reactions forming peroxides. Only at the high VOC/NO_x condition, when there is not sufficient NO_x to react with all the radicals, do radical-radical interactions become important.

The conversion between radical types occurs via reactions with NO, organics, and ozone. The initial OH attack on organics results in conversion to RO_2 or HO_2 radicals. RO_2 then reacts with NO and is converted to HO_2 which can react with NO or O_3 to convert back to OH. It can be seen that conversion to OH depends greatly on the availability of NO. Together with the effect of NO_2 concentration on HNO_3 formation the overall effect of this NO_x dependence is such that at low VOC/NO_x levels RO_2 radicals are ultimately converted to OH and then destroyed by HNO_3 formation, while at high VOC/NO_x, OH radicals tend to be converted to HO_2 and RO_2 radicals and are then removed via radical-radical and PAN formation reactions.

The contribution of the individual VOCs to these radical flows was determined and radical productivities, or the amounts of radical creation or destruction per carbon atom of organic, were calculated. Figures 4-6 indicate distinct behavior for the OH radical, while HO_2 and RO_2 radicals are much more similar to each other. For greater simplicity, in the following radical productivity calculations HO_2 and RO_2 radicals are grouped together, so that only two radical types will be examined. Figure 7 contains

information regarding new OH and new HO_2/RO_2 productivities. Since new OH radicals are formed by O_3 photolysis, the chart of new OH productivities (Figure 7*a*) is very similar to the ozone productivity chart (Figure 2), with the aldehydes, alkenes, and higher aromatics (ARO2) exhibiting the highest productivities, and large variations with VOC/NO_x ratio. New HO_2/RO_2 productivities (Figure 7*b*) are highest for formaldehyde, followed by ARO2, the higher aldehydes, and the alkenes. The alkanes, ketones, and toluene class aromatics (ARO1) had much lower productivities and CO and CH_4 produced virtually no peroxy radicals on a per carbon basis.

Variations with VOC/NO_x are largely determined by the availability of the reacting organic molecule. As VOC/NO_x ratios and OH concentrations increase, the rate of OH initiated reactions increases. Since fast reacting species such as the aldehydes, react nearly completely, reaction with the OH radical competes with photolysis reactions so that as VOC/NO_x increases, photolysis, and therefore new HO_2/RO_2 production, decreases. On the other hand, more slowly reacting species, such as the alkanes, do not react to completion, so that an increase in OH reaction rates causes more of the organic to react, resulting in increased new HO_2/RO_2 production. The relative contributions to new OH and new HO_2/RO_2 radicals of each organic species at the three VOC/NO_x ratios is given in Table 3.

OH and HO_2/RO_2 loss productivities for the individual VOCs, as shown in Figure 8, are generally a reflection of their new radical productivities. This is to be expected since the radicals produced by an organic will eventually be destroyed and attributed back

to that organic. As a result, VOCs that are highly productive with respect to new radicals will also tend to exhibit high radical loss productivities. Losses of OH and HO_2/RO_2 radicals attributable to individual organics, do not, however, correspond directly to their respective new OH and new HO_2/RO_2 productivities since conversion between these two radical types also occurs.

The overall effect of these radical flows can best be understood by examining Figure 9, where net OH and net HO_2/RO_2 productivities are presented. For these figures, the creation, destruction, and conversion flows were all used to calculate the net amount of OH or peroxy radicals produced by each VOC. Net producers of OH radicals are formaldehyde, the aromatics, and the alkenes, species typically regarded as highly reactive with respect to ozone formation, while CO and the alkanes, which are generally thought of as less reactive towards O_3 formation, show a net loss of OH radicals. The productivities for CCHO, RCHO, and MEK are all reported here as zero since the net amount of OH radicals produced by each of these species was extremely small, with fluctuations between positive and negative values, and was indistinguishable from uncertainties in OH concentration.

Net production of HO_2 and RO_2 radicals varied with VOC/NO_x. At VOC/NO_x=4, only the olefins were net sinks for peroxy radicals, due primarily to the conversion of HO_2 radicals to OH and subsequent removal as nitric acid. All other organics were slight net HO_2/RO_2 sources. At VOC/NO_x ratios of 8.2 and 20, many more of the organics exhibit negative net HO_2/RO_2 productivities, particularly the aldehydes, as a result of

large PAN and PPN formation and increased radical-radical reactions. Comparison of Figures 9*a* and 9*b*, as well as Figures 4-6, shows the important role of CO in assisting radical chain propagation by converting OH radicals to HO_2 radicals. While the reported productivities for CO are small, as a result of the large concentration of CO present in the mixture, they represent a major fraction of OH and HO_2 radical flows. Several other organics exhibit similar behavior, most notably the alkenes which produce the opposite conversion from RO_2 to OH radicals.

VOC CONTRIBUTIONS TO PAN AND OTHER PHOTOCHEMICAL PRODUCTS

The reservoir species PAN and HNO_3, which serve as major sinks for both NO_x and radicals, can also be examined to determine the contribution of each organic to their formation. The HNO_3 productivity for each hydrocarbon at three different VOC/NO_x ratios is shown in Figure 10. The productivities shown here are essentially the same as the OH loss productivities shown in Figure 8*a*, for all organics except the aromatics. The major pathway for HNO_3 formation is the reaction of OH and NO_2 and as a result OH loss and HNO_3 productivities are equivalent for most species. The aromatics, however, have an additional pathway for nitric acid formation via the reaction of cresols with NO_3, and therefore exhibit higher HNO_3 productivity than would be predicted by OH loss alone. Table 4 details the relative contribution of each hydrocarbon to HNO_3 production

at the three VOC/NO_x ratios. The majority of nitric acid formation is due to, in order of importance, the aromatics, alkenes, and alkanes. As was the case for OH loss productivity, for all species, nitric acid productivity decreases at high VOC/NO_x, due to a decrease in the available NO_2.

PAN productivities for all relevant hydrocarbons are shown in Figure 11. It should be noted that the SAPRC 90 mechanism includes both PAN and PPN as distinct species. The results here are for PAN only and do not include any PPN formation. CO, CH_4, and HCHO are not included because they produce none of the peroxyacetyl radical that is the precursor to PAN. The higher aldehydes and alkenes are the most effective at producing PAN, but even the alkanes show a significant ability to form PAN. Since PAN formation is dependent on peroxyacetyl radical production, those species that produce, either directly or indirectly, more of this radical will therefore produce the most PAN. For all organics, PAN productivity was highest near the base case VOC/NO_x and was lower at both high and low VOC/NO_x. As was the case with HNO_3 formation, at high VOC/NO_x there is little NO_2 available, thus limiting the amount of PAN that can be formed. At low VOC/NO_x little PAN is formed since few peroxyacetyl radicals are present and most of the available NO_x is converted into HNO_3 instead of PAN.

The relative share of PAN production for each organic is shown in Table 5. Alkenes, aromatics, and alkanes produce over 90% of all the PAN formed. The aldehydes exhibit high productivity, but contribute only slightly to the total PAN production. This results from the manner in which the Ozone Assignment Method

assigns product species to their parent organics. PAN formed from aldehydes that were themselves produced by other hydrocarbons will be assigned back to the originally emitted organic. The small aldehyde contribution to PAN formation (Table 5) includes only that PAN produced from originally emitted aldehydes, which is quite small, while the PAN derived from chemically produced aldehydes is included in the contribution of the parent species.

CONCLUSIONS

The Ozone Assignment Method for tracing the reaction pathways of an atmospheric VOC/NO_x system is a technique that determines the individual contribution of each VOC to ozone and other product species formation. The reactivity measure associated with Ozone Assignment is termed productivity and describes the amount of ozone (or other product species) produced by an organic per amount of that organic emitted.

Using the condensed SAPRC 90 mechanism with a VOC/NO_x mixture representing the South Coast Air Basin, the productivities calculated for formation of ozone, radicals, PAN, and HNO_3 exhibited several similarities. The aldehydes, alkenes, and heavy aromatics were in all cases the most productive, the light aromatics, ketones, and alkanes showed much lower productivities, and CO and CH_4 had extremely low

productivities. Much of this difference can be attributed to the fraction of each VOC that reacted. Those species that react most completely tend to have the highest productivities. The total production of ozone or other products is greatly influenced by the VOC mixture composition. Relatively unproductive species, such as CO and the alkanes, if present in sufficiently high concentration, will lead to significant amounts of ozone, while species showing high productivities, such as the aldehydes, if present in small concentrations, will cause only a small amount of ozone to be formed.

Radical production is shown to involve interactions between new radical creation, radical propagation with conversion of OH, HO_2, and RO_2 radicals, and radical termination. All species exhibit significant production of new radicals, with those species reacting most completely showing the highest productivities. Formaldehyde, xylene class aromatics (ARO2), and alkenes, species that have been viewed as highly reactive regarding ozone formation, provide a net source of OH radicals, with CO and the alkanes acting as net OH radical sinks. The olefins and higher aldehydes are net sinks of RO_2 radicals due to PAN formation and radical-radical reactions, while CO serves as a net source of HO_2 radicals via conversion of OH.

Variations in VOC/NO_x conditions also influence the productivities of the various VOCs, with a peak in production observed at a particular VOC/NO_x ratio. The location of this peak varies among the organics and depends on the product species being assigned. For the particular example studied here, both PAN and O_3 have peak productivities near the base case condition of VOC/NO_x =8.2. New radicals, and nitric

acid, however, exhibited peak productivities at much different VOC/NO_x ratios with HNO_3 peaking near $VOC/NO_x = 5$, and new radical production near $VOC/NO_x = 16$. With the Ozone Assignment Method, these relationships can be studied and a better understanding of the interactions of VOC/NO_x chemistry may be gained.

ACKNOWLEDGMENT

This work was supported by the Coordinating Research Council and the National Renewable Energy Laboratory.

REFERENCES

ARB (1987) South Coast Air Basin emissions inventory for August 27, 1987. Sacramento, CA.

Atkinson R. (1990) Gas-phase tropospheric chemistry of organic compounds: a review. *Atmos. Environ.* **24**, 1-41.

Auto/Oil Air Quality Improvement Research Program (Auto/Oil) (1993*a*) Phase I final report. Coordinating Research Council, Atlanta, GA.

Auto/Oil Air Quality Improvement Research Program (Auto/Oil) (1993*b*) Technical Bulletin No. 12 - Reactivity estimates for reformulated gasolines and methanol/gasoline mixtures. Coordinating Research Council, Atlanta, GA.

Carter W. P. L. (1988) Appendix C. Documentation for the SAPRC atmospheric photochemical mechanism preparation and emissions processing programs for implementation in airshed models. Report, Contract No. A5-122-32, California Air Resources Board, Sacramento, CA.

Carter W. P. L. (1990) A detailed mechanism for the gas-phase atmospheric reactions of organic compounds. *Atmos. Environ.* **24**, 481-518.

Carter W. P. L. (1991) Development of ozone reactivity scales for volatile organic compounds. Final report, EPA Cooperative Agreement CR-814396-01-0, U. S. Environmental Protection Agency, Research Triangle Park, NC.

Carter W. P. L. and Atkinson R. (1987) An experimental study of incremental hydrocarbon reactivity. *Environ. Sci. Technol.* **21**, 670-679.

Carter W. P. L. and Atkinson R. (1989) Computer modeling study of incremental hydrocarbon reactivity. *Environ. Sci. Technol.* **23**, 864-880.

Carter W. P. L. and Lurmann F. W. (1990) Development of a condensed mechanism for urban airshed modeling. Interim progress report - U.S. EPA Cooperative Agreement No. CR-815699-01-0, U.S. Environmental Protection Agency, Research Triangle Park, NC.

Carter W. P. L. and Lurmann F. W. (1991) Evaluation of a detailed gas-phase atmospheric reaction mechanism using environmental chamber data. *Atmos. Environ.* **25**, 2771-2806.

Chang J. S., Brost R. A., Isaken I. S. A., Madronich S., Middleton P., Stockwell W. R. and Walcek C. J. (1987) A three-dimensional Eulerian acid deposition model: physical concepts and formulation. *J. Geophys. Res.* **92**, 14681-14700.

Chang T. Y. and Rudy S. J. (1990) Ozone-forming potential of organic emissions from alternative-fueled vehicles. *Atmos. Environ.* **24**, 2421-2430.

Dunker A. M., Schleyer C. H., Morris R. E. and Pollack A. K. (1992) Effects of methanol/gasoline blends used in flexible/variable fuel vehicles on urban air quality in year 2005/2010. Auto/Oil Air Quality Improvement Research Program, paper 92-119.06, AWMA Annual meeting, Kansas City, MO, June 21-26.

EPA (1988) EPA EKMA base case simulation for Los Angeles, California, on September 3, 1988. Research Triangle Park, NC.

Gery M. W., Whitten G. Z., Killus J. P. and Dodge M. C. (1989) A photochemical kinetics mechanism for urban and regional scale modeling. *J. Geophys. Res.* **94**, 12925-12956.

Harley R. A., Russell A. G., McRae G. J., Cass G. R. and Seinfeld J. H. (1993) Photochemical modeling of the Southern California Air Quality Study. *Environ. Sci. Technol.* **27**, 278-388.

Jeffries H. E. (1993) A different view of ozone formation: fuel reformulation alone may not reduce urban ozone. *Fuel Reformulation,* **3**, 58-68.

Jeffries H. E. and Crouse R. (1990) Scientific and technical issues related to the application of incremental reactivity. Report, University of North Carolina, Chapel Hill, NC.

Lamb R. G. (1983) Regional scale (1000km) model of photochemical air pollution, part 1. theoretical formulation, EPA/600/3-83-035, U. S. Environmental Protection Agency, Research Triangle Park, NC.

Leone J. A. and Seinfeld J. H. (1984) Analysis of the characteristics of complex chemical reaction mechanisms. *Environ. Sci. Technol.* **18**, 280-287.

Leone J. A. and Seinfeld J. H. (1985) Comparative analysis of chemical reaction mechanisms for photochemical smog. *Atmos. Environ.* **19**, 437-464.

Liu S. C., Trainer M., Fehsenfeld F. C., Parrish D. D., Williams E. J., Fahey D. W., Hubler G. and Murphy P. C. (1987) Ozone products in the rural troposphere and the implications for regional and global ozone distribution. *J. Geophys. Res.* **92**, 4191-4207.

Logan J. A., Pather M. J., Wofsy S. C. and McElroy M. B. (1981) Tropospheric chemistry: a global perspective. *J. Geophys. Res.* **86**, 7210-7254, 1981.

Lurmann F. W. and Main H. H. (1992) Analysis of the ambient VOC data collected in the Southern California Air Quality Study. Final report, Contract No. A832-130, California Air Resources Board, Sacramento, CA.

Lurmann F. W., Lloyd A. C. and Atkinson R. (1986) A chemical mechanism for use in long-range transport acid deposition computer modeling. *J. Geophys. Res.* **91**, 905-936.

Madronich S. and Calvert J. G. (1990) Permutation reactions of organic peroxy-radicals in the troposphere. *J. Geophys. Res.* **95**, 5697-5715.

McKeen S. A., Hsie E. Y., Trainer M., Tallamraju R. and Liu S. C. (1991*a*) A regional model study of the ozone budget in the eastern United States. *J. Geophys. Res.* **96**, 10809-10845.

McKeen S. A., Hsie E. Y. and Liu S. C. (1991*b*) A study of the dependence of rural ozone on ozone precursors in the eastern United States. *J. Geophys. Res.* **96**, 15377-15394.

Milford J.B., Russell A. G. and McRae G.J. (1989) A new approach to photochemical pollution control. *Environ. Sci. Technol.* ***23***, 1290-1301.

Morris R. E. and Myers T. C. (1990) User's guide for the Urban Airshed Model - Volume I: user's manual for UAM(CB-IV)1. EPA/450/4-90-007a, U. S. Environmental Protection Agency, Research Triangle Park, NC.

National Research Council (1991*) Rethinking the ozone problem in urban and regional air pollution.* National Academy Press, Washington, D.C.

Paulson S. E. and Seinfeld J. H. (1992) Atmospheric photochemical oxidation of 1-octene - OH, O_3, and $O(^3P)$ reactions. *Environ. Sci. Technol,* **26**, 1165-1173.

Paulson S. E., Flagan R. C. and Seinfeld J. H. (1992) Atmospheric photooxidation of isoprene. *Int. J. Chem. Kin.* **24**, 103-125.

Possiel N. C. and Cox W. M. (1993) The relative effectiveness of NO_x and VOC strategies in reducing northeast U.S. ozone concentrations. *Water, Air, Soil Pollution,* ***67***, 161-179.

Rao S. T. and Sistla G. (1993) Efficacy of nitrogen oxides and hydrocarbon emissions controls in ozone attainment strategies as predicted by the Urban Airshed Model. *Water, Air, Soil Pollution,* **67**, 95-116.

Seinfeld J. H. (1986) *Atmospheric chemistry and physics of air pollution.* Wiley, New York.

Sillman S., Logan J. A. and Wofsy S. C. (1990*a*) A regional scale model for ozone in the United States with subgrid representation of urban and power plant plumes. *J. Geophys. Res.* **95**, 5731-5748.

Sillman S., Logan J. A. and Wofsy S. C. (1990*b*) The sensitivity of ozone to nitrogen oxides and hydrocarbons in regional ozone episodes. *J. Geophys. Res.* **95**, 1837-1851.

Stockwell W. R., Middleton P., Chang J. S. and Tang X. Y. (1990) The 2nd generation regional acid deposition model chemical mechanism for regional air-quality modeling. *J. Geophys. Res.* **95**, 16343-16367.

Trainer M., Hsie E. Y., McKeen S. A., Tallamraju R., Parrish D. D., Fehsenfeld F. C. and Liu S. C. (1987) Impact of natural hydrocarbons on hydroxyl and peroxy radicals at a remote site. *J. Geophys. Res.* **92**, 11879-11894.

Table 1. Base Case Organic Emissions.

	Initial Concentration (ppmC)	Carbon Fraction (%)
CO	1500	34.88
CH4	1700	39.53
aldehydes & ketones		
HCHO	8	0.19
CCHO	5	0.11
RCHO	2	0.04
MEK	16	0.38
alkanes		
ALK1	353	8.21
ALK2	236	5.48
aromatics		
ARO1	147	3.42
ARO2	108	2.52
alkenes		
ETHE	75	1.74
OLE1	60	1.39
OLE2	29	0.67
OLE3	62	1.45
TOTAL	4301	100

Table 2. Percentage of ozone production attributable to each organic.

	VOC/NO_x (ppbC/ppb)		
	4	8.2	20
CO	4.7	5.9	5.0
CH4	0.5	0.8	0.8
aldehydes & ketones			
HCHO	1.8	1.2	1.3
CCHO	1.3	1.0	0.9
RCHO	0.4	0.3	0.3
MEK	0.6	0.6	0.5
alkanes			
ALK1	11.1	16.7	16.7
ALK2	12.6	16.3	17.2
aromatics			
ARO1	5.6	5.5	5.3
ARO2	17.7	12.8	12.9
alkenes			
ETHE	10.8	12.3	11.8
OLE1	13.0	11.5	11.9
OLE2	6.9	5.4	5.3
OLE3	12.8	9.6	10.2
Total Peak Ozone (ppb)	58	378	303

Table 3. Percentage of new radical production attributable to each emitted organic.

	OH Radicals			RO_2 Radicals		
VOC/NO_x	4	8.2	20	4	8.2	20
CO	3.5	5.0	5.4	0.0	0.0	0.0
CH4	0.4	0.7	0.7	0.3	0.4	0.5
aldehydes & ketones						
HCHO	1.1	0.9	1.3	5.3	3.1	2.6
CCHO	1.1	1.3	1.1	1.1	0.7	0.6
RCHO	0.4	0.4	0.3	0.4	0.2	0.2
MEK	0.6	0.8	0.6	0.9	1.0	1.0
alkanes						
ALK1	8.1	17.2	15.1	9.0	14.7	15.4
ALK2	7.0	15.3	14.9	14.1	19.3	19.7
aromatics						
ARO1	3.9	3.4	4.4	7.1	10.6	10.6
ARO2	13.1	10.6	12.7	24.9	20.5	19.6
alkenes						
ETHE	8.9	12.2	12.7	11.3	12.2	13.2
OLE1	18.9	13.7	13.2	10.5	8.1	8.1
OLE2	21.0	7.6	6.4	5.0	3.2	3.1
OLE3	12.0	10.8	11.1	10.1	6.1	5.4
Total New Radical Production (ppb)	9.0	41.6	61.3	93.9	137	142

Table 4. Percentage of nitric acid production attributable to each organic.

	VOC/NO_x (ppbC/ppb)		
	4	8.2	20
CO	3.6	4.1	3.4
CH4	0.4	0.5	0.4
aldehydes & ketones			
HCHO	1.1	0.6	0.8
CCHO	1.2	1.2	0.8
RCHO	0.4	0.4	0.3
MEK	0.6	0.7	0.4
alkanes			
ALK1	8.1	14.0	9.2
ALK2	6.7	11.8	8.7
aromatics			
ARO1	14.7	14.7	23.7
ARO2	26.8	16.3	22.9
alkenes			
ETHE	9.2	10.2	8.2
OLE1	11.0	11.0	9.1
OLE2	5.9	5.6	4.5
OLE3	10.3	8.8	7.6
Total HNO_3 (ppb)	80.1	88.3	27.7

Table 5. Percentage of PAN production attributable to each organic.

	VOC/NOx (ppbC/ppb)		
	4	8.2	20
aldehydes & ketones			
CCHO	3.2	2.6	2.3
RCHO	0.6	0.5	0.5
MEK	1.4	1.4	1.4
alkanes			
ALK1	9.3	18.6	19.1
ALK2	8.2	13.5	15.6
aromatics			
ARO1	9.9	9.4	9.4
ARO2	29.3	15.2	14.4
alkenes			
ETHE	4.0	6.8	6.0
OLE1	14.4	14.9	14.0
OLE2	10.5	8.9	8.4
OLE3	9.2	8.3	8.9
Total PAN (ppb)	2.1	23.7	12.6

LIST OF FIGURES

Figure 11. PAN productivities at high, low, and base case VOC/NO_x conditions.

Figure 1.

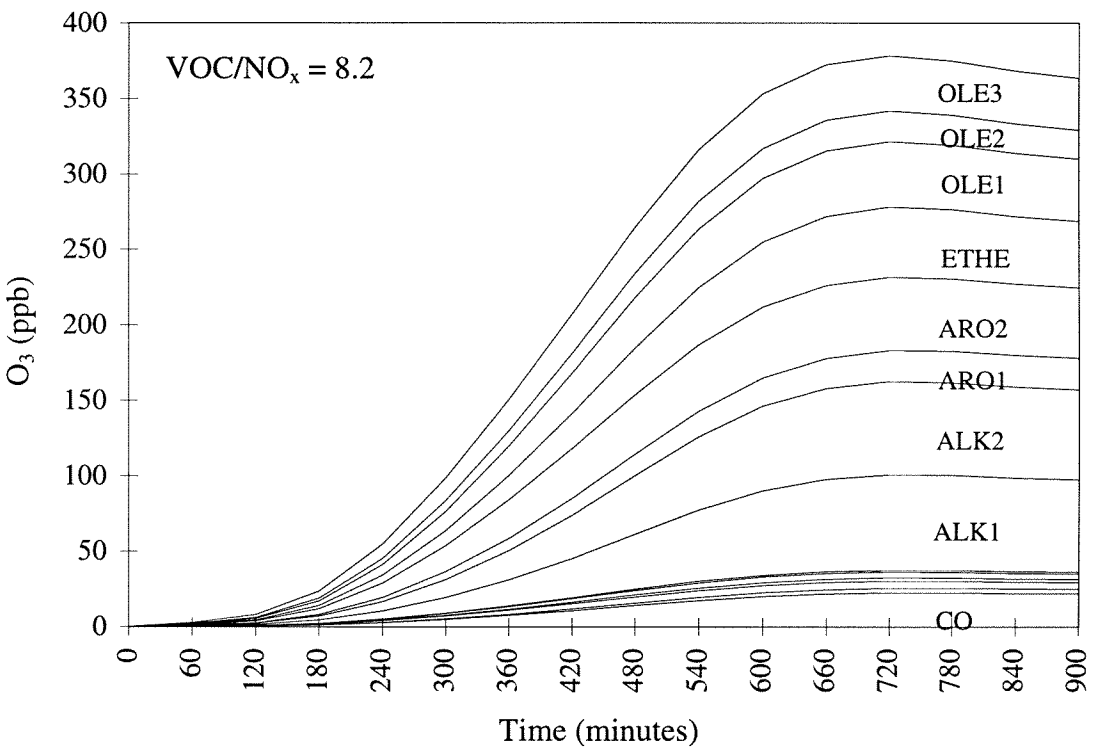
VOC/NOx = 8.2
OLE3
OLE2
OLE1
ETHE
ARO2
ARO1
ALK2
ALK1
CO
O3 (ppb)
Time (minutes)
0
50
100
150
200
250
300
350
400
0
60
120
180
240
300
360
420
480
540
600
660
720
780
840
900

Figure 2.

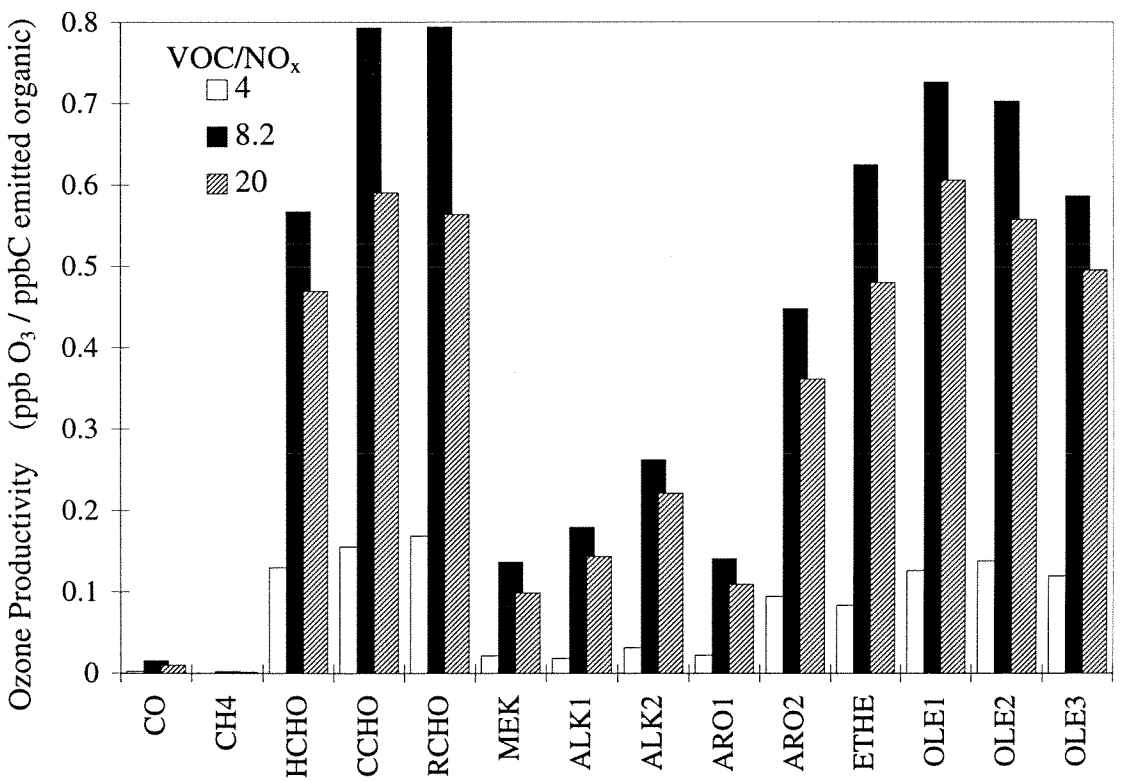
Ozone Productivity (ppb O_3 / ppbC emitted organic)
0.8
0.7
0.6
0.5
0.4
0.3
0.2
0.1
0
VOC/NO_x
4
8.2
20
CO
CH4
HCHO
CCHO
RCHO
MEK
ALK1
ALK2
ARO1
ARO2
ETHE
OLE1
OLE2
OLE3

Figure 3.

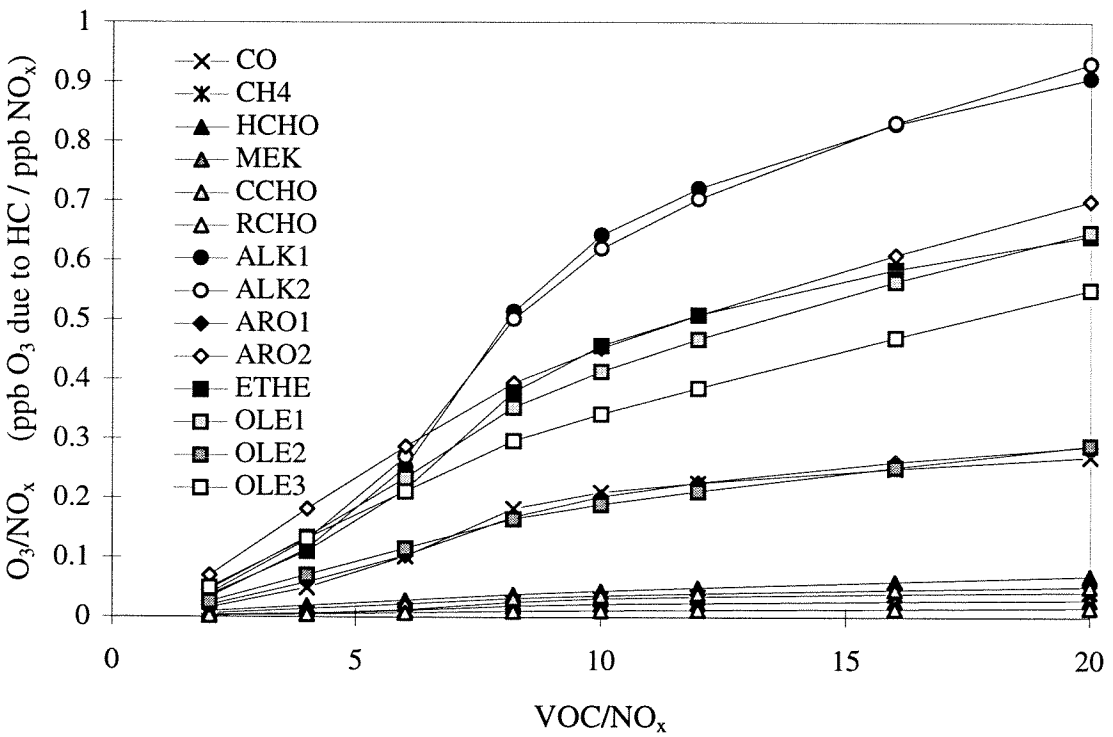
1
0.9
0.8
0.7
0.6
0.5
0.4
0.3
0.2
0.1
0
0
5
10
15
20
O3/NOx (ppb O3 due to HC / ppb NOx)
VOC/NOx
CO
CH4
HCHO
MEK
CCHO
RCHO
ALK1
ALK2
ARO1
ARO2
ETHE
OLE1
OLE2
OLE3

Figure 4.

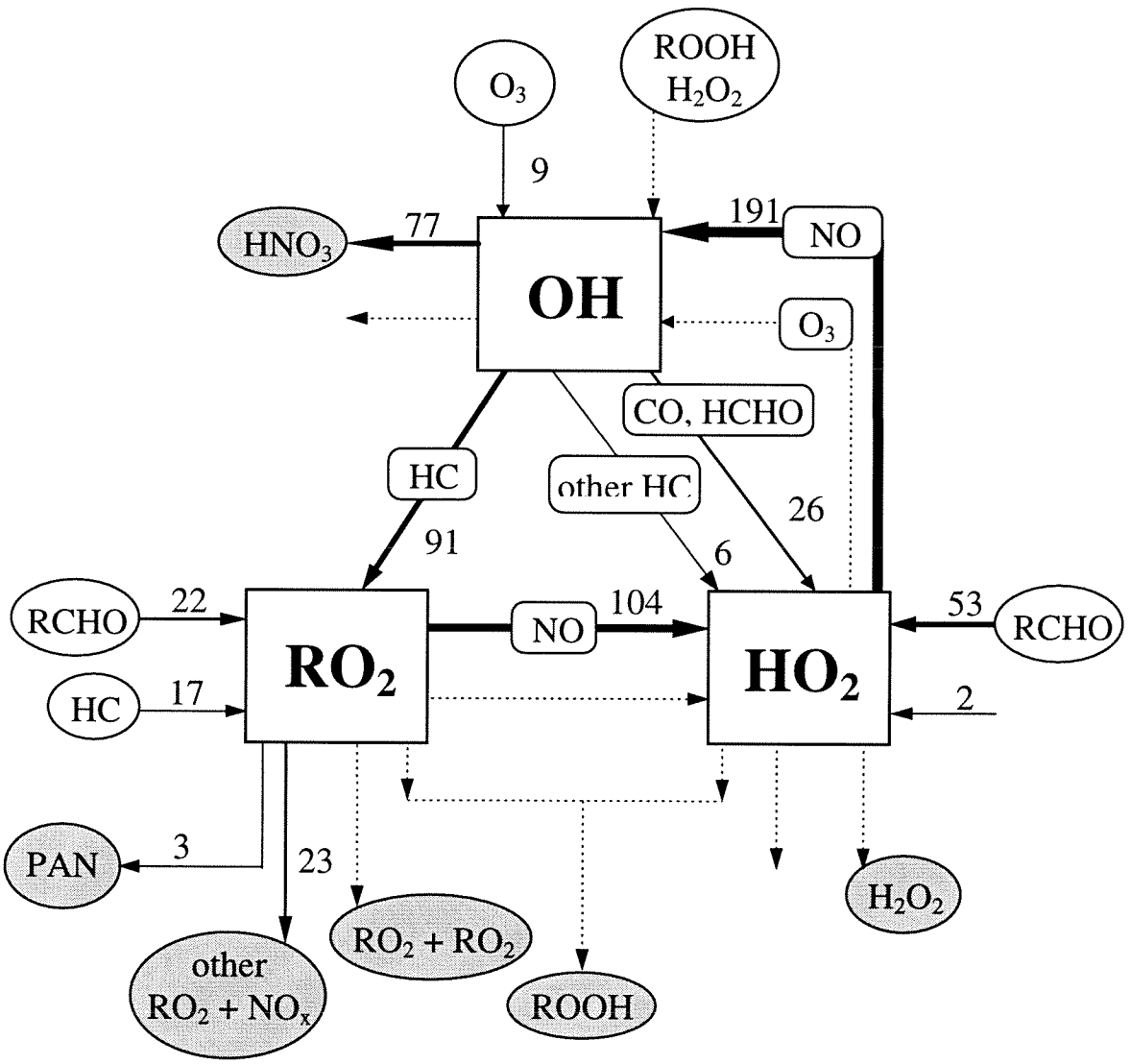
O3
ROOH
H2O2
9
HNO3
77
191
NO
OH
O3
CO, HCHO
HC
other HC
26
91
6
RCHO
22
RO2
NO
104
HO2
53
RCHO
HC
17
2
PAN
3
23
H2O2
RO2 + RO2
other
RO2 + NOx
ROOH

Figure 5.

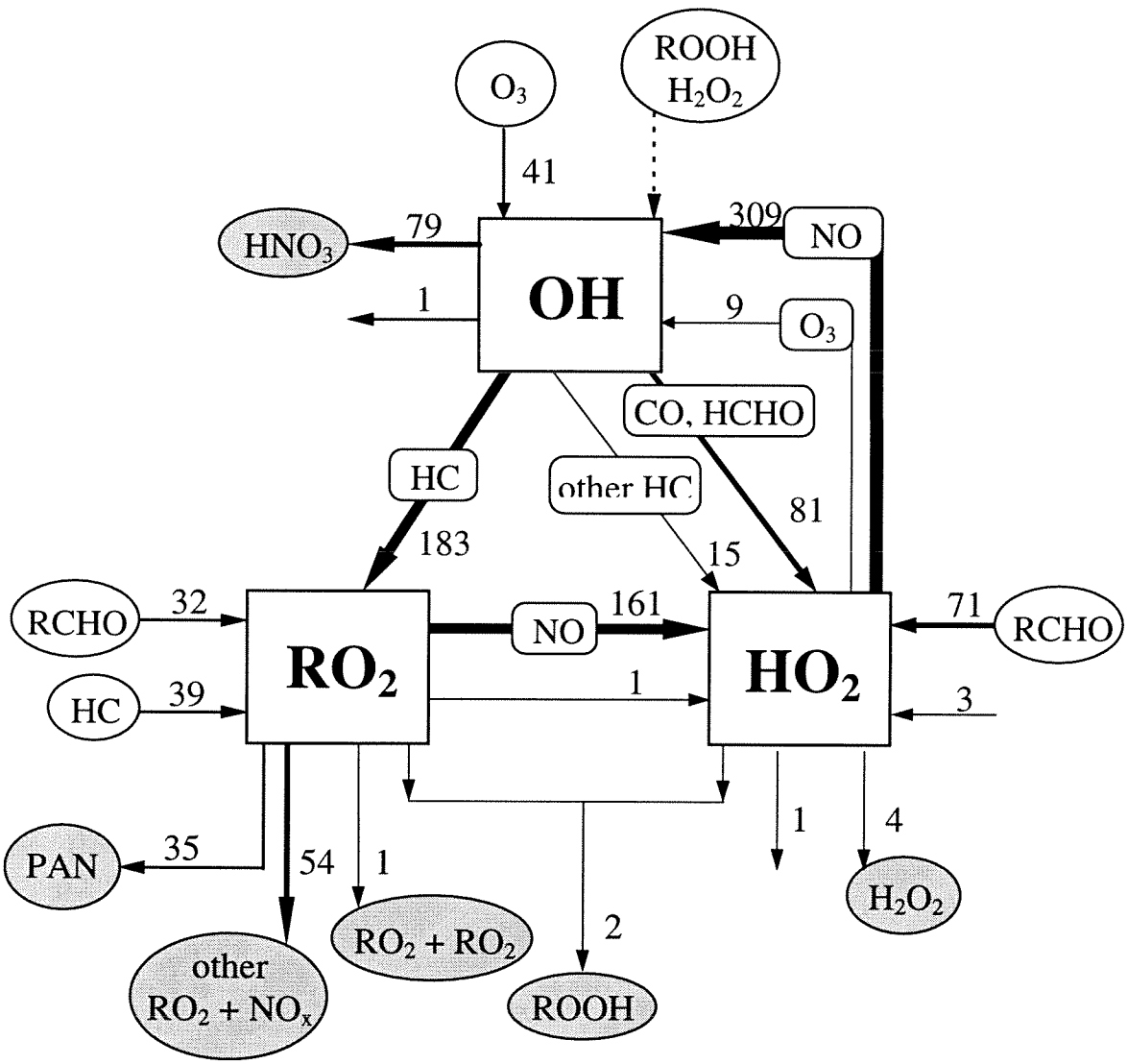
O3
ROOH
H2O2
41
HNO3
79
309
NO
OH
1
9
O3
CO, HCHO
HC
other HC
81
183
15
RCHO
32
RO2
NO
161
HO2
71
RCHO
HC
39
1
3
PAN
35
54
1
1
4
H2O2
other
RO2 + NOx
RO2 + RO2
2
ROOH

Figure 6.

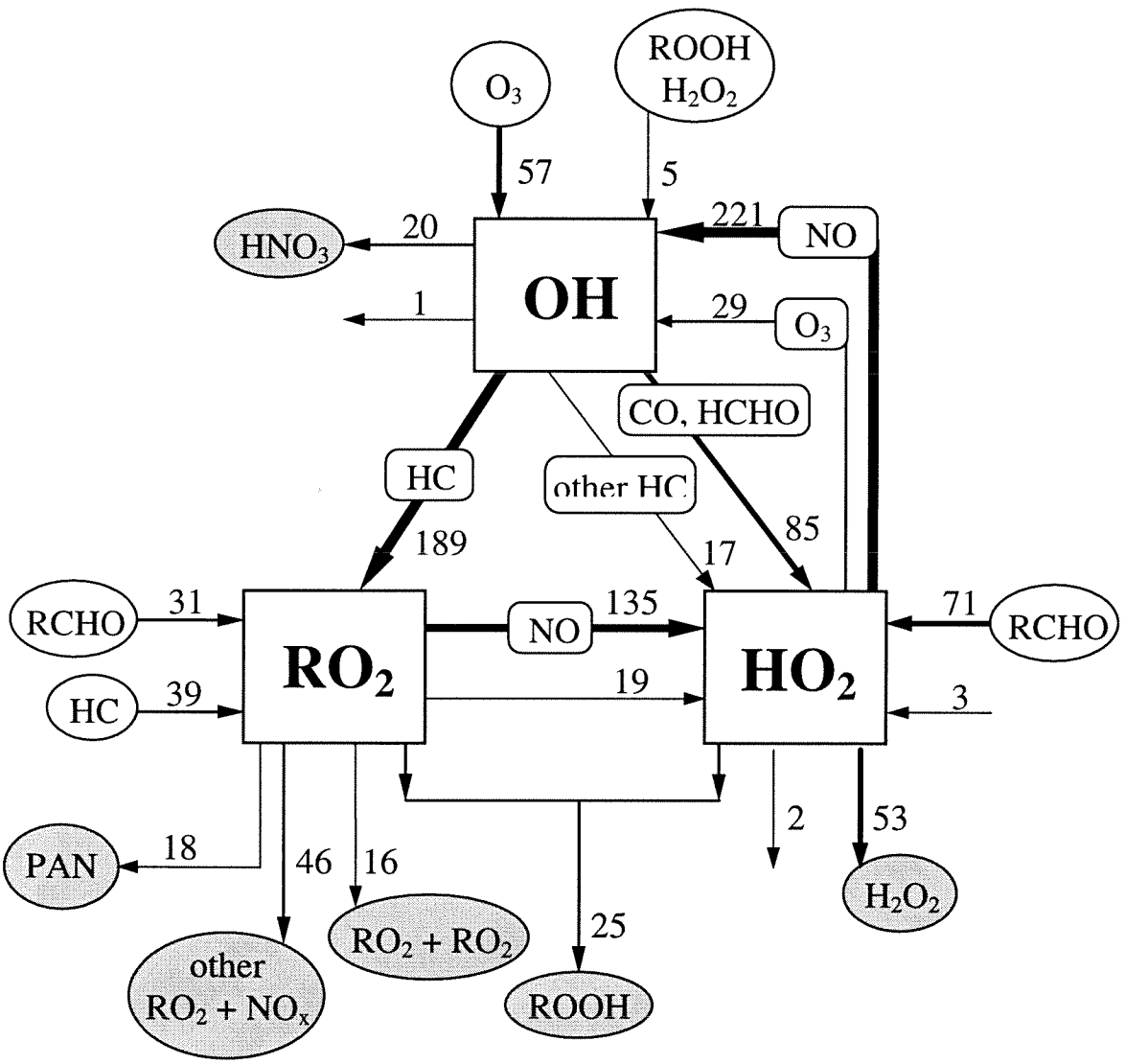
O3
ROOH
H2O2
57
5
HNO3
20
221
NO
OH
1
29
O3
CO, HCHO
HC
other HC
189
17
85
RCHO
31
RO2
NO
135
HO2
71
RCHO
HC
39
19
3
PAN
18
46
16
2
53
H2O2
RO2 + RO2
25
other
RO2 + NOx
ROOH

Figure 7.

(a)

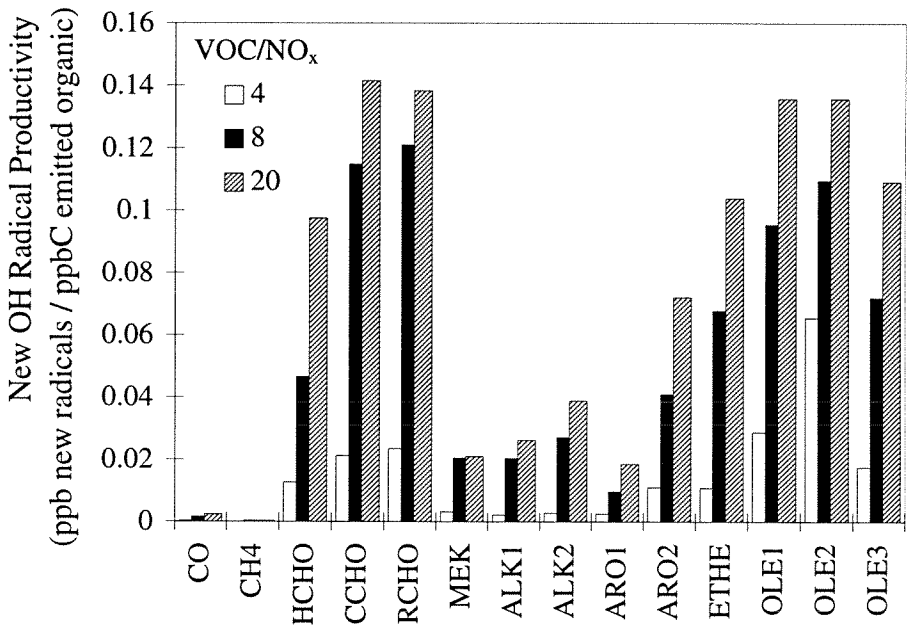
New OH Radical Productivity
(ppb new radicals / ppbC emitted organic)
0.16
0.14
0.12
0.1
0.08
0.06
0.04
0.02
0
VOC/NOx
4
8
20
CO
CH4
HCHO
CCHO
RCHO
MEK
ALK1
ALK2
ARO1
ARO2
ETHE
OLE1
OLE2
OLE3

(b)

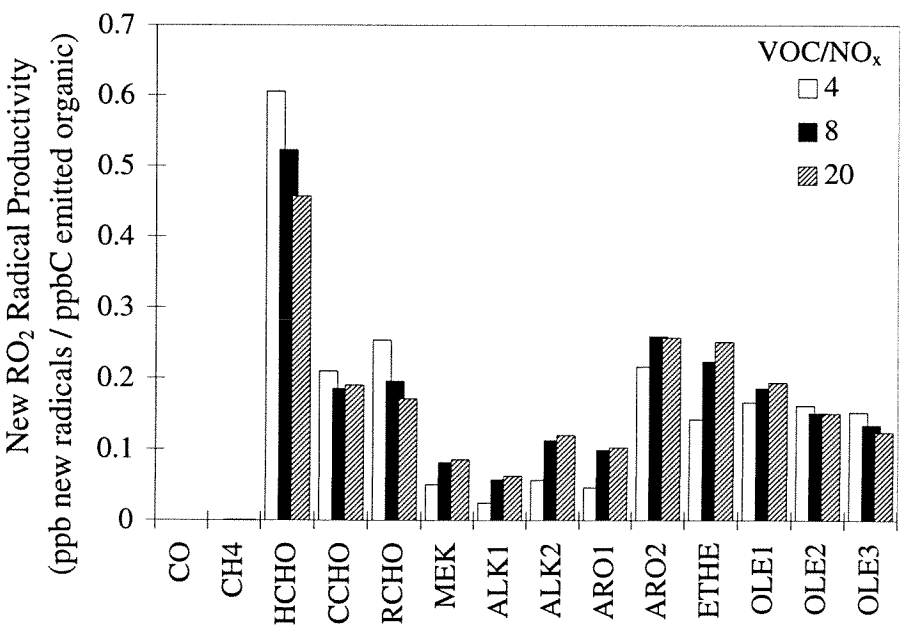
New RO2 Radical Productivity
(ppb new radicals / ppbC emitted organic)
0.7
0.6
0.5
0.4
0.3
0.2
0.1
0
VOC/NOx
4
8
20
CO
CH4
HCHO
CCHO
RCHO
MEK
ALK1
ALK2
ARO1
ARO2
ETHE
OLE1
OLE2
OLE3

Figure 8.

(a)

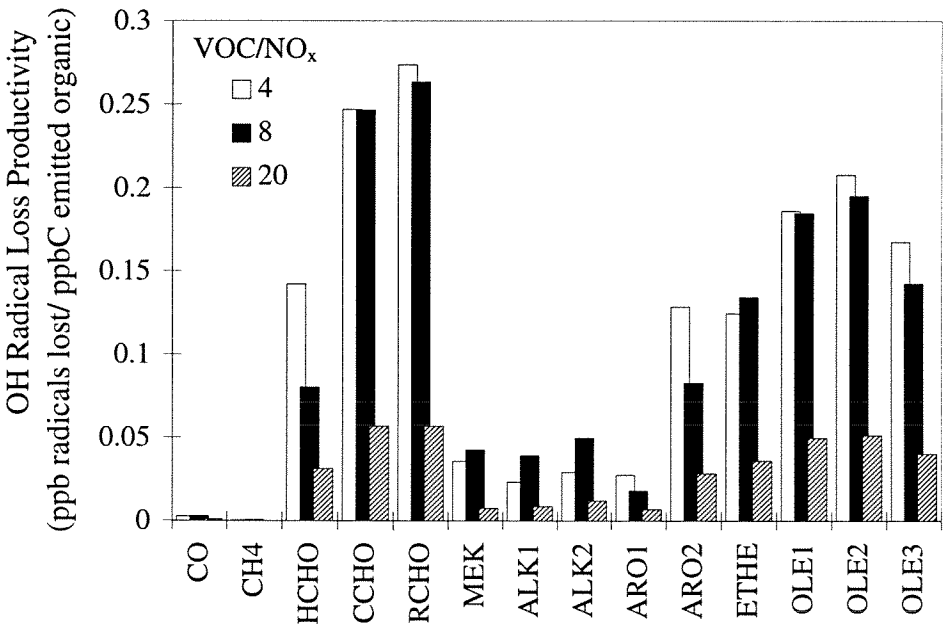
OH Radical Loss Productivity
(ppb radicals lost/ ppbC emitted organic)
VOC/NOx
4
8
20
0.3
0.25
0.2
0.15
0.1
0.05
0
CO
CH4
HCHO
CCHO
RCHO
MEK
ALK1
ALK2
ARO1
ARO2
ETHE
OLE1
OLE2
OLE3

(b)

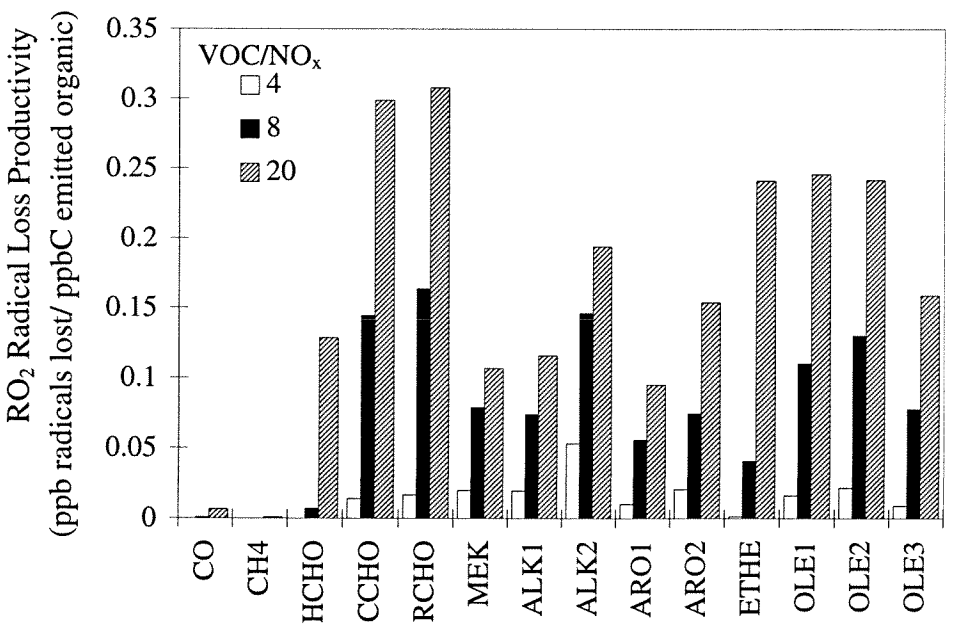
RO2 Radical Loss Productivity
(ppb radicals lost/ ppbC emitted organic)
VOC/NOx
4
8
20
0.35
0.3
0.25
0.2
0.15
0.1
0.05
0
CO
CH4
HCHO
CCHO
RCHO
MEK
ALK1
ALK2
ARO1
ARO2
ETHE
OLE1
OLE2
OLE3

Figure 9.

(a)

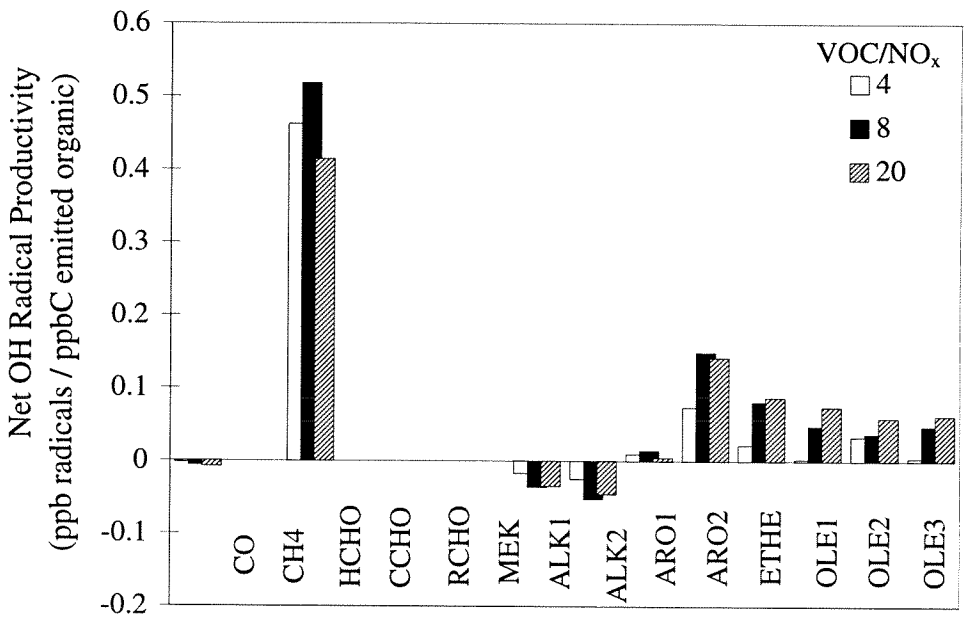
Net OH Radical Productivity
(ppb radicals / ppbC emitted organic)
0.6
0.5
0.4
0.3
0.2
0.1
0
-0.1
-0.2
VOC/NOx
4
8
20
CO
CH4
HCHO
CCHO
RCHO
MEK
ALK1
ALK2
ARO1
ARO2
ETHE
OLE1
OLE2
OLE3

(b)

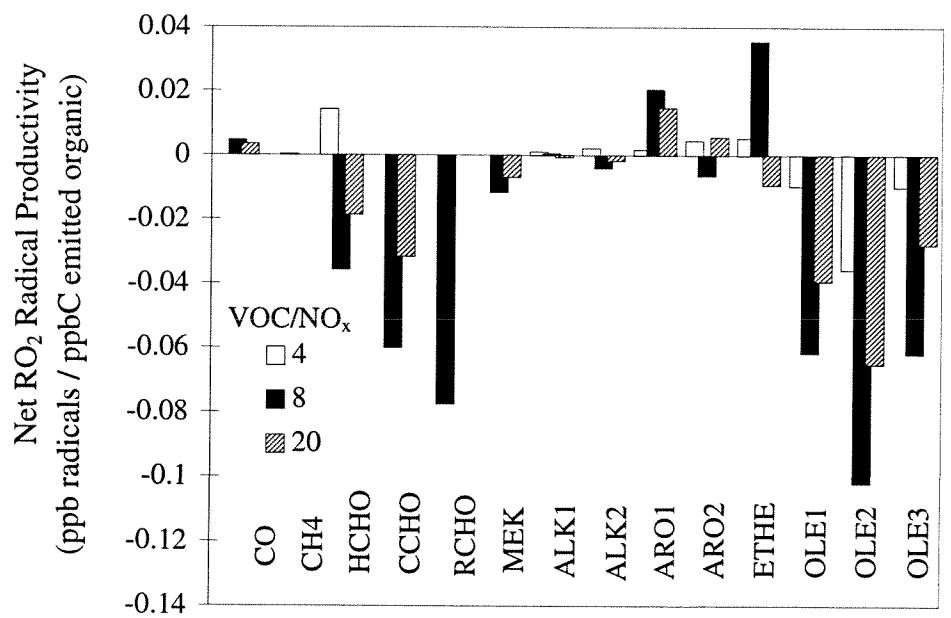
Net RO2 Radical Productivity
(ppb radicals / ppbC emitted organic)
0.04
0.02
0
-0.02
-0.04
-0.06
-0.08
-0.1
-0.12
-0.14
VOC/NOx
4
8
20
CO
CH4
HCHO
CCHO
RCHO
MEK
ALK1
ALK2
ARO1
ARO2
ETHE
OLE1
OLE2
OLE3

Figure 10.

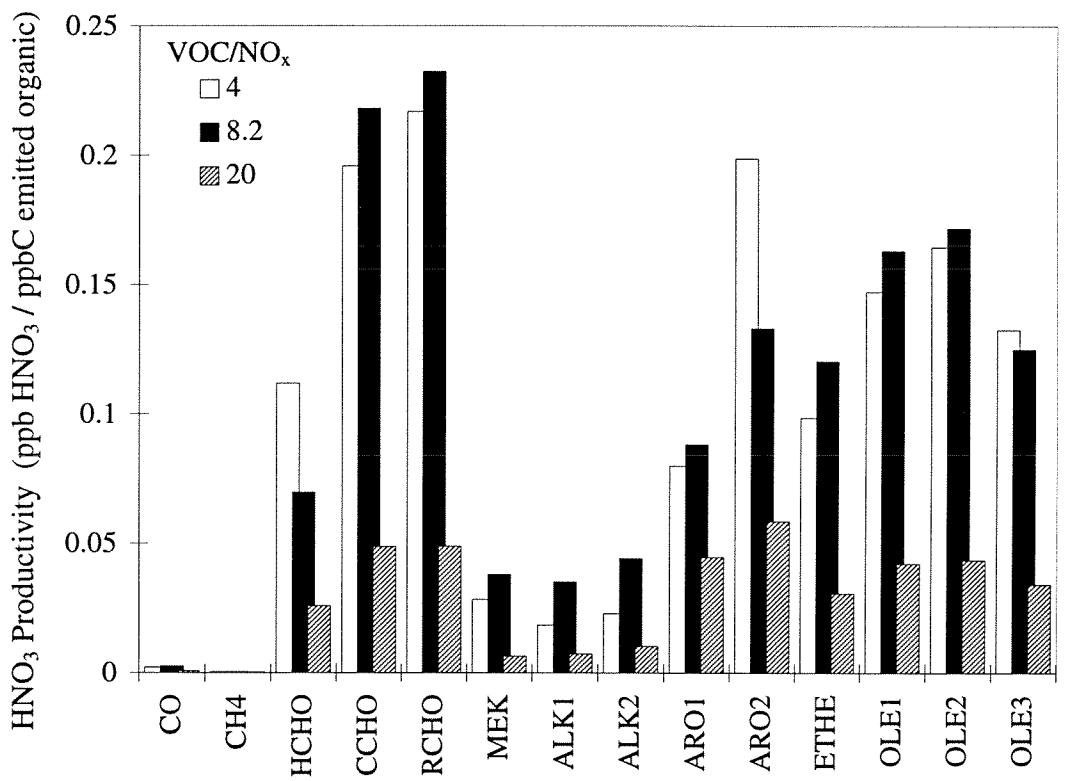
HNO3 Productivity (ppb HNO3 / ppbC emitted organic)
0.25
0.2
0.15
0.1
0.05
0
VOC/NOx
4
8.2
20
CO
CH4
HCHO
CCHO
RCHO
MEK
ALK1
ALK2
ARO1
ARO2
ETHE
OLE1
OLE2
OLE3

Figure 11.

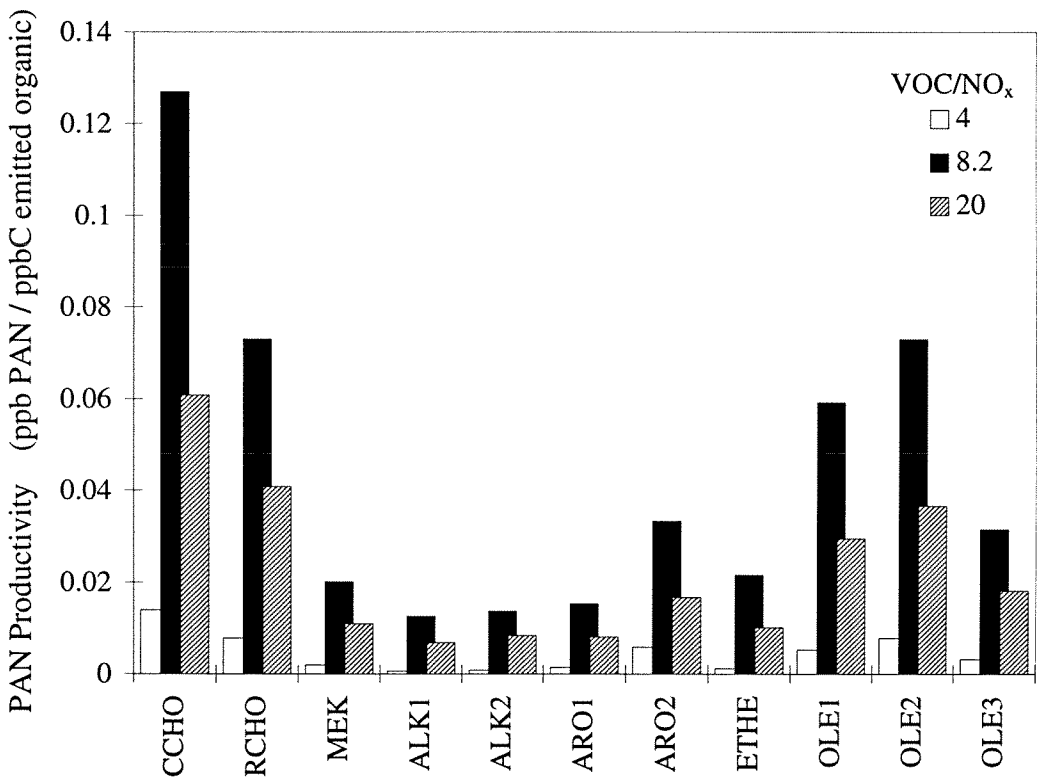
PAN Productivity (ppb PAN / ppbC emitted organic)
0.14
0.12
0.1
0.08
0.06
0.04
0.02
0
VOC/NOx
4
8.2
20
CCHO
RCHO
MEK
ALK1
ALK2
ARO1
ARO2
ETHE
OLE1
OLE2
OLE3

CHAPTER 3:

FUNDAMENTAL BASIS OF INCREMENTAL REACTIVITIES OF ORGANICS IN OZONE FORMATION IN VOC/NO_X MIXTURES

Published in *Atmos. Environ.*, **28**, 3359-3368 (1994).

ABSTRACT

The incremental reactivity of a particular organic species refers to the change in the ozone generated upon addition of a small amount of the organic to a complex organic/NO_x mixture undergoing photooxidation. It is known that the values of the incremental reactivities of organic species depend on the composition of the particular organic/NO_x mixture, the hydrocarbon-to-NO_x ratio, and other environmental conditions. Using a method that enables the assignment of the ozone produced in the photooxidation of a complex organic/NO_x mixture to each of the individual organics present, we show how the incremental ozone reactivity of any one organic species results from changes in the ozone generated by each of the organics present. Thus, we demonstrate explicitly the dependence of the incremental reactivity of each organic present on the nature of the organic/NO_x mixture. Calculations are presented using the SAPRC 90 chemical mechanism to explain the origin of the variation of incremental reactivities with initial hydrocarbon-to NO_x ratio.

INTRODUCTION

It has been recognized for some time that VOCs differ in their ozone-forming capability (Seinfeld, 1986; Carter and Atkinson, 1987, 1989; Chang and Rudy, 1990; Anderson-Sköld *et al.*, 1992; McNair *et al.*, 1992; Derwent and Jenkin, 1991). Smog chamber experiments carried out with a series of single hydrocarbons irradiated in the presence of NO_x provide a measure of the relative amount of ozone formed by individual hydrocarbons (Carter and Atkinson, 1987). Hydrocarbons do not occur singly in the atmosphere, however, and the ozone-forming potential of an individual VOC will depend on the characteristics of the complex mixture of which it is a part, including the NO_x level and the other VOCs that are present (Carter, 1991). It has long been of interest to be able to determine, for any given VOC/NO_x mixture, the contribution of each individual organic species to the total amount of ozone generated in that mixture. That determination has important implications to the relative control of different hydrocarbons in ozone abatement.

One method that is now being used to evaluate the ozone-forming potential of individual VOCs is the incremental reactivity approach (Carter and Atkinson, 1989; Carter, 1991). In this approach, a small amount of an individual organic is added to a base case mixture, either in a smog chamber or in a chemical mechanism, and the change in peak ozone levels due to the additional or incremented organic is simulated. Incremental reactivity (IR) for an organic species *i* is defined as

$$IR_i = \frac{\Delta_i R}{\Delta[VOC_i]} \quad (1)$$

where R is the maximum change of the quantity ([O_3] - [NO]) from its initial value at the beginning of the simulation, $\Delta[VOC_i]$ is the incremental change in concentration, on a carbon basis, of organic species i, and the Δ_i operator represents the change from a base case scenario as a result of an incremental change in species i. The quantity ([O_3] - [NO]) is used to define the ozone-forming potential of the mixture because it more effectively represents the chemical processes leading to ozone formation than ozone concentration alone. When NO is present in excess, any ozone formed will react with NO causing the NO concentration to decrease instead of increasing the O_3 concentration. Analysis of ozone formation should therefore include changes in NO as well as O_3 as represented in the measure ([O_3] - [NO]). Incremental reactivities are intended to be calculated for the limit as $\Delta[VOC_i]$ approaches zero; in practice $\Delta[VOC_i]$ is chosen such that the amount of O_3 formed is within 5% of the amount formed for the base case. While incremental reactivity has even been used as a regulatory tool (Croes *et al.*, 1992), there remains some uncertainty as to exactly what an incremental reactivity value represents and how it can most appropriately be interpreted.

In this paper we examine the fundamental concept of incremental reactivity, explaining how ozone formation changes when an organic compound is added incrementally to a VOC/NO_x mixture. To accomplish this we use incremental reactivity

calculations together with a method that allows one to determine the contributions to ozone formation of individual organics in a VOC/NO_x system.

RELATION OF INCREMENTAL REACTIVITY AND OZONE PRODUCTIVITY

The ozone assignment method is a technique whereby the amount of ozone generated by individual organics in a complex VOC/NO_x mixture is calculated. Full details of this method are presented elsewhere (Bowman and Seinfeld, 1994) and only a brief summary will be given here. In addition, Jeffries and co-workers (Jeffries and Crouse, 1990; Jeffries, 1993) have employed a similar approach to this problem. Ozone assignment follows the reaction pathways of a mechanism and traces the ozone, or other product species, formed back to the original organic precursors. In this way, the total amount of ozone produced in a given scenario attributable to organic species j, designated $[O_3]_j$, may be determined. The change in NO concentration can similarly be assigned to individual organic species and is used to determine contributions to the change in ($[O_3]$-[NO]), or R, such that

$$R_j = \left([O_3]_j - [NO]_j\right)_{peak} - \left([O_3]_j - [NO]_j\right)_{t=0} \qquad (2)$$

where R_j is the change in the quantity ([O_3]-[NO]) attributable to organic species j, and the $[O_3]_j$ and $[NO]_j$ terms are the amount of ozone and NO that are attributable to organic species j initially and at the time of peak ozone concentration.

Using the results of ozone assignment analysis, a measure of the relative ozone-forming potential of each organic, termed its productivity, P_j, can be calculated by normalizing the ([O_3]-[NO]) produced from an organic in a particular situation by the amount of that organic, both initially present and emitted,

$$P_j = \frac{R_j}{[\mathrm{VOC}_j]} = \frac{\text{ppb } (O_3 - \text{NO}) \text{ produced due to VOC}_j}{\text{ppbC VOC}_j \text{ initially present} + \text{ppbC VOC}_j \text{ emitted}} \quad (3)$$

Therefore, ozone assignment and productivity deal with the apportionment of the total amount of ozone produced in a given scenario among each of the organics in a VOC mixture. Also note that a species like formaldehyde which is both emitted and formed photochemically from the oxidation of other organics can be treated by the ozone assignment method.

As noted earlier, the incremental reactivity of species i is the change in the quantity R, due to an additional amount of species i, divided by the incremented amount of species i. Since the sum of individual contributions to the quantity R equals the total observed value of R, the change in R may be represented as the sum of changes in the individual species contributions,

$$\Delta_i R = \sum_j \Delta_i R_j \qquad (4)$$

where $\Delta_i R_j$ denotes the change in the quantity R attributable to organic species j when organic species i is incremented. Using the definition of productivity, equation (3), R_j, the amount of the quantity ([O_3]-[NO]) attributable to organic species j, may be expressed as the product of a productivity coefficient P_j and the organic concentration [VOC_j],

$$R_j = P_j[\mathrm{VOC}_j] \qquad (5)$$

The productivity coefficient, P_j, is the amount of the quantity R attributable to VOC_j that will be produced per carbon atom of VOC_j emitted or initially present. The productivity coefficient may be further separated into kinetic and mechanistic factors, P_j^k and P_j^m, respectively,

$$R_j = P_j^k P_j^m[\mathrm{VOC}_j] \qquad (6)$$

where the kinetic productivity, P_j^k, is the fraction of emitted or initially present species j that reacts during the scenario, and the mechanistic productivity, P_j^m, is the amount of the quantity R attributable to species j per carbon atom of species j reacting. By expressing productivity as the product of kinetic and mechanistic factors, the effect of reaction rates can be separated from the influence of an organic's photooxidation mechanism.

Using equation (6), the change in R_j due to addition of species i may be written as

$$\Delta_i R_j = \Delta_i\{P_j^k P_j^m [\mathrm{VOC}_j]\} \quad (7)$$

which can be expanded to the first order to the following form,

$$\begin{aligned}\Delta_i R_j &= \Delta_i\{P_j^k P_j^m [\mathrm{VOC}_j]\} \\ &= P_j^k P_j^m \Delta_i\{[\mathrm{VOC}_j]\} + P_j^m [\mathrm{VOC}_j]\Delta_i\{P_j^k\} + P_j^k [\mathrm{VOC}_j]\Delta_i\{P_j^m\}\end{aligned} \quad (8)$$

where P_j^k, P_j^m, and $[\mathrm{VOC}_j]$ represent base case values for organic species j and $\Delta_i P_j^k$, $\Delta_i P_j^m$, and $\Delta_i[\mathrm{VOC}_j]$ represent changes in the kinetic productivity, mechanistic productivity, and concentration of organic species j upon adding organic i to the base case. The change in ozone production attributable to organic j upon adding an increment of organic i, $\Delta_i R_j$, may then be viewed as the sum of three terms representing changes in organic concentration, kinetic productivity, and mechanistic productivity.

For all non-incremented species, that is when $j \neq i$, $[\mathrm{VOC}_j]$ is constant and the $\Delta_i[\mathrm{VOC}_j]$ term will be zero. Only the incremented species concentration, $[\mathrm{VOC}_i]$, is changed, making the $\Delta_i[\mathrm{VOC}_j]$ term non-zero only when $j = i$. The $\Delta_i[\mathrm{VOC}_j]$ term represents the effect adding organic i would have if the mixture chemistry remained unchanged by the addition of an increment of species i. That is, the same fraction of all species would react, producing the same amount of ozone per reacting organic, only more of the incremented species, VOC_i, would be available, thus causing an increase in ozone. The $\Delta_i P_j^k$ term represents the change in ozone production that results due to greater or lesser fractions of the available organic species j reacting, while the $\Delta_i P_j^m$ term accounts

for changes in ozone production due to more or less efficient reaction mechanism pathways. Thus, the total change in R upon adding an increment of organic species i can be represented in the following form,

$$\begin{aligned} \Delta_i R_j &= \sum_j \Delta_i R_j \\ &= P_i^k P_i^m \Delta[\mathrm{VOC}_i] + \sum_j P_j^m [\mathrm{VOC}_j] \Delta_i \{P_j^k\} + \sum_j P_j^k [\mathrm{VOC}_j] \Delta_i \{P_j^m\} \end{aligned} \quad (9)$$

Carter and Atkinson have stated that the incremental reactivity of a mixture can be calculated from the sum of the incremental reactivities of its components, weighted by the relative amount of each component present (Carter and Atkinson, 1989).

$$\mathrm{IR}_{\mathrm{mix}} = \sum_i \mathrm{IR}_i \, x_i \quad (10)$$

This property of additivity is based upon the mathematical rules governing partial derivatives which define the total change in the quantity R as,

$$dR = \sum_i \left(\frac{\partial R}{\partial [\mathrm{VOC}_i]} \right) d[\mathrm{VOC}_i] \quad (11)$$

For the addition of an increment of the entire organic mixture, the change in each individual organic concentration will be proportional to its mole fraction in the mixture,

$$d[\mathrm{VOC}_i] = x_i \, d[\mathrm{VOC}_{\mathrm{mix}}] \quad (12)$$

where $d[VOC_{mix}]$ is the overall change in concentration of the organic mixture. Equation (12) can be substituted into (11) and rearranged to yield an expression identical to (10)

$$\frac{dR}{d[VOC_{mix}]} = \sum_i \left(\frac{\partial R}{\partial [VOC_i]} \right) x_i \qquad (13)$$

This derivation is mathematically exact for the limit as $d[VOC_{mix}]$ goes to zero, and should remain valid as long as the changes in organic concentration are sufficiently small. We will show that this is, in fact, the case, and that the incremental reactivity of a mixture can be accurately determined from the incremental reactivities of the individual components.

CHEMICAL MECHANISM AND BASE CASE SCENARIO

The incremental reactivity calculations on which we will focus have been carried out using the condensed SAPRC 90 chemical mechanism (Carter and Lurmann, 1990). The mechanism contains, as organic species, methane, two lumped higher alkanes, termed ALK1 and ALK2, two lumped aromatics, termed ARO1 and ARO2, ethene, three lumped higher alkenes, designated OLE1, OLE2, and OLE3, and four carbonyls, HCHO, CCHO, RCHO, and MEK. The lumped species in the mechanism represent a composite of the individual species present in the organic mixture, with species assigned to the

lumped groups based on their OH radical rate constants. The species ALK1 represents alkanes with $k_{OH} < 10^4$ ppm^{-1} min^{-1}, and contains approximately 4 carbons per molecule. Alkanes with $k_{OH} \geq 10^4$ ppm^{-1} min^{-1} are assigned to ALK2 and contain on average 8 carbons per molecule. The lumped aromatic species ARO1 represents all aromatics with $k_{OH} < 2x10^4$ ppm^{-1} min^{-1} and is composed mostly of toluene. ARO2 represents the aromatics with $k_{OH} \geq 2x10^4$ ppm^{-1} min^{-1} and contains mostly xylene. Alkenes with $k_{OH} < 7.5x10^4$ ppm^{-1} min^{-1} are assigned to OLE1 which are, in general, terminal olefins with 4 carbons per molecule. OLE2 represents the alkenes with $k_{OH} \geq 7.5x10^4$ ppm^{-1} min^{-1} which are mostly internal olefins of approximately 5 carbons. Biogenic alkenes and isoprene are used to form the lumped group OLE3 which has on average 7 carbons per molecule. The carbonyls are modeled after formaldehyde (HCHO), acetaldehyde (CCHO), propionaldehyde (RCHO), and methyl ethyl ketone (MEK).

A photochemical box model, from the Carter mechanism preparation program (Carter, 1988), was used to implement the mechanism for simulations designed to represent summertime conditions in Los Angeles. All reactants were present initially, with no additional emissions or dilution occurring over the course of the simulation. Organic reactant concentrations were determined using the August 27, 1987, California Air Resources Board inventory for the South Coast Air Basin of California (ARB, 1987), from which concentrations for all VOCs except CO were obtained, together with the EPA EKMA scenario for Los Angeles (EPA, 1988), which contains CO levels. The EKMA scenario was also used to select a representative base case VOC/NO_x ratio of 8.2. The

initial reaction mixture contained 1230 ppbC of NMHC, 1700 CH_4, 1500 ppb CO, 120 ppb NO, and 30 ppb NO_2. (See Table 1.) Kinetic parameters for the lumped species in the SAPRC 90 mechanism were calculated from the Carter emissions processing program (Carter, 1988) using the initial organic reactant concentrations. Chemical reactions occurred under the influence of time-varying solar irradiation, corresponding to June 21, and were followed for 15 hours, from 6 am to 9 pm. Calculations were performed at the base case VOC/NO_x ratio of 8.2 as well as VOC/NO_x ratios of 4 and 20, representing high and low NO_x conditions.

The base case scenarios used here differ from Carter's incremental reactivity scenarios (Carter, 1991) in that we used a simple chamber model simulation instead of a more complex trajectory model involving continuous emissions and atmospheric dilution. While these differences do not allow direct comparison of our results with Carter's incremental reactivity values, the scenarios are sufficiently similar that our results should agree qualitatively with the incremental reactivities reported by Carter.

INCREMENTAL REACTIVITY AND PRODUCTIVITY CALCULATIONS

Incremental reactivity calculations were performed for each of the 14 SAPRC mechanism species as well as for the bulk mixture at VOC/NO_x ratios of 4, 8.2, and 20 ppbC/ppb. These values were selected to examine a wide range of VOC/NO_x ratios. For

each VOC/NO_x ratio a base case scenario was run, followed by simulations in which the initial concentration of each mechanism species was individually increased so as to produce a change in ($[O_3]$-[NO]) of less than 5%. For these small changes in *R* we found that incremental reactivities were independent of the amount of organic added, indicating that the change in organic can indeed be viewed as incrementally small. The incremental reactivities calculated in this manner and peak ozone levels for each VOC/NO_x condition are given in Table 2. Incremental reactivities vary with the VOC/NO_x ratio. At VOC/NO_x ratios of 4 and 8.2, the incremental reactivities were highest and decreased considerably at VOC/NO_x = 20. Formaldehyde yielded the highest incremental reactivity at all three VOC/NO_x ratios, followed by the higher aldehydes, CCHO and RCHO, while CO and methane exhibited the smallest incremental reactivities. The aromatics, ARO1 and ARO2, produced negative incremental reactivities for the high VOC/NO_x case.

Incremental reactivities depend on the scenario used for calculation, so a direct comparison of incremental reactivities calculated here with those determined for a different scenario is best done in a qualitative sense. The general trends exhibited in Table 2 do agree qualitatively with literature results calculated using different base case scenarios (Carter and Atkinson, 1987; Carter and Atkinson, 1989), with formaldehyde having the highest incremental reactivity, followed by the higher aldehydes and alkenes, the aromatics exhibiting negative incremental reactivity at high VOC/NO_x, and incremental reactivity dropping off at high VOC/NO_x.

Also given in Table 2 are the incremental reactivities for the overall VOC mixture, calculated directly by adding an increment of the entire mixture to the base case, and indirectly from the weighted sum of the individual components as suggested by Carter and Atkinson (1989). As expected, the incremental reactivity calculated by the indirect method is essentially the same as that determined directly for all three VOC/NO_x ratios. The contributions of individual organics to the incremental reactivities of each organic species and of the mixture as a whole are given in Table 3. Because of the varying magnitude of incremental reactivities among organics, the values in Table 3 are presented as a percentage of the total change in the quantity *R*. In the case of CO at VOC/NO_x=4, for example, the incremented species, CO, is responsible for 164% of the change in *R*, while the remaining organic species in the mixture contribute negatively or not at all. For this example, the 164% means that CO causes an additional amount of ozone to be formed that is partially offset by lower amounts of ozone production from the other mixture species, such that the sum of all species contributions is 100%. For example, the change in ozone production attributable to ALK1 accounts for -9% of the change in *R*, meaning that when CO is added, ALK1 produces less ozone than it did in the base case. Note that at VOC/NO_x=20, where the aromatics (ARO1 and ARO2) have negative incremental reactivities, the positive contribution from the incremented species is entirely offset by decreases in ozone production from the non-incremented species.

Incremental reactivities are also compared by separating the effects of organic concentration, and kinetic and mechanistic factors in Table 4. The contribution of each

term in equation (9) is listed as a percentage of the total incremental reactivity. By definition, the Δ_i[VOC] term, representing the change in ozone production due solely to the presence of additional organic but not to changes in mixture chemistry, is positive indicating that more ozone is formed since additional organic is present. The $\Delta_i P^k$ term is positive when additional ozone is formed due to an increased fraction of available organics reacting, and negative when less ozone is formed as a result of a decrease in the fraction of organics reacting. The $\Delta_i P^m$ term can likewise be positive or negative with positive values indicating additional ozone due to more efficient chemistry, and negative values indicating less ozone due to less efficient chemistry.

ANALYSIS OF CONTRIBUTIONS TO INCREMENTAL REACTIVITY

The results concerning individual VOC contributions found in Table 3 are closely related to the kinetic, mechanistic, and concentration contributions listed in Table 4. As seen from Table 3, the incremented organic generally accounts for only a fraction of the total ozone change, particularly at the high VOC/NO_x ratio. That fraction attributable to the incremented organic (the values found along the diagonals of Table 3) is composed almost entirely of the ozone produced by the additional organic as listed in the Δ_i[VOC] column of Table 4. The remaining portion of the Table 3 diagonal terms, changes in the kinetic and mechanistic productivity of the incremented organic, are relatively minor.

The contribution from the non-incremented species (the off-diagonal elements), on the other hand, arises due to changes in the chemistry of the mixture induced by the addition of the incremented species as evidenced by the significance of the $\Delta_i P^k$ and $\Delta_i P^m$ terms in Table 4. Thus, the Δ_i[VOC] term can be viewed as the change in ozone attributable to the incremented organic, with the $\Delta_i P^k$ and $\Delta_i P^m$ terms attributing changes in ozone to the non-incremented species.

At VOC/NO_x=4, the incremental reactivities of CO and the alkanes, ALK1 and ALK2, include a decrease in ozone production from all the non-incremented species. For all other organics at this VOC/NO_x ratio, the increase in ozone, resulting from adding an increment of an individual species, contains a positive contribution from the non-incremented species. This behavior at VOC/NO_x=4 can be attributed to changes in kinetic productivity, or the fraction of organic that reacts. Table 4 shows a negative ozone contribution from the $\Delta_i P^k$ term for CO, ALK1, and ALK2 at VOC/NO_x =4, while the kinetic productivity contribution for all other organics is positive at this VOC/NO_x ratio. Thus, when CO, ALK1, or ALK2 are added to the base case mixture, less of the other organics react resulting in a decrease in ozone formation attributable to the non-incremented species. When any of the other organics is added to the base case mixture at VOC/NO_x=4, more of the non-incremented species react, causing an increase in ozone formation attributable to the non-incremented organics.

Changes in kinetic productivity can be understood by examining the influence of the radical pool on VOC/NO_x chemistry. The ozone assignment method was also used to

determine the net production of OH radicals by the individual organics. This was accomplished by monitoring separately the OH-creating and OH-destroying reactions and assigning the amount of OH creation and OH destruction to each individual VOC. The net production of OH radicals was calculated from the difference between OH creation and OH destruction. Figure 1 shows that CO, ALK1, and ALK2 are sinks for the OH radical, destroying more than they produce, while the other organics are radical sources of varying strength.

To understand the OH source/sink effect of an organic, OH concentrations were monitored in each simulation and the average OH concentration, over the course of the 15 hour simulation, was determined. The change in average OH concentration from the base case upon adding an organic is shown in Figure 2, with values relative to the change produced by an increment of the entire VOC mixture. Addition of CO, ALK1, and ALK2 in all cases produces a drop in OH concentration, while addition of all other species causes OH levels to increase for VOC/NO_x ratios of 4 and 8.2.

These results indicate that adding an organic that acts as an OH sink to the VOC mixture results in a lower OH concentration which causes the OH-initiated reaction rate of organics to decrease as shown by the drop in the kinetic productivity contribution to ozone when CO, ALK1, and ALK2 are added. At VOC/NO_x = 4 and 8.2, addition of an OH source produces the opposite effect with OH concentrations increasing, more OH-initiated reactions of organics, and higher kinetic productivity. For the high VOC/NO_x scenario, an additional effect, that will be discussed later, becomes important causing OH

concentration and kinetic productivity to decrease upon addition of all species except formaldehyde.

At $VOC/NO_x = 4$, the contribution to ozone from changes in mechanistic productivity is negative for the OH sink species, and near zero for the OH sources. As the VOC/NO_x ratio increases, all of the mechanistic productivity contributions decrease, indicating that adding VOC leads to less efficient reactions. The efficiency of a reaction mechanism can be defined as the fraction of organic-produced RO_2 radicals that react via ozone-forming NO to NO_2 conversions versus radical terminating or other non-ozone-forming pathways. As shown in Figure 3, the overall mechanism efficiency decreases for increased VOC/NO_x ratios, with termination and non-ozone-forming propagation increasing.

At low VOC/NO_x ratios, NO is readily available and virtually all of the RO_2 radicals produced will react with NO. Due to the large excess of NO, addition of organic in this situation has little effect, and changes in mechanistic productivity are near zero for all but the OH sink species. These species tend to increase termination pathways, which results in a decrease in mechanistic productivity. As the VOC/NO_x ratio increases, NO becomes more scarce and organic-produced RO_2 radicals more abundant, resulting in a lesser fraction of RO_2 radicals reacting with NO in NO to NO_2 conversion steps. When an increment of organic is added to the base case mixture under these conditions, mechanism efficiency decreases, which leads to a decrease in mechanistic productivity.

At VOC/NO_x=4, the increases in kinetic productivity upon adding an OH source are sufficiently large to overcome the decreases in mechanistic productivity so that the overall contribution to the ozone change from the non-incremented species is positive. At a VOC/NO_x ratio of 8.2, the decreases in P^m become more significant and for most species the drop in mechanistic productivity dominates the increase in kinetic productivity, causing the overall contribution to ozone from the non-incremented species to be negative.

At VOC/NO_x=20, adding an OH source does not cause the kinetic productivity to increase, but instead results in a decreased fraction of the organics reacting. As was the case for RO_2 radicals, propagation and termination reactions compete for the available OH radicals. One measure of the relative importance of these processes is the OH chain length, L_{OH}, which is the average number of times a newly created OH radical will be recreated through radical chain propagation before it is destroyed. Jeffries and Crouse (1990) have introduced the concept of "new" OH and "old" OH to define the chain length, L_{OH},

$$L_{OH} = \frac{\text{"new" OH + "old" OH}}{\text{"new" OH}}$$

"New" OH radicals, in this context, are those produced directly by photolysis of O_3 as well as those produced from conversion of other "new" radicals to OH, whereas "old" OH radicals are those regenerated after cycling through the radical chain. As shown in Figure 4, OH chain length decreases at both high and low VOC/NO_x ratios, such that at

low VOC/NO_x ratios adding organic increases the chain length, while at high VOC/NO_x ratios additional organic produces a decrease in OH chain length. The chain length is short at low VOC/NO_x ratios due to the high concentration of NO_2, with which OH reacts in a radical-terminating step to form HNO_3. At high VOC/NO_x ratios the small chain length is attributable to increased termination of RO_2 radicals, which prevents OH radicals from being reformed.

Changes in OH concentration upon adding an organic are a result of changes in chain length as well as the OH source/sink behavior of the specific organic added. At higher VOC/NO_x, the drop in OH chain length is sufficient to lower the overall OH concentration as shown in Figure 2. Thus, while adding an OH source has the tendency to increase OH levels, the competing effect of lowered propagation dominates for all OH-source VOCs except formaldehyde, resulting in a lower OH concentration and, therefore, lower kinetic productivity. For the case of the aromatics, ARO1 and ARO2, the lowered kinetic productivity when coupled with a sharp decrease in ozone from changes in mechanistic productivity, is sufficient to overshadow the ozone increase due to the additional organic present, causing an overall decrease in ozone production and a negative incremental reactivity.

CONCLUSIONS

The ozone change measured in an incremental reactivity calculation may be traced to changes in the ozone attributable to individual organic species in a VOC mixture using the ozone assignment method. These changes can be represented as the sum of changes in organic concentration, kinetic productivity, or the fraction of organic reacting, and mechanistic productivity, or the amount of ozone produced per carbon atom of organic reacting.

Incremental reactivity calculations, using the condensed SAPRC 90 mechanism with a VOC mixture representing the South Coast Air Basin, showed significant contributions to the overall ozone change from all organic species in the mixture as a result of changes in concentration and productivity. At VOC/NO_x ratios of 4, 8.2, and 20, the incremented organic accounts for only a fraction of the total ozone change. The ozone attributable to the non-incremented species either increases or decreases depending on VOC/NO_x ratio and radical interactions.

Carbon monoxide, and the alkane species, ALK1 and ALK2, are OH radical sinks, causing OH concentration, and thus kinetic productivity, to decrease upon their addition to a base case mixture at all three VOC/NO_x ratios. The remaining organic species are OH sources and at VOC/NO_x=4 and 8.2, their addition results in higher kinetic productivity. At VOC/NO_x=20, addition of all OH sources, except formaldehyde,

causes OH concentration and kinetic productivity to decrease due to a decrease in OH propagation chain length that overrides the OH source effect.

The ozone contribution from changes in mechanistic productivity decreases or remains constant upon adding any organic at the higher VOC/NO_x ratios due to a shift of RO_2 reactions from NO to NO_2 conversion pathways to termination and non-ozone-forming propagation pathways. At the low VOC/NO_x ratio, where NO is in excess, only the OH sink species, which introduce radical termination, produce a decrease in mechanistic productivity upon their addition to the mixture. These changes in kinetic and mechanistic productivity combine to produce both positive and negative changes in the amount of ozone attributable to the individual non-incremented organics. The drop in kinetic productivity when adding CO, ALK1, or ALK2 results in a decrease in ozone attributable to all of the non-incremented species at all VOC/NO_x ratios. At low VOC/NO_x, the increase in kinetic productivity when adding an OH source leads to an increase in the non-incremented species contribution. At VOC/NO_x=8.2, however, declines in mechanistic productivity offset the kinetic productivity increases for many of the non-incremented organics. At VOC/NO_x=20, the decrease in kinetic productivity together with lowered mechanistic productivity results in lowered ozone production from all non-incremented organics and overall incremental reactivities that are negative for the aromatic species, ARO1 and ARO2.

ACKNOWLEDGMENT

This work was supported by the Coordinating Research Council and the National Renewable Energy Laboratory. The authors wish to acknowledge the referee for helpful comments.

REFERENCES

Anderson-Sköld Y., Greenfelt P. and Pleijel K. (1992) Photochemical ozone creation potentials: a study of different concepts. *J. Air Waste Manage. Assoc.* **42**, 1152-1158.

ARB (1987) South Coast Air Basin emissions inventory for August 27, 1987. California Air Resources Board, Sacramento, CA.

Bowman F. M. and Seinfeld J. H. (1994) Ozone productivity of atmospheric organics. *J. Geophys. Res.* **99**, 5309-5324.

Carter W. P. L. (1988) Appendix C. Documentation for the SAPRC atmospheric photochemical mechanism preparation and emissions processing programs for implementation in airshed models. Report, Contract No. A5-1222-2, California Air Resources Board, Sacramento, CA.

Carter W. P. L. (1991) Development of ozone reactivity scales for volatile organic compounds. EPA 600/3-91/050, Environmental Protection Agency, Research Triangle Park, NC.

Carter W. P. L. and Atkinson R. J. (1987) An experimental study of incremental hydrocarbon reactivity. *Environ. Sci. Technol.* **21**, 670-679.

Carter W. P. L. and Atkinson R. J. (1989) Computer modeling study of incremental hydrocarbon reactivity. *Environ. Sci. Technol.* **23**, 864-880.

Carter W. P. L. and Lurmann. F. W. (1990) Development of a condensed mechanism for urban airshed modeling. Interim report, EPA Cooperative Agreement CR-815699-01-0, U.S. Environmental Protection Agency, Research Triangle Park, NC.

Chang T. Y. and Rudy S. J. (1990) Ozone-forming potential of organic emissions from alternative-fueled vehicles. *Atmos. Environ.* **24A**, 2421-2430.

Croes B. E., Holmes J. R. and Lloyd A. C. (1992) Reactivity based hydrocarbon controls: scientific issues and potential regulatory applications. *J. Air Waste Manage. Assoc.* **42**, 657-661.

Derwent R. G. and Jenkin M. E. (1991) Hydrocarbons and the long-range transport of ozone and PAN across Europe. *Atmos. Environ.* **25A**, 1661-1678.

EPA (1988) EPA EKMA base case simulation for Los Angeles, California, on September 3, 1988. U.S. Environmental Protection Agency, Research Triangle Park, NC.

Jeffries H. (1993) A different view of ozone formation: fuel reformulation alone may not reduce urban ozone. *Fuel Reformulation* Jan/Feb, 58-68.

Jeffries H. E. and Crouse R. (1990) Scientific and technical issues related to the application of incremental reactivity. Report, University of North Carolina, Chapel Hill, NC.

McNair L., Russell A. and Odman M. T. (1992) Airshed calculation of the sensitivity of pollutant formation to organic compound classes and oxygenates associated with alternative fuels. *J. Air Waste Manage. Assoc.* **42**, 174-178.

Seinfeld J. H. (1986) *Atmospheric Chemistry and Physics of Air Pollution*. Wiley, New York.

Table 1. Base case initial organic concentrations.

	Initial Concentration (ppbC)	Carbon Fraction (%)
CO	1500	34.88
CH4	1700	39.53
carbonyls		
HCHO	8	0.19
CCHO	5	0.11
RCHO	2	0.04
MEK	16	0.38
alkanes		
ALK1	353	8.21
ALK2	236	5.48
aromatics		
ARO1	147	3.42
ARO2	108	2.52
alkenes		
ETHE	75	1.74
OLE1	60	1.39
OLE2	29	0.67
OLE3	62	1.45
TOTAL	4301	100

Table 2. Incremental Reactivities (ppb O_3 $ppbC^{-1}$).

	VOC/NO_x		
	4	8.2	20
Maximum Ozone Yield (ppb)	58	378	303
CO	0.0055	0.005	0.0062
CH4	0.0010	0.001	0.0008
carbonyls			
HCHO	3.39	3.26	0.34
CCHO	1.21	1.21	0.078
RCHO	1.49	1.48	0.017
MEK	0.18	0.18	0.008
alkanes			
ALK1	0.065	0.07	0.037
ALK2	0.091	0.09	0.020
aromatics			
ARO1	0.18	0.18	-0.11
ARO2	0.94	0.94	-0.04
alkenes			
ETHE	0.66	0.66	0.17
OLE1	0.85	0.86	0.079
OLE2	1.05	1.05	0.047
OLE3	0.82	0.82	0.056
MIX (direct)	0.0938	0.0942	0.0078
MIX (indirect)	0.0940	0.0940	0.0080
% error	0.2	-0.3	2.7

Incremental reactivity calculations were performed using a chamber model for 15 hour simulations, from 6 am to 9 pm, with time-varying solar irradiation corresponding to June 21.

Table 3. Percent of $\Delta_i R$ attributable to VOC_j.

$VOC/NO_x = 4$

	VOC_j														
VOC_i	CO	CH4	HCHO	CCHO	RCHO	MEK	ALK1	ALK2	ARO1	ARO2	ETHE	OLE1	OLE2	OLE3	Total
CO	164	0	0	-1	0	0	-9	-9	-5	-10	-8	-9	-5	-6	100
CH4	2	84	0	0	0	0	4	4	1	1	2	2	0	1	100
HCHO	5	1	19	1	0	0	12	5	3	15	4	8	7	18	100
CCHO	2	0	0	66	0	0	7	6	1	3	4	5	3	2	100
RCHO	3	0	0	0	57	0	7	8	2	4	5	5	3	5	100
MEK	3	0	0	0	0	63	7	8	2	3	5	4	2	3	100
ALK1	-2	0	0	0	0	0	135	-5	-3	-6	-5	-6	-3	-4	100
ALK2	-3	0	0	-1	0	-1	-9	160	-5	-10	-8	-10	-6	-7	100
ARO1	3	0	0	0	0	0	7	8	63	4	5	5	2	3	100
ARO2	4	0	0	0	0	0	9	9	3	55	7	6	3	4	100
ETHE	3	0	0	0	0	0	7	7	2	4	68	4	1	2	100
OLE1	2	0	0	0	0	0	6	6	1	2	4	77	1	1	100
OLE2	3	0	0	0	0	0	7	7	2	3	5	4	67	3	100
OLE3	2	0	0	0	0	0	6	6	1	2	4	3	1	74	100
MIX	6	1	1	1	0	1	14	15	5	15	12	13	6	11	100

$VOC/NO_x = 8.2$

	VOC_j														
VOC_i	CO	CH4	HCHO	CCHO	RCHO	MEK	ALK1	ALK2	ARO1	ARO2	ETHE	OLE1	OLE2	OLE3	Total
CO	163	0	0	-1	0	0	-9	-9	-5	-10	-8	-9	-5	-6	100
CH4	2	84	0	0	0	0	4	4	0	1	2	2	0	1	100
HCHO	5	1	20	1	0	0	13	10	4	12	8	9	6	12	100
CCHO	2	0	0	66	0	0	6	6	1	2	4	5	3	2	100
RCHO	3	0	0	0	58	0	7	8	2	4	5	5	3	5	100
MEK	3	0	0	0	0	63	7	8	2	3	5	4	2	3	100
ALK1	-2	0	0	0	0	0	134	-4	-3	-6	-5	-6	-3	-4	100
ALK2	-3	0	0	-1	0	0	-9	160	-5	-10	-8	-10	-5	-7	100
ARO1	3	0	0	0	0	0	7	8	63	4	5	5	2	3	100
ARO2	4	0	0	0	0	0	9	9	3	55	7	6	3	4	100
ETHE	3	0	0	0	0	0	7	7	2	4	68	4	1	2	100
OLE1	2	0	0	0	0	0	6	6	1	2	4	77	1	1	100
OLE2	3	0	0	0	0	0	7	7	2	3	5	4	68	2	100
OLE3	2	0	0	0	0	0	6	6	1	2	4	3	1	74	100
MIX	6	1	1	1	0	1	14	15	5	15	12	13	6	11	100

Table 3. (Continued).

VOC/NO_x = 20

	VOC_j														
VOC_i	CO	CH4	HCHO	CCHO	RCHO	MEK	ALK1	ALK2	ARO1	ARO2	ETHE	OLE1	OLE2	OLE3	Total
CO	188	-1	1	0	0	-1	-27	-19	-9	-4	-15	-6	-3	-2	100
CH4	-9	205	-1	-1	0	-1	-19	-15	-8	-12	-16	-11	-5	-7	100
HCHO	-10	0	156	-2	-1	-1	0	5	-68	-33	-14	21	15	31	100
CCHO	-59	-9	-4	888	-1	-4	-168	-146	-61	-72	-126	-71	-21	-48	100
RCHO	-266	-42	-25	-34	3870	-24	-843	-672	-296	-384	-644	-396	-126	-18	100
MEK	-104	-16	-10	-13	-4	1503	-284	-193	-108	-139	-234	-153	-58	-86	100
ALK1	-24	-4	-2	-3	-1	-2	373	-61	-25	-29	-52	-35	-16	-20	100
ALK2	-80	-12	-5	-9	-3	-8	-247	1057	-80	-97	-172	-117	-56	-71	100
ARO1	-17	-2	-2	-2	-1	-2	-47	-39	109	-21	-33	-21	-9	-13	100
ARO2	-91	-11	-15	-14	-5	-8	-219	-192	-82	1010	-189	-137	-55	-92	100
ETHE	-19	-2	-2	-2	-1	-1	-37	-31	-17	-27	291	-24	-12	-16	100
OLE1	-56	-7	-6	-7	-2	-5	-145	-121	-55	-82	-114	791	-40	-52	100
OLE2	-86	-12	-10	-11	-3	-7	-244	-205	-93	-137	-197	-134	1317	-76	100
OLE3	-63	-8	-6	-9	-2	-5	-166	-137	-66	-103	-135	-102	-53	956	100
MIX	-15	-1	7	1	0	0	-11	26	-9	39	-18	25	11	45	100

Table 4. Percent of $\Delta_i R$ attributable to concentration, kinetic, and mechanistic factors.

	VOC/NO_x = 4			VOC/NO_x = 8.2			VOC/NO_x = 20		
VOC_i	ΔVOC	ΔP^k	ΔP^m	ΔVOC	ΔP^k	ΔP^m	ΔVOC	ΔP^k	ΔP^m
CO	167	-23	-44	129	-10	-18	194	-81	-14
CH4	83	25	-9	103	29	-31	206	-33	-73
HCHO	19	62	19	21	78	2	158	100	-157
CCHO	64	32	4	110	41	-51	866	-280	-501
RCHO	57	40	3	101	48	-50	3816	-1349	-2414
MEK	60	38	1	118	27	-47	1453	-479	-890
ALK1	140	-7	-33	194	-22	-71	450	-157	-191
ALK2	171	-26	-44	258	-47	-109	1269	-472	-689
ARO1	61	38	1	87	64	-51	124	-69	-154
ARO2	50	44	5	61	74	-34	1172	-85	-1182
ETHE	63	34	3	87	47	-34	326	-38	-187
OLE1	74	33	-7	114	42	-56	878	-193	-581
OLE2	66	37	-3	104	49	-53	1377	-302	-972
OLE3	72	34	-6	114	46	-60	1018	-210	-706
MIX	72	32	-4	108	39	-46	1050	-292	-655

LIST OF FIGURES

Figure 1.

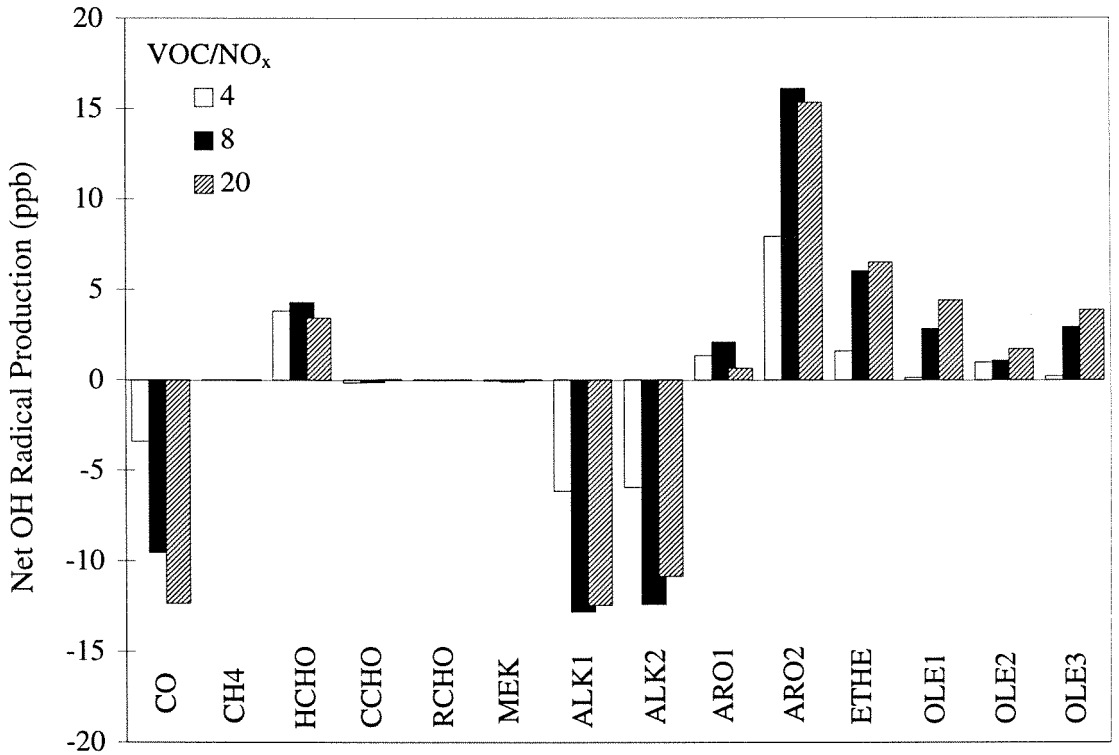
Net OH Radical Production (ppb)
20
15
10
5
0
-5
-10
-15
-20
VOC/NOx
4
8
20
CO
CH4
HCHO
CCHO
RCHO
MEK
ALK1
ALK2
ARO1
ARO2
ETHE
OLE1
OLE2
OLE3

Figure 2.

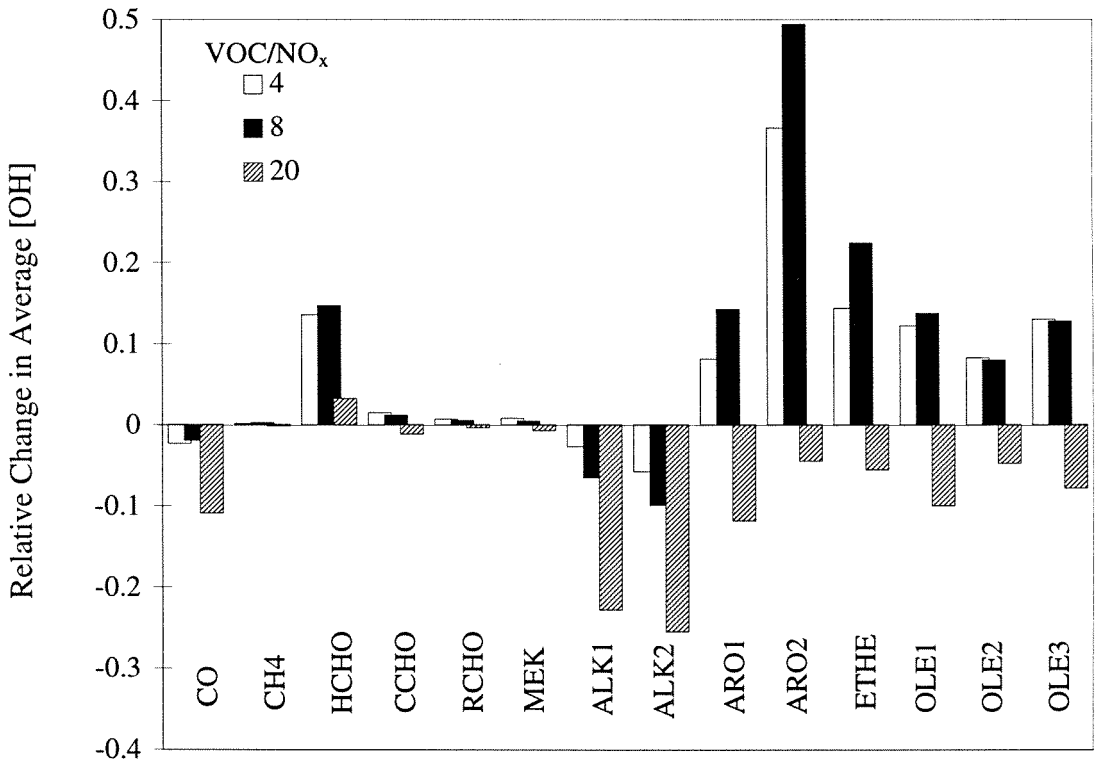
Relative Change in Average [OH]
0.5
0.4
0.3
0.2
0.1
0
-0.1
-0.2
-0.3
-0.4
VOC/NOx
4
8
20
CO
CH4
HCHO
CCHO
RCHO
MEK
ALK1
ALK2
ARO1
ARO2
ETHE
OLE1
OLE2
OLE3

Figure 3.

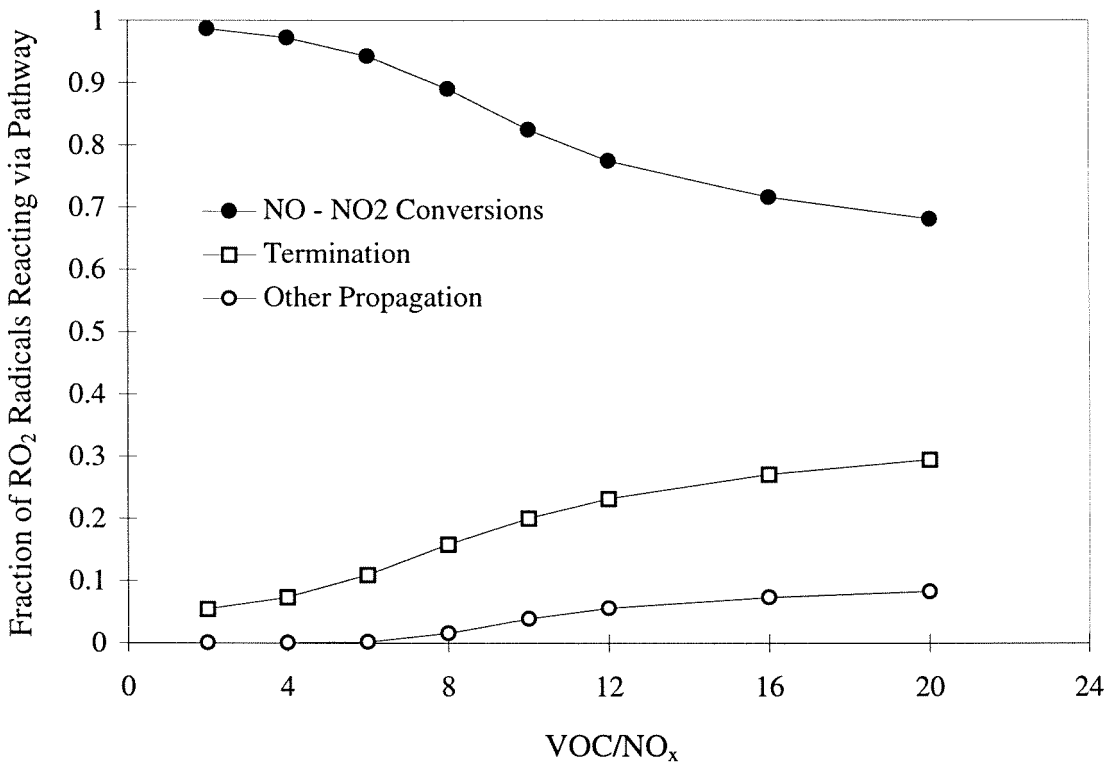
Fraction of RO_2 Radicals Reacting via Pathway
1
0.9
0.8
0.7
0.6
0.5
0.4
0.3
0.2
0.1
0
NO - NO2 Conversions
Termination
Other Propagation
0
4
8
12
16
20
24
VOC/NO_x

Figure 4.

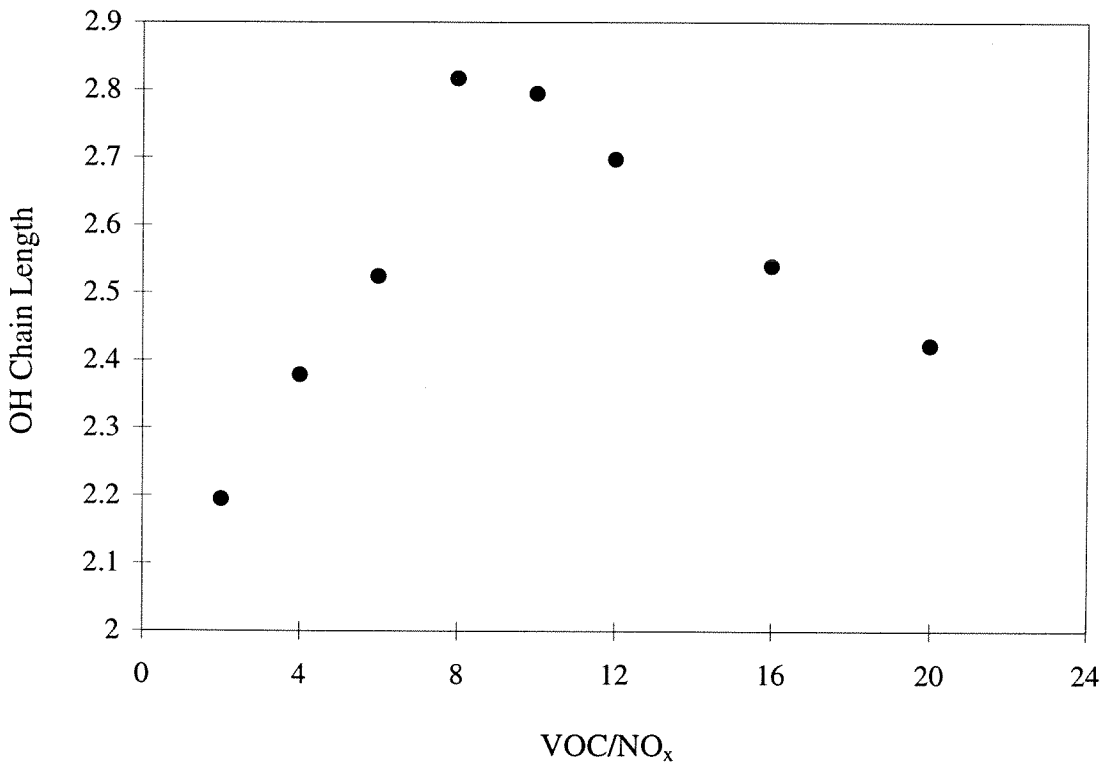

CHAPTER 4:

OZONE AND AEROSOL PRODUCTIVITY OF REACTIVE ORGANICS

Published in *Atmos. Environ.*, **29**, 579-589 (1995).

ABSTRACT

A technique developed to determine the amount of ozone and secondary photochemical species generated by the individual organic components of a complex atmospheric organic/NO_x mixture (Bowman and Seinfeld, 1994*a*) is used to study the individual contributions of carbonyl, aromatic, alkane, and alkene emissions to ozone and secondary organic and inorganic aerosol species in the South Coast Air Basin of California for the Southern California Air Quality Study (SCAQS) air pollution episode of August 27-28, 1987. Aldehydes exhibit the highest ozone productivity followed by alkenes, and lumped reactive aromatics. The aromatic species and formaldehyde enhance the production of secondary organic and secondary sulfate aerosol, because they are effectively OH sources. The same species, through their effect on both OH and O_3 production, are also significant precursors of HNO_3, and, consequently, of nitrate aerosol. This methodology can be used in conjunction with urban airshed models to investigate alternative emission control scenarios.

INTRODUCTION

It has been recognized for some time that volatile organic compounds (VOCs) differ in their ozone-forming capability (Carter and Atkinson, 1987, 1989; Chang and Rudy, 1990; Derwent and Jenkin, 1991; Anderson-Sköld *et al.*, 1992; McNair *et al.*, 1992). The ozone-forming potential of an individual VOC will depend on the characteristics of the complex mixture of which it is a part, including the NO_x level and the other VOCs that are present (Carter, 1991; Bowman and Seinfeld, 1994*ab*). It has long been of interest to be able to determine, for any given VOC/NO_x mixture, the contribution of each individual organic species to the total amount of ozone generated in that mixture. That determination has important implications to the relative control of different organics in ozone abatement.

Atmospheric aerosols can be either primary, directly emitted by sources, or secondary, the result of chemical reactions in the atmosphere that form condensable products (Seinfeld, 1986; Pilinis and Seinfeld, 1988; Pandis *et al.* 1992, 1993). Primary atmospheric aerosols can be controlled by reducing their emissions, while to reduce the levels of secondary aerosol species one has to reduce the emissions of their gaseous precursors. Major reaction pathways for the formation of condensable organic and inorganic gases involve the hydroxyl radical and ozone. Therefore, reducing those VOCs that have ozone and hydroxyl radical-forming capability can be expected to affect the formation of secondary aerosol.

In this study we extend the method of Bowman and Seinfeld (1994*ab*) for determining the contributions of individual VOCs to ozone formation to ozone and secondary aerosol formation along an atmospheric trajectory with simultaneous emissions, dilution, and chemical transformation. The technique is applied to a series of trajectories in the South Coast Air Basin on August 27-28, 1987, during the 1987 Southern California Air Quality Study (SCAQS). Alternative VOC and NO_x control measures are evaluated to determine the relative effectiveness of VOC and NO_x reductions to the abatement of ozone and secondary aerosol.

THE ASSIGNMENT METHOD

The assignment method is a technique whereby the amount of secondary pollutants of interest generated by the individual organics in a complex VOC/NO_x mixture is calculated. Full mathematical details of this method have been presented elsewhere (Bowman and Seinfeld, 1994*a*). The basic objective of the technique is to follow the reaction pathways of a mechanism and trace the ozone, or other product species, formed back to the original organic precursors. This is done by analyzing the concentration predictions of an atmospheric chemical mechanism.

Since reaction stoichiometry is necessary to perform such an analysis, the stoichiometric coefficients for all species in all reactions are initially determined. In order

to trace a product species back to its precursors, one reactant in each reaction must be selected as the controlling, or dominant, reactant to which all products of the reaction will be assigned. This selection provides a necessary simplification of the reaction mechanism where only the effect of the dominant reactant is considered. A limitation in this approach is that products in a reaction can be assigned to only one reactant, making proper selection of dominant reactants, based on the specific product species and reactants of interest, a crucial element. For example, when ozone is being assigned to emitted organics, these organic species have the highest priority for selection as dominant reactants, followed by their immediate products, such as formaldehyde and methyl ethyl ketone, then organic radical species, and, lastly, the nitrogen oxides. Thus in the reaction,

$$HO_2 + NO \rightarrow NO_2 + OH$$

HO_2 would be selected as the dominant reactant so that the ozone-forming NO to NO_2 conversion is attributed to HO_2 and, ultimately, its organic precursor.

The progress of individual reactions within the mechanism is monitored by adding a "counter" species as a product to each reaction. These counters, dummy species with no physical significance, act to "count" the amount of reactant that has undergone each reaction since the beginning of the simulation. For each time step analyzed, the amount of reactant species available for reaction can be determined as the sum of initially present reactant, emitted reactant, and reactant formed in other reactions during the time step. With the change in concentration during a time step of a given reaction's counter

species and the amount of reactant available for that reaction, the fraction of available reactant passing through that reaction during the time step can be calculated. Starting with an organic precursor, these fractions reacting, together with product stoichiometry, can be used to calculate the amount of various species that will be formed as direct products in reactions involving the organic as dominant reactant. Of course, these products generally undergo reaction themselves forming additional products, which, in turn, react once again, creating a complex web of reaction pathways.

For each successive step in the VOC/NO_x photooxidation, products are assigned back to the precursor organic. For simple reaction mechanisms of only a few reactions, all of these calculations may be performed by hand. For more complicated mechanisms, however, with hundreds of reactions, or where species are regenerated in a reaction cycle, the required calculations are executed by solving a system of linear equations consisting of one equation for each chemical species in the mechanism. At each time step a new set of linear equations, formed from the fractions reacting calculated for that time step, is solved and products are assigned back to species present at the beginning of the time step from which they were formed.

Initially, all species present are assigned to themselves, and then after the first time step all product species are assigned back to these initially present organic precursors. In subsequent time steps, when these "primary" products react, the resultant "secondary" products are assigned back first to the primary product from which they were generated, and then back to the organic precursor from which the primary product was

formed. Organic emissions during a time step are treated similarly, being assigned to themselves and added to the amount of that organic species present at the beginning of the time step. In this way, at any given time the concentration of each chemical species is assigned among all of the initially present or emitted organic precursors. When taken together, the contributions of the individual organics to a given product species, such as ozone, add up to the total concentration of that species.

The current study applies the assignment method to a trajectory model and represents an extension of the technique to include deposition of chemical species and continuous emissions of organic species and NO_x. The manner in which emissions are included is described by the matrix equation (Bowman and Seinfeld, 1994*a*),

$$\mathbf{X}(t) = \mathbf{X}(t-\Delta t) + \mathbf{X}(t-\Delta t)\,\mathbf{G}(t) + \mathbf{E}'(t)\,\mathbf{G}(t) \qquad (1)$$

where the first term on the right-hand side is the assignment of species from the previous time step, t-Δt, the second term represents changes due to reactions of these species during the time step, and the third term represents reactions during the time step of newly emitted species.

Specifically, the matrix $\mathbf{X}(t)$ is composed of elements, $x_{ik}(t)$, the concentration of species i attributable to species k at time t, and carries information on the assignment of all species to their original precursors. $\mathbf{G}(t)$ is produced by solving the aforementioned set of linear equations, and is composed of elements $g_{ik}(t)$, that are defined such that

$$g_{ik}(t) = \frac{\text{net amount of species } k \text{ produced or destroyed attributable to the reactions of species } i \text{ and its products during the time step ending at } t}{\text{amount of reactant species } i \text{ available during the time step ending at } t}$$

Emissions data from an array $\mathbf{e}(t)$, composed of the elements, $e_k(t)$, the concentration of species k emitted during the time step ending at t, are used to construct the matrix $\mathbf{E}'(t)$ such that emitted species are assigned to themselves,

$$e'_{ik}(t) = e'_i(t) \qquad \text{for } i = k$$

$$e'_{ik}(t) = 0 \qquad \text{for } i \neq k$$

Inclusion of the third term in equation (1) allows emissions of organic precursors to be properly accounted for when assigning product species. Dry deposition can be described by the assignment method using a dummy reaction in which the depositing species is destroyed and no products are formed. In this way deposition processes are viewed as additional reactions in the chemical mechanism and changes in concentration due to deposition can be included in the matrix $\mathbf{G}(t)$. Unfortunately, obtaining deposition loss information from the SRSOAM model is quite cumbersome and, therefore, in order to simplify the analysis, deposition was not included in our calculations. Since the assignment method requires mass conservation for correct results, the trajectory calculations within this study to which the assignment method was applied were run without deposition. Other calculations, used to asses the performance of the model, contain appropriate deposition velocities as described in the following section.

While neglecting deposition leads to increased concentrations of organic aerosols, nitric acid, and sulfates, this does not pose a major problem since the aim of the assignment calculations is to determine the relative contributions of organic precursors to aerosol and ozone production. Deposition affects these contributions equally, such that the amount of aerosol attributable to a given precursor will be higher by not including deposition, but the fraction of the total aerosol concentration attributable to the precursor will remain unchanged.

Adding counter species to the reaction mechanism and performing the additional calculations necessary for the assignment method causes only a modest increase in computational time. Using a VAX workstation the time required for a 38 hour run of the trajectory model increased from 12 cpu minutes to 16 cpu minutes upon adding counter species to each reaction. The productivity calculations, performed using a post processing program to analyze the model output data, required approximately 4 minutes on a 486/66 MHz PC.

SECONDARY PHOTOCHEMICAL AEROSOLS

As noted above, secondary photochemical aerosols result from the conversion of organic and inorganic species into products capable of condensing into the particulate phase. The inclusion of secondary photochemical aerosols into a trajectory model has

been accomplished with the Size Resolved Secondary Organic Aerosol Model (SRSOAM), a Lagrangian trajectory box model (Pandis *et al.*, 1992, 1993) that is based on a numerical solution of the Lagrangian trajectory form of the atmospheric diffusion equation presented by McRae *et al.* (1982). As the air parcel moves along the trajectories its height may increase or decrease, depending on the mixing depth. The model contains modules describing gas-phase chemistry, inorganic and organic aerosol thermodynamics, condensation and evaporation of aerosol species, dry deposition, and emissions of primary gaseous and particulate pollutants. The gas-phase chemistry module is based on the detailed SAPRC gas-phase chemical mechanism (Carter, 1990), as extended by Pandis *et al.* (1992) to include production of condensable organic gases. Each reaction involving an organic aerosol gas precursor includes a condensable product species with its corresponding aerosol yield coefficient, as shown in Table 1. These aerosol yield coefficients are based on smog chamber results and the estimation techniques of Grosjean and Seinfeld (1989) and represent a major source of uncertainty in predicting the amount of secondary organic aerosol formed. Also included in Table 1 is a listing of the organic species within the mechanism together with their chemical description. The mechanism includes four classes of lumped alkanes, AAR1 to AAR4, in order of increasing reactivity with respect to the OH radical, three classes of lumped alkenes, OLE1 to OLE3, and three classes of lumped aromatics, AAR5 to AAR7. The lumped species in the mechanism represent a composite of the individual species present in the organic mixture, with species assigned to the lumped groups based on their OH radical rate constants. The

carbonyl species RCHO and MEK are modeled after propionaldehyde and methyl ethyl ketone, respectively, but are lumped species used to represent all higher aldehydes and ketones. The mechanism was modified, using the mechanism processing software of Carter (1988), to include one counter species for each reaction of the mechanism, as required by the assignment method. Thus the expanded chemical mechanism contains 195 counter species, in addition to the 100 species of the original mechanism.

The method we have presented allows one, in a sense, to unravel the complex chemistry of VOC/NO_x photooxidation, as described by a given chemical mechanism, to determine individual VOC contributions to ozone, OH, and secondary products. How valid a particular mechanism is in representing actual atmospheric chemistry is a separate issue. Aromatic chemistry is a case in point. All VOC/NO_x reaction mechanisms include the oxidation of aromatics such as toluene and the xylenes. In the troposphere benzene and the alkyl-substituted benzenes such as toluene and the xylenes react virtually exclusively with the OH radical. The major reaction pathway involves initial OH radical addition to the aromatic ring to yield a hydroxycyclohexadienyl type radical. The minor pathway (about 10%) involves H-atom abstraction from the substituent groups to form a benzyl type radical. Rate constants for these initial steps are well known and the reaction path following H-atom abstraction is reasonably well established. The OH-radical addition path leads to both ring-retaining products such as phenols and ring-cleavage products such as α- and γ-dicarbonyls. However, the detailed mechanism of reaction subsequent to formation of the hydroxycyclohexadienyl radical is not yet known, and only

about 50% of the original aromatic carbon has been accounted for experimentally. Nonetheless, atmospheric VOC/NO_x mechanisms include complete carbon-conserving aromatic oxidation mechanisms in which secondary ring-cleavage products such as carbonyl or dicarbonyl compounds are the precursors for NO to NO_2 conversions. The product splits are generally chosen to match observed ozone formation in aromatic/NO_x smog chamber systems. The accuracy of these mechanisms is yet to be established. Thus, the detailed results of mechanism analysis studies such as that presented here will change as the specific reaction steps are changed.

In modeling photochemical aerosol formation and growth, the volatile inorganic aerosol species are usually assumed to be distributed between the aerosol and the gas phases from thermodynamic equilibrium. This assumption is valid as long as equilibrium is established over time scales smaller than the 10 minute time step used by the model (Hildemann *et al.*, 1984; Pilinis and Seinfeld, 1987; Wexler and Seinfeld, 1992; Pandis *et al.*, 1992, 1993). The sectional equilibrium aerosol model of Pilinis and Seinfeld (1987), SEQUILIB, is used here for the calculation of the composition and distribution of volatile inorganic aerosol at equilibrium. The model predicts the gas-phase concentrations of NH_3, HNO_3, and HCl, as well as the aerosol-phase concentrations of H_2O, NO_3^-, SO_4^{2-}, HSO_4^-, NH_4^+, Na^+, Cl^-, H_2SO_4, Na_2SO_4, $NaHSO_4$, NaCl, NH_4Cl, NH_4NO_3, $(NH_4)_2SO_4$, NH_4HSO_4 and $(NH_4)_3H(SO_4)_2$. Thermodynamic equilibrium is also assumed for the various condensable organic aerosol species with saturation concentrations assumed to be

on the order of a few parts per trillion such that virtually all of the condensable gases are found in the aerosol phase (Pandis *et al.*, 1992).

TRAJECTORIES DURING THE SOUTHERN CALIFORNIA AIR QUALITY STUDY (SCAQS)

In the summer and fall of 1987, a comprehensive air pollution data set was collected in the Los Angeles area during the Southern California Air Quality Study (SCAQS) (Hering and Blumenthal, 1989). Our analysis focuses on one of the intensive periods of measurement, that of August 27-28, 1987.

The first step in the analysis is to examine the performance of the SRSOAM model when applied to two receptor sites in the South Coast Air Basin, Rubidoux and Fontana. Hourly ozone data are available at both sites, while 4-hour averaged aerosol concentrations are available at Rubidoux. Air parcel trajectories were computed by specifying the trajectory end points and the time of arrival of the parcel at the receptor site. Integrating back in time using the gridded wind field, which was prepared using the method of Goodin *et al.* (1979), 24 trajectories were constructed for each of the two receptor sites, each corresponding to an hour of August 28, 1987. Once the trajectories were computed, the necessary meteorological data and pollutant emissions were extracted from the corresponding gridded meteorological and emission fields (Pandis *et al.*, 1992).

The meteorological input data needed for the simulations are interpolated gridded data constructed from measured meteorological data using objective analysis techniques (Goodin *et al.*, 1979; Harley *et al.*, 1991). Other meteorological data required are temperature, humidity, mixing depth, surface winds, and solar radiation. The grid used in our simulations was the standard 5 x 5 km grid used in previous studies in the South Coast Air Basin (Pandis *et al.*, 1992, 1993).

Emissions inventories for the South Coast Air Basin for the two days of interest were provided by the California Air Resources Board (ARB, 1987; Allen, 1993). The emissions inventory consists of emissions of NO_x, reactive organic gases (ROG), SO_2, CO, and speciated PM_{10}. Recent evaluations of the South Coast Air Basin emissions inventory indicate that the motor vehicle emissions in that 1987 inventory were likely substantially underestimated (Pierson *et al.*, 1990; Chico and Lester, 1992; Harley *et al.*, 1991, 1993; Fujita *et al.*, 1992). In order to account for this underprediction, total hot and cold start organic emissions from mobile sources were increased by a factor of four, and CO emissions by a factor of 2.5 in our simulations, as suggested by Pierson *et al.* (1990). A biogenic emission inventory matching the isoprene emission estimates of Winer *et al.* (1983) has also been included. The organic gas emissions are subdivided into the 28 organic species required by the chemical mechanism (Table 1) using the emissions processing software of Carter (1988). All trajectories were initiated over the Pacific Ocean; initial conditions for the model (Table 2) were estimated based on measurements

made at San Nicholas Island (Chan and Durkee, 1989). The initial secondary organic aerosol concentrations were set equal to zero.

Trajectory models are not expected to exhibit the detailed spatial and temporal resolution of three-dimensional Eulerian models, but they should represent the qualitative behavior of major pollutants of interest, such as ozone and secondary aerosol species. Uncertainties, including organic emissions, aerosol yields, and the partitioning of the condensable gases between phases, exist in both ozone and secondary organic aerosol predictions (Pandis *et al.*, 1992, 1993). The predicted ozone concentrations at the two sites for trajectories arriving at each of the 24 hours of August 28, 1987 are presented in Figure 1. With the motor vehicle hydrocarbon emissions increased by a factor of four, the model is capable of reproducing observed ozone behavior at both sites, whereas when using the reported emissions, ozone predictions by the model are much lower than observed levels. These results, together with those of a previous application of the model for Claremont, CA, for the same period (Pandis *et al.*, 1992), indicate that SRSOAM can be used as a tool in the assignment technique for estimating the contribution of individual VOC species to ozone and aerosol formation.

OZONE AND AEROSOL PRODUCTIVITY

The assignment method was used to analyze the contributions of individual VOCs to ozone and aerosol formation along two trajectories that arrived at Rubidoux on August

28, 1987. The first trajectory arrived at 2 pm (PST), which corresponds to the time of peak ozone levels, while a second trajectory, arriving at 8 am, was selected to examine the effect of varying the time of day. A summary of the organics emitted along the trajectories to Rubidoux is listed in Table 3. Also included in Table 3 is a listing of basin-wide emissions for comparison. While the composition of emissions along the trajectories to Rubidoux varies somewhat from the average basin composition, with MEK and RCHO higher for Rubidoux, the overall chemistry is not expected to be altered significantly. The fraction of emissions from mobile and stationary sources for each organic is presented in Table 4. The ozone concentration at Rubidoux was assigned back to the emitted organic species as shown in Figure 2. The contribution to the amount of ozone at Rubidoux varies significantly among each of the organics. That contribution is a result of two factors, the amount of ozone generated per molecule of organic and the amount of the organic species present as a result of emissions. The relatively large contribution to ozone by CO in Figure 2, for example, is largely a result of the emissions of CO along the trajectory to Rubidoux (see Table 3). In order to normalize for the effect of varying organic concentrations, ozone production for each species is divided by the total emitted and initially present concentration of that species to give an ozone productivity value,

$$P_i = \frac{[O_3]_i}{[VOC_i]_{total}}$$

where P_i is the ozone productivity of species i, in units of ppb O_3/ppbC VOC_i, $[O_3]_i$ is that portion of the final ozone concentration attributable to species i, and $[VOC_i]_{total}$ is the total amount of emitted and initially present species i available for reaction, in units of ppbC. Ozone productivity represents the net amount of ozone formed per carbon atom of each organic species present.

Figure 3 compares ozone productivity values for each VOC. Among the general classes of organics, the aldehydes exhibit the highest productivity followed by the alkenes, higher aromatics, and alkanes. CO produces very little ozone per molecule, but as a result of its relatively higher concentration (Table 3) when compared to the VOCs, a significant amount of ozone is attributed to CO in Figure 2. Exact numerical values of ozone productivities can vary considerably, depending upon scenario conditions such as VOC/NO_x ratio and organic mixture composition. In a trajectory calculation, ozone productivities of VOCs relative to each other may also be affected by the timing of organic emissions, with species emitted later having less time to react and, therefore, showing lower overall productivity.

The results for ozone production at 2 pm, as shown in Figures 2 and 3, can be compared to the results for the 8 am trajectory shown in Figures 3 and 4. As the total ozone concentration increases from 19 ppb at 8 am to 272 ppb at 2 pm (Figure 1), the amount of ozone assigned to each of the organic precursors increases proportionately. The relative contributions of the organic species at 8 am and 2 pm tend to be similar, and when ozone productivities are compared (Figure 3), the amount of ozone produced per

molecule is shown to remain relatively constant. This same behavior was observed to a greater extent for aerosol assignment calculations, with both the 8 am and 2 pm trajectories producing similar results. As results for both times of day are comparable, aerosol results are presented only for the 2 pm trajectory.

Aerosol formation was analyzed to determine the contributions of the VOC classes to the individual aerosol components. Vapor phase aerosol precursors include nitric acid, sulfate, and a variety of condensable organics generated in the gas phase. Nitric acid is formed via the following reactions,

$$NO_2 + OH \rightarrow HNO_3 \qquad \text{(R1)}$$

$$NO + NO_3 \leftrightarrow N_2O_5 \qquad \text{(R2}a\text{)}$$

$$N_2O_5 + H_2O \rightarrow 2\ HNO_3 \qquad \text{(R2}b\text{)}$$

with the first reaction occurring during the day, and the second tow predominantly at night. Sulfate (denoted SULF) is formed primarily by the reaction of SO_2 and the OH radical

$$SO_2 + OH \rightarrow SULF \qquad \text{(R3)}$$

As an example of a secondary organic aerosol constituent, the species denoted AEA4 is assumed to be produced as a result of the initial OH attack on the lumped higher alkane AAR4,

$$\text{AAR4} + \text{OH} \rightarrow \text{products} + y\,\text{AEA4} \qquad \text{(R4)}$$

where y is the aerosol yield for the reaction of AAR4, which has a value of 383 $\mu g\ m^{-3}$ ppm^{-1} reacted (Table 1).

The most straightforward manner of assigning these secondary aerosol constituents back to their precursors is to attribute HNO_3 to NO_2, SULF to SO_2, and AEA4 to AAR4. Clearly, if emissions of NO_x, SO_2, or AAR4 are decreased, formation of the associated aerosol will also decrease (but not necessarily in a one-to-one manner). Aerosol production does not, however, depend solely on these precursors, but is also influenced by the OH and NO_3 radicals with which they must react. Using the ozone assignment method, with OH and NO_3 selected as the dominant reactants in reactions R1-R4, it is possible to trace the aerosol constituents back to the organic species that were responsible for the formation of these radicals. Virtually all NO_3 radicals are produced in the reaction of O_3 and NO_2,

$$O_3 + NO_2 \rightarrow O_2 + NO_3 \qquad \text{(R5)}$$

Nighttime nitric acid can, therefore, be traced back to NO_3, to O_3, and then to the initial or emitted species that contributed to O_3.

The VOC assignments for AEA4, performed on the basis of the OH concentrations, are shown in Figure 5. Note that in Figure 5 none of the AEA4 produced is attributed to its organic precursor AAR4 since, in this case, all products in reaction R4

have been assigned back to OH instead of AAR4. By assigning AEA4 back to the OH radical instead of AAR4, we can measure the net OH production of the individual organics. Thus, Figure 5 is actually more a measure of OH production than AEA4 formation since AEA4 is only created by AAR4. The remaining organic species do, however, influence the rate at which AAR4 reacts to form AEA4. Species that act as OH sources, such as AAR6 and formaldehyde, increase radical levels and therefore accelerate aerosol formation, while OH sinks, like CO and the alkanes, tend to lower OH concentrations depressing aerosol formation. Results for assignment of SULF are virtually identical to those in Figure 5, with the aromatic species AAR6 and formaldehyde emerging as the largest contributors to aerosol, and the higher aldehydes, toluene and the alkenes, particularly ethene, also leading to significant amounts of aerosol. Since they are OH sinks rather than sources, CO and the alkanes (AAR1-AAR4) exhibit negative contributions.

The assignment of nitric acid back to initial and emitted species can be traced through reactions R1 and R2 to determine the effect of OH and NO_3 on nitric acid formation. Approximately 85% of HNO_3 at 2 pm at Rubidoux is formed during the day by reaction of OH with NO_2. Production of nitric acid via this reaction can be traced through the OH radical and, therefore, the relative contributions of the organics are the same as those found for AEA4 in Figure 5. The remaining 15% of the HNO_3 originates from N_2O_5, which is formed by the nighttime reaction of NO_3 with NO_2. Assignment of HNO_3 produced along this pathway is shown in Figure 6. Because ozone is the primary

intermediate controlling the nighttime production of HNO_3, Figure 6 reflects the ozone contributions of each species, and is, in many ways, similar to Figure 2. Figure 6, however, reflects only ozone production on August27, since any ozone created during August 28 is unavailable for nighttime reaction to form the nitric acid present at 2 pm on August 28 at Rubidoux. Additionally, the relative contribution of alkenes is smaller for HNO_3 formation than for O_3 production as a result of the alkene + NO_3 reaction that removes NO_3 radicals from the system. By combining daytime and nighttime contributions, the overall assignment of HNO_3 in Figure 7 is created. The aldehydes and the lumped aromatic AAR6, through their effect on OH and ozone, are the most significant non-NO_x precursors to nitric acid. These species are also the main contributors to organic aerosol and sulfate formation, and are large producers of ozone as well.

ACKNOWLEDGMENT

This work was supported by the Coordinating Research Council and the National Renewable Energy Laboratory.

REFERENCES

Air Resources Board (ARB) (1987) South Coast Air Basin emissions inventory for August 27-28, 1987. Sacramento, CA.

Allen P. D. (1993) Technical Support Division, California Air Resources Board, Sacramento, CA, personal communication.

Anderson-Sköld Y., Greenfelt P. and Pleijel K. (1992) Photochemical ozone creation potentials: a study of different concepts. *J. Air Waste Manage. Assoc.* **42**, 1152-1158.

Bowman F. M. and Seinfeld J. H. (1994*a*) Ozone productivity of atmospheric organics. *J. Geophys. Res.* **99**, 5309-5324.

Bowman F. M. and Seinfeld J. H. (1994*b*) Fundamental basis of incremental reactivities of organics in ozone formation in VOC/NO_x mixtures. *Atmos. Environ.* **28**, 3359-3368.

Carter W. P. L. (1991) Development of ozone reactivity scales for volatile organic compounds. EPA 600/3-91/050, U. S. Environmental Protection Agency, Research Triangle Park, NC.

Carter W. P. L. (1990) A detailed mechanism for the gas-phase atmospheric reactions of organic compounds. *Atmos. Environ.* **24**, 481-518.

Carter W. P. L. (1988) Documentation of a gas phase photochemical mechanism for use in airshed modeling. Final Report for the California Air Resources Board, Sacramento, CA.

Carter W. P. L. and Atkinson R. J. (1987) An experimental study of incremental hydrocarbon reactivity. *Environ. Sci. Technol.* **21**, 670-679.

Carter W. P. L. and Atkinson R. J. (1989) Computer modeling study of incremental hydrocarbon reactivity. *Environ. Sci. Technol.* **23**, 864-880.

Chan M. and Durkee K. (1989) Southern California air quality study B-site operations. Final report to the California Air Resources Board, Sacramento, CA.

Chang T. Y. and Rudy S. J. (1990) Ozone-forming potential of organic emissions from alternative-fueled vehicles. *Atmos. Environ.* **24**, 2421-2430.

Chico T. and Lester J. (1992) Application of the Urban Airshed Model for two SCAQS episodes in the South Coast Air Basin. Southern California Air Quality Study Data Analysis Conference, Los Angeles, CA.

Derwent R. G. and Jenkin M. E. (1991) Hydrocarbons and the long-range transport of ozone and PAN across Europe. *Atmos. Environ.* **25**, 1661-1678.

Fujita E. M., Croes B. E., Bennett C. L., Lawson D. R., Lurmann, F. W. and Main H. H. (1992) Comparison of emission inventory and ambient concentration ratios of CO, NMOG and NO_x in California's South Coast Air Basin. *J. Air Waste Manage. Assoc.* **42**, 264-276.

Goodin W. R., McRae G. J. and Seinfeld J. H. (1979) A comparison of interpolation methods for sparse data: Application to wind and concentration fields. *J. Appl. Met.* **18**, 761-771.

Grosjean D. and Seinfeld J. H. (1989) Parameterization of the formation potential of secondary organic aerosols. *Atmos. Environ.* **23**, 1733-1744.

Harley R. A., Russell A. G., McRae G. J., McNair L. A., Winner D. A., Odman M. T., Dabdub D., Cass G. R. and Seinfeld J. H. (1991) Continued development of a photochemical model and application to the Southern California Air Quality Study (SCAQS) intensive monitoring periods. Final report submitted to the Coordinating Research Council, Atlanta, GA.

Harley R. A., Russell A. G., McRae G. J., Cass G. R. and Seinfeld J. H. (1993) Photochemical modeling of the Southern California Air Quality Study. *Environ. Sci. Technol.* **27**, 378-388.

Hering S. V. and Blumenthal D. L. (1989) Southern California Air Quality Study (SCAQS), Description of the measurement activities. Final Report to the California Air Resources Board, Sacramento, CA.

Hildemann L. M., Russell A. G. and Cass G. R. (1984) Ammonia and nitric acid concentrations in equilibrium with atmospheric aerosol: experiment vs. theory. *Atmos. Environ.* **18**, 1737-1750.

McNair L., Russell A. and Odman M. T. (1992) Airshed calculation of the sensitivity of pollutant formation to organic compound classes and oxygenates associated with alternative fuels. *J. Air Waste Manage. Assoc.* **42**, 174-178.

McRae G. J., Goodin W. R. and Seinfeld J. H. (1982) Development of a second generation mathematical model for urban air pollution-I. Model formulation. *Atmos. Environ.* **16**, 679-696.

Pandis S. N., Harley R. A., Cass G. R. and Seinfeld J. H. (1992) Secondary aerosol formation and transport. *Atmos. Environ.* **26**, 2269-2282.

Pandis S. N., Wexler A. S. and Seinfeld J. H. (1993) Secondary aerosol formation and transport-II. Predicting the ambient secondary aerosol size distribution. *Atmos. Environ.* **27**, 2403-2416.

Pierson W. R., Gertler A. W. and Bradow R. L. (1990) Comparison of the SCAQS tunnel study with other on-road vehicle emission data. *J. Air Waste Manage. Assoc.* **40**, 1495-1504.

Pilinis C. and Seinfeld J. H. (1987) Continued development of a general equilibrium model for inorganic multicomponent atmospheric aerosols. *Atmos. Environ.* **21**, 2453-2466.

Seinfeld J. H. (1986) *Atmospheric Chemistry and Physics of Air Pollution*, Wiley, New York.

Wexler A. S. and Seinfeld J. H. (1992) Analysis of aerosol ammonium nitrate: departures from equilibrium during SCAQS. *Atmos. Environ.* **26**, 579-591.

Winer A. M. (1983) Investigation of the role of natural hydrocarbons in photochemical smog formation in California. Final Report to the California Air Resources Board, Sacramento, CA.

Table 1. Summary of organic species with corresponding aerosol species and aerosol yields.

Gas-phase Species[a]	Chemical Description	Aerosol Species	Aerosol Yield[b] ($\mu g\ m^{-3} ppm^{-1}$)
AAR1	lumped C2-C4 alkanes	AEA1	0
AAR2	lumped C5-C6 alkanes	AEA2	3.1
AAR3	lumped C7-C9 alkanes	AEA3	78
AAR4	lumped C10 + alkanes	AEA4	383
C6H6	benzene	-	-
TOLU	toluene	AETL	424
AAR5	mono-substituted benzenes	AEA5	426
AAR6	xylenes	AEA6	390
AAR7	naphthalenes, trimethyl benzenes	AEA7	563
ETHE	ethene	-	-
OLE1	lumped terminal alkenes	AEO1	9.2
OLE2	isobutene	AEO2	0
OLE3	lumped internal alkenes	AEO3	19
ISOP	isoprene	-	-
C7OL	heptene	AEC7	78
C8OL	octene	AEC8	227
C9OL	nonene	AEC9	306
APIN	α-pinene	AEAP	762
BPIN	β-pinene	AEBP	720
HCHO	formaldehyde	-	-
CCHO	acetaldehyde	-	-
RCHO	lumped aldehyde	-	-
ACET	acetone	-	-
MEK	lumped ketone	-	-
BALD	benzaldehyde	AEBA	5
C2H2	acetylene	-	-
ROH1	lumped alcohol	-	-
PBZN	peroxybenzoyl nitrate	AEPB	5
PHEN	phenol	AEPH	192
CRES	cresol	AECR	221
NPHE	nitropehenol	AENP	285

[a] Species names from the SAPRC mechanism (Carter, 1990) as extended by Pandis *et al.* (1992).

[b] Aerosol yields derived by Pandis *et al.* (1992).

Table 2. Initial mixing ratios for trajectories.[a]

Model Species	Initial Mixing Ratio (ppb)	Model Species	Initial Mixing Ratio (ppb)
inorganic		alkenes	
NO	5	ETHE	0.7
NO2	5	OLE1	0.3
HNO3	1	OLE3	0.3
SO2	1	ISOP	0.2
		C8OL	0.1
CO	113	carbonyls	
alkanes		HCHO	3.8
AAR1	2.3	CCHO	3.5
AAR2	0.5	RCHO	5.2
AAR3	0.6	ACET	0.7
AAR4	0.1	MEK	11
aromatics			
C6H6	0.1	C2H2	0.5
TOLU	0.6		
AAR5	0.1		
AAR6	0.9		

[a] Allen (1993)

Table 3. Summary of emissions compositions for the South Coast Air Basin and along trajectories terminating at 8 am and 2 pm on August 28, 1987 at Rubidoux, CA.

	Rubidoux, 8 am		Rubidoux, 2 pm		Basin Average
	Mixing Ratio (ppbC)	Fraction of VOC (% of Carbon)	Mixing Ratio (ppbC)	Fraction of VOC (% of Carbon)	Fraction of VOC (% of Carbon)
CO	1464		2881		
alkanes		**44.8**		**46.8**	**47.2**
AAR1	71	8.9	135	9.9	9.5
AAR2	137	17.3	250	18.3	18.2
AAR3	107	13.5	192	14.1	15.5
AAR4	40	5.1	62	4.5	4.0
aromatics		**24.8**		**25.3**	**27.5**
C6H6	25	3.1	45	3.3	3.8
TOLU	84	10.6	149	10.9	10.9
AAR5	13	1.6	22	1.6	1.9
AAR6	66	8.3	112	8.2	9.3
AAR7	10	1.2	17	1.3	1.5
alkenes		**11.9**		**13.3**	**15.5**
ETHE	40	5.1	81	6.0	6.4
OLE1	36	4.5	70	5.1	5.7
OLE2	2	0.2	3	0.2	0.3
OLE3	10	1.2	16	1.2	1.4
ISOP	2	0.2	2	0.2	0.9
C7OL	2.1	0.3	4	0.3	0.4
C8OL	1.4	0.2	2	0.1	0.2
C9OL	1.1	0.1	2	0.1	0.2
APIN	0.1	0.0	0.1	0.0	0.0
BPIN	0.2	0.0	0.5	0.0	0.0
carbonyls		**13.1**		**9.2**	**3.8**
HCHO	10	1.3	17	1.2	1.0
CCHO	13	1.6	19	1.4	0.9
RCHO	17	2.1	18	1.3	0.2
ACET	11	1.4	18	1.3	0.9
MEK	53	6.6	54	4.0	0.8
BALD	0.3	0.0	0.6	0.0	0.0
other					
C2H2	26	3.3	51	3.7	4.1
ROH1	17	2.1	23	1.7	1.9
Total VOC	792	100	1368	100	100

Table 4. Sources of emitted organic species for the South Coast Air Basin.

Organic Species	Chemical Description	Sources (%) Mobile	Stationary
alkanes			
AAR1	lumped C2-C4 alkanes	50.7	49.3
AAR2	lumped C5-C6 alkanes	67.9	32.1
AAR3	lumped C7-C9 alkanes	79.4	20.6
AAR4	lumped C10 + alkanes	39.4	60.6
aromatics			
C6H6	benzene	91.8	8.2
TOLU	toluene	71.7	28.3
AAR5	mono-substituted benzenes	85.6	14.4
AAR6	xylenes	88.4	11.6
AAR7	naphthalenes, trimethyl benzenes	92.1	7.9
alkenes			
ETHE	ethene	89.3	10.7
OLE1	lumped terminal alkenes	91.9	8.1
OLE2	isobutene	100.0	0.0
OLE3	lumped internal alkenes	92.9	7.1
ISOP	isoprene	3.2	96.8
C7OL	C7 alkenes	93.3	6.7
C8OL	C8 alkenes	49.2	50.8
C9OL	C9 alkenes	94.2	5.8
APIN	α-pinene	10.4	89.6
BPIN	β-pinene	100.0	0.0
carbonyls			
HCHO	formaldehyde	91.5	8.5
CCHO	acetaldehyde	95.7	4.3
RCHO	lumped higher aldehydes	81.7	18.3
ACET	acetone	47.6	52.4
MEK	lumped higher ketones	17.5	82.5
other			
C2H2	acetylene	92.1	7.9
ROH1	lumped alcohols	0.0	100.0

LIST OF FIGURES

Figure 1.

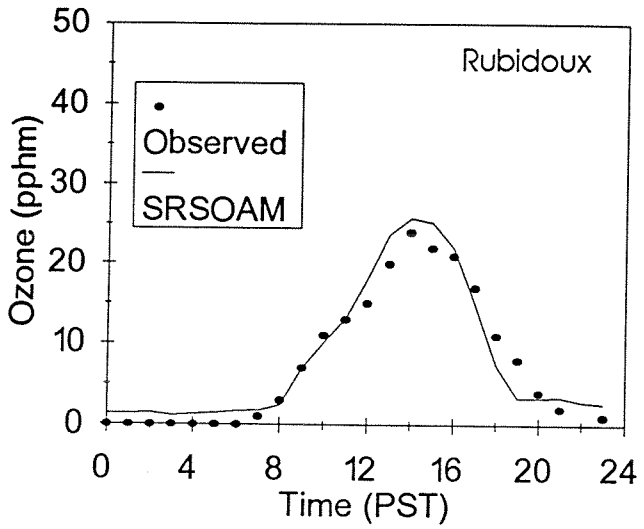
Rubidoux
Observed
SRSOAM
Ozone (pphm)
Time (PST)
0
10
20
30
40
50
0
4
8
12
16
20
24

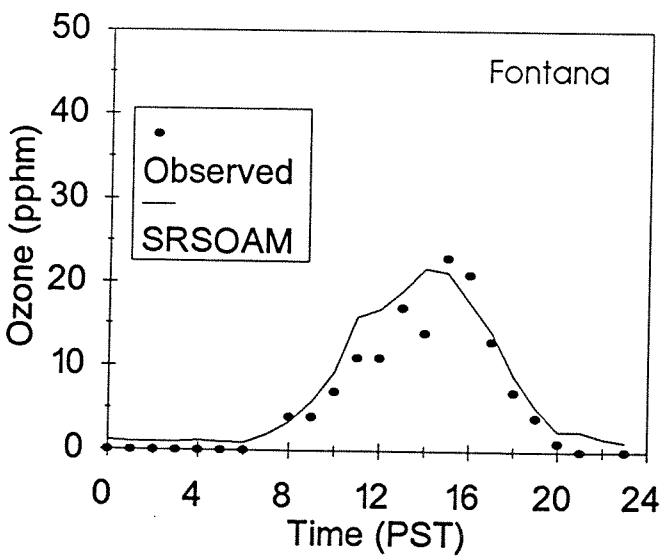
Fontana
Observed
SRSOAM
Ozone (pphm)
Time (PST)
0
10
20
30
40
50
0
4
8
12
16
20
24

Figure 2.

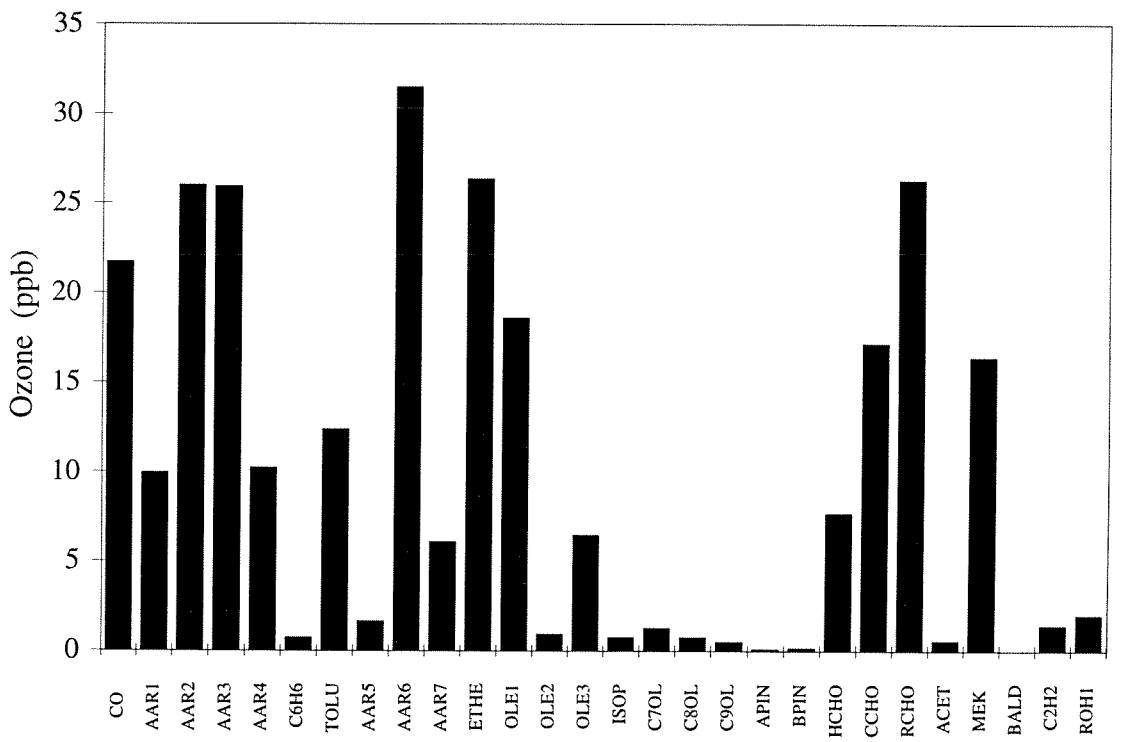
Ozone (ppb)
35
30
25
20
15
10
5
0
CO
AAR1
AAR2
AAR3
AAR4
C6H6
TOLU
AAR5
AAR6
AAR7
ETHE
OLE1
OLE2
OLE3
ISOP
C7OL
C8OL
C9OL
APIN
BPIN
HCHO
CCHO
RCHO
ACET
MEK
BALD
C2H2
ROH1

Figure 3.

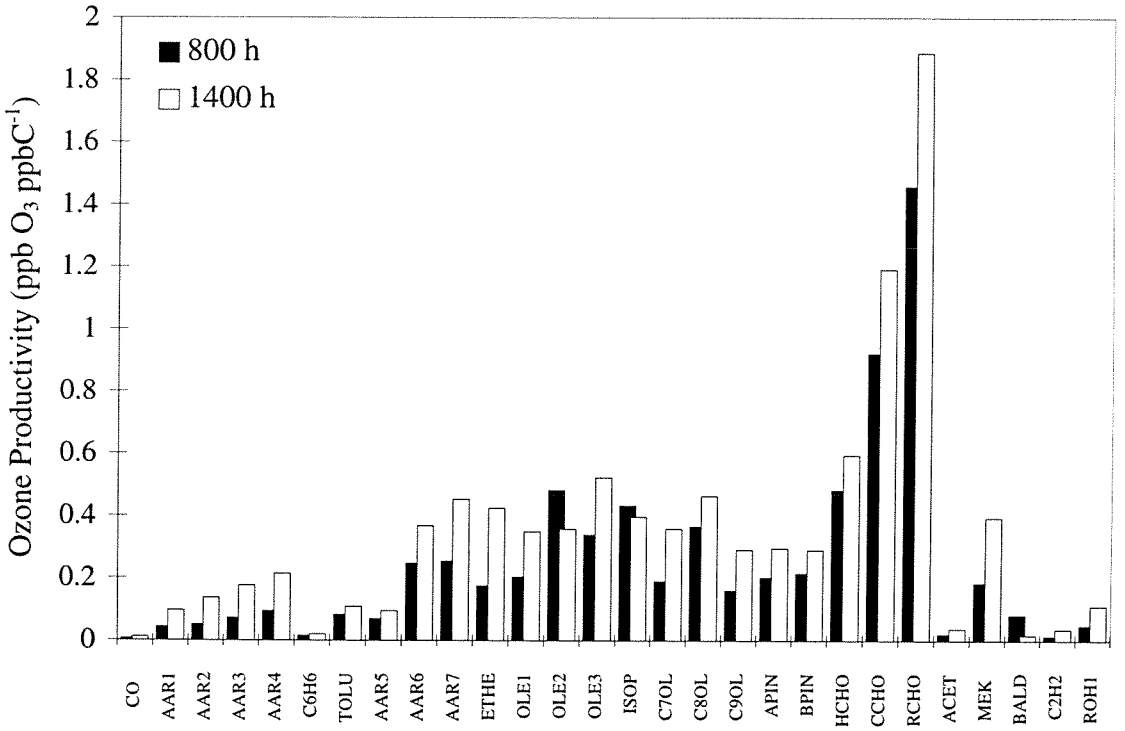
Ozone Productivity (ppb O_3 ppbC^{-1})
800 h
1400 h
2
1.8
1.6
1.4
1.2
1
0.8
0.6
0.4
0.2
0
CO
AAR1
AAR2
AAR3
AAR4
C6H6
TOLU
AAR5
AAR6
AAR7
ETHE
OLE1
OLE2
OLE3
ISOP
C7OL
C8OL
C9OL
APIN
BPIN
HCHO
CCHO
RCHO
ACET
MEK
BALD
C2H2
ROH1

Figure 4.

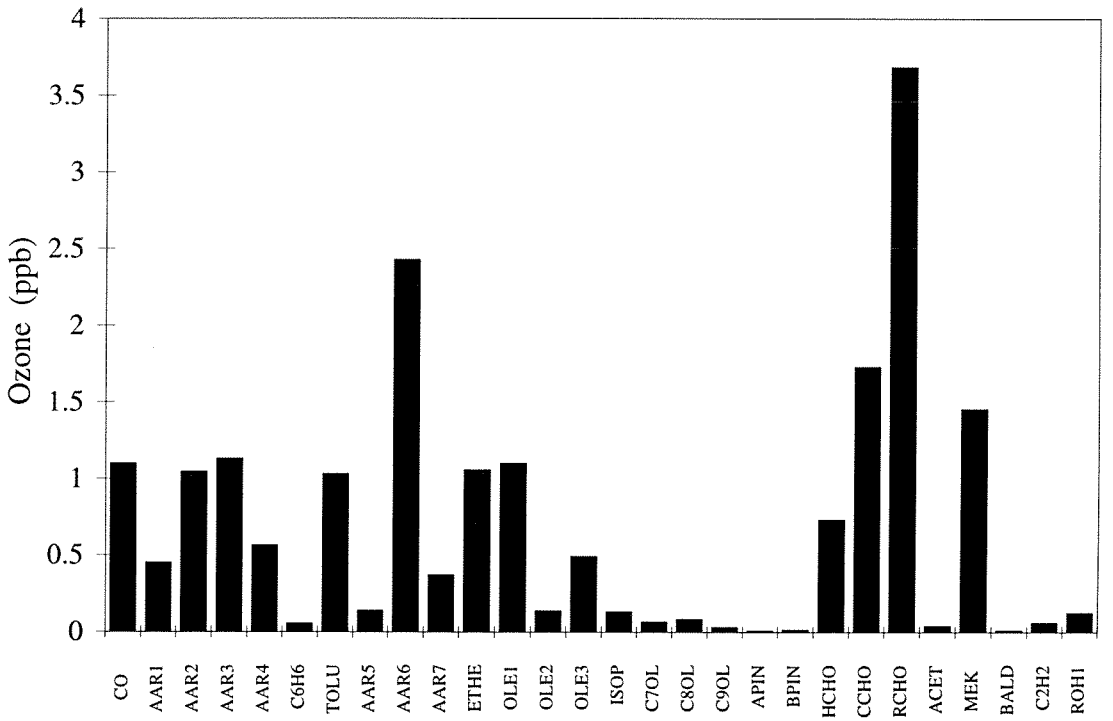
Ozone (ppb)
4
3.5
3
2.5
2
1.5
1
0.5
0
CO
AAR1
AAR2
AAR3
AAR4
C6H6
TOLU
AAR5
AAR6
AAR7
ETHE
OLE1
OLE2
OLE3
ISOP
C7OL
C8OL
C9OL
APIN
BPIN
HCHO
CCHO
RCHO
ACET
MEK
BALD
C2H2
ROH1

Figure 5.

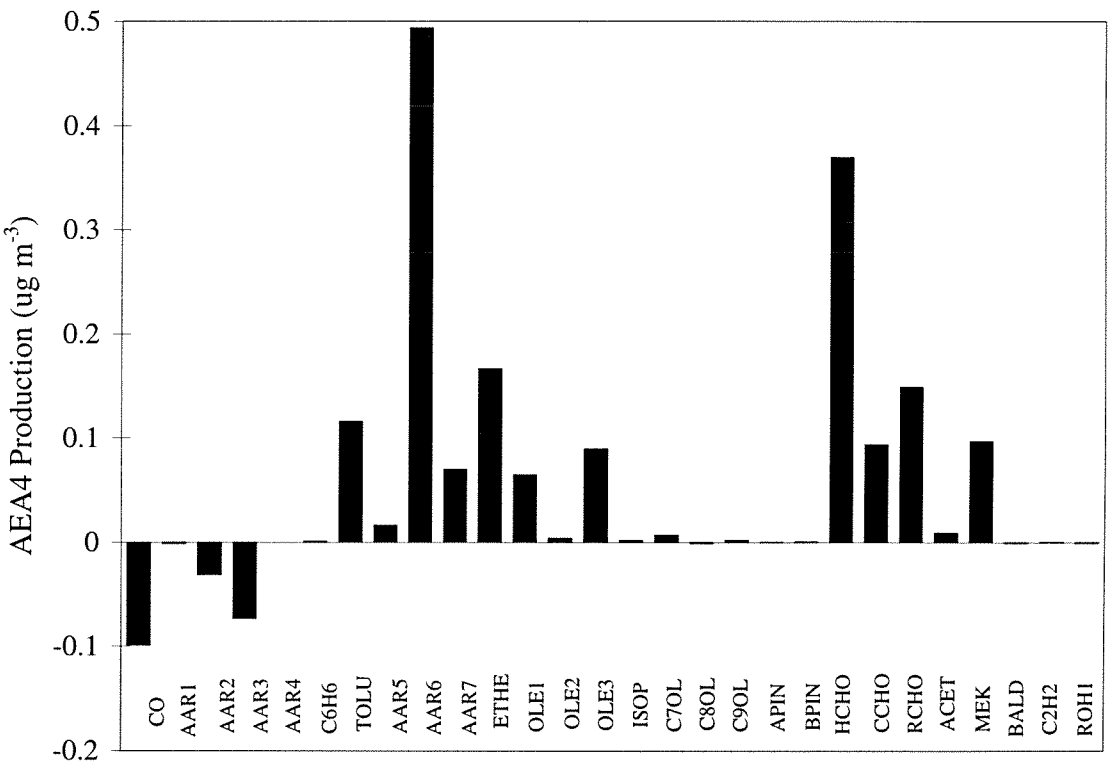
AEA4 Production (ug m-3)
0.5
0.4
0.3
0.2
0.1
0
-0.1
-0.2
CO
AAR1
AAR2
AAR3
AAR4
C6H6
TOLU
AAR5
AAR6
AAR7
ETHE
OLE1
OLE2
OLE3
ISOP
C7OL
C8OL
C9OL
APIN
BPIN
HCHO
CCHO
RCHO
ACET
MEK
BALD
C2H2
ROH1

Figure 6.

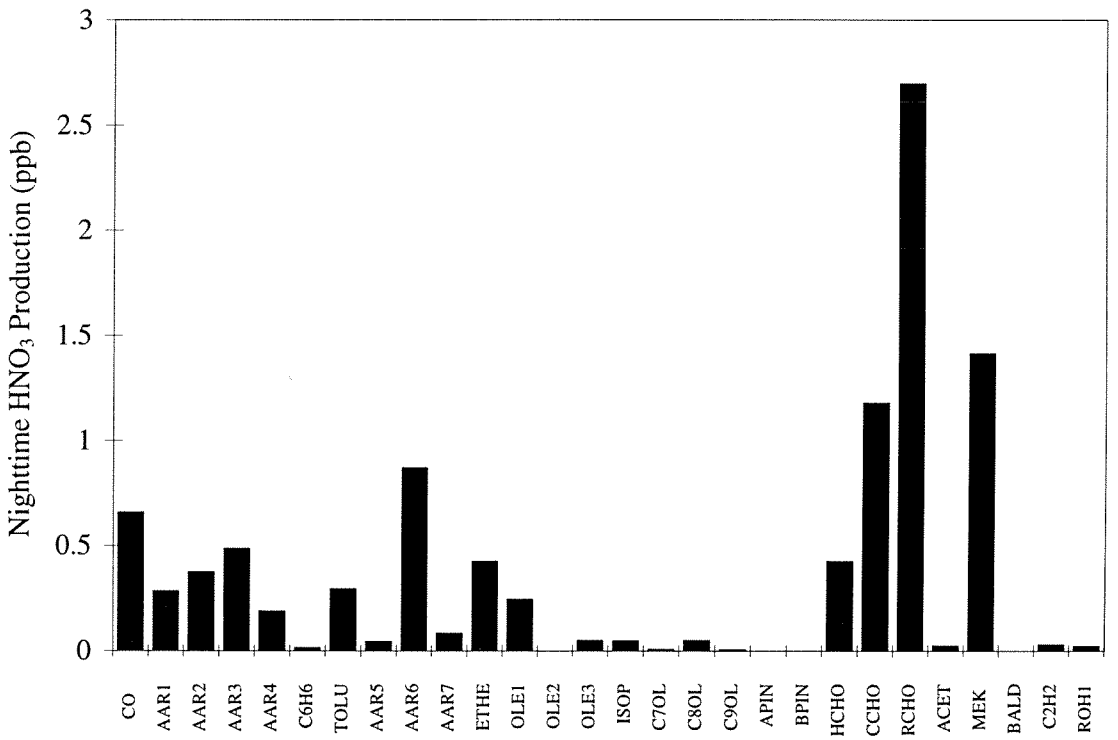
Nighttime HNO_3 Production (ppb)
3
2.5
2
1.5
1
0.5
0
CO
AAR1
AAR2
AAR3
AAR4
C6H6
TOLU
AAR5
AAR6
AAR7
ETHE
OLE1
OLE2
OLE3
ISOP
C7OL
C8OL
C9OL
APIN
BPIN
HCHO
CCHO
RCHO
ACET
MEK
BALD
C2H2
ROH1

Figure 7.

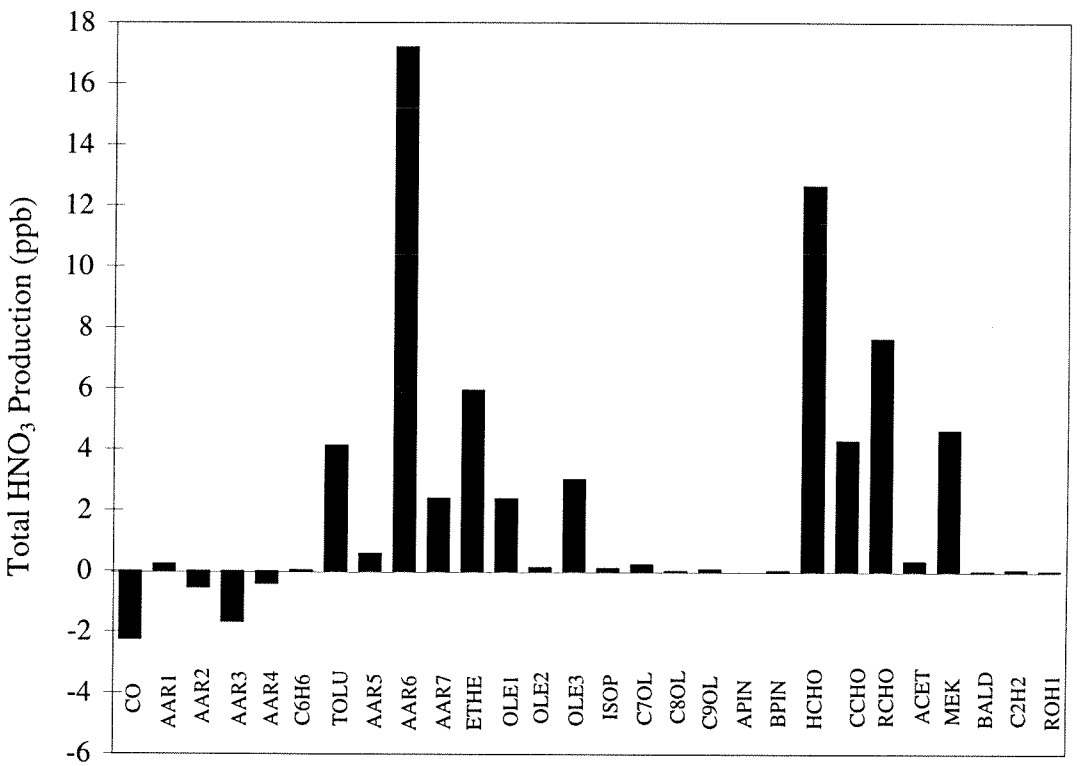
Total HNO_3 Production (ppb)
18
16
14
12
10
8
6
4
2
0
-2
-4
-6
CO
AAR1
AAR2
AAR3
AAR4
C6H6
TOLU
AAR5
AAR6
AAR7
ETHE
OLE1
OLE2
OLE3
ISOP
C7OL
C8OL
C9OL
APIN
BPIN
HCHO
CCHO
RCHO
ACET
MEK
BALD
C2H2
ROH1

CHAPTER 5:

ATMOSPHERIC CHEMISTRY OF ALTERNATE FUELS AND REFORMULATED GASOLINE COMPONENTS

Published in *Progress in Energy Combust. Sci.*, **21**, 387-417, (1995).

ABSTRACT

Recent air quality regulations have mandated the use of reformulated gasoline and alternate fuels in motor vehicles. Reformulated fuels are intended to reduce both ozone-forming volatile organic compound (VOC) emissions and air toxic emissions from vehicles. A method that allows the determination of the individual contributions of a single VOC to the ozone formation in a complex VOC/NO_x mixture is outlined and applied to eight reformulated fuel components. In calculations using a current comprehensive atmospheric chemical reaction mechanism, a wide variety of organics are shown to be responsible for ozone production. The incremental reactivities of the fuel components, which are defined as the additional amount of ozone formed per amount of organic compound added to a base mixture, include both the direct production of ozone by the oxygenate itself and additional ozone produced by the VOC mixture when the oxygenate is added. The enhancement of ozone production attributable to the organic mixture upon adding the oxygenates is shown to be a result of changes to the organic free radical pool. Most of the fuel oxygenates have relatively low incremental reactivities due to their slow reaction rates and to the formation of relatively unreactive formate and acetate products. The more reactive fuel oxygenates are those containing ethyl groups, which react faster than their counterparts containing only methyl and *tert*-butyl groups.

INTRODUCTION

The 1990 Clean Air Act Amendments mandate the use of reformulated gasoline in motor vehicles. Beginning in January 1995, so-called Phase I reformulated gasoline is intended to provide a 15 to 17% reduction in both ozone-forming volatile organic compound (VOC) emissions and air toxics emissions from vehicles. Then, beginning in January 2000, Phase II reformulated gasoline is intended to provide a 25 to 29% reduction in VOC emissions, a 20 to 22% reduction in air toxics emissions, and a 5 to 7% reduction in nitrogen oxides emissions from vehicles. The reformulated gasoline provisions of the Amendments require the addition of oxygenates to gasoline.

In 1990 the California Air Resources Board (CARB) adopted motor vehicle emissions regulations that included a reactivity adjustment (CARB, 1992). The reactivity adjustment factors (RAFs) are calculated from the measured composition of emissions associated with a particular fuel, with the emissions fraction of each organic compound weighted by an "incremental reactivity" that is calculated from an atmospheric chemical mechanism. The mechanism used to compute these incremental reactivities is that developed by Carter (1990).

Atmospheric ozone formation is the result of a complex series of sunlight-driven reactions involving volatile organic compounds (VOCs) and oxides of nitrogen (NO_x) (NRC, 1991). The rate of ozone formation is governed mainly by the reactivity of the total organic gases (TOG) in the atmosphere and the ratio of TOG to nitrogen oxides

(NO_x). TOG consists of thousands of compounds, including hydrocarbons and oxygenated hydrocarbons (alcohols, carbonyls, ethers, and esters). The reactivity, or the rate at which ozone is formed, varies widely for different TOG compounds. The reactive species in TOG are frequently referred to as volatile organic compounds (VOCs). Two other definitions of the organic mixture are also used: NMOG, which is nonmethane organic gases (TOG minus methane), and, for methanol fuels only, organic matter hydrocarbon equivalent (OMHCE), which is defined as TOG minus the oxygen in methanol and formaldehyde. The reformulated gasoline provisions of the 1990 Clean Air Act Amendments are aimed primarily at reducing both the total mass emissions of VOCs from motor vehicles and the atmospheric ozone-forming potential, or reactivity, of those emissions. A number of programs have assessed the effect of the use of reformulated gasolines on vehicle emissions; the most comprehensive of these is the Auto/Oil Air Quality Improvement Research Program (Cohen *et al.*, 1994).

The effect of changing vehicle emissions on atmospheric ozone formation is assessed using chemical kinetic models of atmospheric chemistry. These models are based on chemical oxidation mechanisms of the array of organic species present in vehicle emissions and in the atmosphere. The atmospheric VOC/NO_x chemistry that leads to ozone formation is highly complex and determining the influence of changing a single VOC's emissions on the amount of ozone formed is accomplished by solving the chemical kinetic model after perturbing each VOC by a small amount one VOC at a time. The result is the so-called incremental reactivity with respect to ozone formation of each

VOC. Then given a set of exhaust and evaporative emissions profiles from a vehicle or fleet of vehicles corresponding to a set of fuels, the relative ozone-forming potential can be assessed. This procedure is emerging as the regulatory approach to evaluating the atmospheric impact of a reformulated gasoline or alternate fuel.

This article reviews the methodology to determine the ozone-forming potential of individual organic molecules and applies that methodology to reformulated gasoline and alternate fuel components. We focus particularly on elucidating mechanistically the ozone-forming potential of each component.

We begin with a summary of the 1990 Clean Air Act Amendments provisions relating to motor vehicle emissions and reformulated fuels. We then discuss general aspects of atmospheric chemical mechanisms and approaches to computing incremental reactivities. A method that allows the determination of the individual contribution of a single VOC to the ozone formed in a complex VOC/NO_x mixture is then outlined and applied to eight reformulated fuel components.

MOTOR VEHICLE EMISSIONS AND REFORMULATED FUEL REGULATIONS

As a result of the 1990 Clean Air Act Amendments, there now exist in federal law five categories of ozone non-attainment - in increasing order of severity: marginal, moderate, serious, severe, and extreme (Section 181), as shown in Table 1. A region's

attainment status is based upon the fourth highest one-hour ozone concentration measured at a site over a three-year period. One violation per year is deemed acceptable, thus the fourth highest recorded value represents the so-called design value for non-attainment classification purposes. There exist a number of mandatory provisions of the Act aimed at reducing the contribution of motor vehicle emissions to urban ozone formation.

Stage II vapor recovery is required at the gasoline pump, to trap and retain evaporative VOC emissions (Section 182). This requirement applies to gasoline dispensing operations with throughputs of 10,000 gallons per month or more for all areas classified as moderate, serious, severe, and extreme.

Enhanced vehicle inspection and maintenance programs are required, replacing the existing test with the IM 240 test procedure that simulates the drive cycle. The test is to be performed biennially and the program is to become operational January 1, 1995. Enhanced vehicle inspection and maintenance is mandatory for all serious, severe, and extreme non-attainment areas as well as in metropolitan statistical areas with populations greater than 100,000 that lie within the Northeast ozone transport region (OTR).

Federal Tier I cars are required in model year 1994 (Section 203(a)(g)). Tier I cars and other light-duty vehicles must meet stricter tailpipe emissions standards than earlier model-year vehicles (Table 2). The standards apply to three pollutants: non-methane hydrocarbons (NMHC), carbon monoxide, and, nitrogen oxides. As well, these standards apply to two in-use milestones: 5 years/50,000 miles and 10 years/ 100,000 miles, as shown in Table 2. The implementation schedule for Tier I vehicles is: 40% of a

manufacturer's sales volume must be Tier I vehicles in 1994; 80% in 1995; and 100% beyond 1995.

Federal reformulated gasoline (RFG) must be introduced as Phase I RFG in 1995 (Tables 3 and 4) and Phase II RFG in 2000. The goal of reformulating gasoline is to reduce total emission levels, both exhaust and evaporative emissions, to reduce emissions of toxic compounds, and to reduce the reactivity of emissions. Compositional changes usually associated with gasoline reformulation include lower Reid Vapor Pressure (RVP), lower sulfur content, lighter distillation (as expressed by T_{50} and/or T_{90}, the temperature at which 50% or 90%, respectively, of the fuel vaporizes), lower aromatic content, lower benzene content (benzene is a toxic compound), lower olefin content, and addition of oxygenates. There are two types of oxygenates sold today--nonrenewable oxygenates made from natural gas (methanol and methyl tertiary butyl ether, MTBE) and renewable oxygenates (ethanol and ethyl tertiary butyl ether, ETBE), which can be made from corn, other grains, wood, and even garbage, but are currently produced primarily via nonrenewable processes. The addition of alcohols has been found to lead to increased evaporative emissions. Whereas it is possible to lower the volatility of the base blend stock gasoline to offset part of this problem, this approach results in additional costs for alcohol blended reformulated gasoline.

Exhaust compositions differ from fuel compositions in several important areas:

- Generation of light olefins
- Generation of carbonyls

- Depletion of paraffins and ethers
- Enrichment of benzene

Exhaust NMOG is not simply unburned fuel; a significant fraction is composed of products of partial combustion, and in general combustion products have higher reactivity than unburned fuel. Some changes in fuel composition lead to directly offsetting reactivity effects. For example, methyl tertiary butyl ether (MTBE) in the fuel, which has relatively low reactivity, produces olefins and aldehydes in exhaust emissions, which have relatively high reactivity. Also, paraffins in the fuel, of relatively low reactivity, produce olefins in the exhaust. Since a decrease in high-reactivity fuel components is offset by an increase in high-reactivity exhaust components, the specific reactivity of exhaust emissions is less sensitive to changes in gasoline composition than might be imagined. It is, in fact, the reduction in overall NMOG emissions that is most responsible for a reduction in the ozone generated when reformulated gasoline is in use.

Preparing an EPA approved plan for achieving attainment, and eventually reaching attainment, are mandatory provisions of the 1990 Act. Faced with the prospect of possibly not reaching attainment through mandatory control measures, those options labeled in the Act as supplemental may indeed be mandatory with respect to the attainment goals of the Act.

California reformulated gasoline could be adopted in the states. California Reformulated Gasoline (RFG) is essentially a more severely reformulated gasoline than either federal Phase I or Phase II RFG (Table 5). Federal Phase I RFG sales begin in

1995. This gasoline differs primarily from current fuels in that a minimum oxygen weight is prescribed (2%), maximum benzene by volume is 1%, and NO_x emissions must meet a yet-to-be determined standard, using a baseline vehicle and gasoline type. Phase II federal RFG sales must commence in 2000. In this fuel, no lead is allowed and detergent additives are required. California (Phase II) RFG goes beyond the federal Phase II requirements by stipulating greater hydrocarbon reductions, lower RVP and California RFG would be introduced earlier.

The important process of modeling the emissions changes associated with changing fuel parameters is currently in a state of transition. The previous EPA model used for such purposes (the "Simple" model) has now been replaced with the "Complex Model." In the Simple Model, which is to be applied from 1995 to 1997, the fuel variables used to predict VOC emissions are RVP and oxygen content; those to predict toxics emissions are RVP, oxygen, benzene, and aromatics content. The NO_x emissions standard is deemed satisfied as long as the fuel oxygen content is less than 2.7 weight percent. The Complex Model is to be applied after 1998. In it, the fuel variables are RVP, oxygen, benzene, aromatic, olefin, and sulfur contents, and E200 (the percent of the fuel that evaporates at 200°F) and E300 (the same at 300°F).

The states could choose to adopt the California Low Emission Vehicle (CALEV) Program. The CALEV program was designed by the California Air Resources Board (CARB) to address the worst ozone problem extant in the United States - the Los Angeles

region (in the South Coast Air Basin) which is the sole extreme non-attainment area in the country. Defined within the CALEV program are five types of light-duty vehicles,

- conventional
- transitional low emission vehicle (TLEV)
- low emission vehicle (LEV)
- ultra-low emission vehicle (ULEV)
- zero-emission vehicle (ZEV)

These new vehicle definitions are based, in part, on increasingly strict 50,000 mile tailpipe emission rate standards (expressed in grams per mile), shown in Table 6. With one exception (zero emission vehicles) the CALEV program does not explicitly mandate when certain categories of vehicles must be offered for sale; rather, the mix of vehicle types is established indirectly by setting an increasingly tighter (i.e., lower) fleet average tailpipe emissions rate goal that must be achieved.

The EPA may, in 1997, decide that Federal Tier II vehicles (with lower emissions than Tier I) are necessary to reach attainment, and mandate their sale by model year 2004. Section 203 of the 1990 Clean Air Act Amendments sets emissions standards for the Federal Tier II vehicle. If required, then the Tier II vehicle would have to be available for model years after January 1, 2003. The Tier II car does not precisely fit into any of the categories of the CALEV program, as shown by the tailpipe emissions standards for the TLEV, LEV, and Tier II vehicles given in Table 7.

An important difference between Tier II and LEV standards is that the Tier II numbers shown in Table 7 are 100,000 mile standards, and must be compared to LEV standards at the corresponding mileage. Recognizing that vehicle emissions deteriorate with time and mileage, the Tier II vehicle will have to produce substantially lower emissions at the 5 year/50,000 mile point than at 10 years/100,000 miles. The Tier II car therefore falls somewhere between the TLEV and LEV vehicles in terms of hydrocarbon emissions performance. The actual difference in the effect of the hydrocarbon standards would be somewhat reduced if California reformulated gasoline were not available for in-use operation of LEV vehicles. When it is considered that the Tier II car has equal or lower NO_x emissions, and lower CO emissions than its LEV-family counterpart, it is probably most comparable to the LEV standard vehicle.

OZONE FORMATION AND ORGANIC REACTIVITY

Ozone is formed when an oxygen atom is added to the oxygen molecule. Oxygen atoms are produced in the atmosphere through photolysis of NO_2, which results in an oxygen atom and a molecule of nitric oxide (NO). In turn, the NO reacts with ozone to produce O_2 and NO_2, and in this cycle, pumped by sunlight, the net ozone remains constant. When organic compounds are present, however, their oxidation leads to peroxy radicals that convert NO to NO_2 without destroying an ozone molecule, resulting in a net

ozone increase over that available from the $NO_2/NO/O_3$ photolytic cycle (NRC, 1991; Seinfeld, 1986; Atkinson, 1990). Thus, organic compounds are key components in the formation of ozone, and the importance of each organic compound is measured by reactivity. One measure of the ozone formation potential of an organic/NO_x mixture is its VOC-to-NO_x concentration ratio. At low VOC-to-NO_x ratios the rate of ozone formation is governed by the amount of VOC present (i.e., the rate is VOC limited). At higher ratios the air parcel is considered to be NO_x limited; that is, ozone formation is limited mainly by the availability of NO_x rather than VOCs. The addition of more VOCs to a NO_x-limited air mixture increases ozone very little. In the unpolluted troposphere ozone formation is usually NO_x limited.

There has been considerable research into methodologies for ranking organic compounds based on their ozone formation potential. One approach is to rank compounds by their rate constant for reaction with the hydroxyl (OH) radical, which for most compounds is the principal reaction that initiates ozone formation. However, this OH, or kinetic, reactivity does not consider further reactions of the products of the initial reaction with the hydroxyl radical - what might be called the mechanistic reactivity. Recently, Carter developed an ozone reactivity scale that addresses both the kinetic reactivity and the mechanistic reactivity of individual organic compounds (Carter and Atkinson, 1989; Carter, 1991, 1994). Carter used a photochemical box model to estimate ozone formation potentials for individual organic compounds, that is, incremental reactivity factors that estimate the amount of ozone formed per amount of organic

compound added to a base mixture. Incremental reactivity factors were calculated for two different regimes: (1) maximum incremental reactivity (MIR) factors that estimate the maximum ozone formation potential of an organic compound and are representative of low VOC-to-NO_x ratios (about 4 to 6 ppb $ppbC^{-1}$) and moderate ozone concentration conditions; and (2) maximum ozone reactivity (MOR) factors that estimate the incremental ozone formation potential of an organic compound under moderate VOC-to-NO_x ratio conditions (about 6 to 8 ppb $ppbC^{-1}$) that are most conducive to ozone formation.

The Carter MIR and MOR factors represent a methodology for ranking individual organic compounds based on their ozone formation potential under the conditions used in developing them. Reactivity factors depend on the particular conditions used as inputs to the model calculations and on the chemical mechanism employed. The input conditions used for the Carter factors are EPA's Empirical Kinetic Modeling Approach (EKMA) scenarios, representing conditions from 39 urban areas in the United States and developed using atmospheric measurements and hourly emissions estimates for the various areas. Uncertainties in the input parameters, as well as variations among scenarios, contribute to reactivity uncertainties. The formulation of the chemical mechanism contains some uncertainty; differently formulated chemical mechanisms result in different reactivity factors (see next section). In addition, the reactivity factors themselves contain uncertainties because box model calculations provide a simplistic representation of ozone formation. Specifically, box models do not treat three-dimensional spatial variation in

pollutant concentrations and carry-over of pollutants from one day to the next. Three-dimensional transport and dispersion effects are always important in determining the ozone maximum achieved in a region; thus, where possible, a three-dimensional airshed model is preferred to the use of box-model derived reactivity factors. Consequently, MIR and MOR factors are best used to estimate ratios of reactivities between different compounds and emissions.

The MIR and MOR factors are used to estimate the relative reactivity of an organic mixture (e.g., of an exhaust or evaporative test) by summing the products of the mass of the individual compounds in the mixture times the MIR or MOR factor for that compound and dividing the sum by the total mass of the organic mixture. This procedure assumes that the mass-weighted incremental reactivity of individual organic species is additive. Given the nonlinear nature of ozone formation, this assumption is valid only when the mixture being evaluated is a minor part of the overall total VOC in the atmosphere. MIR and MOR reactivities are expressed in terms of either potential grams ozone per gram organic compound or as potential moles ozone per mole carbon in the organic compound. For exhaust and engine-out tests, since one knows the amount of organic compounds emitted per mile, the MIR and MOR reactivities for a test can be expressed as potential grams ozone per mile.

DEVELOPMENT AND TESTING OF ATMOSPHERIC CHEMICAL REACTION MECHANISMS

Assessment of the reactivity of a given organic compound is done by means of an atmospheric chemical reaction mechanism. The mechanism development process begins with the assembly of reactions and rate parameters from chemical and thermodynamic theory, the chemical literature, and from recommendation and evaluation studies. Not all rate data or mechanistic pathways of interest are available in the literature. Laboratory kinetic measurements must often be performed to determine these, but frequently at conditions significantly different from those in the atmosphere. The required extrapolation introduces uncertainty into the mechanism. Also, important competing processes may not have been present in the laboratory kinetics measurement system leading to either unintentionally ignoring important reactions or, where this problem is recognized, requiring the use of estimation methods to account for their absence. As a result, throughout the mechanism development process some form of testing is used to determine the importance of inclusion or exclusion of a given reaction and to assess the sensitivity of the mechanism's predictions to the choice of rate parameters. These parameters generally have some uncertainty as a result of the use of estimation techniques or of experimental measurement uncertainty. In addition, some form of testing for completeness of the mechanism must be performed.

In most cases, these tests have included the simulation of smog chamber experiments. In analyzing the data from smog chamber experiments, one must identify and quantify any chamber conditions that influence the chemical transformation processes, such as the magnitude and spectral distribution of the photolytic rates in the chamber, the temperature, humidity, and mixing characteristics of the chamber, the magnitude and production mechanisms of chamber radical sources, and chamber walls as sinks for intermediate and final products (e.g., HNO_3, H_2O_2). The lack of analytical techniques that are both highly sensitive and specific for important chemical species, such as OH and HO_2, present limitations on the data available for analysis.

Chemical mechanisms that have enough detail to describe the features of large sets of smog chamber data may be too detailed to be used in three-dimensional air quality models. Therefore, generalization processes are applied to these more complex models to produce a more practically sized mechanism for use in air quality models without sacrificing significant accuracy of prediction. This step is generally described as producing a "condensed chemical mechanism" by a process referred to as "lumping."

Current reaction mechanisms for urban and regional-scale ozone formation have important elements of uncertainty. For most organic compounds the main atmospheric oxidation reaction is with the OH radical, and while the primary OH rate constant is usually known, product yields and chemistry occurring subsequent to the primary OH attack are not. Values of rate constants and product yields obviously influence the predictions of a mechanism. Stockwell *et al.* (1993) have compiled uncertainty estimates

for the primary reactions of approximately 25 organic compounds of specific interest to incremental reactivity studies in the detailed chemical mechanism of Carter (1990), that used by the CARB to calculate the incremental reactivities for its reformulated gasoline regulations and that employed in the present study. (Uncertainties arising from yields (especially branching ratios), unknown or obsolete chemistry, alternative lumping schemes, and covariance between different parts of the mechanism were not considered in the Stockwell *et al.* (1993) study.) With respect to lumping schemes, in the Carter mechanism MEK, RCHO, -OOH, CRES, and some other model species represent classes of compounds that are assumed to react similarly. This is sometimes referred to as the "lumped molecule approach." In this case there is additional uncertainty, beyond that associated with the rate constants of individual compounds, arising from the adequacy with which a single rate constant for the class represents the rate constant for the mixture of compounds being represented. For example, MEK is used to represent some of the alkane bi- and poly-functional products as well as higher ketones and other compounds. These compounds might react with OH radicals and photolyze at quite different rates than is assumed for the class MEK. Moreover, methyl ethyl ketone itself may only be a small component of the mixture of compounds represented by MEK in the mechanism. Of the eight reformulated gasoline components considered in the present study, Stockwell *et al.* (1993) estimated the uncertainty factors in the 298 K OH rate constants of methanol, ethanol, methyl tertiary butyl ether, and ethyl tertiary butyl ether as 1.58, 1.58, 1.4, and 1.4, respectively. We will not address the effect of these uncertainty factors in this work.

SIMULATION OF URBAN OZONE FORMATION

For our study we have used the detailed mechanism developed by Carter (1990) in a one-cell trajectory model to explore the VOC/NO_x chemistry of a typical urban ozone scenario. The version of Carter's mechanism used contains 29 organic species, including four lumped alkanes, three lumped aromatics, three lumped alkenes (two anthropogenic and one biogenic), and eight explicitly represented oxygenates. Mechanisms for the eight fuel component oxygenates are based on recent mechanistic studies and have been added to the Carter mechanism. A full listing of the mechanism is contained in Appendix A, and a later section will discuss the oxygenate mechanisms in detail. The lumped species within the mechanism represent a composite of the individual species present in an organic mixture, with species assigned to the lumped groups based on their OH radical rate constants. A list of each organic species within the mechanism, together with a chemical description, is found in Table 8.

The trajectory model that w have employed is a software program developed at the Statewide Air Pollution Research Center, University of California, Riverside (SAPRC) (Carter, 1988) to conduct calculations identical to the EPA's OZIPM4 computer program (EPA, 1989) and is the same model used by Carter for his incremental reactivity calculations. As noted earlier, the model is a single-cell box that includes continuous emissions, entrainment of pollutants from aloft as the inversion height

changes, and time-varying temperature, humidity, and photolysis rates. Model inputs were based on Carter's "averaged conditions scenario," (Carter, 1994) an average of the 39 EPA EKMA scenarios, and is designed to be representative of conditions in urban areas of the United States.

The VOC mixture used for initially present and emitted hydrocarbons was that used by Carter and is based on EPA data for hydrocarbons and the 1987 Southern California Air Quality Study (SCAQS) data for oxygenates. A small amount of several oxygenated alternate fuel and reformulated gasoline components were also added to Carter's base mixture for our study. Concentrations in the aloft mixture, which contained 30 ppbC VOC, 500 ppb CO, and 70.4 ppb O_3, are an average of concentrations from the EKMA scenarios. Methane was assumed present at a global background level of 1790 ppb in both initial and aloft mixtures. NO_x was present initially as 73.5% NO, 24.5% NO_2, and 2% HONO, while NO_x emissions contained 94.9% NO, 5% NO_2, and 0.1% HONO. NO_x levels were selected to correspond to the situation of maximum incremental reactivity (MIR), where changes in organic concentration have the greatest effect on ozone levels. The MIR condition was selected for consistency with Carter's incremental reactivity studies (Carter, 1991, 1994) and to minimize the sensitivity to scenario inputs (Carter, 1994). The total available concentration of each reactant, comprised of initial concentration, emissions, and entrainment from aloft, are listed in Table 8. Note that the concentrations are reported in units of mmoleC m^{-2} so as to be independent of mixing

height, which increased from 293 m, at 8 am, to 1823 m, at 6 pm. Table 9 presents a summary of the scenario conditions used for our calculations.

CONTRIBUTIONS TO OZONE FORMATION BY INDIVIDUAL VOCS

Incremental Reactivity

The incremental reactivity method developed by Carter and Atkinson (1989) produces a measure that is best used for evaluating the relative effects on ozone of changing individual organic emissions. In this approach, a small amount of an individual organic is added to a base case mixture in a chemical mechanism, and the change in peak ozone levels resulting from the additional or incremented organic is simulated. The incremental reactivity (IR) for an organic species *i* is then defined as

$$IR_i = \frac{\Delta_i[O_3]}{\Delta[VOC_i]} \qquad (1)$$

where $\Delta_i[O_3]$ is the change in peak ozone concentration from a base case scenario as a result of an incremental change in species *i*, and $\Delta[VOC_i]$ is the incremental change in concentration, on a carbon atom basis, of organic species *i*. Incremental reactivities are intended to be calculated in the limit as $\Delta[VOC_i]$ approaches zero; in practice $\Delta[VOC_i]$ is chosen such that the incremental amount of ozone formed is larger than numerical errors

associated with the calculation, but still within the range where the change in ozone is linearly proportional to the amount of VOC_i added.

For a given species *i*, incremental reactivity can be expressed as the product of kinetic and mechanistic reactivities (Carter and Atkinson, 1989).

$$IR_i = KR_i\ MR_i \qquad (2)$$

Kinetic reactivity, KR_i, is the fraction of total emitted* species *i* that reacts during the scenario, and is a measure of the species' overall reaction rate under the given conditions. Mechanistic reactivity, MR_i, is, therefore, the ratio of total incremental reactivity to kinetic reactivity and can be viewed as the amount of additional ozone produced by each additional amount of species *i* reacting. By expressing incremental reactivity as the product of kinetic and mechanistic factors, the effect of the initial rate of reaction of a species (usually with OH) can be separated from the influence of its photooxidation mechanism.

We have performed incremental reactivity calculations, using the previously described scenario, for each of the organic mechanisms species as well as the entire VOC mixture itself. Results of these calculations are summarized in Table 10. The relative ranking of incremental reactivity values among the different organics is the same as that

* For the purposes of this paper the term "emitted species" refers to the total amount of the species that is introduced into the model cell, and is defined as the sum of the initially present amount, emissions, and entrainment from aloft.

obtained by Carter in previous studies (Carter and Atkinson, 1987, 1989; Carter 1994). Formaldehyde has the highest incremental reactivity of the species in the mechanism, followed by the higher aromatics, the aldehydes, and alkenes; next highest are the lower aromatics and then the alkanes. Benzaldehyde actually causes a decrease in peak ozone when added to the mixture, resulting in a negative incremental reactivity. The oxygenated fuel species, showing relatively low incremental reactivities in the range of the alkanes and lower aromatics, will be discussed in detail later.

The effect of reaction rate on incremental reactivity can be seen clearly by examining the results for methane. While methane has one of the highest mechanistic reactivities, expressing the efficiency with which a molecule of methane produces ozone, its very slow rate of reaction leads to an incremental reactivity near zero. Conversely, the lumped alkene species, OLE1 and OLE2, have lower mechanistic reactivities, but react almost completely, resulting in relatively high overall incremental reactivities.

Mechanistic reactivity values represent the overall effect on the reaction mixture of an individual VOC's photooxidation mechanism. This includes both the amount of ozone produced directly by the additional VOC that has been added to the mixture as well as changes in ozone production by the other VOCs as a result of changes to the mixture chemistry upon adding the individual VOC. Formaldehyde, which creates over 5 additional ozone molecules for each additional molecule of formaldehyde that reacts, an amount that is not possible if due only to the direct reactions of HCHO, does so by enhancing the ozone-forming capability of the entire VOC mixture. Addition of

benzaldehyde, which has strong radical loss pathways that lead to lower overall radical levels, produces the opposite effect, reducing ozone production by the organic mixture, resulting in a negative mechanistic reactivity. These changes in the VOC/NO_x chemistry of the mixture are the result of changes in the radical pool and will be discussed further in the following sections.

Ozone Assignment

The assignment method is a technique whereby the amount of secondary pollutants of interest generated by the individual organics in a complex VOC/NO_x mixture is calculated (Bowman and Seinfeld, 1994*ab*; Bowman *et al.*, 1995). Full mathematical details of this method are presented in Appendix B. The basic objective of the technique is to follow the reaction pathways of a mechanism and trace the ozone, or other product species, formed back to the original organic precursors. This is done by analyzing the concentration predictions of an atmospheric chemical mechanism.

Since reaction stoichiometry is necessary to perform such an analysis, the stoichiometric coefficients for all species in all reactions are initially determined. In order to trace a product species back to its precursors, one reactant in each reaction must be selected as the controlling, or dominant, reactant to which all products of the reaction will be assigned. This selection provides a necessary simplification of the reaction mechanism where only the effect of the dominant reactant is considered. A limitation in this approach is that products in a reaction can be assigned to only one reactant, making

proper selection of dominant reactants, based on the specific product species and reactants of interest, a crucial element. For example, when ozone is being assigned to emitted organics, these organic species have the highest priority for selection as dominant reactants, followed by their immediate oxidation products, such as formaldehyde and methyl ethyl ketone, then organic radical species, and, lastly, the nitrogen oxides. Thus in the reaction,

$$HO_2 + NO \rightarrow NO_2 + OH \qquad (3)$$

HO_2 would be selected as the dominant reactant so that the ozone-forming NO to NO_2 conversion is attributed to HO_2 and, ultimately, its organic precursor.

The progress of individual reactions within the mechanism is monitored by adding a "counter" species as a product to each reaction. These counters, dummy species with no physical significance, act to "count" the amount of reactant that has undergone each reaction since the beginning of the simulation. For each time step analyzed, the amount of reactant species available for reaction can be determined as the sum of initially present reactant, emitted reactant, and reactant formed in other reactions during the time step. With the change in concentration during a time step of a given reaction's counter species and the amount of reactant available for that reaction, the fraction of available reactant passing through that reaction during the time step can be calculated. Starting with an organic precursor, these fractions reacting, together with product stoichiometry, can be used to calculate the amount of various species that will be formed as direct

products in reactions involving the organic as dominant reactant. Of course, these products generally undergo reaction themselves forming additional products, which, in turn, react once again, creating a complex web of reaction pathways.

For each successive step in the VOC/NO_x photooxidation, products are assigned back to the precursor organic. For simple reaction mechanisms of only a few reactions, all of these calculations may be performed by hand. For more complicated mechanisms, however, with hundreds of reactions, or where species are regenerated in a reaction cycle, the required calculations are executed by solving a system of linear equations consisting of one equation for each chemical species in the mechanism. At each time step a new set of linear equations, formed from the fractions reacting calculated for that time step, is solved and products are assigned back to species present at the beginning of the time step from which they were formed.

Initially, all species present are assigned to themselves, and then after the first time step all product species are assigned back to these initially present organic precursors. In subsequent time steps, when these "primary" products react, the resultant "secondary" products are assigned back first to the primary product from which they were generated, and then back to the organic precursor from which the primary product was formed. Organic emissions during a time step are treated similarly, being assigned to themselves and added to the amount of that organic species present at the beginning of the time step. In this way, at any given time the concentration of each chemical species is assigned among all of the initially present or emitted organic precursors. When taken

together, the contributions of the individual organics to a given product species, such as ozone, add up to the total concentration of that species.

The ozone assignment values give the total amount of ozone produced in a given scenario attributable to species j, designated $[O_3]_j$. The total O_3 attributable to each organic is influenced greatly by the relative concentrations of each species. A measure of the ozone-forming potential of each organic, termed its productivity, P_j, normalizes the ozone produced from an organic in a particular scenario by the amount of that organic available for reaction,

$$P_j = \frac{[O_3]_j}{[VOC_j]} = \frac{\text{ppb } O_3 \text{ produced due to VOC}_j}{\text{ppbC VOC}_j \text{ emitted}} \qquad (4)$$

Therefore, ozone assignment and productivity deal with the apportionment of the total amount of ozone produced in a given scenario among each of the organics in a VOC mixture. As with incremental reactivities, productivities may also be represented as the product of kinetic and mechanistic factors,

$$P_j = P_j^k \; P_j^m \qquad (5)$$

where the kinetic productivity, P_j^k, is identical to kinetic reactivity and represents the fraction of emitted species j that reacts during the scenario, while the mechanistic productivity, P_j^m, is the amount of ozone attributable to species j that is formed per carbon atom of species j reacting.

Table 11 presents ozone assignment and productivity results for the base case scenario. The largest single source of ozone in the simulation, responsible for 14% of the peak ozone level, is classified as inorganic, and represents the net effect of ozone entrainment from aloft and ozone-destruction by NO_x. Carbon monoxide is also a major contributor to ozone, accounting for 14% of total ozone produced. The other major sources, which taken together are responsible for 56% of the ozone produced, are the lumped alkanes, ethene, the lumped alkenes, and the higher molecular weight aromatics. The remaining ozone is mainly attributable to methane, the lower aromatics, and the aldehydes. As noted earlier, the total O_3 attributable to each species is, to a large extent, a reflection of the species' relative abundance. CO, for example, has a very low ozone productivity, indicating that only a small amount of ozone is produced by each CO molecule, but as a result of its high concentration, a relatively large amount of ozone is created.

The productivity results provide a meaningful evaluation of each species' ozone-forming potential. The most productive species, on a per carbon basis, are the higher aldehydes, followed by the alkenes, then the higher aromatics and formaldehyde, and lastly the alkanes and lower aromatics. The kinetic and mechanistic productivity values show the relative importance of both a species reaction rate and its reaction mechanism. Under the scenario conditions, methane is the most efficient contributor to ozone, producing over two molecules of ozone for each reacting molecule, but since methane reacts so slowly, it exhibits a very low overall productivity. In general, the species with

the highest ozone productivities have relatively high values of both kinetic and mechanistic productivities.

Factors Contributing to Incremental Reactivity

Upon comparison of an organic's incremental reactivity (Table 10) and its ozone productivity (Table 11), it can be seen that in most instances the incremental reactivity value (mole O_3 mole C^{-1}) is higher than the ozone productivity value (mole O_3 mole C^{-1}). This difference would seem to indicate that the increment of organic added to the base case mixture generally produces ozone more efficiently than that amount which is already a part of the mixture. This behavior can be explained by using the concept of productivity to examine how ozone formation changes when an organic is added incrementally to a VOC/NO_x mixture.

As noted earlier, the incremental reactivity of species *i* is the change in peak ozone concentration, due to an additional amount of species *i*, divided by the incremented amount of species *i*. Since the sum of individual contributions to ozone equals the total observed value of O_3, the change in O_3 may be represented as the sum of changes in the individual species contributions,

$$\Delta_i[O_3] = \sum_j \Delta_i[O_3]_j \qquad (6)$$

where $\Delta_i[O_3]_j$ denotes the change in ozone attributable to organic species j when organic species i is incremented. Using the definition of productivity, equation (4), $[O_3]_j$, the amount of ozone attributable to organic species j, may be expressed as the product of a productivity coefficient P_j and the organic concentration $[VOC_j]$,

$$[O_3]_j = P_j[VOC_j] \tag{7}$$

The productivity coefficient, P_j, is the amount of O_3 attributable to VOC_j that will be produced per carbon atom of VOC_j emitted. As expressed in equation (5), the productivity coefficient may be further separated into kinetic and mechanistic factors, P_j^k and P_j^m,

$$[O_3]_j = P_j^k P_j^m[VOC_j] \tag{8}$$

Using equation (8), the change in O_3 due to addition of species i may be written as

$$\Delta_i[O_3]_j = \Delta_i\{P_j^k P_j^m[VOC_j]\} \tag{9}$$

which can be expanded to the first order to the following form,

$$\begin{aligned}\Delta_i[O_3]_j &= \Delta_i\{P_j^k P_j^m[VOC_j]\} \\ &= P_j^k P_j^m \Delta_i\{[VOC_j]\} + P_j^m[VOC_j]\Delta_i\{P_j^k\} + P_j^k[VOC_j]\Delta_i\{P_j^m\}\end{aligned} \tag{10}$$

where P_j^k, P_j^m, and [VOC_j] represent base case values for organic species j and $\Delta_i P_j^k$, $\Delta_i P_j^m$, and Δ_i[VOC_j] represent changes in the kinetic productivity, mechanistic productivity, and concentration of organic species j upon adding organic i to the base case. The change in ozone production attributable to organic j upon adding an increment of organic i, $\Delta_i[O_3]_j$, may then be viewed as the sum of three terms representing changes in organic concentration, kinetic productivity, and mechanistic productivity.

For all non-incremented species, that is when $j \neq i$, [VOC_j] is constant and the Δ_i[VOC_j] term will be zero. Only the incremented species concentration, [VOC_i], is changed, making the Δ_i[VOC_j] term non-zero only when $j = i$. The Δ_i[VOC_j] term represents the effect adding organic i would have if the mixture chemistry remained unchanged by the addition of an increment of species i. That is, the same fraction of all species would react, producing the same amount of ozone per reacting organic, only more of the incremented species, VOC_i, would be available, thus causing an increase in ozone. The $\Delta_i P_j^k$ term represents the change in ozone production that results due to greater or lesser fractions of the available organic species j reacting, while the $\Delta_i P_j^m$ term accounts for changes in ozone production due to more or less efficient reaction mechanism pathways. Thus, the total change in ozone upon adding an increment of organic species i can be represented in the following form,

$$\Delta_i[O_3] = \sum_j \Delta_i[O_3]_j$$
$$= P_i^k P_i^m \Delta[VOC_i] + \sum_j P_j^m[VOC_j]\Delta_i\{P_j^k\} + \sum_j P_j^k[VOC_j]\Delta_i\{P_j^m\} \quad (11)$$

The contributions of individual organics to the incremental reactivities of each organic species are given in Table 12. Because of the varying magnitude of incremental reactivities among organics, the values in Table 12 are presented as a percentage of the total change in ozone. In the case of CH_4, for example, the incremented species, CH_4, is responsible for 59% of the change in ozone, while the remaining species in the mixture contribute additional amounts. For this example, the 59% means that the addition of CH_4 causes an additional amount of ozone to be formed, 59% of which is due to the new molecules of CH_4. This amount is then augmented by additional amounts of ozone produced from the other mixture species, such that the sum of all species contributions is 100% of the total ozone change. For example, with the addition of CH_4, the change in ozone production attributable to AAR1 accounts for 5% of the change in O_3, meaning that when CH_4 is added, AAR1 produces more ozone than it did in the base case. Note that for benzaldehyde (BALD), the positive contribution from the incremented species is entirely offset by decreases in ozone production from the non-incremented species, which react more slowly since BALD lowers radical concentrations. In this case, the addition of benzaldehyde causes the remaining organic species to produce less ozone than in the base case, with the net result being an overall decrease in ozone.

Incremental reactivities are also compared by separating the effects of organic concentration, and kinetic and mechanistic factors in Table 13. The contribution of each term in equation (11) is listed as a percentage of the total incremental reactivity. By definition, the Δ_i[VOC] term, representing the change in ozone production due solely to the presence of additional organic but not to changes in mixture chemistry, is positive indicating that more ozone is formed since additional organic is present. The $\Delta_i P^k$ term is positive when additional ozone is formed due to an increased fraction of available organics reacting, and negative when less ozone is formed as a result of a decrease in the fraction of organics reacting. The $\Delta_i P^m$ term can likewise be positive or negative with positive values indicating additional ozone due to more efficient chemistry, and negative values indicating less ozone as a result of less efficient chemistry.

The results concerning individual VOC contributions found in Table 12 are closely related to the kinetic, mechanistic, and concentration contributions listed in Table 13. As seen from Table 12, the incremented organic accounts for only a fraction of the total ozone change. That fraction attributable to the incremented organic (the values found along the diagonals of Table 12) is composed almost entirely of the ozone produced by the additional organic as listed in the Δ_i[VOC] column of Table 13. The remaining portion of the Table 12 diagonal terms, changes in the kinetic and mechanistic productivity of the incremented organic, are relatively minor. The contribution from the non-incremented species (the off-diagonal elements), on the other hand, arises due to changes in the mixture chemistry induced by adding the incremented species, as

evidenced by the significance of the $\Delta_i P^k$ and $\Delta_i P^m$ terms in Table 13. Thus, the Δ_i[VOC] term can be viewed as the change in ozone attributable to the incremented organic, with the $\Delta_i P^k$ and $\Delta_i P^m$ terms attributing changes in ozone to the non-incremented species.

The incremental reactivities of most organics are characterized by an increase in ozone from the non-incremented species. This behavior can be attributed primarily to changes in kinetic productivity, or the fraction of organic that reacts. For most organics, the kinetic productivity term in Table 13 is positive, indicating that when these organics are added to the base case mixture, more of the non-incremented species react, leading to greater ozone formation on the part of the non-incremented species. Exceptions to this pattern are the lumped alkane, AAR4, and benzaldehyde, BALD, which, when added to the base case, cause less of the remaining species to react, resulting in decreased ozone formation by the non-incremented species and a negative kinetic productivity.

Changes in mechanistic productivity are also important for many species, but in this scenario they are not as significant as the effect on kinetic productivity. Benzaldehyde, BALD, and all of the lumped alkanes, AAR1-4, have negative mechanistic productivity terms in Table 13 due to nitrate-forming pathways in their mechanisms. Adding an increment of these organics to the reaction mixture causes the non-incremented organics to react less efficiently, producing less ozone. All other organics produce the opposite effect when added to the base case, increasing the efficiency of the non-incremented species, leading to additional ozone formation.

Changes in the Radical Pool

These changes in kinetic and mechanistic productivity are the result of changes to the radical pool which controls VOC/NO_x chemistry. We used the assignment method to track the formation, propagation, and destruction of radical species. In order to accurately track radical species, both radical-creating reactions and radical-destroying reactions can be identified for OH, HO_2, and RO_2 radicals. The chemical mechanism represents OH and HO_2 radicals explicitly and employs several other radical species to represent the various peroxy radicals. For our purposes all of these higher peroxy radicals can be defined as RO_2 radicals. A radical-creating reaction is one in which more radicals are created than destroyed, and, likewise, a radical-destroying reaction is one where more radicals are destroyed than created. Propagation reactions that involve conversions between RO_2, HO_2, and OH radicals are also identified, but those propagation reactions where one type of RO_2 radical is converted into another type of RO_2 radical were not considered since no net change to the RO_2 pool occurs.

The interrelation among these various radical flows for the entire VOC mixture is shown in Figure 1, where the numbers by each arrow indicate the amount of radicals, in units of mmole m^{-2}, that follow each pathway integrated over the entire time of the simulation. Sources of radical creation are identified by lightly shaded ovals, and radical-destroying sinks are denoted by more heavily shaded ovals. Conversion flows between the three radical types and the species that cause the conversion are listed within rounded rectangles.

New radical species are created through photolysis of O_3, aldehydes, and other species, and their production is offset by losses due primarily to formation of HNO_3 and, to a lesser extent, nitrates and PAN. The maximum incremental reactivity condition for the scenario represents a VOC-controlled environment where NO_x is in excess. As a result, radical reactions with NO_x are favored over other radical pathways. As can be seen from Figure 1, the conversion of RO_2 radicals to HO_2 radicals, and HO_2 radicals to OH radicals occurs almost exclusively through reaction with NO.

Kinetic productivity is essentially a measure of OH levels within the scenario, since the majority of all organic degradation is through OH attack. An increase in kinetic productivity, therefore, is an indication that OH radical levels have increased. Under the NO_x-rich conditions of the scenario, addition of most organics increases OH concentrations by increasing the fraction of OH radicals that are converted to RO_2 and HO_2 radicals, pathways that lead to the re-creation of OH. As a result, OH radicals can cycle through the radical propagation chain more times before combining with NO_2 to form HNO_3, thus increasing OH concentrations. The only VOCs that exhibit negative kinetic productivity terms in Table 13, benzaldehyde (BALD) and AAR4, offset the increased propagation effect with strong RO_2 radical loss pathways via nitrophenol and nitrate formation. These RO_2 radical losses prevent OH radicals from being re-created, thus reducing OH levels and the amount of VOCs that react.

Changes in mechanistic productivity are also dependent on the balance between radical propagation and termination pathways. Mechanistic productivity can be viewed

as a measure of the efficiency with which RO_2 radicals react. When RO_2 and HO_2 react with NO, NO is converted to NO_2, leading to ozone formation. When RO_2 radicals form nitrates or PAN, the ozone-forming NO to NO_2 conversion does not occur and the radical is removed from circulation. Thus, when a nitrate-forming VOC is added to the base case mixture, the overall reaction mechanism efficiency decreases as a result of increased radical losses and ozone production by the non-incremented species will tend to drop. The mechanistic productivity results in Table 13 reflect the fact that the alkanes and benzaldehyde are the organics with significant nitrate-forming capacity. All other organics increase radical propagation, leading to greater ozone formation, and higher mechanistic productivities.

The combined effect of increase VOC concentration, and changes in kinetic and mechanistic productivities results in the observed incremental change in ozone. The species with the highest incremental reactivities are not merely species that produce the most ozone themselves, i.e., species with the highest ozone productivities, but are those that increase radical flows which then lead to increased ozone production by the non-incremented organics as well.

REFORMULATED GASOLINE EFFECTS ON OZONE

The effects of alternate fuels and reformulated gasoline components on ozone formation can be investigated by examining their incremental reactivities and ozone

productivities together with their individual OH reaction mechanisms. Reaction mechanisms and rate constants for the eight oxygenates included in this study were developed from recent experimental studies. Table 14 contains a listing of the OH reaction of each compound, together with its OH rate constant.

Methanol

The incremental reactivity of methanol is characterized by a low kinetic reactivity and a rather high mechanistic reactivity (Table 10). The low kinetic reactivity is due to the presence of primary hydrogen atoms in the methanol molecule which undergo OH abstraction relatively slowly. The formaldehyde produced by methanol, on the other hand, leads to a high mechanistic reactivity value, as HCHO is a strong radical source. A large fraction of the ozone change upon addition of methanol to the VOC mixture is attributable to additional reactions of non-incremented species as a result of the HCHO formed by OH attack on methanol. Overall, methanol's incremental reactivity is relatively low and falls within the range of those of the lumped alkanes.

Ethanol

Ethanol reacts much faster with OH than methanol, due to the presence of secondary hydrogen atoms. Ethanol's reaction mechanism, however, does not lead to as much formaldehyde formation as methanol and, therefore, ethanol has a mechanistic reactivity that is lower than methanol. The increased rate of reaction dominates over the

lower mechanistic reactivity and, as a result, ethanol has an incremental reactivity considerably higher than that of methanol, with a value comparable to those of the lower aromatics. Both alcohols have similar mechanistic productivities, but since ethanol reacts faster it has an ozone productivity three times larger than methanol. The majority of additional ozone formed by adding ethanol to a VOC mixture is attributable, therefore, directly to ethanol itself, and changes in the productivities of the non-incremented species are less significant.

tert-Butyl Alcohol

Like methanol, *tert*-butyl alcohol (TBA), offers only primary hydrogen atoms for reaction and, as a result, has a correspondingly low rate of OH reaction. Unlike methanol, however, when TBA does react, it forms little ozone itself, with a single HCHO molecule being formed as the only reactive product. The formaldehyde formed from TBA leads to some additional ozone formation by the non-incremented species, but the incremental reactivity of TBA is still very low, with CH_4 and CO the only species in the mechanism having lower incremental reactivities.

Dimethyl Ether

Dimethyl ether (DME) is oxidized to form relatively unreactive methyl formate. Since information on the OH reactions of methyl formate is limited to rate constant data, with no mechanistic studies available in the literature, methyl formate is represented in

the mechanism as 0.2 MEK, based on the ratio of their OH rate constants. Approximately a third of the emitted DME reacts during the 10-hour scenario, with each reacting carbon forming one ozone molecule. Ozone contributions from non-incremented species are only 14%, since few radical-forming products are created by the DME photooxidation. The overall incremental reactivity of DME is similar to that of methanol and falls in the range of those of the lumped alkanes.

Diethyl Ether

Diethyl ether (DEE) reacts fairly rapidly with OH and is mostly consumed during the 10-hour scenario. Ethyl formate, formed as a reaction product, is represented, like methyl formate, as MEK in the mechanism. DEE also forms HCHO, which increases radical levels and leads to greater non-incremented organic ozone contributions than is seen with DME. The greater kinetic and mechanistic reactivities for DEE result in an incremental reactivity value that is considerably higher than those of the alkanes and is even higher than those of the lower aromatics.

Methyl tert-Butyl Ether

The relationship between the reactivities of methyl *tert*-butyl ether (MTBE) and DME is similar to that between TBA and methanol. As with TBA, which has a much lower incremental reactivity than does methanol, MTBE's incremental reactivity is significantly lower than that of DME. Both ethers have comparable reaction rates, but

MTBE has fewer ozone-forming pathways, as much of the carbon from MTBE ends up relatively unreactive as *tert*-butyl formate and methylacetate. MTBE does produce some HCHO, accounting for a small contribution to ozone from the non-incremented species. MTBE's incremental reactivity is quite low and is similar to that of the least reactive alkanes.

Ethyl tert-Butyl Ether

As could be expected from its structure, ethyl *tert*-butyl ether (ETBE) reacts considerably faster than MTBE, accounting for much of the increase in incremental reactivity over that of MTBE. Also serving to increase ETBE's incremental reactivity, relative to MTBE, is the increased fraction of the ETBE carbon that ends up as aldehyde products. These aldehydes produce additional ozone themselves as well as enhancing the ozone formation of the entire VOC mixture. As a result, ETBE has an incremental reactivity higher than those of the alkanes and similar to those of the lower aromatics.

tert-Amyl Methyl Ether

tert-Amyl methyl ether (TAME) is similar to ETBE, with the difference that the ethyl group is placed on the other end of the molecule. TAME has a slightly lower rate of reaction than ETBE, but makes up for the difference with greater ozone and radical forming products. Both ethers have comparable incremental reactivities and ozone

productivities and show similar relative contributions to ozone. As with ETBE, TAME's incremental reactivity is closest to the lower aromatics.

Summary

A summary of results for each of the fuel oxygenates is contained in Table 15. Incremental reactivities and productivities are presented both on a per carbon basis and on a per molecule basis. The effect of larger molecule size is seen in the higher incremental reactivity and productivity values when represented on a per molecule basis, as opposed to a per carbon basis, but the relative ranking of compounds is changed little. Methanol and ethanol, due to their small size, rank as more reactive when represented on a per carbon basis than they do on a per molecule basis.

Incremental reactivities and productivities for the fuel species as a function of the number of carbon atoms in each molecule are presented in Figure 2. Productivity values for the fuel oxygenates (shown as triangles in Figure 2) indicate the amount of ozone that is produced directly by the given species in the scenario considered in this paper. Incremental reactivity values (shown as circles in Figure 2) include both the direct production of ozone by the oxygenate itself and additional ozone produced by the VOC mixture. The difference between incremental reactivity and productivity for an individual compound is a measure of the degree to which that compound enhances ozone production by other VOCs in the mixture. The enhancement of ozone production is primarily a result of radical-forming products, such as formaldehyde, that increase overall OH levels

and, thus, the amount of other species that react. Consequently, methanol, whose sole organic product is formaldehyde, has an incremental reactivity that is over twice the value of its productivity, due to the enhancement of ozone produced by other VOCs. Conversely, DME produces the relatively unreactive methyl formate molecule when it reacts with OH and, as a result, has an incremental reactivity that is only slightly higher than its productivity.

As can be seen from Figure 3, where incremental reactivities and productivities for the oxygenates are plotted against their OH rate constants, the ozone-forming potential of a given compound is highly dependent on its rate of reaction with OH. The most reactive oxygenates are those that are the fastest reacting. Since reaction rates depend on molecular structure, those compounds with ethyl groups (ETOH, TAME, ETBE, and DEE) react faster and produce more ozone than those compounds containing only methyl or *tert*-butyl groups (MEOH, TBA, DME, MTBE). For two or three day scenarios, where there is more time for the methyl and *tert*-butyl compounds to react, a greater fraction of these oxygenates will react and the difference between reaction rates will be less pronounced.

CONCLUSIONS

The ability to accurately determine the different contributions to ozone formation by individual organic species is important in developing pollution control strategies.

Using the assignment method, the amount of ozone attributable to each reaction species can be determined. In calculations using a version of the SAPRC mechanism in one of Carter's maximum incremental reactivity (MIR) scenarios, a wide variety of organics were found to be responsible for ozone production. Examining ozone formation using productivity values shows the most productive species, on a per carbon basis, are the higher aldehydes, followed by the alkenes, then the higher aromatics and formaldehyde, and lastly the alkanes and lower aromatics. Both kinetic and mechanistic factors are important in determining relative productivities between VOCs, where the species with the highest ozone productivities have relatively high values of both kinetic and mechanistic productivities.

The ozone change measured in an incremental reactivity calculation may be traced to changes in the ozone attributable to individual organic species in a VOC mixture using the ozone assignment method. These changes can be represented as the sum of changes in organic concentration, kinetic productivity, or the fraction of organic reacting, and mechanistic productivity, or the amount of ozone produced per carbon atom of organic reacting. Incremental reactivity calculations showed significant contributions to the overall ozone change from all organic species in the mixture as a result of changes in concentration and productivity. The ozone attributable to the non-incremented species either increases or decreases depending on changes in the radical pool upon adding the test organic.

Since only a small concentration of each oxygenated fuel component was included in the VOC mixture, little of the overall ozone produced was attributable to these species. For the most part, the fuel oxygenates have relatively low incremental reactivities with values similar to those of the alkanes and lower aromatics. This is, in most cases, due to their slow reaction rates, as well as the formation of relatively unreactive formate and acetate products. The more reactive fuel oxygenates are those containing ethyl groups, which react faster than their counterparts containing only methyl and *tert*-butyl groups.

ACKNOWLEDGMENT

This work was supported by the Coordinating Research Council and the National Renewable Energy Laboratory.

REFERENCES

Aschmann S. M. and Atkinson R. (1994) Formation yields of methyl vinyl ketone and methacrolein from the gas-phase reaction of O_3 with isoprene. *Environ. Sci. Technol.* **28**, 1539.

Atkinson R. (1990) Gas-phase tropospheric chemistry of organic compounds - a review. *Atmos. Environ.* **24**, 1-41.

Atkinson R., Baulch D. L., Cox R. A., Hampson R. F., Kerr J. A. and Troe J. (1992) Evaluated kinetic and photochemical data for atmospheric chemistry. Supplement-IV. IUPAC subcommittee on gas kinetic data evaluation for atmospheric chemistry. *J. Phys. Chem. Ref. Data.* **21**, 1125.

Bennett P. J. and Kerr J. A. (1990) Kinetics of the reactions of hydroxyl radicals with aliphatic ethers studied under simulated atmospheric conditions- temperature dependences of the rate constants. *J. Atmos. Chem.* **10**, 29.

Bowman F. M. and Seinfeld J. H. (1994*a*) Ozone productivity of atmospheric organics. *J. Geophys. Res.*, **99** 5309.

Bowman F. M. and Seinfeld J. H. (1994*b*) Fundamental basis of incremental reactivities of organics in ozone formation in VOC/NO_x mixtures. *Atmos. Environ.* **28**, 3359-3368.

Bowman F. M., Pilinis C. and Seinfeld J. H. (1995) Ozone and aerosol productivity of reactive organics. *Atmos. Environ.* **29**, 579-589.

California Air Resources Board (CARB) (1992) Development and evaluation of ozone reactivity scale for low-emission vehicles and clean fuels regulations. Sacramento, CA.

Carter W. P. L. (1988) Appendix C. Documentation for the SAPRC atmospheric photochemical mechanism preparation and emissions processing programs for implementation in airshed models. Report, Contract No. A5-122-32, California Air Resources Board, Sacramento, CA.

Carter W. P. L. (1990) A detailed mechanism for the gas-phase atmospheric reactions of organic compounds. *Atmos. Environ.* **24**, 481.

Carter W. P. L. (1991) Development of ozone reactivity scales for volatile organic compounds. EPA 600/3-91/050, Environmental Protection Agency, Research Triangle Park, NC.

Carter W. P. L. (1994) Development of ozone reactivity scales for volatile organic compounds. *J. Air & Waste Manage. Assoc.* **44**, 881.

Carter W. P. L. and Atkinson R. J. (1987) An experimental study of incremental hydrocarbon reactivity. *Environ. Sci. Technol.* **21**, 670.

Carter W. P. L. and Atkinson R. J. (1989) Computer modeling study of incremental hydrocarbon reactivity. *Environ. Sci. Technol.* **23**, 864.

Carter W. P. L. and Lurmann F. W. (1991) Evaluation of a detailed gas-phase atmospheric reaction mechanism using environmental chamber data. *Atmos. Environ.* **25A**, 2771.

Cohen J. P., Yarwood G., Noda A. M., Pollack A. K. and Morris R. E. (1994) Auto/Oil Air Quality Improvement Research Program: Development of emissions reactivity values for phase II results. SYSAPP94-94/053, Systems Applications International, San Rafael, CA.

EPA (1989) User's manual for OZIPM-4 Volume I. EPA-450/4-84-005.

Grosjean D., Grosjean E. and Williams E. L. (1994) Atmospheric removal of MPAN. *Abs. Papers Amer. Chem. Soc.* **207**, 187-ENVR.

Grosjean D., Williams E. L. and Grosjean E. (1993) Atmospheric chemistry of isoprene and its carbonyl products. *Environ. Sci. Technol.* **27**, 830.

Japar S. M., Wallington T. J., Richert J. F. O. and Ball J. C. (1990) The atmospheric chemistry of oxygenated fuel additives - tert-butyl alcohol, dimethyl ether, and methyl tert-butyl ether. *Int. J. Chem. Kin.* **22**, 1257.

National Research Council (1991) *Rethinking the ozone problem in urban and regional air pollution.* National Academy Press, Washington, D.C.

Paulson S. E. and Seinfeld J. H. (1992) Development and evaluation of a photochemical mechanism for isoprene. *J. Geophys. Res.* **97**, 20703.

Saunders S. M., Baulch D. L., Cooke K. M., Pilling M. J. and Smurthwaite P. I. (1994) Kinetics and mechanisms of the reactions of OH with some oxygenated compounds of importance in tropospheric chemistry. *Int. J. Chem. Kin.* **26**, 113.

Seinfeld J. H. (1986) *Atmospheric chemistry and physics of air pollution*. Wiley, New York.

Semadeni M., Stocker D. W. and Kerr J. A. (1993) Further studies of the temperature dependence of the rate coefficients for the reactions of OH with a series of ethers under simulated atmospheric conditions. *J. Atmos. Chem.* **16**, 79.

Smith D. F., Kleindienst T. E., Hudgens E. E., McIver C. D. and Bufalini J. J. (1992) Kinetics and mechanism of the atmospheric oxidation of ethyl tertiary butyl ether. *Int. J. Chem. Kin.* **24**, 199.

Stockwell W. R., Yang Y. J. and Milford J. B. (1993) A compilation of estimated uncertainty factors for rate constants in W.P.L. Carter's detailed mechanism. prepared for Coordinating Research Council, Atlanta, GA.

Tuazon E. C., Carter W. P. L., Aschmann S. M. and Atkinson R. (1991) Products of the gas-phase reaction of methyl tert-butyl ether with the OH radical in the presence of NOx. *Int. J. Chem. Kin.* **23**, 1003.

Tully F. P. and Droege A. T. (1987) Kinetics of the reactions of the hydroxyl radical with dimethyl ether and diethyl ether. *Int. J. Chem. Kin.* **19**, 251.

Wallington T. J., Andino J. M., Skewes L. M., Siegl W. O. and Japar S. M. (1989) Kinetics of the reaction of OH radicals with a series of ethers under simulated atmospheric conditions at 295 K. *Int. J. Chem. Kin.* **21**, 993.

Wallington T. J., Dagaut P., Liu R. Z. and Kurylo M. J. (1988) Rate constants for the gas-phase reactions of OH with C-5 through C-7 aliphatic alcohols and ethers - predicted and experimental values. *Int. J. Chem. Kin.* **20**, 541.

Wallington T. J. and Japar S. M. (1991) Atmospheric chemistry of diethyl ether and ethyl tert-butyl ether. *Environ. Sci. Technol.* **25**, 410.

Wallington T. J., Potts A. R., Andino J. M., Siegl W. O., Zhang Z., Kurylo M. J. and Huei R. E. (1993) Kinetics of the reaction of OH radicals with t-amyl methyl ether revisited. *Int. J. Chem. Kin.* **25**, 265.

Whitten G. Z. and Yarwood G. (1992) Unpublished report. Systems Applications International, San Rafael, CA.

APPENDIX A. CHEMICAL REACTION MECHANISM

The reaction mechanism we have used was developed by Carter, and for a more complete description we refer the reader to the original literature describing the development of the mechanism (Carter, 1990; Carter and Lurmann, 1991). The species used in the mechanism are described in Table A1. We have added reactions for isoprene and eight fuel oxygenates based on recent experimental studies. Rate parameters and product coefficients for the lumped groups (AAR*n* and OLE*n*) are represented in Carter's mechanism as variable coefficients that depend on the composition of the lumped group. The listing of the mechanism in Table A2 contains numerical values of these parameters determined for the base case VOC mixture.

Table A1. List of reaction mechanism species.

Name	Chemical description
Inorganic species	
O3	Ozone
NO	Nitric oxide
NO2	Nitrogen dioxide
NO3	NO_3 radical
N2O5	N_2O_5
HNO3	Nitric acid
HONO	Nitrous acid
HNO4	Peroxynitric acid
HO2H	Hydrogen peroxide
Organic product species	
CO	Carbon monoxide
HCHO	Formaldehyde
CCHO	Acetaldehyde
RCHO	Propionaldehyde and lumped higher aldehydes
PAN	Peroxy acetyl nitrate
PPN	Peroxy propionyl nitrate and higher PAN analogues
ACET	Acetone
MEK	Methylethyl ketone and lumped higher ketones
RNO3	Lumped organic nitrates
GLY	Glyoxal
GPAN	PAN analogue formed from glyoxal
MGLY	Methyl glyoxal
PHEN	Phenol
CRES	Cresol and other alkyl phenols
BALD	Benzaldehyde and other aromatic aldehydes
PBZN	Peroxy benzoyl nitrate
NPHE	Nitrophenols and other aromatic nitro-compounds
AFG1	Unknown aromatic fragmentation product #1. (Formed from benzene, tetralin, and naphthalenes)
AFG2	Unknown aromatic fragmentation product #2. (Formed from aromatics containing alkyl groups)
MVK	Methyl vinyl ketone
MACR	Methacrolein
MPAN	PAN analogue formed from methacrolein

OH-CCHO	Hydroxyacetaldehyde
OH-ACET	Hydroxyacetone

Emitted organic species

CH4	Methane
AAR*n*	*n*'th lumped alkane/aromatic group. (AAR1-AAR4 are lumped alkanes. AAR5-AAR7 are lumped aromatics)
TOLU	Toluene
ETHE	Ethene
OLE*n*	*n*'th lumped alkene group
ISOP	Isoprene
BPIN	β-pinene and lumped biogenic alkenes

Fuel oxygenate species

MEOH	Methanol
ETOH	Ethanol
TBA	*tert*-Butyl alcohol
DME	Dimethyl ether
DEE	Diethyl ether
MTBE	Methyl *tert*-butyl ether
ETBE	Ethyl *tert*-butyl ether
TAME	*tert*-Amyl methyl ether

Radical and atomic species

O	Ground state oxygen atoms
O*1D2	Excited oxygen atoms
HO.	Hydroxyl radicals
HO2.	HO_2 radicals
HOCOO.	Intermediate formed in the HCHO + HO_2 reaction
CCO-O2.	Peroxy acetyl radicals
C2CO-O2.	Higher peroxy acyl radicals
BZ-CO-O2.	Peroxy benzoyl radicals
HCOCO-O2.	Peroxyacyl radicals formed from glyoxal
BZ-O.	Phenoxy radicals
BZ(NO2)-O.	Phenoxy-type radical containing nitro-groups
MCO3.	Peroxyacyl radicals formed from methacrolein

Product only species

CO2	Carbon dioxide
H2SO4	Sulfuric acid
H2	Hydrogen
-C	"Lost carbon." Used to account for carbon balance.

Constant species

O2	Oxygen
M	Air
H2O	Water
HV	Light factor (1.0 = normal intensity)

Chemical operators

-OOH	Used to represent reactions at hydroperoxy groups
RO2.	Total alkyl peroxy radicals
RCO3.	Total peroxyacyl radicals
RO2-R.	Used to represent NO to NO_2 conversion with generation of HO_2 radicals
RO2-N.	Used to represent NO consumption and RNO_3 formation
RO2-XN.	Used to represent NO sink reactions
RO2-NP.	Used to represent NO consumption and NPHE formation
R2O2.	Used to represent extra NO to NO_2 conversions

Table A2. List of reactions and rate constant parameters in Carter mechanism.

Reaction label	Rate parameters [a]			Reaction [b]
Inorganic reactions				
1	Photolysis set = NO2			NO2 + HV = NO + O + F1
2	6.0E-34	0.0	-2.3	O + O2 + M = O3 + M + F2
3A	6.5E-12	-0.238		O + NO2 = NO + O2 + F3A
3B	Falloff			O + NO2 = NO3 + M + F3B
	9.0E-32	0.0	-2.0	
	2.2E-11	0.0	0.0	
	0.6	1.0		
4	2.00E-12	2.782		NO + O3 = NO2 + O2 + F4
5	1.400E-13	4.968		NO2 + O3 = O2 + NO3 + F5
6	1.7E-11	-0.298		NO3 + NO = #2 NO2 + F6
7	3.300E-39	-1.05		NO + NO + O2 = #2 NO2 + F7
8	Falloff			NO3 + NO = N2O5 + F8
	2.2E-30	0.0	-4.3	
	1.5E-12	0.0	-0.5	
	0.6	1.0		
9	Equilibrium with reaction 8			
	9.09E+26	22.26		N2O5 = NO2 + NO3 + F9
10	1.0E-21			N2O5 + H2O = #2 HNO3 + F10
11	2.5E-14	2.44		NO3 + NO2 = NO + NO2 + O2 + F11
12A	Photolysis set = NO3NO			NO3 + HV = NO + O2 + F12A
12B	Photolysis set = NO3NO2			NO3 + HV = NO2 + O + F12B
13A	Photolysis set = O3O3P			O3 + HV = O + O2 + F13A
13B	Photolysis set = O3O1D			O3 + HV = O*1D2 + O2 + F13B
14	2.2E-10			O*1D2 + H2O = #2 HO. + F14
15	1.919E-11	-0.251		O*1D2 + M = O + M + F15
16	Falloff			NO + HO. = HONO + F16
	7.0E-31	0.0	-2.6	
	1.5E-11	0.0	-0.5	
	0.6	1.0		
17	Photolysis set = HONO			HONO + HV = HO. + NO + F17

18	Falloff			NO2 + HO. = HNO3 + F18
	2.6E-30	0.0	-3.2	
	2.4E-11	0.0	-1.3	
	0.6	1.0		
19	6.45E-15	-1.652		HNO3 + HO. = H2O + NO3 + F19
21	2.4E-13			CO + HO. = HO2. + CO2 + F2
22	1.600E-12	1.87		O3 + HO. = HO2. + O2 + F22
23	3.700E-12	-0.48		HO2. + NO = HO. + NO2 + F23
24	Falloff			NO2 + HO2. = HNO4 + F24
	1.8E-31	0.0	-3.2	
	4.7E-12	0.0	-1.4	
	0.6	1.0		
25	Equilibrium with reaction 24			
	4.76E+26	21.66		HNO4 = HO2. + NO2 + F25
27	1.3E-12	-0.755		HNO4 + HO. = H2O + NO2 + O2 + F27
28	1.100E-14	0.994		O3 + HO2. = HO. + #2 O2 + F28
29A	2.2E-13	-1.23		HO2. + HO2. = HO2H + O2 + F29A
29B	1.9E-33	-1.95		HO2. + HO2. + M = HO2H + O2 + F29B
29C	3.1E-34	-5.60		HO2. + HO2. + H2O = HO2H + O2 + H2O + F29C
29D	6.6E-35	-6.32		HO2. + HO2. + H2O = HO2H + O2 + H2O + F29D
30A	Same *k* as 29A			NO3 + HO2. = HNO3 + O2 + F30A
30B	Same *k* as 29B			NO3 + HO2. + M = HNO3 + O2 + F30B
30C	Same *k* as 29C			NO3 + HO2. + H2O = HNO3 + O2 + H2O + F30C
30D	Same *k* as 29D			NO3 + HO2. + H2O = HNO3 + O2 + H2O + F30D
31	Photolysis set = H2O2			HO2H + HV = #2 HO. + F31
32	3.300E-12	0.397		HO2H + HO. = HO2. + H2O + F32
33	4.60E-11	-0.457		HO2. + HO. = H2O + O2 + F33

Peroxy radical reactions

B1	4.200E-12	-0.360		RO2. + NO = NO + FB1
B2	5.100E-12	-0.397		RCO3. + NO = NO + FB2
B4	Falloff			RCO3. + NO2 = NO2 + FB3
	1.95E-28	0.0	-4.0	
	8.40E-12	0.0	0.0	
	0.27	1.0		
B5	3.40E-13	-1.590		RO2. + HO2. = HO2. + FB5
B6	3.40E-13	-1.590		RCO3. + HO2. = HO2. + FB6
B7	Photolysis set = CO2H			-OOH + HV = HO2. + HO. + FB7

B7A	1.18E-12	-0.254	-OOH + HO. = HO. + FB7A
B7B	1.79E-12	-0.435	-OOH + HO. = RO2-R. + RO2. + FB7B
B8	1.0E-15		RO2. + RO2. = FB8
B9	1.86E-12	-1.053	RO2. + RCO3. = FB9
B10	2.8E-12	-1.053	RCO3. + RCO3. = FB10
B11	Same *k* as B1		RO2-R. + NO = NO2 + HO2. + FB11
B12	Same *k* as B5		RO2-R. + HO2. = -OOH + FB12
B13	Same *k* as B8		RO2-R. + RO2. = RO2. + #.5 HO2. + FB13
B14	Same *k* as B9		RO2-R. + RCO3. = RCO3. + #.5 HO2. + FB14
B15	Same *k* as B1		R2O2. + NO = NO2 + FB15
B16	Same *k* as B5		R2O2. + HO2. = FB16
B17	Same *k* as B8		R2O2. + RO2. = RO2. + FB17
B18	Same *k* as B9		R2O2. + RCO3. = RCO3. + FB18
B19	Same *k* as B1		RO2-N. + NO = RNO3 + FB19
B20	Same *k* as B5		RO2-N. + HO2. = -OOH + MEK + #1.5 -C + FB20
B21	Same *k* as B8		RO2-N. + RO2. = RO2. + #.5 HO2. + MEK + #1.5 -C + FB21
B22	Same *k* as B9		RO2-N. + RCO3. = RCO3. + #.5 HO2. + MEK + #1.5 -C +FB22
B23	Same *k* as B1		RO2-XN. + NO = -N + FB23
B24	Same *k* as B5		RO2-XN. + HO2. = -OOH + FB24
B25	Same *k* as B8		RO2-XN. + RO2. = RO2. + #.5 HO2. + FB25
B26	Same *k* as B9		RO2-XN. + RCO3. = RCO3. + HO2. + FB26

Reactions of aldehydes and other alkane products

C1	Photolysis set = HCHOAVGR			HCHO + HV = #2 HO2. + CO + FC1
C2	Photolysis set = HCHOAVGM			HCHO + HV = H2 + CO + FC2
C3	1.125E-12	-1.288	2.0	HCHO + HO. = HO2. + CO + H2O + FC3
C4	9.7E-15	-1.242		HCHO + HO2. = HOCOO. + FC4
C4A	2.4E+12	13.91		HOCOO. = HO2. + HCHO + FC4A
C4B	Same *k* as B1			HOCOO. + NO = -C + NO2 + HO2. + FC4B
C9	2.8E-12	5.00		HCHO + NO3 = HNO3 + HO2. + CO + FC9
C10	5.55E-12	-0.618		CCHO + HO. = CCO-O2. + H2O + RCO3. + FC10
C11A	Photolysis set = CCHOR			CCHO + HV = CO + HO2. + HCHO + RO2-R. + RO2. + FC11A

C12	1.4E-12	3.696		CCHO + NO3 = HNO3 + CCO-O2. + RCO3. + FC12
C13	Same *k* as B2			CCO-O2. + NO = CO2 + NO2 + HCHO + RO2-R. + RO2. + FC13
C14	Same *k* as B4			CCO-O2. + NO2 = PAN + FC14
C15	Same *k* as B6			CCO-O2. + HO2. = -OOH + CO2 + HCHO + FC15
C16	Same *k* as B9			CCO-O2. + RO2. = RO2. + #.5 HO2. + CO2 + HCHO + FC16
C17	Same *k* as B10			CCO-O2. + RCO3. = RCO3. + HO2. + CO2 + HCHO + FC17
C18	Falloff			PAN = CCO-O2. + NO2 + RCO3. + FC18
	6.30E-02	25.406	0.0	
	2.20E+16	26.698	0.0	
	0.27	1.00		
C25	8.5E-12	-0.50		RCHO + HO. = C2CO-O2. + RCO3. + FC25
C26	Photolysis set = RCHO			RCHO + HV = CCHO + RO2-R. + RO2. + CO + HO2. + FC26
C27	1.4E-12	3.696		RCHO + NO3 = HNO3 + C2CO-O2. + RCO3. + FC27
C28	Same *k* as B2			C2CO-O2. + NO = CCHO + RO2-R. + CO2 + NO2 + RO2. + FC28
C29	8.4E-12			C2CO-O2. + NO2 = PPN + FC29
C30	Same *k* as B6			C2CO-O2. + HO2. = -OOH + CCHO + CO2 + FC30
C31	Same *k* as B9			C2CO-O2. + RO2. = RO2. + #.5 HO2. + CCHO + CO2 + FC31
C32	Same *k* as B10			C2CO-O2. + RCO3. = RCO3. + HO2. + CCHO + CO2 + FC32
C33	1.6E+17	27.966		PPN = C2CO-O2. + NO2 + RCO3. + FC33
C38	1.92E-13	-0.11	2.0	ACET + HO. = #.8 MGLY + #.8 RO2-R. + #.2 R2O2. + #.2 HCHO + #.2 CCO-O2. + #.2 RCO3. + RO2. + FC38
C39	Photolysis set = ACETONE			ACET + HV = CCO-O2. + HCHO + RO2-R. + RCO3. + RO2. + FC39
C44	2.92E-13	-0.823	2.0	MEK + HO. = H2O + #.5 CCHO + #.5 HCHO + #.5 CCO-O2. + #.5 C2CO-O2. + RCO3. + #1.5 R2O2. + #1.5 RO2. + FC44
C57	Photolysis set = KETONE			MEK + HV = CCO-O2. + CCHO + RO2-R. + RCO3. + RO2. + FC57

C58A	Photolysis set = GLYOXAL1		GLY + HV = #.8 HO2. + #.45 HCHO + #1.55 CO + FC58A
C58B	Photolysis set = GLYOXAL2		GLY + HV = #.13 HCHO + #1.87 CO + FC58B
C59	1.14E-11		GLY + HO. = #.6 HO2. + #1.2 CO + #.4 HCOCO-O2. + #.4 RCO3. + FC59
C60	Same *k* as C12		GLY + NO3 = HNO3 + #.6 HO2. + #1.2 CO + #.4 HCOCO-O2. + #.4 RCO3. + FC60
C62	Same *k* as B2		HCOCO-O2. + NO = NO2 + CO2 + CO + HO2. + FC62
C63	Same *k* as B4		HCOCO-O2. + NO2 = GPAN + FC63
C64	Same *k* as C18		GPAN = HCOCO-O2. + NO2 + RCO3. + FC64
C65	Same *k* as B6		HCOCO-O2. + HO2. = -OOH + CO2 + CO + FC65
C66	Same *k* as B9		HCOCO-O2. + RO2. = RO2. + #.5 HO2. + CO2 + CO + FC66
C67	Same *k* as B10		HCOCO-O2. + RCO3. = RCO3. + HO2. + CO2 + CO + FC67
C68	Photolysis set = MEGLYOX		MGLY + HV = HO2. + CO + CCO-O2. + RCO3. + FC68
C69	1.72E-11		MGLY + HO. = CO + CCO-O2. + RCO3. + FC69
C70	1.4E-12	3.696	MGLY + NO3 = HNO3 + CO + CCO-O2. + RCO3. + FC70
C95	2.191E-11	1.408	RNO3 + HO. = NO2 + #.155 MEK + #1.05 RCHO + #.48 CCHO + #.16 HCHO + #.11 -C + #1.39 R2O2. + #1.39 RO2. + FC95

Reactions of aromatic products

G2	Same *k* as B1	RO2-NP. + NO = NPHE + FG2
G3	Same *k* as B5	RO2-NP. + HO2. = -OOH + #6 -C + FG3
G4	Same *k* as B8	RO2-NP. + RO2. = RO2. + #.5 HO2. + #6 -C + FG4
G5	Same *k* as B9	RO2-NP. + RCO3. = RCO3. + HO2. + #6 -C + FG5
G7	1.14E-11	AFG1 + HO. = HCOCO-O2. + RCO3. + FG7
G8	Photolysis set = AROMUNKN	AFG1 + #0.1 HV = HO2. + HCOCO-O2. + RCO3. + FG8
G9	1.72E-11	AFG2 + HO. = C2CO-O2. + RCO3. + FG9

G10	Photolysis set = AROMUNKN			AFG2 + HV = HO2. + CO + CCO-O2. + RCO3. + FG10
G30	1.29E-11			BALD + HO. = BZ-CO-O2. + RCO3. + FG30
G31	Photolysis set = BZCHO			BALD + HV = #7 -C + FG31
G32	1.4E-12	3.747		BALD + NO3 = HNO3 + BZ-CO-O2. + FG32
G33	Same *k* as B2			BZ-CO-O2. + NO = BZ-O. + CO2 + NO2 + R2O2. + RO2. + FG33
G34	8.4E-12			BZ-CO-O2. + NO2 = PBZN + FG34
G35	1.6E+15	25.90		PBZN = BZ-CO-O2. + NO2 + RCO3. + FG35
G36	Same *k* as B6			BZ-CO-O2. + HO2. = -OOH + CO2 + PHEN + FG35
G37	Same *k* as B9			BZ-CO-O2. + RO2. = RO2. + #.5 HO2. + CO2 + PHEN + FG37
G38	Same *k* as B10			BZ-CO-O2. + RCO3. = RCO3. + HO2. + CO2 + PHEN + FG38
G43	1.3E-11	-0.596		BZ-O. + NO2 = NPHE + FG43
G44	Same *k* as B5			BZ-O. + HO2. = PHEN + FG44
G45	1.0E-3			BZ-O. = PHEN + FG45
G46	2.63E-11			PHEN + HO. = #.15 RO2-NP. + #.85 RO2-R. + #.2 GLY + #4.7 -C + RO2. + FG46
G51	3.6E-12			PHEN + NO3 = HNO3 + BZ-O. + FG51
G52	4.2E-11			CRES + HO. = #.15 RO2-NP. + #.85 RO2-R. + #.2 MGLY + #5.5 -C + RO2. + FG52
G57	2.1E-11			CRES + NO3 = HNO3 + BZ-O. + -C + FG57
G58	3.6E-12			NPHE + NO3 = HNO3 + BZ(NO2)-O. + FG58
G59	Same *k* as G43			BZ(NO2)-O. + NO2 = #2 -N + #6 -C + FG59
G60	Same *k* as B5			BZ(NO2)-O. + HO2. = NPHE + FG60
G61	Same *k* as G45			BZ(NO2)-O. = NPHE + FG61

Reactions of methane and the lumped alkanes

RCH4	6.255E-13	2.548	2.0	CH4 + HO. = HCHO + RO2-R. + RO2. + FRCH4

A1OH	2.95E-12	0.229	AAR1 + HO. = #.924 RO2-R. + #.043 RO2-N. + #.007 RO2-XN. + #.025 HO2. + #.345 R2O2. + #1.319 RO2. + #.148 HCHO + #.329 CCHO + #.170 RCHO + #.265 ACET + #.262 MEK + #.025 CO + #.059 GLY + #.051 -C + FA1OH
A2OH	2.67E-12	-0.309	AAR2 + HO. = #.904 RO2-R. + #.093 RO2-N. + #.003 RO2-XN. + #.738 R2O2. + #1.738 RO2. + #.003 HCHO + #.368 CCHO + #.204 RCHO + #.380 ACET + #.566 MEK + #.020 CO + #.043 -C + FA2OH
A3OH	4.58E-12	-0.358	AAR3 + HO. = #.776 RO2-R. + #.222 RO2-N. + #.002 RO2-XN. + #.918 R2O2. + #1.918 RO2. + #.035 HCHO + #.049 CCHO + #.332 RCHO + #.036 ACET + #1.065 MEK + #.055 CO + #.021 CO2 + #.769 -C + FA3OH
A4OH	7.25E-12	-0.323	AAR4 + HO. = #.653 RO2-R. + #.347 RO2-N. + #.001 RO2-XN. + #.794 R2O2. + #1.794 RO2. + #.008 HCHO + #.045 CCHO + #.130 RCHO + #1.249 MEK + #.007 CO2 + #3.072 -C + FA4OH

Reactions of toluene and the lumped aromatics

TOLU	1.810E-12	-0.705	TOLU + HO. = #.085 BALD + #.26 CRES + #.118 GLY + #.131 MGLY + #.41 AFG2 + #.74 RO2-R. + #.26 HO2. + #2.726 -C + #.74 RO2. + FTOLU
A5OH	2.04E-12	-0.565	AAR5 + HO. = #.746 RO2-R. + #.254 HO2. + #.746 RO2. + #.064 PHEN + #.190 CRES + #.062 BALD + #.142 GLY + #.096 MGLY + #.132 AFG1 + #.299 AFG2 + FA5OH
A6OH	7.68E-12	-0.591	AAR6 + HO. = #.82 RO2-R. + #.18 HO2. + #.82 RO2. + #.18 CRES + #.039 BALD + #.101 GLY + #.387 MGLY + #.662 AFG2 + FA6OH

A7OH	2.13E-11	-0.591	AAR7 + HO. = #.82 RO2-R. + #.18 HO2. + #.82 RO2. + #.18 CRES + #.03 BALD + #.62 MGLY + #.6 AFG2 + FA7OH

Reactions of ethene

D1	1.96E-12	-0.870	ETHE + HO. = #.22 CCHO + #1.56 HCHO + RO2-R. + RO2. + FD1
D6	1.2E-14	5.226	ETHE + O3 = HCHO + #.44 CO + #.56 -C + #.12 HO2. + FD6
D8	1.04E-11	1.574	ETHE + O = HCHO + CO + HO2. + RO2-R. + RO2. + FD8
D9	5.43E-12	6.043	ETHE + NO3 = NO2 + #2 HCHO + R2O2. + RO2. + FD9

Reactions of the lumped alkenes

O1OH	2.24E-12	-1.585	OLE1 + HO. = #.871 RO2-R. + #.129 RO2-N. + RO2. + #.871 HCHO + #.256 CCHO + #.615 RCHO + FO1OH
O1O3	1.89E-15	3.025	OLE1 + O3 = #.06 HO. + #.165 HO2. + #.135 RO2-R. + #.135 RO2. + #.544 HCHO + #.253 CCHO + #.353 RCHO + #.189 MEK + #.295 CO + FO1O3
O1OA	2.24E-12	3.115	OLE1 + O = #.4 HO2. + #.5 RCHO + #.5 MEK + FO1OA
O1N3	4.55E-12	0.056	OLE1 + NO3 = NO2 + HCHO + #.294 CCHO + #.706 RCHO + FO1N3
O2OH	4.39E-12	-1.587	OLE2 + HO. = #.918 RO2-R. + #.082 RO2-N. + RO2. + #.270 HCHO + #.745 CCHO + #.544 RCHO + #.128 ACET + #.070 MEK + #.065 BALD + FO2OH
O2O3	1.97E-15	1.426	OLE2 + O3 = #.124 HO. + #.167 HO2. + #.206 RO2-R. + #.029 R2O2. + #.235 RO2. + #.004 CCO-O2. + #.004 C2CO-O2. + #.008 RCO3. + #.273 HCHO + #.501 CCHO + #.296 RCHO + #.069 ACET + #.355 MEK + #.014 MGLY + #.189 CO + #.035 BALD + #.018 BZ-O. + FO2O3

O2OA	6.97E-13	-0.034	OLE2 + O = #.4 HO2. + #.5 RCHO + #.5 MEK + FO2OA
O2N3	8.50E-12	-0.645	OLE2 + NO3 = NO2 + R2O2. + RO2. + #.295 HCHO + #.812 CCHO + #.593 RCHO + #.139 ACET + #.077 MEK + #.070 BALD + FO2N3

Reactions of α-pinene

APOH	1.210E-11	-0.882	APIN + HO. = RO2-R. + RCHO + RO2. + #7 -C + FAPOH
APO3	9.900E-16	1.366	APIN + O3 = #.05 HCHO + #.2 CCHO + #.5 RCHO + #.61 MEK + #.075 CO + #.05 CCO-O2. + #.05 C2CO-O2. + #.1 RCO3. + #.105 HO2. + #.16 HO. + #.135 RO2-R. + #.15 R2O2. + #.285 RO2. + #5.285 -C + FAPO3
APOA	3.000E-11		APIN + O = #.4 HO2. + #.5 MEK + #.5 RCHO + #6.5 -C + FAPOA
APN3	1.190E-12	-0.974	APIN + NO3 = NO2 + R2O2. + RCHO + RO2. + #7 -C + FAPN3

Reactions of isoprene and products[c]

IOH	1.0E-10		ISOP + HO. = #.36 MACR + #.48 MVK + #.84 HCHO + #.16 RO2-N. + #.89 RO2-R. + #.09 R2O2. + #1.14 RO2. + FIOH
IO3	1.2E-17		ISOP + O3 = #.39 MACR + #.16 MVK + #.07 CCHO + #.97 HCHO + #.44 CO + #.27 HO2. + #.27 HO. + #.07 RO2-R. + #.07 RO2. + #1.25 -C + FIO3
INO3	7.8E-13		ISOP + NO3 = #.95 NO2 + #.1 MACR + #.05 MVK + #.15 HCHO + #.85 RO2-N. + #.8 RO2-R. + #.2 R2O2. + #1.85 RO2. + #.05 -N + FINO3
IO	5.8E-11		ISOP + O = #.26 MACR + #.66 MVK + #.07 HCHO + #.01 RO2-N. + #.07 RO2-R. + #.01 R2O2. + #.09 RO2. + #1.2 -C + FIO

MVOH	1.9E-11	MVK + HO. = #.68 OH-CCHO + #.27 HCHO + #.27 MGLY + #.68 CCO-O2. + #.27 RO2-R. + #.68 RO2-N. + RO2. + #.68 RCO3. + #-0.05 -C + FMVOH
MVO3	4.8E-18	MVK + O3 = #.06 HCHO + #.94 MGLY + #.41 CO + #.11 HO2. + #.71 -C + FMVO3
MAOH	3.3E-11	MACR + HO. = #.08 HCHO + #.08 MGLY + #.4 OH-ACET + #.4 CO + #.5 MCO3. + #.48 RO2-R. + #.02 RO2-N. + #.5 RO2. + #.5 RCO3. + #-0.02 -C + FMAOH
MAO3	1.1E-18	MACR + O3 = #.9 MGLY + #.2 HCHO + #.6 CO + #.3 HO2. + FMAO3
I7	Photolysis set = CCHOR	OH-CCHO + HV = HCHO + CO + #2 HO2. + FI7
I8	1.0E-11	OH-CCHO + HO. = #.78 CCO-O2. + #.22 GLY + #.22 HO2. + #.78 RCO3. + FI8
I11	8.4E-12	MCO3. + NO2 = MPAN + FI11
I12	1.4E-11	MCO3. + NO = HCHO + NO2 + #3 -C + FI12
I13	3E-12	MCO3. + HO2. = HCHO + -OOH + #3 -C + FI13
I14	3.5E-12	MCO3. + RO2. = HCHO + CO + #.5 HO2. + RO2. + #2 -C + FI14
I15	5.3E-12	MCO3. + RCO3. = HCHO + HO2. + RCO3. + #3 -C + FI15
I16	2.2E-4	MPAN = MCO3. + NO2 + RCO3. + FI16
I17	8.2E-18	MPAN + O3 = #.6 HCHO + #3.4 -C + FI17
II8	3.6E-12	MPAN + HO. = #.6 OH-ACET + #.4 HCHO + #1.8 -C + FI18
I19	Photolysis set = ACETONE	OH-ACET + HV = HCHO + HO2. + CCO-O2. + RCO3. + FI19
I20	3E-12	OH-ACET + HO. = MGLY + HO2. + FI20

Reactions of fuel oxygenates [d]

MEOH	9.2E-13	MEOH + HO. = HCHO + HO2. + FMEOH
ETOH	3.2E-12	ETOH + HO. = #.95 CCHO + #.011 OH-CCHO + #.078 HCHO + #.05 RO2-R. + #.95 HO2. + #.05 RO2. + FETOH

TBA	1E-12	TBA + HO. = ACET + HCHO + RO2-R. + RO2. + FTBA
DME	3E-12	DME + HO. = #.2 MEK + RO2-R. + RO2. + #1.2 -C + FDME
DEE	1.2E-11	DEE + HO. = #.8 MEK + HCHO + RO2-R. + R2O2. + #2 RO2. + #-0.2 -C + FDEE
MTBE	3.1E-12	MTBE + HO. = #.22 MEK + #.02 ACET + #.38 HCHO + #.95 RO2-R. + #.05 RO2-N. + #.31 R2O2. + #1.31 RO2. + #3.43 -C + FMTBE
ETBE	9E-12	ETBE + HO. = #.26 MEK + #.16 CCHO + #.88 HCHO + #.97 RO2-R. + #.03 RO2-N. + #.85 R2O2. + #1.85 RO2. + #3.61 -C + FETBE
TAME	5.5E-12	TAME + HO. = #.68 MEK + #.96 HCHO + #.36 CCHO + RO2-R. + #1.3 R2O2. + #2.3 RO2. + #1.6 -C + FTAME

---

[a] Kinetic parameters in the mechanism are specified in one of the following ways:

1. *Simple thermal reactions*

   Parameters are listed in the form,

   $$A \quad E_a \quad B$$

   and rate constants are given by the expression

   $$k=A(T/300)^B \exp(-E_a/RT)$$

   where k and A are given in cm, molecule, s units, E_a is given in kcal mole^{-1}, T is temperature in K, and R is 0.0019872 kcal deg^{-1} mole^{-1}. When only one number is listed, E_a and B are zero, and if only two numbers are listed, then B is zero.

2. *"Falloff" thermal reactions*

   Rate constants denoted as "falloff" are both temperature and pressure dependent. Parameters are listed in the following order,

A_0 E_0 B_0

A_∞ E_∞ B_∞

f n

and the rate constant is determined from the expression

$$k = [(k_0 M)/(1+[k_0 M/k_\infty])]\, f^g$$

where

$$g=1/[1+(\log_{10}[k_0 M/k_\infty]/n)^2].$$

and

$$k_0 = A_0 (T/300)^{B}0 \exp(-E_0/RT)$$

$$k_\infty = A_\infty (T/300)^{B}{}_\infty \exp(-E_\infty/RT)$$

3. *Reactions with the same rate constants as other reactions*

The notation "Same *k* as *RXN#*", where *RXN#* is the reaction label of another reaction, indicates that this reaction has the same rate constant as reaction *RXN#*.

4. *Reactions in equilibrium with other reactions*

Equilibrium reactions are indicated by the notation "Equilibrium with reaction *RXN#*". The rate parameters listed refer to the equilibrium constant which can be calculated using the expression for simple thermal reactions. The rate constant used for the reaction is found by multiplying the equilibrium constant by the rate constant for reaction *RXN#*.

5. *Photolysis reactions*

Photolysis reactions are indicated by the notation "Photolysis set = *NAME*", where *NAME* refers to a set of absorption cross-section and quantum yield data that is

used to calculate the photolysis rate constants. The photolysis data sets used in this mechanism are listed in Table 3 of Carter (1990).

[b] The symbol "#" denotes a product yield coefficient. When no coefficient is given the yield is unity.

[c] The reactions of isoprene, methyl vinyl ketone, methacrolein, and their products are based on Paulson and Seinfeld (1992), Grosjean *et al.* (1993), Ashmnann and Atkinson (1994), and Grosjean *et al.* (1994).

[d] The reactions of the fuel oxygenates are based on recent experimental work. The references used to develop their mechanisms and rate constants are listed in Table 14 of the main paper.

APPENDIX B. MATHEMATICAL DEVELOPMENT OF THE ASSIGNMENT METHOD

The aim of the assignment method is to follow the reaction pathways of a mechanism and trace the ozone, or other product species, formed back to the original organic precursors. The essential concept is to track the progress of each reaction in the chemical mechanism through the use of dummy products added to each reaction, termed counter species (since they "count" the number of times a particular reaction occurs), and then, by appropriate stoichiometric manipulations of these products, to unravel the complex chemistry.

Given a mechanism with N species, A_i, i=1,2,...,N, and M reactions, a generalized reaction using the species, A_i, and the stoichiometric coefficients, s_{ij}, can be written

$$(-s_{1j})A_1 + (-s_{2j})A_2 \xrightarrow{j} s_{3j}A_3 + s_{4j}A_4 + \ldots + s_{Nj}A_N, \qquad j = 1,2,\ldots,M$$

where the stoichiometric coefficient s_{ij} is, by convention, negative for reactants and positive for products. As noted, a counter species, C_j, is added to each reaction,

$$(-s_{1j})A_1 + (-s_{2j})A_2 \xrightarrow{j} s_{3j}A_3 + s_{4j}A_4 + \ldots + s_{Nj}A_N + C_j$$

The concentrations of the chemical species, A_i, and the counter species, C_j, at any time can be represented by the vectors, $\mathbf{x}(t)$ and $\mathbf{f}(t)$, the elements of which are $x_i(t)$, the concentration of species A_i at time t, i=1,2,...,N, and $f_j(t)$, the concentration of the counter

species C_j for reaction j at time t, j=1,2,...,M. To allow for changes in mixing height, concentrations are best represented in height independent units, such as ppm-m or mmole-m^{-2}.

This technique for following the reaction pathways of a mechanism, which we call the assignment method, requires that one reactant in each reaction be selected as the "dominant" or controlling reactant. The dominant reactant for a given reaction will be the precursor to which the product species formed in the reaction will be assigned. Thus for the reaction

$$A_1 + A_2 \longrightarrow A_3 + A_4$$

the product species A_3 and A_4 can be "assigned" to either A_1 or A_2 depending on which species is specified as the dominant reactant. The selection of dominant reactants is based upon the information sought from the mechanism. The selection process is straightforward for reactions that have essentially only one reactant. Examples are photolysis reactions and those involving a constant species such as O_2 or H_2O. Since the main goal of the assignment method is to assign ozone back to the emitted organics, for our calculations when more than one reactant was present, the emitted species were given priority for selection as dominant reactant followed by organic radical species and, lastly, the nitrogen oxides. When, for example, an organic reacts with the OH radical, the organic species will be designated the dominant reactant. For the case of peroxy-peroxy reactions, the larger radical is selected as the dominant reactant such that a peroxyalkyl

radical has preference over an HO_2 radical which itself takes priority over an OH radical. In this way the organics and their more immediate products are selected as dominant reactants. Dominant reactant information can be placed in a vector **d**, composed of the elements d_j, where d_j is the index number of the species selected as the dominant reactant for reaction j, j=1,2,...,M. Thus for the reaction above, if A_2 is selected as the dominant reactant, the vector element d_j for this reaction will be 2. In this way the dominant reactant for any reaction j will be the species A_{d_j}.

Using the concentration vectors, $\mathbf{x}(t)$ and $\mathbf{f}(t)$, together with the stoichiometric coefficient matrix **S**, with elements s_{ij}, i=1,2,...,N, j=1,2,...,M, and the above vector **d**, all the necessary manipulations to trace the mechanism pathways may be performed. The first step is to determine the fraction, $h_j(t)$, of the dominant reactant A_{d_j} that passes through each reaction j. This fraction can be expressed in the following form,

$$h_j(t) = \frac{\Delta f_j(t)}{x_{d_j}(t-\Delta t) + \sum_{\substack{k=1 \\ s_{d_j k}>0}}^{M} s_{d_j k}\Delta f_k(t) + e_{d_j}(t)}$$

$$= \frac{\text{amount of reactant passing through reaction } j \text{ during time step } \Delta t \text{ ending at } t}{\text{amount of reactant available during time step } \Delta t \text{ ending at } t}$$

where $\Delta f_j(t)$ is the change in counter species j during the time step ending at t, $x_{d_j}(t-\Delta t)$ is the concentration at the beginning of the time step of species A_{d_j} (the dominant reactant for reaction j), $s_{d_j k}$ is the stoichiometric coefficient of A_{d_j} in reaction k, and $e_{d_j}(t)$, an element of the vector $\mathbf{e}(t)$, is the concentration of species A_{d_j} emitted during the time step

ending at t. In the development of the assignment method, the term emissions represents emissions from ground sources, entrainment from aloft, and any other non-chemical additions of species to the model cell. Deposition and other processes for removal from the gas-phase are best described by additional dummy reactions in which the removed species reacts and no products are formed. The summation in the above expression is over all reactions k, k=1,2,...,M, in which species A_{d_j} is produced (that is, when $s_{d_jk} > 0$). The variables $h_j(t)$, j=1,2,...,M, constitute the elements of a vector $\mathbf{h}(t)$.

To illustrate this consider the following three reactions, with counter species C_1, C_2, and C_3 added, that occur in all VOC/NO_x mechanisms:

$$\mathrm{HCHO} + h\nu \xrightarrow{1} 2\,\mathrm{HO_2} + \mathrm{CO} + \mathrm{C_1}$$
$$\mathrm{CO} + \mathrm{OH} \xrightarrow{2} \mathrm{HO_2} + \mathrm{CO_2} + \mathrm{C_2}$$
$$\mathrm{HO_2} + \mathrm{NO} \xrightarrow{3} \mathrm{OH} + \mathrm{NO_2} + \mathrm{C_3}$$

For the reactions above, the fraction of HO_2, the dominant reactant in reaction (3), reacting via reaction (3) is obtained by calculating $h_3(t)$,

$$h_3(t) = \frac{\Delta[\mathrm{C_3}]}{[\mathrm{HO_2}]_{t-\Delta t} + 2\,\Delta[\mathrm{C_1}] + \Delta[\mathrm{C_2}]}$$

The numerator of the above expression is the amount of HO_2 that has passed through reaction (3) during the time step from t-Δt to t. The denominator is the total amount of HO_2 available for reaction during the time step, being composed of the HO_2 present at the

beginning of the time step as well as any HO_2 produced during the time step by reactions (1) and (2), with, in this case, no HO_2 emitted.

The next quantities to be calculated are termed production factors, and can be placed in an $N \times N$ matrix, $\mathbf{G}(t)$, composed of the elements $g_{ik}(t)$, defined such that

$$g_{ik}(t) = \frac{\text{net amount of species } k \text{ produced or destroyed attributable to the reactions of species } i \text{ and its products during the time step ending at } t}{\text{amount of reactant species } i \text{ available during the time step ending at } t}$$

That is, g_{ik} is the amount of species k attributable to species i that is produced per amount of species i available for reaction. The production factor, $g_{ik}(t)$, when multiplied by a species concentration $x_i(t-\Delta t)$ will give the net amount of species k produced (or destroyed) by species i during the time step Δt ending at time t. It is in defining the production factors that the degradation pathways of the mechanism are traced. The production of species k due to species i is not merely the amount of species k formed or destroyed directly by reactions of species i, but includes also any amount of species k that is formed or destroyed by the reaction products of species i. Using the simple three-reaction mechanism from above, with HO_2 as the assigned species k, the following production factors can be written

$$\begin{aligned} g_{HCHO,HO_2}(t) &= h_1(t)\,[2 + 2\,g_{HO_2,HO_2}(t) + g_{CO,HO_2}(t)] \\ g_{CO,HO_2}(t) &= h_2(t)\,[1 + g_{HO_2,HO_2}(t) + g_{CO_2,HO_2}(t)] \\ g_{HO_2,HO_2}(t) &= h_3(t)\,[-1 + g_{OH,HO_2}(t) + g_{NO_2,HO_2}(t)] \end{aligned}$$

Production factors are obtained by multiplying the reaction probability, $h_j(t)$, for each reaction j in which species i is the dominant reactant, by the production factor of each product species in reaction j. When the assigned species k is formed, as is the case for HO_2 in reactions (1) and (2), a factor of +1 is included for each molecule of species k created; when species k is destroyed, as occurs for HO_2 in reaction (3), a factor of -1 is included. For more complicated mechanisms each production factor will contain several terms corresponding to each reaction in which species i is the dominant reactant. Production factors are, therefore, interdependent and can be determined by solving the system of linear equations for $\mathbf{G}(t)$,

$$\mathbf{A}(t)\,\mathbf{G}(t) = \mathbf{B}(t)$$

where the $N \times N$ matrices $\mathbf{A}(t)$ and $\mathbf{B}(t)$ are formed according to

$$\mathbf{A}(t) = \mathbf{S''}\,\mathbf{h}(t)$$

$$\mathbf{B}(t) = \mathbf{S'}\,\mathbf{h}(t)$$

where the $N \times N \times M$ matrices $\mathbf{S'}$ and $\mathbf{S''}$ are composed of the elements s'_{ik} and s''_{ikj}, i=1,2,...,N, k=1,2,...,N, j=1,2,...,M, with

$$s'_{ikj} = 0 \quad \text{for } i \neq d_j \qquad\qquad s''_{ikj} = 0 \quad \text{for } i \neq d_j$$

$$s'_{ikj} = -s_{kj} \quad \text{for } i = d_j \qquad\qquad s''_{ikj} = s_{kj} \quad \text{for } i = d_j,\ s_{kj} > 0$$

$$s''_{ikj} = 0 \quad \text{for } i = d_j,\ s_{kj} \leq 0$$

such that

$$a_{ik}(t) = \frac{\text{amount of species } k \text{ formed as a product in reactions of species } i \text{ during the time step ending at } t}{\text{amount of reactant species } i \text{ available during the time step ending at } t}$$

$$b_{ik}(t) = \frac{\text{net amount of species } k \text{ produced (amount formed as product minus amount destroyed as reactant) in reactions of species } i \text{ during the time step ending at } t}{\text{amount of reactant species } i \text{ available during the time step ending at } t}$$

Once the matrices $\mathbf{A}(t)$ and $\mathbf{B}(t)$ are calculated, the system of equations is solved for the matrix $\mathbf{G}(t)$. $\mathbf{A}(t)$, $\mathbf{B}(t)$, and $\mathbf{G}(t)$ are all square $N \times N$, non-singular matrices, thus permitting a variety of methods for solving the equations. The computer code we used for our calculations employed simple Gauss-Jordan reduction. The set of production factors, $\mathbf{G}(t)$, once calculated, may then be used to create a matrix of assigned species, $\mathbf{X'}(t)$, composed of the elements $x'_{ik}(t)$, the concentration of species i attributable to species k at time t, i=1,2,...,N, k=1,2,...,N. At time $t = 0$, the initially present species will be assigned to themselves such that

$$x'_{ik}(t) = x_i(t) \qquad \text{for } i = k$$

$$x'_{ik}(t) = 0 \qquad \text{for } i \neq k$$

Similarly, emitted species, whose concentrations are listed in $\mathbf{e}(t)$, are also assigned to themselves by forming a diagonal $N \times N$ matrix, $\mathbf{E}'(t)$, composed of the elements $e'_{ik}(t)$, $i=1,2,...,N$, $k=1,2,...,N$, where

$$e'_{ik}(t) = e'_i(t) \qquad \text{for } i = k$$

$$e'_{ik}(t) = 0 \qquad \text{for } i \neq k$$

The matrix $\mathbf{X}'(t)$ is then calculated as follows

$$\mathbf{X}'(t) = \mathbf{X}'(t-\Delta t) + \mathbf{X}'(t-\Delta t)\,\mathbf{G}(t) + \mathbf{E}'(t)\,\mathbf{G}(t)$$

The concentration of a species i, attributable to species k, at a given time is, therefore, the sum of the concentration at the previous time step plus any change in the concentration of species i during the time step due to the reactions of all the species attributable to species k, including emissions of species k during the time step. Once calculations are completed for all time steps, the matrix $\mathbf{X}'(t)$ will contain full information assigning all species within the mechanism back to the initially present or emitted species.

Table 1. Categories of Ozone Non-Attainment Regions (1990 Clean Air Act Amendments).

Area Class	Design Value (ppm)	Attainment Date[a]
Marginal	0.121-0.138	3 years
Moderate	0.138-0.160	6 years
Serious	0.160-0.180	9 years
Severe	0.180-0.280	15 years
Extreme	0.280 and above	20 years

[a] From 1990.

Table 2. Federal Tier I Tailpipe Emissions Standards (g/mile).

Vehicle Type	5 years/50,000 miles			10 years/100,000 miles		
	NMHC	CO	NO_x	NMHC	CO	NO_x
0-3750 lb.	0.25	3.4	0.4	0.31	4.2	0.6
3751-5750 lb.	0.32	4.4	0.7	0.40	5.5	0.97

Table 3. Federal Requirements for Reformulated Gasoline (1995-1997).

Each Gallon:

Controlled Emission/ Parameter	VC Control Region 1 (Southern Areas)	VC Control Region 2 (Northern Areas)
RVP (psi)	7.2	8.1
Oxygen (wt%)	2.0 Min., 2.7 Max	2.0 Min., 2.7 Max
Benzene (vol%)	1.0 Max	1.0 Max
Toxics (% reduction)	15.0	15.0

or

Average of All Gallons:

Controlled Emission/ Parameter	VC Control Region 1 (Southern Areas)	VC Control Region 2 (Northern Areas)
RVP (psi)	7.2	8.1
Oxygen (wt%)	2.1 Min., 2.7 Max	2.1 Min., 2.7 Max
Benzene (vol%)	0.95, 1.3 Max	0.95, 1.3 Max
Toxics (% reduction)	16.5	16.5

Table 4. Expected Properties of Reformulated Gasoline.

	Pre-1995 Industry Average	Federal	
		Phase I	Phase II
Benzene, vol%	1.53	0.95	0.95
Oxygen, wt%	0.0	2.1	2.1
RVP, psi	8.7	8.1/7.2	6.5-6.8
Aromatics, vol%	32	25-30	25-30
Sulfur, ppm wt	339	300-330	100-150
Olefins, vol%	9.2	small reduction likely	
T_{50}, °F	218	reduction of 0 to 20 likely	
T_{90}, °F	330	reduction of 0 to 20 likely	

Table 5. California Phase II Reformulated Gasoline Specifications.

		Averaging Option	
	Flat Limit	Average	Cap
Aromatics, vol%	25	22	30
Oxygen, wt%	1.8-2.2	--	--
Olefins, vol%	6	4	10
RVP, psi	7	--	--
Sulfur, ppm wt	40	30	80
T_{50}, °F	210	200	220
T_{90}, °F	300	290	310
Benzene, vol%	1.0	0.8	1.2

Table 6. California Low Emission Vehicle Program Emissions (g/mile).

Category	NMOG	CO	NO_x
Conventional (Federal Tier 1)	0.250 (NMHC)	3.4	0.4
TLEV	0.125	3.4	0.4
LEV	0.075	3.4	0.2
ULEV	0.040	1.7	0.2
ZEV	0	0	0

Table 7. Federal Tier II Vehicle Emissions as Compared to California TLEV and LEV Standards (g/mile).

	5 years/50,000 miles			10 years/100,000 miles		
Category	HC	CO	NO_x	HC	CO	NO_x
TLEV	0.125	3.4	0.4	0.156	4.2	0.6
LEV	0.075	3.4	0.2	0.090	4.2	0.3
Tier II	-	-	-	0.125	1.7	0.2

Table 8. Reactant species concentrations in reactivity calculations.

Mechanism Species	Chemical description	Total Emitted[a] (mmoleC/m^2)	Percent of VOC (% carbon)
NO		3.19	
NO_2		0.52	
HONO		0.04	
O_3		4.37	
CH_4		132.50	
CO		62.77	
alkanes			
AAR1	lumped C2-C4 alkanes	3.51	20.22
AAR2	lumped C5-C6 alkanes	2.89	16.63
AAR3	lumped C7-C9 alkanes	2.07	11.90
AAR4	lumped C10+ alkanes	0.76	4.38
aromatics			
TOLU	toluene	1.22	7.05
AAR5	benzene, monosubstituted benzenes	0.47	2.71
AAR6	xylenes, disubstituted benzenes	1.61	9.25
AAR7	trisubstituted benzenes	0.81	4.64
alkenes			
ETHE	ethene	0.49	2.83
OLE1	lumped terminal alkenes	0.93	5.33
OLE2	lumped internal alkenes	1.05	6.05
ISOP	isoprene	0.14	0.80
APIN	a-pinene, biogenics	0.11	0.65
carbonyls			
HCHO	formaldehyde	0.27	1.54
CCHO	acetaldehyde	0.19	1.12
RCHO	lumped aldehyde	0.14	0.78
ACET	acetone	0.15	0.86
MEK	lumped ketone	0.07	0.41
BALD	benzaldehyde	0.02	0.11
oxygenates			
MEOH	methanol	0.02	0.09
ETOH	ethanol	0.03	0.18
TBA	*tert*-butyl alcohol		
DME	dimethyl ether	0.03	0.18
DEE	diethyl ether	0.06	0.35
MTBE	methyl *tert*-butyl ether	0.08	0.44
ETBE	ethyl *tert*-butyl ether	0.09	0.53
TAME	*tert*-amyl methyl ether	0.09	0.53
Total VOC		17.37	100.00

[a] Total emitted reactant is sum of initially present, emitted, and entrained from aloft.

Table 9. Scenario conditions for urban ozone simulation.

Reactant Inputs (mmole m^{-2})		
	Initial	Emitted
VOC	9.51	6.25
NO_x	1.71	2.04
CO	24.12	7.58
CH_4	21.29	0

Aloft Concentrations (ppb)	
VOC	30
CO	500
CH_4	1790
O_3	70.4

	Initial	Final
Time of Day	8:00 am	6:00 pm
Mixing Height (m)	293	1823
Temperature (K)	295.5	305

Latitude (deg)	36.22
Longitude (deg)	16.50
Peak Ozone (ppb)	999

Table 10. Incremental Reactivities.

Mechanism Species	Incremental Reactivity (ppb O_3 / ppbC)	Kinetic Reactivity (ppb reacted / ppb emitted)	Mechanistic Reactivity (ppb O_3 / ppbC reacted)
CH_4	0.005	0.001	3.747
CO	0.037	0.038	0.969
AAR1	0.297	0.266	1.119
AAR2	0.412	0.490	0.842
AAR3	0.405	0.703	0.576
AAR4	0.233	0.823	0.283
TOLU	0.805	0.575	1.400
AAR5	0.575	0.541	1.063
AAR6	2.178	0.959	2.272
AAR7	2.917	0.975	2.992
ETHE	2.313	0.734	3.149
OLE1	1.736	0.967	1.795
OLE2	2.077	0.993	2.091
ISOP	2.196	0.989	2.219
APIN	1.012	0.993	1.020
HCHO	4.901	0.918	5.341
CCHO	2.733	0.866	3.156
RCHO	2.836	0.921	3.078
ACET	0.243	0.084	2.877
MEK	0.478	0.208	2.295
BALD	-0.191	0.910	-0.210
MEOH	0.394	0.131	3.014
ETOH	0.649	0.382	1.701
TBA	0.122	0.141	0.861
DME	0.393	0.363	1.082
DEE	1.361	0.811	1.678
MTBE	0.230	0.373	0.616
ETBE	0.697	0.733	0.951
TAME	0.660	0.557	1.185
VOC Mixture	1.056	0.638	1.657

Table 11. Assigned Ozone and Ozone Productivities.

Mechanism Species	Assigned Ozone (mmole m^{-2})	Productivity (ppb O_3 $ppbC^{-1}$)	Kinetic Productivity (ppb reacted / ppb emitted)	Mechanistic Productivity (ppb O_3 / ppbC reacted)
Inorganic	1.761			
CH_4	0.410	0.003	0.001	2.113
CO	1.719	0.027	0.038	0.727
AAR1	0.873	0.249	0.266	0.936
AAR2	1.104	0.382	0.490	0.781
AAR3	0.883	0.427	0.703	0.608
AAR4	0.244	0.320	0.823	0.389
TOLU	0.346	0.283	0.575	0.492
AAR5	0.103	0.219	0.541	0.405
AAR6	0.929	0.578	0.959	0.603
AAR7	0.590	0.731	0.975	0.750
ETHE	0.505	1.026	0.734	1.397
OLE1	0.903	0.976	0.967	1.009
OLE2	0.922	0.878	0.993	0.884
ISOP	0.162	1.167	0.989	1.180
APIN	0.056	0.497	0.993	0.500
HCHO	0.181	0.677	0.918	0.738
CCHO	0.243	1.256	0.866	1.450
RCHO	0.184	1.356	0.921	1.472
ACET	0.011	0.074	0.084	0.871
MEK	0.018	0.247	0.208	1.187
BALD	0.001	0.036	0.910	0.039
MEOH	0.003	0.164	0.131	1.250
ETOH	0.016	0.508	0.382	1.331
TBA	0.005	0.065	0.141	0.462
DME	0.010	0.338	0.363	0.929
DEE	0.050	0.810	0.811	0.998
MTBE	0.013	0.175	0.373	0.469
ETBE	0.040	0.434	0.733	0.592
TAME	0.040	0.432	0.557	0.776
TOTAL	12.325			

Table 12. Percent of Ozone Change Attributable to Individual Species.

Incremented Species	Species to which ozone is attributable										
	INORG	CH4	AAR1	AAR2	AAR3	AAR4	TOLU	AAR5	AAR6	AAR7	ETHE
CH4	12	59	5	6	4	1	1	0	0	0	1
AAR1	8	1	87	2	1	0	0	0	-1	0	0
AAR2	7	1	1	94	1	0	0	0	-1	-1	0
AAR3	6	0	0	0	105	0	-1	0	-1	-1	0
AAR4	6	-2	-4	-5	-4	136	-2	-1	-2	-1	-2
TOLU	10	4	8	10	7	2	37	1	0	0	3
AAR5	10	4	8	9	6	2	2	38	1	0	3
AAR6	9	4	10	11	8	2	2	1	28	0	3
AAR7	6	5	10	12	8	2	2	1	1	25	3
ETHE	9	3	7	8	6	1	1	0	0	0	47
OLE1	7	3	6	7	5	1	1	0	0	0	2
OLE2	7	3	8	9	6	2	1	0	0	0	2
ISOP	7	3	7	8	5	1	1	0	0	-1	2
APIN	6	3	7	8	6	1	1	0	0	0	2
HCHO	-4	4	10	11	8	2	1	0	30	-3	3
CCHO	7	3	7	8	5	1	1	0	0	0	2
RCHO	6	3	7	8	6	1	1	0	0	0	2
ACET	10	4	9	10	7	2	2	1	0	0	3
MEK	7	2	6	7	7	2	1	0	0	0	2
BALD	12	-7	-17	-19	-14	-4	-4	-1	-1	-1	-7
CO	13	1	2	2	1	0	0	0	-1	-1	0
MEOH	13	3	7	8	6	1	1	0	0	0	2
ETOH	9	1	3	3	2	1	0	0	0	0	1
MTBE	9	1	3	3	2	1	0	0	0	-1	1
ETBE	8	2	5	6	4	1	1	0	0	0	1
TBA	11	3	6	7	5	1	1	0	0	0	2
TAME	8	2	5	5	4	1	1	0	0	0	1
DME	8	1	2	2	1	0	0	0	-1	-1	0
DEE	7	3	6	6	4	1	1	0	0	0	2
MIX	7	3	11	14	11	3	3	1	6	3	5

Table 12. (continued)

Incremented Species	Species to which ozone is attributable											
	OLE1	OLE2	ISOP	APIN	HCHO	CCHO	RCHO	ACET	MEK	BALD	CO	MEOH
CH4	1	1	0	0	0	0	0	0	0	0	6	0
AAR1	0	-1	0	0	0	0	0	0	0	0	2	0
AAR2	-1	-1	0	0	0	0	0	0	0	0	0	0
AAR3	-2	-2	0	0	0	0	0	0	0	0	-2	0
AAR4	-4	-5	-1	0	0	-1	-1	0	0	0	-9	0
TOLU	3	2	0	0	0	1	0	0	0	0	12	0
AAR5	3	2	0	0	0	1	0	0	0	0	11	0
AAR6	3	3	1	0	0	1	1	0	0	0	14	0
AAR7	4	3	1	0	0	1	1	0	0	0	15	0
ETHE	2	2	0	0	0	0	0	0	0	0	10	0
OLE1	58	1	0	0	0	0	0	0	0	0	8	0
OLE2	3	44	0	0	0	0	0	0	0	0	11	0
ISOP	1	0	54	0	0	0	0	0	0	0	9	0
APIN	2	2	0	49	0	0	0	0	0	0	10	0
HCHO	3	3	0	0	14	0	0	0	0	0	15	0
CCHO	3	3	0	0	0	48	1	0	0	0	9	0
RCHO	4	4	0	0	0	0	49	0	0	0	9	0
ACET	3	3	0	0	0	1	0	33	0	0	12	0
MEK	1	2	0	0	0	0	0	0	54	0	7	0
BALD	-8	-11	-1	-1	0	-1	-1	0	0	19	-30	0
CO	0	0	0	0	0	0	0	0	0	0	81	0
MEOH	2	2	0	0	0	0	0	0	0	0	10	42
ETOH	0	0	0	0	0	0	0	0	0	0	3	0
MTBE	0	0	0	0	0	0	0	0	0	0	3	0
ETBE	1	1	0	0	0	0	0	0	0	0	7	0
TBA	2	1	0	0	0	0	0	0	0	0	7	0
TAME	1	0	0	0	0	0	0	0	0	0	6	0
DME	0	-1	0	0	0	0	0	0	0	0	1	0
DEE	1	1	0	0	0	0	0	0	0	0	7	0
MIX	7	7	1	0	1	2	1	0	0	0	10	0

Table 12. (continued)

Incremented Species	Species to which ozone is attributable							
	ETOH	MTBE	ETBE	TBA	TAME	DME	DEE	TOTAL
CH4	0	0	0	0	0	0	0	100
AAR1	0	0	0	0	0	0	0	100
AAR2	0	0	0	0	0	0	0	100
AAR3	0	0	0	0	0	0	0	100
AAR4	0	0	0	0	0	0	0	100
TOLU	0	0	0	0	0	0	0	100
AAR5	0	0	0	0	0	0	0	100
AAR6	0	0	0	0	0	0	0	100
AAR7	0	0	0	0	0	0	0	100
ETHE	0	0	0	0	0	0	0	100
OLE1	0	0	0	0	0	0	0	100
OLE2	0	0	0	0	0	0	0	100
ISOP	0	0	0	0	0	0	0	100
APIN	0	0	0	0	0	0	0	100
HCHO	0	0	0	0	0	0	0	100
CCHO	0	0	0	0	0	0	0	100
RCHO	0	0	0	0	0	0	0	100
ACET	0	0	0	0	0	0	0	100
MEK	0	0	0	0	0	0	0	100
BALD	0	0	0	0	-1	0	-1	-100
CO	0	0	0	0	0	0	0	100
MEOH	0	0	0	0	0	0	0	100
ETOH	78	0	0	0	0	0	0	100
MTBE	0	76	0	0	0	0	0	100
ETBE	0	0	63	0	0	0	0	100
TBA	0	0	0	54	0	0	0	100
TAME	0	0	0	0	66	0	0	100
DME	0	0	0	0	0	86	0	100
DEE	0	0	0	0	0	0	60	100
MIX	0	0	0	0	0	0	0	100

Table 13. Percent of ozone change attributable to concentration, kinetic, and mechanistic factors.

Incremented Organic	Δ[VOC]	ΔP^k	ΔP^m
CH4	56	31	13
CO	75	13	12
AAR1	84	17	-1
AAR2	93	12	-5
AAR3	106	6	-11
AAR4	137	-15	-22
TOLU	35	50	14
AAR5	38	50	12
AAR6	27	55	18
AAR7	25	59	16
ETHE	44	43	12
OLE1	56	39	5
OLE2	42	48	10
ISOP	53	43	4
APIN	49	44	7
HCHO	14	54	33
CCHO	46	42	12
RCHO	48	40	12
ACET	30	50	18
MEK	52	34	13
BALD	19	-87	-33
MEOH	41	41	17
ETOH	78	21	1
TBA	54	35	11
DME	86	14	0
DEE	59	35	5
MTBE	76	20	3
ETBE	62	33	5
TAME	65	30	4
MIX	67	44	10

Table 14. Oxygenate fuel component mechanisms.

Reaction	k_{OH} (298 K) (10^{13} cm^3 molecule^{-1} s^{-1})	Reference [a]
methanol $CH_3OH + OH \rightarrow HCHO + HO_2$	9.2	(Atkinson *et al.*, 1992) / (Atkinson *et al.*, 1992)
ethanol $C_2H_5OH + OH \rightarrow 0.95\ CH_3CHO + 0.011\ CH(O)CH_2OH + 0.078\ HCHO + HO_2 + 0.05\ (NO \rightarrow NO_2)$	32	(Atkinson *et al.*, 1992) / (Atkinson *et al.*, 1992)
tert-butyl alcohol $(CH_3)_3COH + OH \rightarrow (CH_3)_2CO + HCHO + HO_2 + (NO \rightarrow NO_2)$	10	(Japar *et al.*, 1990) / (Japar *et al.*, 1990; Saunders *et al.*, 1994)
dimethyl ether $CH_3OCH_3 + OH \rightarrow HCOOCH_3 + HO_2 + (NO \rightarrow NO_2)$	30	(Japar *et al.*, 1990) / (Wallington *et al.*, 1988; Tully and Droege, 1987; Bennett and Kerr, 1990)
diethyl ether $C_2H_5OC_2H_5 + OH \rightarrow HCOOC_2H_5 + HCHO + HO_2 + 2\ (NO \rightarrow NO_2)$	120	(Wallington and Japar, 1991) / (Semadeni *et al.*, 1993)
methyl *tert*-butyl ether $CH_3OC(CH_3)_3 + OH \rightarrow 0.76\ HCOOC(CH_3)_3 + 0.17\ CH_3COOCH_3 + 0.38\ HCHO + 0.02\ (CH_3)_2CO + 0.95\ HO_2 + 0.05\ RNO_3 + 1.31\ (NO \rightarrow NO_2)$	31	(Tuazon *et al.*, 1991) / (Bennett and Kerr, 1990)
ethyl *tert*-butyl ether $C_2H_5OC(CH_3)_3 + OH \rightarrow 0.64\ HCOOC(CH_3)_3 + 0.13\ CH_3COOC(CH_3)_3 + 0.97\ HO_2 + 0.04\ CH_3COOC_2 + 0.16\ CH_3CHO + 0.88\ HCHO + 0.03\ RNO_3 + 1.85\ (NO \rightarrow NO_2)$	90	(Smith *et al.*, 1992) / (Wallington *et al.*, 1988, 1989; Smith *et al.*, 1992)
tert-amyl methyl ether $CH_3O(CH_3)_2C_2H_5 + OH \rightarrow 0.4\ HCOOC(CH_3)_2C_2H_5 + 0.12\ C_2H_5COOCH_3 + 0.48\ CH_3COOCH_3 + 0.36\ CH_3CHO + 0.96\ HCHO + HO_2 + 2.3\ (NO \rightarrow NO_2)$	55	(Whitten and Yarwood, 1992) / (Wallington *et al.*, 1993)

[a] The first reference is for the mechanism; the second set is references for the rate constant.

Table 15. Comparison of fuel oxygenates.

	k_{OH} (x 10^{13} cm^3 $molecule^{-1}$ sec^{-1})	*Ozone per carbon atom* Incremental Reactivity (mole O_3 mole C^{-1})	Productivity (mole O_3 mole C^{-1})	*Ozone per molecule* Incremental Reactivity (mole O_3 $mole^{-1}$)	Productivity (mole O_3 $mole^{-1}$)
MeOH	9.2	0.394	0.164	.394	.164
EtOH	32	0.649	0.508	1.298	1.016
TBA	10	0.122	0.065	.488	.260
DME	30	0.393	0.338	.786	.676
DEE	120	1.361	0.810	5.444	3.240
MTBE	31	0.230	0.175	1.150	.875
ETBE	90	0.697	0.434	4.182	2.604
TAME	55	0.660	0.432	3.960	2.592

LIST OF FIGURES

Figure 1.

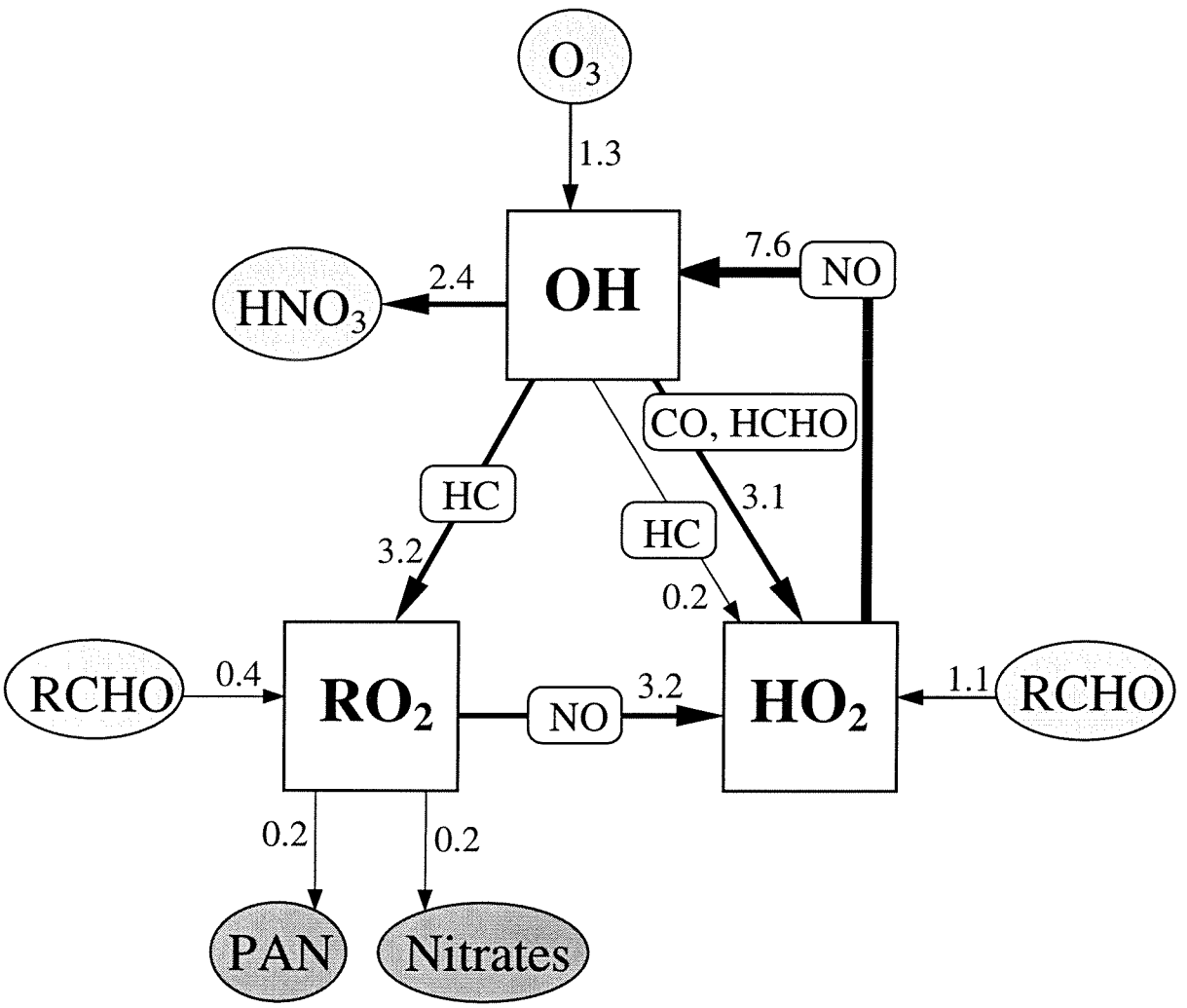
O_3
1.3
OH
7.6
NO
2.4
HNO_3
CO, HCHO
HC
3.2
HC
3.1
0.2
RCHO
0.4
RO_2
NO
3.2
HO_2
1.1
RCHO
0.2
0.2
PAN
Nitrates

Figure 2.

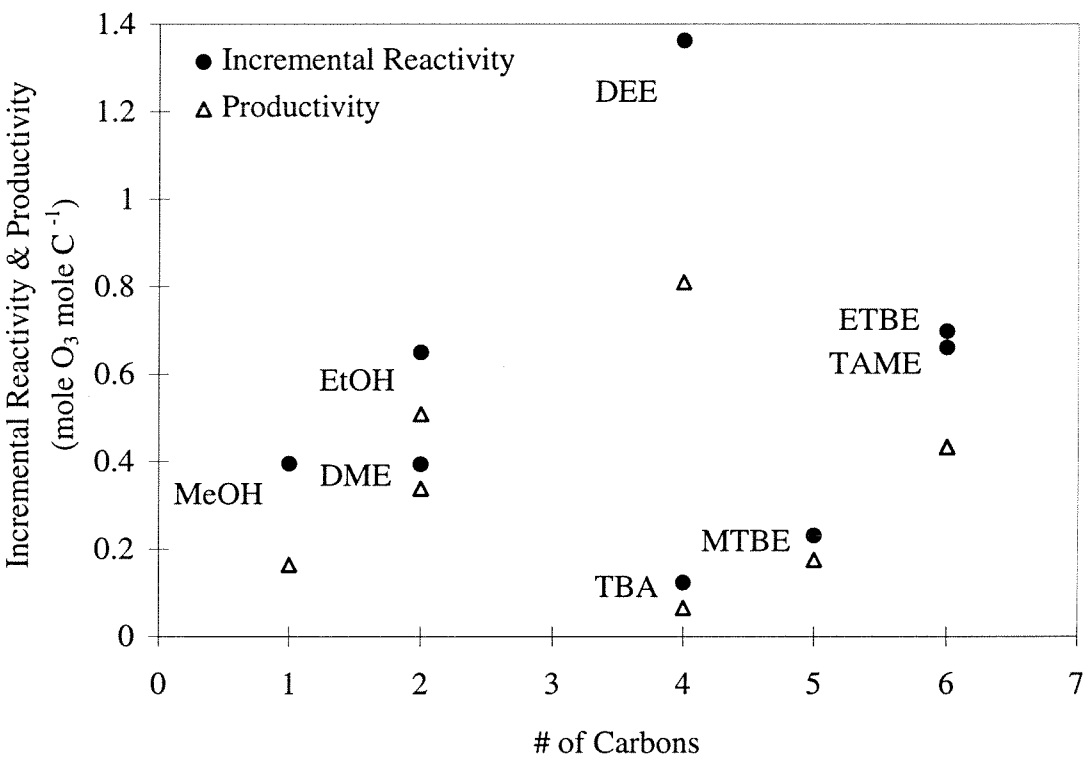
Incremental Reactivity & Productivity
(mole O_3 mole C^{-1})
Incremental Reactivity
Productivity
DEE
ETBE
TAME
EtOH
MeOH
DME
MTBE
TBA
# of Carbons
0
0.2
0.4
0.6
0.8
1
1.2
1.4
0
1
2
3
4
5
6
7

Figure 3.

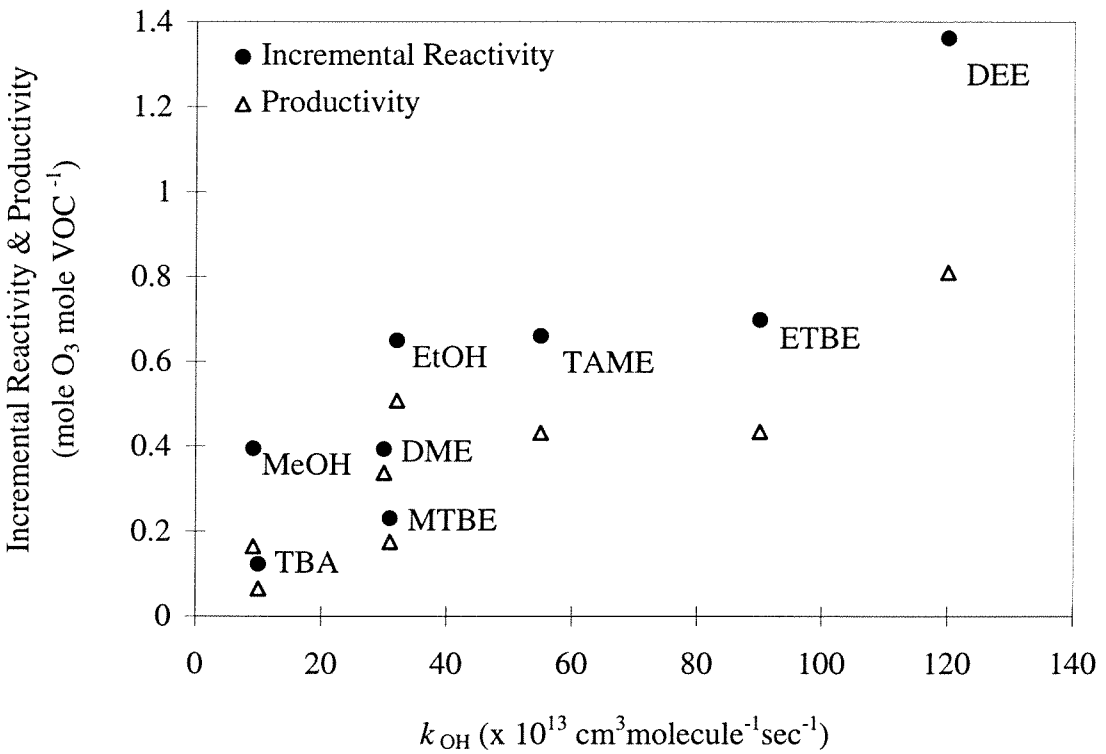
Incremental Reactivity & Productivity
(mole O_3 mole VOC^{-1})
1.4
1.2
1
0.8
0.6
0.4
0.2
0
Incremental Reactivity
Productivity
DEE
EtOH
TAME
ETBE
MeOH
DME
MTBE
TBA
0
20
40
60
80
100
120
140
k_{OH} (x 10^{13} $cm^3 molecule^{-1} sec^{-1}$)

CHAPTER 6:

FORMATION OF ORGANIC AEROSOLS FROM THE OXIDATION OF BIOGENIC HYDROCARBONS

Submitted to *J. Atmos. Chem.*

Formation of organic aerosols from the oxidation of biogenic hydrocarbons

Thorsten Hoffmann[1], Jay R. Odum[2], Frank Bowman[3], Donald Collins[2], Dieter Klockow[1], Richard C. Flagan[3], John H. Seinfeld[3]*

[1] Institut fuer Spektrochemie und angewandte Spektroskopie, 44139 Dortmund, Germany

[2] Department of Environmental Engineering Science and

[3] Department of Chemical Engineering, California Institute of Technology, Pasadena, CA 91125, USA

* To whom correspondence should be addressed

Abstract

Measurements of aerosol formation during the photooxidation of α-pinene, β-pinene, d-3-carene, d-limonene, ocimene, linalool, terpinene-4-ol, and trans-caryophyllene were conducted in an outdoor smog chamber. Daylight experiments in the presence of NO_x and dark experiments with elevated ozone concentrations were performed. The evolution of the aerosol was simulated by the application of a gas/particle absorption model. Ozone and, for selected hydrocarbons, the NO_3 reaction of the compounds were found to represent efficient routes to the formation of condensable products. For initial hydrocarbon mixing ratios of about 100 ppb, the fractional aerosol yields from daylight runs have been estimated to be ~ 5% for open-chain hydrocarbons, such as ocimene and linalool, 5 - 25% for monounsaturated cyclic monoterpenes, such as α-pinene, d-3-carene, or terpinene-4-ol, and ~ 40% for a cyclic monoterpene with two double bonds like d-limonene. For the only sesquiterpene investigated, trans-caryophyllene, a fractional aerosol yield of close to 100% was observed. The majority of the compounds studied showed an even higher aerosol yield during dark experiments in the presence of ozone.

Key words: biogenic hydrocarbons, ozone, nitrate radicals, aerosol formation, gas/particle partitioning.

1. Introduction

Terrestrial vegetation releases a variety of reactive organic compounds into the atmosphere, especially isoprene, monoterpenes, sesquiterpenes, as well as oxygen-containing compounds, such as alcohols or ketones. The atmospheric chemistry of these biogenic non-methane hydrocarbons (NMHCs) has received particular attention because of the large quantities emitted globally in comparison with the release of anthropogenic NMHCs and the high reactivity of the mostly unsaturated biogenic NMHCs. The total annual global emission of biogenic hydrocarbons has been estimated between 825 and 1150 $TgCyr^{-1}$ (Fehsenfeld et al., 1992, Guenther et al., 1995), whereas anthropogenic hydrocarbons have been estimated to account for less than 100 Tg C per year (Mueller, 1992, Hough and Johnson, 1991). Because of the considerable reactivity of the natural alkene emissions, they play an important role in tropospheric chemistry. For example, there is substantial evidence that biogenic hydrocarbons influence the regional distribution of ozone (Simpson et al., 1995, Chameides et al., 1992, Trainer et al., 1993, Roselle et al., 1991, McKeen et al., 1991a, McKeen et al., 1991b, Vogel et al., 1995).

One of the major uncertainties of the impact of biogenic hydrocarbons on atmospheric processes is the quantitative understanding of their ability to form organic aerosols. Although the aerosol formation potential of biogenic NMHCs was noted as early as 1960 (Went, 1960), the magnitude of the natural contribution to the particulate burden in the atmosphere is still not well characterized. Some studies have focused on isoprene and a few monoterpenes as precursors for organic aerosol but even less is known about the aerosol formation potential of other important biogenic compounds, such as sesquiterpenes and oxygenated compounds. The few available studies have shown a considerable contribution of biogenic NMHCs (especially monoterpenes) to total secondary organic aerosols (Pandis et al., 1991, Pandis et al., 1992, Palen et al., 1992, Zhang et al., 1992, Paulson et al., 1990, Hatakeyama et al., 1989, Hatakeyama et al., 1991, Kamens, 1981 , Hooker et al., 1985).

In addition to their importance in the urban and regional atmosphere, the formation of aerosols from the conversion of naturally emitted hydrocarbons is a matter of great interest because of the need to distinguish natural and anthropogenic contributions to direct radiative forcing of climate by aerosols (Andreae, 1995, Jonas et al., 1995,

Pilinis et al., 1995, Twomey, 1991, National Research Council, 1996). To evaluate the biogenic impact on atmospheric aerosols, reliable data about natural source strength and composition of organic particles has to be included in respective models. In addition to the direct influence of aerosols on the radiation budget of the cloudless atmosphere, aerosol particles can serve as cloud condensation nuclei (CCN) on which water vapor condenses to form cloud droplets. Organics can play a key role in the interaction between aerosols and water in the atmosphere (Novakov and Penner, 1993, Saxena et al., 1995, Shulman et al., 1996). The purpose of this paper is to determine the relative aerosol-forming potential of biogenic hydrocarbons and which reaction pathways are most important.

2. Experimental procedure

The experimental system of the Caltech outdoor smog chamber has been described previously (Odum et al., 1996). A short description of the facility and the experimental procedure employed in the present experiments is given here. All experiments used a collapsible Teflon bag in a dual-chamber mode in which the bag was divided in the center, resulting in two chambers with approximately the same bag volume (~ 20 m^3). The chamber was mounted on nets on a metal framework ~ 0.7 m above the ground on the roof of a laboratory building. To reduce the amount of residual material in the bag prior to each experiment, the chamber was flushed with purified particle free air for at least 38 hours and exposed to sunlight for at least one day. The night before each experiment the chamber was flushed with rehumidified air.

Two sets of experiments were carried out: daylight experiments to investigate the aerosol formation in the presence of NO_x and dark reactions with elevated ozone concentrations to assess the potential of ozonolysis reactions of the natural alkenes to form condensable species.

For each daylight experiment, the chamber, covered with a black tarpaulin, was filled with NO, NO_2, propene (as a photochemical initiator), the hydrocarbons of interest, and, for most of the runs, ammonium sulfate seed particles. The latter were produced

by nebulizing an aqueous solution of $(NH_4)_2SO_4$ with a constant rate atomizer (Liu and Lee, 1975) followed by a diffusion dryer and an ^{85}Kr aerosol neutralizer. The seed particle injection was maintained until a particle concentration of 5,000 - 10,000 particles cm^{-3} was achieved (number mean diameter ~ 100 nm). Then, the desired amounts of propene, NO_2 and NO were added to both chamber halves through Teflon tubing using certified cylinders of the gases in nitrogen. Afterwards, the biogenic hydrocarbons were injected into the chambers by slowly evaporating the pure liquids within a heatable glass bulb into the purified air supply. Additionally, hexafluorobenzene was injected into the chambers as an internal standard for the hydrocarbon measurements. The low reactivity of this compound towards gas-phase oxidation results in lifetimes much longer than the time scale of the experiments, and it therefore represents an ideal substance against which to normalize the hydrocarbon measurements. Before removing the tarpaulin, the reactants were allowed to mix in the bag over a period of several minutes and the initial concentrations of the reactants were then measured.

The gas-phase concentrations of NO_2 and NO were monitored using a chemiluminescence NO_x analyzer (Model 42, Thermo Environmental Instruments, Franklin (MA), USA). The NO_2 channel of the instrument showed a significant interference from PAN and PPN, a characteristic that has to be considered in the later stage of the experiments when PAN concentrations are an important fraction of NO_y. A Dasibi Environmental Corp. (Glendale, CA) Model 1008-PC O_3 analyzer was used to monitor ozone concentrations. Both instruments were calibrated on a regular basis. This equipment was used to measure the gas-phase concentrations of the compounds on both sides of the chamber, alternately switching the sample flow every 10 minutes between the two halves of the Teflon bag. For measurement of the hydrocarbon concentrations, two GC systems were employed. One system consisted of a 2 mL heated sample loop (100 °C) mounted on a Hewlett-Packard Gas Chromatograph (Model 5890) equipped with a flame ionization detector. Separate Teflon sampling lines from each side of the bag to the GC inlet valve were used to prevent memory effects after the injection of the compounds as well as to minimize these effects when switching between the two sides. In order to separate propene from methane, the GC

oven was cooled to -60 °C. After hydrocarbon injection, this temperature was held for 1 min and then increased rapidly (typically 40 °C min^{-1}) until the elution of the biogenic compound was detected. Depending on the retention behavior of the chosen compounds, the hydrocarbon concentrations could be measured every 10 to 15 min. Calibration was performed on a daily basis by producing a suitable standard gas atmosphere, either by diluting the test gas from certified cylinders (propene, α-pinene in N_2) with purified lab air or by evaporating a calibration solution of the analytes in CH_2Cl_2 in a Teflon bag of known volume. Comparison of both calibration methods for selected substances showed excellent agreement.

The second technique to measure hydrocarbon concentrations allowed the preconcentration of the compounds on solid adsorbents (Tenax TA/Carbosieve (Tekmar, Cincinnati (OH), USA)) immediately underneath the Teflon ports of the chambers, avoiding long sampling lines that could alter the measured hydrocarbon concentration due to memory effects. Especially for measurement of rapid concentration changes associated with higher and more reactive biogenic hydrocarbons, such as sesquiterpenes, this method was found to be favorable. Prior using the cartridges, conditioning of the tubes was performed by heating at 275 °C for 12 h under a flow of nitrogen (30 mL min^{-1}). A sequential sampler device containing 8 sampling tubes was used on each side to measure the change in the hydrocarbon concentration during the experiments. Sampling volumes of 0.4 to 2 L with a sample flow rate of about 130 mL min^{-1} were chosen to preconcentrate the analytes. The loaded tubes were thermally desorbed with a Tekmar 6000 AEROTrap equipped with a cryo-focusing module and finally separated and analyzed with a Hewlett Packard G1800A GCD system.

The aerosol instrumentation included two scanning electrical mobility spectrometers (SEMS) and two condensation nucleus counters (CNC) acting as particle detectors on each side of the bag. Complete number and size distribution measurements were obtained with a 1 min time resolution throughout the experiments using one radial SEMS (Zhang et al., 1995) (size range 5-80 nm) and one cylindrical SEMS (TSI, St.

Paul (MN), USA) (size range 30-850 nm) simultaneously. A more complete description of the operation conditions for the aerosol measurements has been published previously (Odum et al., 1996).

Ozone reactions of the biogenic hydrocarbons were studied in the same chamber with excess ozone, but exclusively in the absence of sunlight (chamber covered with the black tarpaulin). The protocol for conditioning of the chamber was identical to that described for the daylight experiments. Ozone was produced using an ozone generator and introduced into the bag until an O_3 mixing ratio of 150-330 ppb was reached. At the same time, ammonium sulfate seed particles were injected into the bag. When ozone and seed particles were well mixed and their concentrations became stable, the chamber was divided and the hydrocarbons were injected in the same manner described above. The precise chamber volumes were determined by adding known amounts of C_6F_6 to the chambers and measuring its concentrations using the pre-calibrated sample loop GC system. These experiments were carried out without cyclohexane, which is usually added to scavenge the OH radicals formed in the O_3 reactions of alkenes. Although a fraction of the natural alkenes was degraded by OH produced by the O_3 reactions, and therefore complicated the exact quantification of the amount of hydrocarbon that reacted with O_3, the additional contribution of cyclohexane oxidation products to the particle phase was avoided.

In selected chamber runs (daylight as well as dark experiments), bulk aerosol samples were collected on quartz filters and subsequently analyzed by supercritical-fluid extraction using carbon dioxide, followed by gas chromatography-mass spectrometry. The main focus of this aerosol sampling was to obtain qualitative information about the chemical composition of the organic aerosol formed during the smog chamber experiments.

3. Results and Discussion

3.1 AEROSOL YIELDS

The aerosol formation of each hydrocarbon was investigated at different initial concentrations and consequently a range of aerosol yields was found. Table 1 shows the experimentally determined fractional aerosol yields from the daylight experiments of the biogenic hydrocarbons investigated. The fractional aerosol yield (Y) is defined as the fraction of a hydrocarbon that is converted to aerosol and can be calculated by

$$Y = \frac{M_o}{\Delta ROG} \qquad (1)$$

where M_o is the organic aerosol mass concentration (μg m^{-3}) and ΔROG the amount of reactive organic gas that reacted (μg m^{-3}). Total organic aerosol mass concentration was calculated from the observed total organic aerosol volume, assuming a density of 1 g cm^{-3}. Overall, the yields increased with increasing initial hydrocarbon concentration. Observed aerosol yields can be explained to a large extent in the framework of a gas/particle partitioning model, in which the yield is a function of the organic aerosol mass concentration (Odum et al., 1996).

To demonstrate the correlation between aerosol yield and organic aerosol mass, Figure 1 displays the overall yields from nine α-pinene experiments as a function of the final organic aerosol mass concentration. It can be seen that the aerosol yield (Y) is a strong function of the organic aerosol mass, in which Y increases rapidly at small values of M_o and becomes flatter at higher values. This behavior is expected when the gas/aerosol partitioning of the oxidation products is governed by equilibrium partitioning into an absorptive organic matter phase (Pankow, 1994a, Pankow, 1994b, Odum et al., 1996). The functional form of this dependence is expressed as

$$Y = \sum_i Y_i = M_o \sum_i \left(\frac{\alpha_i K_{om,i}}{1 + K_{om,i} M_o} \right) \qquad (2)$$

$$K_{om,i} = \frac{760RT}{MW_{om}10^6\zeta_i p^0_{L,i}} \quad (3)$$

for a series of individual products i, where $K_{om,i}$ is the partitioning coefficient for species i in terms of the organic mass concentration, α_i is the individual formation yield of i, M_o is the absorbing organic mass concentration, MW_{om} is the mean molecular weight of the absorbing organic material, ζ_i is the activity coefficient of compound i in the organic material phase, and $p^0_{L,i}$ is the vapor pressure of compound i at the temperature of interest. The model line through the data in Figure 1, generated from equation (2), uses a two-product model and the $K_{om,i}$ and α_i values were chosen to fit the data points. Although the knowledge about the precise degradation pathway for α-pinene is limited (i.e. the exact number and yields of the products as well as their individual partitioning coefficients are unknown), the close agreement between measured and modeled aerosol yields implies that the organic aerosol yield from biogenic hydrocarbon oxidation is described by equilibrium gas/particle partitioning. Similar results have been obtained for aromatic systems, such as m-xylene and 1,2,4-trimethylbenzene (Odum et al., 1996).

3.2 OZONE-ALKENE REACTIONS IN THE DARK

Initial concentrations and experimental conditions used in the dark experiments are summarized in Table 2. Because of the fact that no OH radical scavengers, such as cyclohexane, was added to the chamber, the discrepancy between the amounts of the biogenics and ozone that reacted ($\Delta O_3/\Delta ROG$, see Table 2) is most likely attributed to reaction of the alkenes with OH radicals generated in the O_3 reaction mechanism. Although the aerosol yields given in the table reflect simultaneous O_3 and OH reactions, the ozonolysis always represents the major reaction pathway (typically 80 % of the hydrocarbons reacted with O_3).

Analogous to the daylight experiments, aerosol formation from α-pinene was investigated at different initial concentrations. The first five chamber runs listed in Table 2 were performed during the day the chamber was covered with a tarpaulin. Consequently, the temperature in the bag was relatively high (47.7 ± 1.1 °C). Figure 2 shows the fractional aerosol yields (Y) observed in the α-pinene experiments, again plotted as a function of the organic mass concentration (M_o). A comparison with the results from the daylight experiments (Figure 1) reveals several interesting differences. First, the aerosol yield of α-pinene is generally higher for the dark experiments and, secondly, the dependence of the yields on the total aerosol organic mass concentration is less pronounced. In connection with equation (2) and (3), the second observation can be used to predict some physico-chemical properties of the products formed from α-pinene ozonolysis. The type of partitioning behavior observed is expected when very nonvolatile products are produced in the reaction. These compounds will virtually completely condense on preexisting particles (or even homogeneously nucleate), and consequently the aerosol yield will be nearly independent of the organic aerosol concentration. The line through the data shown in Figure 2 has been generated from equation (2) using the two-product model, where again the $K_{om,i}$ and α_i values were chosen in order to fit the experimental data. One product (product 1) was assumed to possesses an absorption equilibrium constant ($K_{om,1}$) of 0.2 and a product yield (α_1) of 0.12, the second product (product 2) 5×10^{-3} and 0.19, respectively. It should be noted here that the fit of the model line through the data is more or less insensitive to the exact value of K_{om} for product 1 as long as this number exceeds approximately 0.1.

A relatively nonvolatile product that is expected to be formed during α-pinene oxidation is pinonic acid. In principle, equation (3) could be used to obtain an estimate of the absorption equilibrium constant for this compound by substituting values for the various parameters in the equation. Since only very limited data on vapor pressures of semi- and nonvolatile substances are available in the literature, it is difficult to calculate K values theoretically. However, in order to demonstrate that the constants chosen are appropriate for chemical species like pinonic acid, we can perform this procedure for adipic acid, an oxidation product of cyclohexene.

Following the suggestions for the various parameters made by Pankow (1994b) for secondary organic aerosol ($MW_{om} \cong 200$ and $\zeta_i \cong 1$) and using the vapor pressure of adipic acid as a subcooled liquid (Pankow, 1994a), an absorption equilibrium constant of approximately 1 can be estimated. This value lies well above the K of 0.1 necessary to explain the experimental data. Although the molecular nature of the two organic acids is not identical, these results support the general idea that ozone/α-pinene reactions immediately produce nonvolatile compounds, such as multifunctional carboxylic acids.

One experiment with α-pinene was conducted during the night and therefore the temperature in the bag was substantially lower than that during the day ($\Delta T_{night/day} \sim$ 32 °C). The fractional aerosol yield estimated in this run, also shown in Figure 2, exceeds the yields of the other dark experiments by a factor of about three. Again, this behavior can be explained qualitatively by the gas/particle partitioning absorption model. Since $K_{om,i}$ is inversely proportional to the vapor pressure (equation (3)), the individual aerosol yields for more volatile products will be very sensitive to temperature. For the given system, compounds like pinonic aldehyde or similar species are likely to represent these kind of products.

One of the major assumptions underlying the derivation of equation (2) is that the total amount of a product that is produced in the reaction is proportional to the amount of the parent hydrocarbon reacted. For the dark experiments, where almost exclusively ozone/alkene reactions take place, this is likely to be the case and therefore not only the final yield, but also the yield at any time $Y(t)$, should be described by equation (2). In practice, the high rate of biogenic/ozone reactions complicates this approach, because hydrocarbon and aerosol measurements have to be accurately synchronized. Consequently, we applied this procedure only for β-pinene and d-3-carene, both relatively unreactice biogenics towards ozone. Figure 3 shows the $Y(t)$ values versus organic aerosol mass for the β-pinene experiment of October 10, 1995. Usually, at least two products are necessary to describe the measured aerosol yields by the application of equation (2). For this particular compound, only an one-product model

is sufficient to represent the shape of the curve (K_{om} = 0.11, α = 0.35), although this observation does not necessarily exclude the possibility that many condensable products with similar vapor pressures are produced. However, analogous to the α-pinene/ozone reaction, the products in the particle phase are nonvolatile compounds with vapor pressures in the range of 10^{-6} to 10^{-7} torr.

3.3 MODELING THE CHEMISTRY OF BIOGENIC NMHCs DURING DAYLIGHT EXPERIMENTS

The dominant loss processes for volatile organic compounds in the troposphere are chemical transformations by reaction with hydroxyl radicals (OH), nitrate radicals (NO_3) and ozone. Especially for the oxidation of the mostly unsaturated biogenic hydrocarbons, all three of these reactions must be considered in assessing the transformation processes of a given alkene (Atkinson, 1994). The initial step of these reactions proceeds exclusively via the addition of the oxidizing species to the double bond of the hydrocarbon, except the OH radical reaction, in which H-atom abstraction is also possible. However, for this group of compounds H-atom abstraction can be assumed to be of minor importance.

Since the individual products and the product distribution from the three reactions are quite different, the fractional aerosol yields from the particular oxidation reactions can also be expected to be different. In order to assess the potential of each of these reactions to form condensable organic species, it is necessary to estimate the contribution of the individual reactions during the course of an experiment and to connect this information with the actual aerosol evolution in the chamber. Because the concentrations of the biogenic hydrocarbons and ozone were measured during the experiments, and the reaction rate constants are well known, the fraction of the hydrocarbon that reacted with ozone can be determined directly (Zhang et al., 1992). However, because of a lack of measurements of OH and NO_3 mixing ratios in the chamber, the consumption of the hydrocarbons due to their radical reactions must be estimated using a chemical mechanism. The detailed mechanism for gas-phase reactions of organic compounds developed by Carter (1990) (so-called SAPRC

mechanism) was employed to simulate the chemistry of the organics during the chamber runs. Rate constants of the investigated hydrocarbons with OH, NO_3 and O_3 were taken from the literature (Atkinson, 1994, Shu and Atkinson, 1995).

3.4 EVIDENCE FOR NITRATE RADICAL REACTIONS

Figure 4 shows the measured and modeled concentrations of NO, NO_2, NO_x, ozone and the biogenic hydrocarbon for a smog chamber experiment with β-pinene at October 6, 1995. The performance of the mechanism in simulating the chamber data is quite reasonable for this hydrocarbon and therefore provides means to calculate the concentrations of radical species, such as the NO_3 radical which is displayed as a function of time in the figure.

NO_3 radicals are formed by (Atkinson, 1991, Wayne, 1991),

$$NO_2 + O_3 \xrightarrow{1} NO_3 + O_2$$

Two major processes remove NO_3 radicals, photolysis {2,3} and reaction with NO {4}, whereas the reaction with NO_2 {5} temporarily sequesters the radical as N_2O_5,

$$NO_3 + h\nu \xrightarrow{2} NO + O_2$$

$$NO_3 + h\nu \xrightarrow{3} NO_2 + O$$

$$NO_3 + NO \xrightarrow{4} 2\,NO_2$$

$$NO_3 + NO_2 \xrightleftharpoons{5} N_2O_5$$

Because of the rapid photolysis of NO_3 radicals (lifetime ~ 5s for an overhead sun), their concentration usually remains low during daylight hours. Nevertheless, as a result of the high ozone and NO_2 concentrations in the smog chamber in the later

stages of the runs (see Figure 4), even for daylight experiments nitrate radical chemistry has to be taken into account for the interpretation of the β-pinene data. Figure 5 shows the total β-pinene that reacted and the portions attributable to the reaction with OH, NO_3 and O_3 for this particular experiment. Evolution of the aerosol mass concentration is also plotted. During the first approximately 60 minutes, the biogenic hydrocarbon was degraded essentially by OH radicals and no aerosol growth was observed in this stage of the experiment. When the ozone concentration began to build up (after ~ 60 min), the importance of the O_3 and NO_3 reactions emerged. Whereas the contribution of ozonolysis reactions remained relatively unimportant, the attack of nitrate radicals represented the major pathway of degradation of β-pinene in the final stage of the chamber experiment. At the same time a significant condensation growth of the seed particles was observed. The coincidence between the formation of condensable products and the onset of NO_3/β-pinene reactions clearly indicates the potential of the nitrate/alkene reactions to produce organic aerosols. A more quantitative approach to interpret aerosol formation from NO_3 reactions will be presented later.

The conclusion that aerosol growth in the chamber in the β-pinene experiment can most probably be ascribed to the nitrate radical reaction is a consequence of the relative low reactivity of β-pinene towards ozone in comparison with NO_3. Because elevated ozone concentrations are a key requisite for nitrate radical formation in the chamber, ozonolysis represents an important competing reaction and the majority of the other hydrocarbons investigated were mainly degraded by ozone and not by NO_3. Consequently, it was more difficult for these compounds to separate the individual contribution to the measured change in aerosol mass caused by ozone and NO_3 reactions.

To find additional potential candidates for which reaction with nitrate radicals might be important it is useful to compare their individual reactivities. Table 3 gives the reaction rate constants of the compounds investigated in this study with the three relevant oxidizing species. According to Table 3, d-3-carene shows similar features in terms of its relative reactivity to β-pinene.

The measured and simulated gas-phase concentrations of the reactants for a d-3-carene experiment (10/06 (A)) are shown in Figure 6. Once again, a good fit between experimental and theoretical data was observed, pointing out that the main characteristics of the chemistry are adequately described by the mechanism.

It is worthwhile to discuss the NO_2 concentration during the runs in more detail in connection with NO_3 chemistry. As mentioned above, the signal from the NO_2 channel of the NO_x instrument was considered to represent the sum of NO_2 and PAN concentrations. Especially in the later stage of the runs this interference has to be accounted for in interpretation of the data. Therefore, when NO_2 is mentioned in the following text it is implicit that it refers to NO_2 plus PAN. Figure 7 shows the measured (dots) and modeled (lines) NO_2 plus PAN concentration during the smog chamber experiment with d-3-carene. The dotted line results from the model simulation using the original reaction scheme from the SAPRC mechanism, which assumes that the alkene-NO_3-reaction proceeds as follows (Carter, 1990),

$$NO_3 + R_1R_2C{=}CR_3R_4 \xrightarrow{6} R_1R_2C(ONO_2)\dot{C}R_3R_4$$

$$R_1R_2C(ONO_2)\dot{C}R_3R_4 \xrightarrow[(+O_2,+NO,-NO_2)]{7} R_1R_2C(ONO_2)\underset{\displaystyle O\cdot}{\overset{\displaystyle |}{C}}R_3R_4$$

$$R_1R_2C(ONO_2)\underset{\displaystyle O\cdot}{\overset{\displaystyle |}{C}}R_3R_4 \xrightarrow{8} NO_2 + R_1R_2C{=}O + R_3R_4C{=}O$$

This is analogous to the scheme used for the reactions of OH radicals with alkenes, except that NO_2 is generated instead of HO_2. The addition of NO_3 to the double bond {6} forms β-nitratoalkyl radicals, which rapidly add O_2 {7} to form peroxy radicals. The latter are expected to convert NO to NO_2 and the β-nitratoalkoxy radicals formed are believed to thermally decompose and generate NO_2 {8}. However, at least the last step of the reaction sequence is not in good agreement with the measured NO_2

concentration. A close evaluation of the data reveals a rapid decrease in the NO_2 concentration after the onset of NO_3 reactions. The fit between measured and modeled NO_2 concentrations can be improved if the mechanism is modified to exclude formation of NO_2 in reaction {8}. Several alternative pathways that do not involve NO_2 formation are given by Atkinson (1991), for example the reaction of the β-nitratoalkoxy radicals with O_2,

$$R_1R_2C(ONO_2)\overset{O\cdot}{\overset{|}{C}}R_3R_4 + O_2 \xrightarrow{9} R_1R_2C(ONO_2)\overset{O}{\overset{||}{C}}R + HO_2 \quad (\text{if } R_{3\text{ or }4} = H)$$

The results of the model substituting reaction {8} by {9} is also shown in Figure 7. A third alternative pathway is the reaction of the β-nitratoalkoxy radicals with NO_2 to yield dinitrates,

$$R_1R_2C(ONO_2)\overset{O\cdot}{\overset{|}{C}}R_3R_4 + NO_2 \xrightarrow{10} R_1R_2C(ONO_2)C(ONO_2)R_3R_4$$

If this reaction is included in the mechanism, assuming instantaneous formation of dinitrates, the model predicts a temporal behavior of the NO_2 concentration in excellent agreement with the measured data (see Figure 7). The close fit is further evidence that NO_3 reactions actually occur during selected chamber runs and implies that the formation of organic dinitrates is occurring.

3.5 MODELING AEROSOL FORMATION

Derivation of equation (2) is based on the assumption that the product concentrations (c_i) resulting from the photooxidation of a hydrocarbon are proportional to the amount of the primary hydrocarbon that reacts (ΔROG), where α_i represents the stoichiometry of the reaction regarding product *i*,

$$\alpha_i \Delta ROG = c_i \qquad (4)$$

For alkenes, three oxidation reactions have to be considered:

$$\alpha_i \Delta ROG_{OH} = c_i \tag{4a}$$

$$\alpha_j \Delta ROG_{ozone} = c_j \tag{4b}$$

$$\alpha_k \Delta ROG_{NO3} = c_k \tag{4c}$$

The total concentration of an individual product formed is the sum of its concentrations in the gas- (A_i) and particle phases (F_i):

$$c_i = A_i + F_i \tag{5}$$

If the definition of Odum et al. (1996) for a partitioning coefficient in terms of the organic mass concentration,

$$K_{om,i} = \frac{F_{i,om}}{A_i M_o} \tag{6}$$

is used and combined with (4) and (5), the following expression for the amount of an individual product in the particle phase can be derived, taking the OH reaction as an example:

$$F_{i,om} = \frac{\Delta ROG_{OH} \alpha_i K_{om,j} M_o}{1 + K_{om,i} M_o} \tag{7}$$

The total organic aerosol is composed of the individual contributions of each condensable species,

$$M_o = \sum_i F_i \qquad (8)$$

In principle, if we know the product yield (α_i), the absorption equilibrium constant of the compound i ($K_{om,i}$) and the total aerosol organic mass (M_o) as well as the formation rate of i ($\Delta ROG(t)$), we can use equation (7) to calculate the fraction of i in the aerosol phase as a function of time. In connection with the results of the chemical model employed, equations (7) and (8) can be used to estimate the aerosol mass in the chamber as a function of time. However, in the beginning of a smog chamber experiment no organic aerosol is present and the solution of equation (7) would predict all products to be in the gas-phase, independent of their chemical nature. Therefore, in order to calculate the gas/particle equilibrium at a given time t, an initial absorptive non-zero aerosol mass concentration has to be defined. For the following example calculations the initial aerosol mass ($M_{o,i}$) was assumed to be 1×10^{-4} μg m^{-3}. If the partitioning is believed to include also physical adsorption on the inorganic seed particles then there is no need to make such an assumption. In either case, this assumption has no effect on aerosol yields calculated.

Now, the desired functional form for the temporal behavior of the aerosol mass can be obtained using an iterative solution,

$$M_o(t) = M_{o,n} = M_{o,i} + \Delta ROG(t)\, M_{o,n-1} \sum_i \left(\frac{\alpha_i K_{om,i}}{1 + K_{om,i} M_{o,n-1}} \right) \qquad (9)$$

$$(n = 1 \rightarrow \infty)$$

For alkenes we have to consider all relevant oxidation reactions,

$$M_{o,n} = M_{o,i} + \Delta ROG_{OH}(t)\, M_{o,n-1} \sum_i \left(\frac{\alpha_i K_{om,i}}{1 + K_{om,i} M_{o,n-1}} \right)$$
$$+ \Delta ROG_{ozone}(t)\, M_{o,n-1} \sum_j \left(\frac{\alpha_j K_{om,j}}{1 + K_{om,j} M_{o,n-1}} \right) \qquad (10)$$
$$+ \Delta ROG_{NO3}(t)\, M_{o,n-1} \sum_k \left(\frac{\alpha_k K_{om,k}}{1 + K_{om,k} M_{o,n-1}} \right)$$

As an example, equation (10) is applied to the smog chamber experiment (10/06 (B)) with β-pinene described earlier. The individual contributions of OH, NO_3 and O_3 reactions to the β-pinene degradation ($\Delta ROG's$) are shown in Figure 5. To solve equation (10) we have the to chose appropriate $K's$ and $\alpha's$. As a first approximation, we can describe aerosol formation for products of the β-pinene/ozone reaction with a one-product model with $K_{om,j} = 0.11$ and $\alpha_j = 0.35$ (see Figure 3), although the actual absorption equilibrium constants can be expected to be smaller because of the higher temperature during the daylight experiment. Few quantitative product studies of the β-pinene/OH reaction have been carried out and the only major product found was nopinone (with nopinone formation yields of 0.79 (Hatakeyama et al., 1991) and 0.27 (Hakola et al., 1994), analogous to the reaction of β-pinene with ozone (Hatakeyama et al. 1989). Taking the estimated vapor pressure of this compound (Tu, 1994) we can roughly assess an absorption equilibrium constant in the range of 10^{-6} to 10^{-7} for nopinone. Finally, the products of the reaction of β-pinene with nitrate radicals have to be included in equation (10). Because of the lack of experimental data, the formation of a single product from the NO_3/β-pinene reaction was assumed with the yield (α_k) to be unity. The $K_{om,k}$ value of the unknown product was selected in order to fit the measured aerosol mass. Figure 8 shows a comparison of the measured and simulated aerosol evolution, where $K_{om,k}$ was chosen to be 0.5 and a molecular weight of the products (O_3 and NO_3 products) of 170 was assumed.

The excellent agreement between the experimental and theoretical evolution of the organic aerosol has to be qualified, especially because the close agreement of the final

aerosol mass is a consequence of the choice of the unknown parameters, such as the yield and molecular weight of the NO_3-product. For example, if we assume a molecular weight of 260 (MW of the β-pinene dinitrate) instead of 170 and a formation yield of 0.65 instead of unity, the application of equation (10) would give exactly the same result as shown in Figure 8. However, some interesting features of the β-pinene photooxidation system with respect to aerosol formation can be discussed applying equation (10). First, the result of the model indicates that the yield of nonvolatile products from the β-pinene/OH reaction is quite low; otherwise an earlier onset of aerosol growth would be expected. Secondly, the dominant fraction of the aerosol observed in the β-pinene experiment consisted of the product of the NO_3/β-pinene reaction. According to the chemical mechanism, at the termination of the experiment 68 % of the total β-pinene consumption was a result of reaction with OH, 10 % had reacted with O_3, and 22 % with NO_3. At the same time the aerosol formed consisted of < 0.1 % OH-products, 12 % O_3-products and 88 % NO_3-products.

A second experiment was investigated in detail applying equation (10), the chamber run with d-3-carene as parent hydrocarbon. The individual *ΔROG's* as a function of time were estimated using the chemical mechanism model (Figure 6) and the *K*'s and α's for the ozone products from the dark experiment, again ignoring the temperature difference between dark and daylight experiments ($K_{om,1}$=0.08, $K_{om,2}$=0.01, α_1=0.2, α_2=0.16). The OH reaction is expected to form a ketoaldehyde, ($C_{10}H_{16}O_2$, (2,2-dimethyl-3-(2-oxopropyl)-cyclopropaneacetaldehyde)) as the main product (α=0.34) (Hakola et al., 1994). This substance has a chemical structure almost identical to that of pinonic aldehyde, an α-pinene oxidation product with a vapor pressure of about 1×10^{-4} torr under experimental conditions (Zhang et al., 1992). Substituting this value for $p^0_{L,i}$ in equation (3) we obtain a *K*-value of approximately 1×10^{-3}.

The β-pinene experiment (10/06 (B)) implied that the reaction products of the NO_3 reaction are nonvolatile compounds, rapidly transferring to the aerosol phase. As can be seen in Figure 9, the d-3-carene system behaves differently. In contrast to the chamber run with β-pinene (Figure 9a), we observed a time delay between the beginning of d-3-carene/NO_3 reactions and the onset of aerosol growth (Figure 9b).

In order to match this behavior with equation (10), the absorption equilibrium constant for the nitrate reaction products of d-3-carene has to be much smaller than $K_{om,k}$ for the β-pinene products. Figure 10 shows the measured and predicted aerosol evolution during the d-3-carene experiment, using a $K_{om,k}$ of 5×10^{-3}. Again, an excellent fit between theoretical and experimental data is obtained, demonstrating the general ability of the simple approach to simulate organic aerosol formation. The large differences in the choice of $K_{om,k}$ for the two biogenics necessary to explain the aerosol evolution can be expected as a consequence of different reaction pathways leading to different products.

Assuming that aerosol formation can actually be described using the K's and α's given above, another interesting feature appears in the d-3-carene system. Analogous to the β-pinene run, OH reaction was the most important degradation pathway in the beginning of the experiment. The total amount of the $C_{10}H_{16}O_2$-product is also shown in Figure 10. The relatively high vapor pressure does not allow a significant amount to condense and consequently the gas-phase concentration of the product increased during the course of the experiment. After approximately 50 minutes, the onset of O_3 and NO_3 reactions produced an organic aerosol phase and at this time also a fraction of the ketoaldehyde underwent gas-to-particle conversion. This phenomenon is demonstrated by the condensation rate for this particular compound (dF_i/dt) (Figure 10). According to our simulation, the maximum conversion of the compound to the particle phase occurred at t=75 min and subsequently the rate decreased gradually until the parent hydrocarbon was consumed.

3.6 SECONDARY REACTIONS AND AEROSOL FORMATION

Unlike the daylight experiments with β-pinene and d-3-carene, in which the maximum aerosol mass was observed at the time the hydrocarbons were consumed, most of the other biogenics produced the maximum aerosol mass a certain time after the hydrocarbons had completely reacted. This behavior points to the contribution of secondary oxidation reactions of the primary ozone-, OH- and NO_3-products to the particle phase. Especially for polyunsaturated hydrocarbons, the photooxidation can

be assumed to proceed via the formation of 'first generation products', which are still unsaturated compounds and consequently highly reactive towards OH, NO_3, and O_3.

As an example, Figure 11 shows a smog chamber run with d-limonene (08/25(A)). Again, the chemical mechanism was used to estimate the relative contribution of the three oxidation reactions to limonene degradation during the experiment. At the time limonene was entirely consumed (~ 0.7 h) approximately 64% had reacted with OH, 23% with ozone and 13% with NO_3. It is obvious from Figure 11 that the aerosol continued to build up in the bag, although the parent hydrocarbon was consumed. Hakola et al. (1994) investigated the reaction of d-limonene with OH radicals and they could identify two main products, 4-Acetyl-1-methylcyclohexene (product yield 0.29) and 3-Isopropenyl-6-one-heptanal (product yield 0.2). Rate constants for the gas-phase reactions of these primary oxidation products were experimentally determined by Atkinson and Aschmann (1993). If these data are integrated into the chemical mechanism, the formation of secondary products as a consequence of O_3-, NO_3- and OH-reactions of the two main OH products can be simulated as a function of time. Figure 11 also shows the expected temporal behavior of the two first generation products and the total amount of secondary products, formed from their subsequent oxidation. The similarity of the shape of the curve for the aerosol evolution and the formation rate of secondary products in the final stage of the experiment implies that these secondary oxidation products are mainly responsible for the increase of the aerosol mass when the parent hydrocarbon is exhausted. However, a quantitative understanding of the individual contribution of the different products to the particle phase is still lacking, since only subsequent reactions of the OH reaction products were considered in the simulation. A rough estimate of the particular contributions gives ~ 70 % of the organic aerosol phase resulting from gas-to-particle conversion of primary products and 30 % from secondary products in the d-limonene system.

The influence of secondary reactions on aerosol formation is even more pronounced for the sesquiterpene investigated. A typical example of the trans-caryophyllene and aerosol mass concentration time profiles is shown in Figure 12. The highly reactive

C_{15}-compound is degraded rapidly after the removal of the bag cover and the dominant degradation pathway is represented by the attack of ozone ($\Delta ROG_{(ozone)}$ ~ 81 %). Although the sesquiterpene was completely consumed after approximately 0.6 h, the major part of the aerosol formation occurred later. Again, this behavior can be described using the chemical mechanism in connection with equation (10). We can match the observed aerosol evolution if we make a couple of assumptions. First, the reaction of trans-caryophyllene with ozone leads directly to the formation of a relatively nonvolatile product (K ~ 0.05) with a product yield of about 20 % (product I) and a more volatile reaction product ($K < 1\times10^{-5}$, $p^0_{L,i} > \sim 0.01$ torr) (product II) . Secondly, product II (which is still an olefin) behaves in the gas-phase like a monounsaturated terpene (here, we assumed the same rate constants than for α-pinene) and the secondary products formed (product III) are nonvolatile compounds ($K > 0.05$):

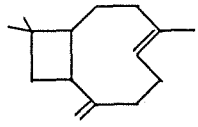

trans-caryophyllene

+ ozone ⟶ 0.2 product I + 0.8 product II

product II $\xrightarrow{OH,\ NO_3,\ O_3}$ product III

The resulting prediction is also shown in Figure 12. Again, the excellent correlation between simulated and measured aerosol mass shows that we can explain the important features of aerosol evolution, especially the distinct increase of aerosol mass after approximately one hour of the experiment. This second burst can be attributed to ozone and nitrate radical reactions of product II since the ozone concentration began to build up at this time.

It was shown earlier that the application of the chemical mechanism in connection with equation (10) is particularly useful in revealing some general physico-chemical

properties of the oxidation products of the natural alkenes. However, the simulation of the trans-caryophyllene/NO_x/air experiments indicates also some mechanistic information. Usually, it is assumed that the ozone reaction of alkenes, which is the dominant degradation pathway for the sesquiterpene, proceeds by initial O_3 addition to the >C=C< bond to yield an energy-rich ozonide that rapidly decomposes to a carbonyl and an energy-rich biradical (Atkinson, 1994). The fate of the biradical is presently not well understood but it is expected that a fraction will be collisonally stabilized and the remain will decompose by a number of pathways. One important feature of the decomposition pathway is the formation of various radicals, including organic peroxy and OH radicals, which strongly influence the NO to NO_2 ratios in the chamber. However, in order to simulate the temporal behavior of the NO-, NO_2-, O_3- and ROG-concentration during the sesquiterpene experiment, the radical yields normally used to represent the ozonolysis of cyclic alkenes have to be reduced drastically. Figure 13 shows the measured concentrations of NO, NO_2, and trans-caryophyllene during the experiment already discussed above. Although a major fraction of the C_{15}-compound reacted within the first 20 min, the NO_x concentrations showed no particular response in this period. In order to match the observed time profiles for NO_x the radical yields have to be adjusted to be smaller than 0.04. These results are consistent with published data of OH radical formation yields from the ozone/trans-caryopyllene reaction. Shu and Atkinson (1996) recommended a value for this reaction of 0.06. Altogether these observations suggest that other reaction channels are operative for the C_{15}-compound and that the sesquiterpene acts substantially like an efficient sink for ozone without major influences on the radical balance in the system. The question whether this behavior is a consequence of the formation of mainly stabilized biradicals, which subsequently react, for example, with water vapor or rearrange intramolecularly (Hatakeyama and Akimoto, 1994), or if non-radical forming decompositions are predominant cannot be answered without detailed product studies.

3.7 INDIVIDUAL OXIDATION REACTIONS AND AEROSOL YIELDS

It was mentioned earlier that some experiments indicated that the OH radical reaction of certain hydrocarbons (e.g. β-pinene) leads to the formation of relatively volatile products without a major contribution to the organic aerosol phase. In contrast, the dark reactions with ozone revealed remarkably high SOA yields (Table 2). These observations can be summarized if the overall aerosol yields are plotted as a function of the fraction of the individual hydrocarbons that had reacted with ozone ($\Delta ROG(O_3)/ \Delta ROG(total)$) during the experiments (Figure 14). For the daylight experiments, $\Delta ROG(O_3)$ was estimated using the chemical mechanism, for the dark experiments from the $\Delta O_3/\Delta ROG$ values shown in Table 2. Except for β-pinene and linalool, aerosol yields increased with increasing importance of the ozone reaction.

One evident explanation is the temperature difference between the two data sets. Usually, the temperature was lower during the dark experiments, resulting in lower vapor pressures of the products. Therefore, a larger fraction of the products can be expected to undergo gas-to-particle conversion. Nevertheless, the comparison of the temporal behavior of aerosol formation with the portion of ROG that reacted with OH (Fig. 5 and 10) indicates that the OH reaction does not lead to a significant aerosol formation. If we also take into account the results from α-pinene experiments carried out in the same temperature range, showing a higher aerosol yield during dark than during daylight experiments (Fig. 1 and 2), Figure 14 points to a significant aspect of the aerosol formation of biogenic hydrocarbons, the importance of ozonolysis reactions as a direct source of nonvolatile products. The unusual β-pinene result can most probably be explained by the additional contribution of NO_3-products to the particle phase during the daylight experiments

3.8 MOLECULAR SPECIATION OF THE ORGANIC AEROSOL

To date, knowledge about the chemical composition of the aerosol formed from the oxidation of hydrocarbons is limited. A number of investigators have reported on monoterpene reaction products found in the aerosol phase (Hull, 1981 , Hatakeyama et al., 1989, Hatakeyama et al., 1991, Palen et al., 1992). Because information about

the chemical nature of particulate products is helpful for the understanding of the routes to aerosol formation, we performed gas chromatographic screening of organic compounds in the aerosol during selected chamber runs. A typical GC/MS chromatogram of an α-pinene aerosol generated in the smog chamber during daylight experiments is shown in Figure 15. It can be seen in the chromatogram that the photooxidation of the biogenic hydrocarbon produced a variety of products, the majority of which could not be clearly identified. The main problem in ascertaining the identity of unknown oxidation products is the lack of suitable reference mass spectra together with complex EI-fragmentation pathways of aliphatic compounds. Nevertheless, the mass spectra of two important product peaks are consistent with the reported spectra of pinonaldehyde and pinonic acid (Hakola et al., 1994, Swigar and Silverstein, 1981). The most important compound comprising the organic aerosol phase that is visible in this chromatogram is the carboxylic acid. This compound is expected to be formed from the ozone reaction of α-pinene by the following reaction sequence (Hatakeyama et al., 1989):

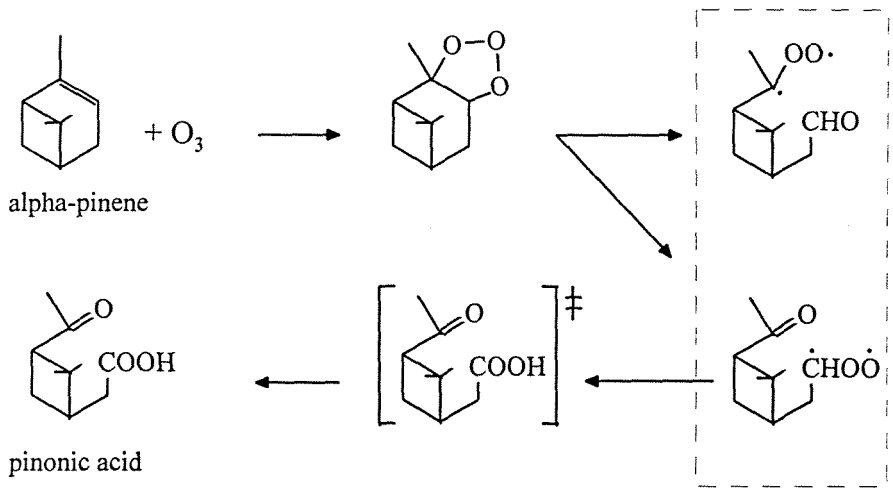

One of the two possible Criegee intermediates are speculated to rearrange to vibrationally excited carboxylic acid, a portion of which is deactivated to a ground state molecule. A second route would be the reversible reaction of the intermediate with water vapor in the gas phase (Hatakeyama and Akimoto, 1994).

It should be mentioned that aerosol sampling and analysis was performed to obtain qualitative chemical information about the organics in the particle phase since the collection methods applied here are expected to result in sampling artifacts (Eatough et al., 1993, Grosjean, 1992). However, the finding that the ketocarboxylic acid is present in high quantities in the organic aerosol supports conclusions drawn from the dark experiments that especially the ozone reaction directly leads to nonvolatile compounds. Furthermore, these results might be interesting with respect to other atmospheric processes due to an intrinsic feature of carboxylic acids, their surface activity. Compounds like pinonic acid, which are slightly soluble in water, can affect the surface tension of cloud droplets and therefore alter the droplet growth process (Shulman et al., 1996).

3.9 ATMOSPHERIC IMPLICATIONS

The reaction rate constants given in Table 3 can be combined with ambient concentrations of ozone, OH, and NO_3 radicals to calculate tropospheric lifetimes of the hydrocarbons studied with respect to gas-phase reactions with the three oxidizing species. For OH radicals a 12-hour daytime average of 1.6×10^6 molecules cm^{-3} was assumed (Prinn et al., 1992), for NO_3 radicals a 12-hour nighttime average concentration of 5×10^8 molecules cm^{-3} (Atkinson, 1991) and for ozone a daytime mixing ratio of 50 ppb. Obviously, the compounds investigated are all highly reactive toward OH, NO_3, and ozone with atmospheric lifetimes between a few minutes and several hours. During the day, the reaction with ozone represents the major tropospheric degradation pathway for most of the terpenes studied. This is shown in the last row of Table 4, in which the relative contribution of the O_3 reaction is calculated for daytime conditions. The comparison of these data with the fraction of the hydrocarbons that had reacted with ozone during daylight smog chamber experiments, in which the fraction that reacted with ozone was usually below 30 % (except trans-caryophyllene, see Fig. 14), reveals that degradation by ozone is more important under typical environmental conditions. Consequently, aerosol yields from

the daylight chamber runs might represent lower limits for the aerosol formation potential of biogenics in the ambient atmosphere.

However, the conclusions drawn here are based on experimental results in the presence of relatively high levels of NO_x and therefore the organic peroxy radicals formed, for example, from the OH reaction of the hydrocarbons will react almost exclusively with NO to yield NO_2. In the remote atmosphere under low NO_x conditions, e.g. in the tropics, permutation reactions of the peroxy radicals gain importance, presumably causing a completely different product distribution. The relatively high aerosol yields from the reaction of α-pinene with OH radicals estimated by Hatakeyama et al. (1991), which are not consistent with the findings of our study, can probably be explained by this reaction sequence.

Another interesting result obtained is the high aerosol formation potential of biogenics as a result of their reaction with nitrate radicals, an observation that could be relevant for the night-time chemistry in forested areas. Tropospheric lifetimes of the biogenic hydrocarbons with respect to their reaction with NO_3 lie in the order of minutes (Table 4), hence could represent an important degradation pathway if NO_3 is available. As mentioned earlier, a close evaluation of the experimental data gave evidence of the formation of dinitrates. High NO_2 concentrations can be expected to be a prerequisite for the formation of dinitrates and consequently it is not clear if the high aerosol yields will be observed also under typical tropospheric conditions. However, if the high aerosol yields from nitrate radical reactions also hold under ambient conditions and if this result is combined with the indicated dependence of the aerosol yield from the HC fraction that reacted with ozone, these observations would imply another aspect of the aerosol formation of natural alkenes, namely the increase of organic aerosol mass in rural areas due to increasing tropospheric O_3 and NO_x concentrations.

Because of still incomplete understanding of the chemical pathways leading to the formation of condensable species during the oxidation of biogenic hydrocarbons in the troposphere only a rough assessment of their contribution to the atmospheric particle phase is possible to date. Furthermore, ambient aerosol yields cannot be represented

by a unique value for a given compound, because they are dependent on organic mass concentration and temperature. Nevertheless, considering the experimental indications particularly that O_3/biogenic alkene reactions play a major role in the formation of condensable products and that these reactions also take place under tropospheric conditions, SOA yield data from smog chamber studies will most likely be close to the yields of individual hydrocarbons when applied to the ambient atmosphere. The expected small dependence of the individual yields from the organic mass concentration for very nonvolatile products, such as some ozonolysis products, support this conclusion.

4. Conclusions

Outdoor smog chamber experiments investigating the formation of aerosol during the oxidation of a series of biogenic hydrocarbons have been performed. Two sets of experiments were carried out: daylight experiments to investigate the photochemical aerosol formation in the presence of NO_x and dark reactions with elevated ozone concentrations to assess the potential of ozonolysis reactions of the natural alkenes to form condensable species. Aerosol formation in selected runs has been simulated by applying a gas/particle partitioning absorption model in connection with a chemical reaction mechanism. The results of these simulations strongly indicate the occurrence of NO_3/alkene reactions, and for β-pinene and d-3-carene, indirect evidence that the products of these reactions can contribute significantly to the particle phase. Furthermore, both sets of experiments have shown that especially the ozonolysis of the natural alkenes leads to the formation of nonvolatile compounds and consequently has to be considered for the evaluation of the aerosol potential of unsaturated hydrocarbons. In general, the potential to form SOA was found to be higher for cyclic parent hydrocarbons (like α-pinene and d-3-carene) than for acyclic compounds (e.g. ocimene), most likely due to the formation of polyfunctional oxidation products without molecular scission. Polyunsaturated biogenic alkenes, such as limonene, exhibit an even higher aerosol yield. For these compounds, secondary oxidation reactions of the primary formed degradation products are shown to be responsible for this observation. For trans-caryophyllene, a naturally emitted sesquiterpene, a fractional aerosol yield of close to 1.0 was found. With respect to recent findings that

sesquiterpenes are present in ambient air (Helmig and Arey, 1992, Hoffmann, 1995) and that they can be emitted in large quantities from vegetation (Helmig et al., 1994, Arey et al., 1991, Winer et al., 1992, Koenig et al., 1995), future estimations of the SOA formation from biogenic hydrocarbons should consequently also consider these group of compounds as aerosol precursors.

Acknowledgments

This work was supported by U.S. Environmental Protection Agency Exploratory Environmental Research Center on Airborne Organics (R-819714-01-0), National Science Foundation grant ATM-9307603, the Coordinating Research Council (A-5-1), and the Chevron Corporation. T.H. thanks the German Research Association (DFG) for financial support and the BMBF (Bundesministerium für Bildung, Wissenschaft, Forschung und Technologie) for agreeing with the stay at Caltech during his participation in the research programme 'cycles of trace constituents'.

References

Andreae, M.O., (1995), Climatic effects of changing atmospheric aerosol levels, *in: World Survey of Climatology, Vol. 16: Future Climates of the World (A. Henderson-Sellers (Ed.))*.

Arey, J., Winer, A.M., Atkinson, R., Aschmann, S.M., Long, W.D., Morrison, C.L. and Olszyk, D.M., (1991), Terpenes emitted from agricultural species found in California's central valley, *J. Geophys. Res.* **96**, 9329-9336.

Atkinson, R., (1991), Kinetics and mechanisms of the gas-phase reactions of the NO_3 radical with organic compounds, *J. Phys. Chem. Ref. Data* **20**, 459-507.

Atkinson, R., (1994), Gas-phase tropospheric chemistry of organic compounds, *J. Phys. Chem. Ref. Data (Monograph No.2)* 1-216.

Atkinson, R. and Aschmann, S. M., (1993), Atmospheric chemistry of the monoterpene reaction products Nopinone, Camphenilone, and 4-Acetyl-1-Methylcyclohexene, *J. Atmos. Chem.* **16**, 337-348.

Carter, W.P.L., (1990), A detailed mechanism for the gas-phase atmospheric reactions of organic compounds, *Atmos. Environ.* **24A**, 481-518.

Chameides, W. L., Fehsenfeld, F., Rodgers, M. O., Cardelino, C., Martinez, J., Parrish, D., Lonneman, W., Lawson, D. R., Rasmussen, R. A., Zimmerman, P., Greenberg, J., Middleton, P. and Wang, T., (1992), Ozone precursor relationships in the ambient atmosphere, *J. Geophys. Res.* **97**, 6037-6055.

Eatough, D.J., Wadsworth, A., Eatough, D.A., Crawford, J.W., Hansen, L.D. and Lewis, E.A., (1993), A multiple-system, multi-channel diffusion denuder sampler for the determination of fine-particulate organic material in the atmosphere, *Atmos. Environ.* **27A**, 1213-1219.

Fehsenfeld, F., Calvert, J., Fall, R., Goldan, P., Guenther, A.B., Hewitt, C.N., Lamb, B., Liu, S., Trainer, M., Westberg, H. and Zimmerman, P., (1992), Emissions of volatile organic compounds from vegetation and the implications for atmospheric chemistry, *Global Biogeochem. Cycles* **6**, 389-430.

Grosjean, D., (1992), In situ organic aerosol formation during a smog episode: Estimated production and chemical functionality, *Atmos. Environ.* **26A**, 953-963.

Guenther, A., Hewitt, C.N., Erickson, D., Fall, R., Geron, C., Graedel, T., Harley, P., Klinger, L., Lerdau, M., McKay, W.A., Pierce, T., Scholes, B., Steinbrecher, R., Tallamraju, R., Taylor, J. and Zimmerman, P., (1995), A global model of natural volatile organic compound emissions, *J. Geophys. Res.* **100**, 8873-8892.

Hakola, H., Arey, J., Aschmann, S.A. and Atkinson, R., (1994), Product formation from the gas-phase reactions of OH-radicals and O3 with a series of monoterpenes, *J. Atmos. Chem.* **18**, 75-102.

Hatakeyama, S. and Akimoto, H., (1994), Reactions of Criegee intermediates in the gas phase, *Res. Chem. Intermed.* **20**, 503-524.

Hatakeyama, S., Izumi, K., Fukuyama, T. and Akimoto, H., (1989), Reactions of ozone with α-pinene and ß-pinene in air: Yields of gaseous and particulate products, *J. Geophys. Res.* **94**, 13013-13024.

Hatakeyama, S., Izumi, K., Fukuyama, T., Akimoto, H. and Washida, N., (1991), Reactions of OH with α-pinene and ß-pinene in air: Estimate of global CO production from the atmospheric oxidation of terpenes, *J. Geophys. Res.* **96**, 947-958.

Helmig, D. and Arey, J., (1992), Organic chemicals in the air of Whitaker's forest/Sierra Nevada Mountains, California, *Sci. Total Environ.* **112**, 233-250.

Helmig, D., Klinger, L.F., Greenberg, J. and Zimmerman, P., (1994), Emissions and identification of individual organic compounds from vegetation in three ecosystems in the U.S., *paper presented at the 207th ACS Meeting, Am. Chem. Soc., San Diego, Calif., March 13-18*

Hoffmann, T., (1995), Adsorptive preconcentration technique including oxidant scavenging for the measurement of reactive natural hydrocarbons in ambient air, *Fresenius J. Anal. Chem.* **351**, 41-47.

Hooker, C. L., Westberg, H. H. and Sheppard, J. C., (1985), Determination of carbon balances for smog chamber terpene oxidation experiments using a carbon-14 tracer technique , *J. Atmos. Chem.* **2**, 307-20 .

Hough, A.M. and Johnson, C.E., (1991), Modelling the role of nitrogen oxides, hydrocarbons and carbon monoxide in the global formation of tropospheric oxidants, *Atmos. Environ.* **25A**, 1819-1835.

Hull, L.A., (1981), Terpene ozonolysis products, in: Atmos. Biog. Hydrocarbons, Vol. 2, (J.J. Bufalini, and R.R. Arnts (Eds.)), Ann Arbor Science, Ann Arbor.

Jonas, P.R., Charlson, R.J. and Rohde, H., (1995), Aerosols, in: Climate change 1994, Reports of Working Groups I and III of the IPCC (J.T. Houghton, L.G. Meira Filho, J. Bruce, H. Lee, B.A. Callander, E. Haites, N. Harris and K. Maskell (Eds.)), University Press, Cambridge.

Kamens, R.M., (1981), The impact of α-pinene on urban smog formation: an outdoor smog chamber study, in: Atmos. Biog. Hydrocarbons, Vol. 2, (J.J. Bufalini, and R.R. Arnts (Eds.)), Ann Arbor Science, Ann Arbor.

Koenig, G., Brunda, M., Puxbaum, H., Hewitt, C.N., Duckham, S.C. and Rudolph, J., (1995), Relative contribution of oxygenated hydrocarbons to the total biogenic VOC emissions of selected Mid-European agricultural and natural plant species, *Atmos. Environ.* **29**, 861-874.

Liu, B.Y. and Lee, K.W., (1975), An aerosol generator of high stability, *Am. Ind. Hyg. Assoc. J.* **36**, 861-865.

McKeen, S.A., Hsie, E.-Y., Trainer, M., Tallamraju, R. and Liu, S.C., (1991a), A regional model study of the ozone budget in the Eastern United States, *J. Geophys. Res.* **96**, 10809-10845.

McKeen, S.A., Hsie, E.-Y. and Liu, S.C., (1991b), A study of the dependence of rural ozone on ozone precursors in the eastern United States, *J. Geophys. Res.* **96**, 15377-15394.

Müller, J. F., (1992), Geographical distribution and seasonal variation of surface emissions and deposition velocities of atmospheric trace gases, *J. Geophys. Res.* **97**, 3787-3804.

National Research Council, (1996), Aerosol radiative forcing and climate change, National Academy Press, Washington, DC.

Novakov, T. and Penner, J. E., (1993), Large contribution of organic aerosols to cloud-condensation-nuclei concentrations, *Nature* **365**, 823-826.

Odum, J.R., Hoffmann, T., Bowman, F., Collins, D., Flagan, R.C. and Seinfeld, J.H., (1996), Gas/particle partitioning and secondary aerosol formation, *Environ. Sci. Technol. (in press)*

Palen, E.J., Allen, D.T., Pandis, S.N., Paulson, S.E., Seinfeld, J.H. and Flagan, R.C., (1992), Fourier transform infrared analysis of aerosol formed in the photo-oxidation of isoprene and ß-pinene, *Atmos. Environ.* **26A**, 1239-1251.

Pandis, S.N., Paulson, S.E., Seinfeld, J.H. and Flagan, R.C., (1991), Aerosol formation in the photooxidation of isoprene and ß-pinene, *Atmos. Environ.* **25A**, 997-1008.

Pandis, S.N., Harley, R.A., Cass, G.R. and Seinfeld, J.H., (1992), Secondary organic aerosol formation and transport, *Atmos. Environ.* **26A**, 2269-2282.

Pankow, J.F., (1994a), An absortion model of the gas/aerosol partitioning involved in the formation of secondary organic aerosol, *Atmos. Environ.* **28**, 189-193.

Pankow, J.F., (1994b), An absortion model of gas/particle partitioning of organic compounds in the atmosphere, *Atmos. Environ.* **28**, 185-188.

Paulson, S.E., Pandis, S.N., Baltensperger, U., Seinfeld, J.H., Flagan, R.C., Palen, E.J., Allen, D.T., Schaffner, C., Giger, W. and Portmann, A., (1990), Characterization of photochemical aerosols from biogenic hydrocarbons, *J. Aerosol Sci.* **21**, 245-248.

Pilinis, C., Pandis, S. and Seinfeld, J.H., (1995), Sensitivity of direct climate forcing by atmospheric aerosols to aerosol size and composition, *J. Geophys. Res.* **100**, 18739-18754.

Prinn, R. et al., (1992), Global average concentration and trend for OH radicals deduced from ALE/GAGE trichloroethane (methyl chloroform) data for 1978-1990, *J. Geophys. Res.* **97**, 2445-2461.

Roselle, S.J., Pierce, T.E. and Schere, K.L., (1991), The sensitivity of regional ozone modeling to biogenic hydrocarbons, *J. Geophys. Res.* **96**, 7371-7394.

Saxena, P., Hidlemann, L., McMurry, P.H. and Seinfeld, J.H., (1995), Organics alter hygroscopic behavior of atmospheric particles, *J. Geophys. Res.* **100**, 18755-18770.

Shu, Y. and Atkinson, R.,, Rate constants gor the gas-phase reactions of O3 with a series of terpenes and OH radical formation from the O3 reactions with sesquiterpenes at 296 ± 2K, *International J. Chem. Kinetics (in press)*

Shu, Y. and Atkinson, R., (1995), Atmospheric lifetimes and fates of a series of sesquiterpenes, *J. Geophys. Res.* **100**, 7275-7281.

Shulman, M., Jacobson, M., Charlson, R.J., Synovec, R.E. and Young, T.E., (1996), Dissolution behavior and surface tension effects of organic compounds in nucleating cloud droplets, *Geophys. Res. Lett.* **23**, 277-280.

Simpson, D., Guenther, A., Hewitt, C.N. and Steinbrecher, R., (1995), Biogenic emissions in Europe: 1. Estimates and uncertainties, *J. Geophys. Res.* **100**, 22875-22890.

Swigar, A.A. and Silverstein, R.M., (1981), Monoterpenes. Infrared, Mass, ^{1}H NMR, and ^{13}C NMR Spectra, and Kovats Indices, Aldrich Chem. Comp., Milwaukee, Wisconsin.

Trainer, M., Parrish, D. D., Buhr, M. P., Norton, R. B., Fehsenfeld, F. C., Anlauf, K. G., Bottenheim, J. W., Tang, Y. Z., Wiebe, H. A., Roberts, J. M., Tanner, R. L., Newman, L., Bowersox, V. C., Meagher, J. F., Olszyna, K. J., Rodgers, M. O., Wang, T., Berresheim, H., Demerjian, K. L. and Roychowdhury, U. K., (1993), Correlation of ozone with NOy in photochemically aged air, *J. Geophys. Res.* **98**, 2917-2925.

Tu, C.-H., (1994), Group-contribution method for the estimation of vapor pressures, *Fluid Phase Equilibria* **99**, 105-120.

Twomey, S., (1991), Aerosols, clouds and radiation, *Atmos. Environ.* **25A**, 2435-2442.

Vogel, B., Fiedler, F. and Vogel, H., (1995), Influence of topography and biogenic volatile organic compounds emission in the state of Baden-Wuerttemberg on ozone concentrations during episodes of high air temperatures, *J. Geophys. Res.* **100**, 22907-22928.

Wayne, R.P., (1991), The nitrate radical: Physics, chemistry and the atmosphere, *Atmos. Environ.* **25A**, 1-206.

Went, F.W., (1960), Blue hazes in the atmosphere, *Nature* **187**, 641-643.

Winer, A. M., Arey, J., Atkinson, R., Aschmann, S. M., Long, W. D., Morrison, C. L. and Olszyk, D. M., (1992), Emission rates of organics from vegetation in California's Central Valley, *Atmos. Environ.* **26**, 2647-2659.

Zhang, S. H., Shaw, M., Seinfeld, J. H. and Flagan, R. C., (1992), Photochemical aerosol formation from α-pinene- and β-pinene, *J. Geophys. Res.* **97**, 20717-20729.

Zhang, S.-H., Akutsu, Y., Russell, L.M., Flagan, R.C. and Seinfeld, J.H., (1995), Radial differential mobility analyzer, *Aerosol Sci. Technol.* **23**, 357-372.

List of Figures

List of Tables

Table 1.

	date (side of bag)	ROG_0 [ppb]	M_o [$\mu g\ m^{-3}$]	NO_x [ppb]	$\Delta ROG/NO_x$ (incl. C_3H_6) [pppbC/ppb]	yield [%]
α-pinene	08/14 (A)	136.0	87.0	240	9.4	12.00
	08/14 (B)	144.0	96.0	240	9.8	12.50
	08/17 (A)	72.0	22.7	203	8.0	5.91
	08/17 (B)	19.5	1.3	113	9.7	1.22
	09/15 (B)	53.0	8.0	206	6.9	2.83
	09/22 (A)	94.5	33.0	135	13.7	6.54
	09/22 (B)	87.4	38.2	125	14.2	8.19
	09/25 (A)	95.5	39.3	124	15.0	7.71
	09/25 (B)	94.6	34.2	122	15.1	6.77
d-limonene	08/19 (A)	159.0	302.7	134	18.6	35.68
	08/21 (B)	95.0	205.3	205	9.0	40.50
	08/25 (A)	89.2	192.3	174	10.3	40.40
d-3-carene	10/04 (A)	117.0	143.0	200	10.4	22.90
	10/06 (A)	112.0	161.4	210	9.6	27.00
β-pinene	10/06 (B)	95.0	153.0	204	9.1	30.20
ocimene	10/04 (B)	104.1	30.6	238	8.2	5.51
linalool	08/25 (B)	79.7	43.6	186	9.1	9.05
	08/28 (B)	75.8	19.1	153	10.8	4.17
	09/08 (A)	230.0	136.7	394	8.1	9.83
terpinene-4-ol	08/30 (A)	70.5	21.3	141	11.4	5.00
	09/01 (B)	76.8	14.0	190	8.8	3.02
	09/08 (B)	228.8	82.8	413	7.7	6.00
trans-caryophyllene	08/23 (A)	102.2	845.0	283	8.6	103.25
	08/23 (B)	99.5	998.3	268	8.9	125.29

Table 2.

	date (side of bag)	ROG_0 [ppb]	HC_{final} [ppb]	ΔHC [ppb]	M_o [$\mu g\ m^{-3}$]	Temp. [°C]	O_3(ini) [ppb]	$\Delta O_3/\Delta ROG$	yield [%]
α-pinene	09/27 (A)	91.0	3.0	88.0	82.0	48.1	210	0.64	18.0
	09/27 (B)	41.0	3.0	38.0	29.9	48.9	220	0.85	15.2
	09/29 (B)	168.0	13.9	154.1	183.5	48.1	327	0.74	23.0
	09/29 (A)	110.5	8.6	101.9	80.4	47.2	320	0.71	15.2
	10/02 (A)	141.9	9.0	132.9	94.9	46.1	210	0.71	13.7
	10/08 (A)	91.5	3.0	88.5	341.0	16.1	242	0.94	67.1
d-3-carene	10/08 (B)	96.4	6.7	89.7	390.0	16.7	249	0.80	75.9
β-pinene	10/10 (B)	85.4	32.04	53.4	97.1	19.4	271	0.92	32.1
ocimene	10/09 (A)	85.4	0.0	85.4	85.0	17.8	150	0.78	17.4
linalool	10/09 (B)	77.8	0.0	77.8	39.5	17.2	154	0.85	7.8
terpinene-4-ol	10/10 (A)	90.4	0.0	90.4	200.0	17.5	270	0.91	34.2

Table 3.

	$k(OH) \times 10^{12}$ [cm^3 $molecule^{-1}$ s^{-1}]	$k(O_3) \times 10^{18}$ [cm^3 $molecule^{-1}$ s^{-1}]	$k(NO_3) \times 10^{12}$ [cm^3 $molecule^{-1}$ s^{-1}]	$k(NO_3)/k(O_3)$ $\times 10^{-5}$
β-pinene	78.9	15.0	2.5	1.67
d-3-carene	88.0	37.1	9.1	2.45
d-limonene	171.0	200.0	12.2	0.61
terpinene-4-ol	170.0	250.0	14.6	0.58
α-pinene	53.7	86.6	6.2	0.71
cis/trans-ocimene	252.0	540.0	22.0	0.41
linalool	159.0	430.0	11.7	0.27
trans-caryophyllene	200.0	11600	19.0	0.02

Table 4.

	lifetime due to reaction with			rel. contribution of O_3- reaction to tropospheric degradation
	OH *daytime* [min]	O_3 *daytime* [min]	NO_3 *nighttime* [min]	*daytime* [%]
β-pinene	132	902	13	13
d-3-carene	118	365	4	24
d-limonene	61	68	3	47
terpinene-4-ol	61	54	2	53
α-pinene	194	156	5	55
cis/trans-ocimene	41	25	2	62
linalool	66	31	3	68
trans-caryophyllene	52	1	2	98

Figure 1.

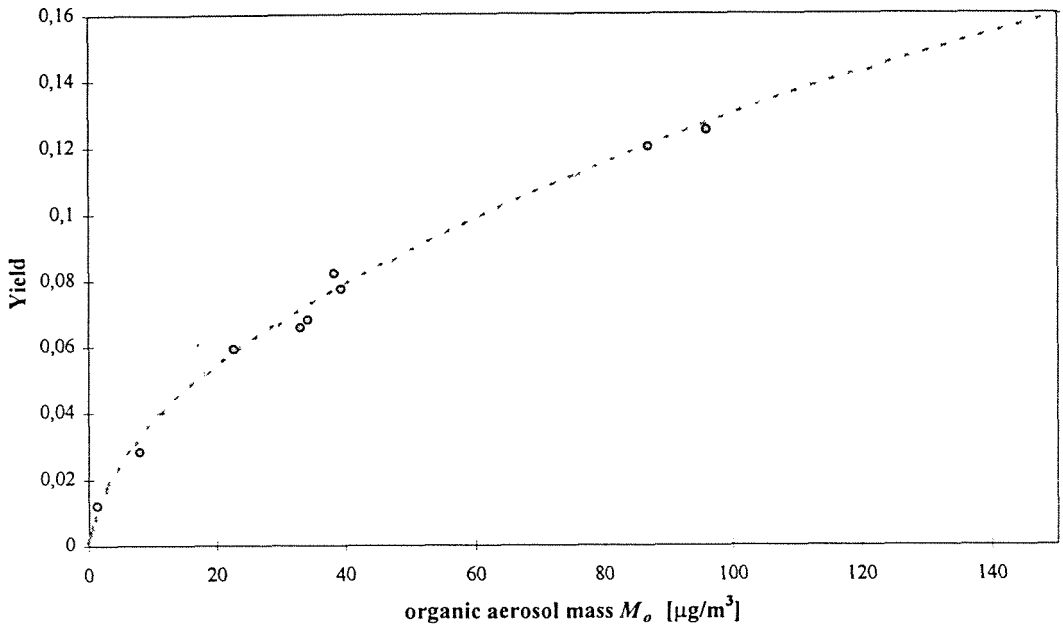
0,16
0,14
0,12
0,1
0,08
0,06
0,04
0,02
0
Yield
0
20
40
60
80
100
120
140
organic aerosol mass M_o [µg/m^3]

Figure 2.

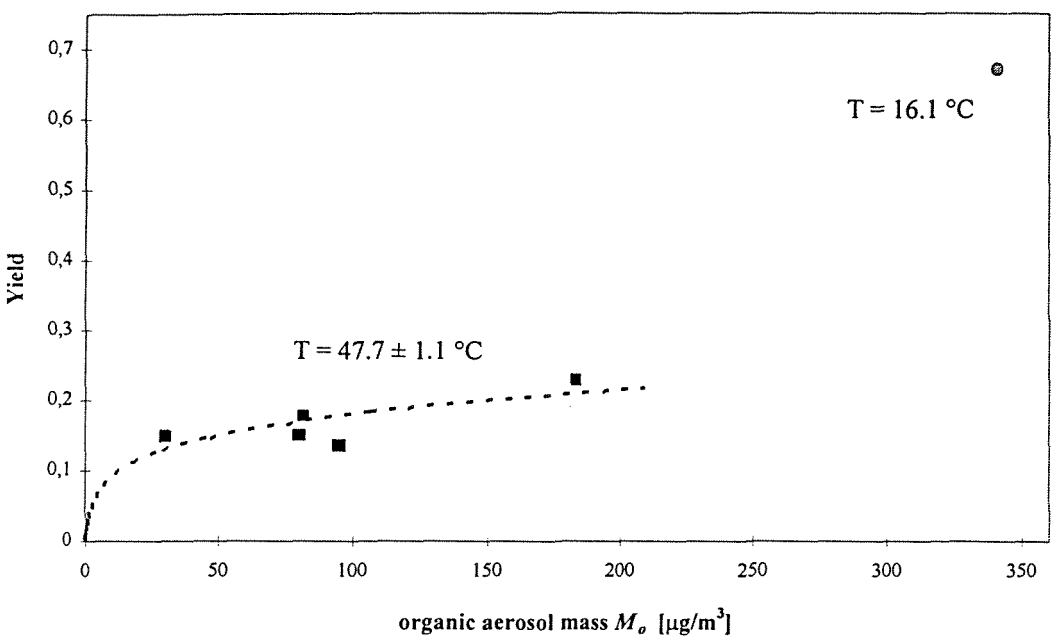
0,7
0,6
0,5
0,4
0,3
0,2
0,1
0
Yield
T = 16.1 °C
T = 47.7 ± 1.1 °C
0
50
100
150
200
250
300
350
organic aerosol mass M_o [µg/m^3]

Figure 3.

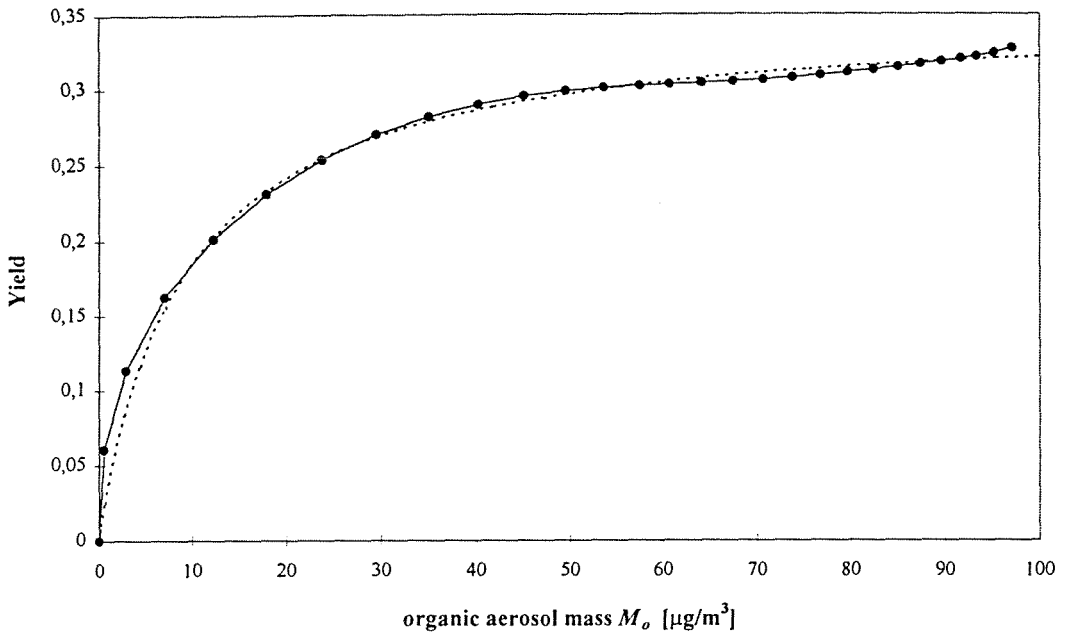
0,35
0,3
0,25
0,2
0,15
0,1
0,05
0
Yield
0
10
20
30
40
50
60
70
80
90
100
organic aerosol mass M_o [μg/m^3]

Figure 4.

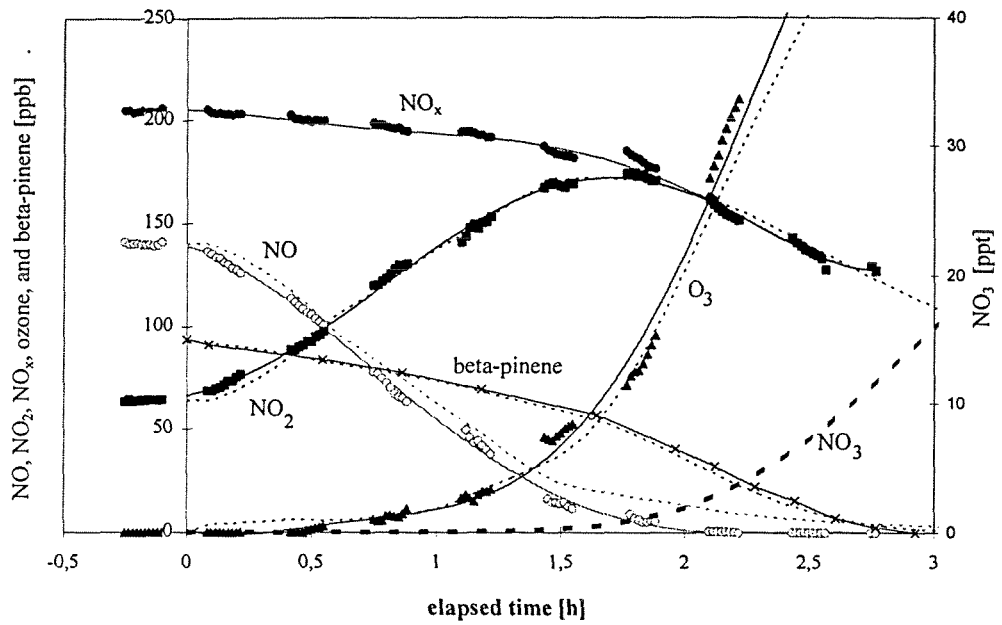
NO, NO2, NOx, ozone, and beta-pinene [ppb]
NO3 [ppt]
elapsed time [h]
NOx
NO
NO2
O3
beta-pinene
NO3
250
200
150
100
50
0
40
30
20
10
0
-0,5
0
0,5
1
1,5
2
2,5
3

Figure 5.

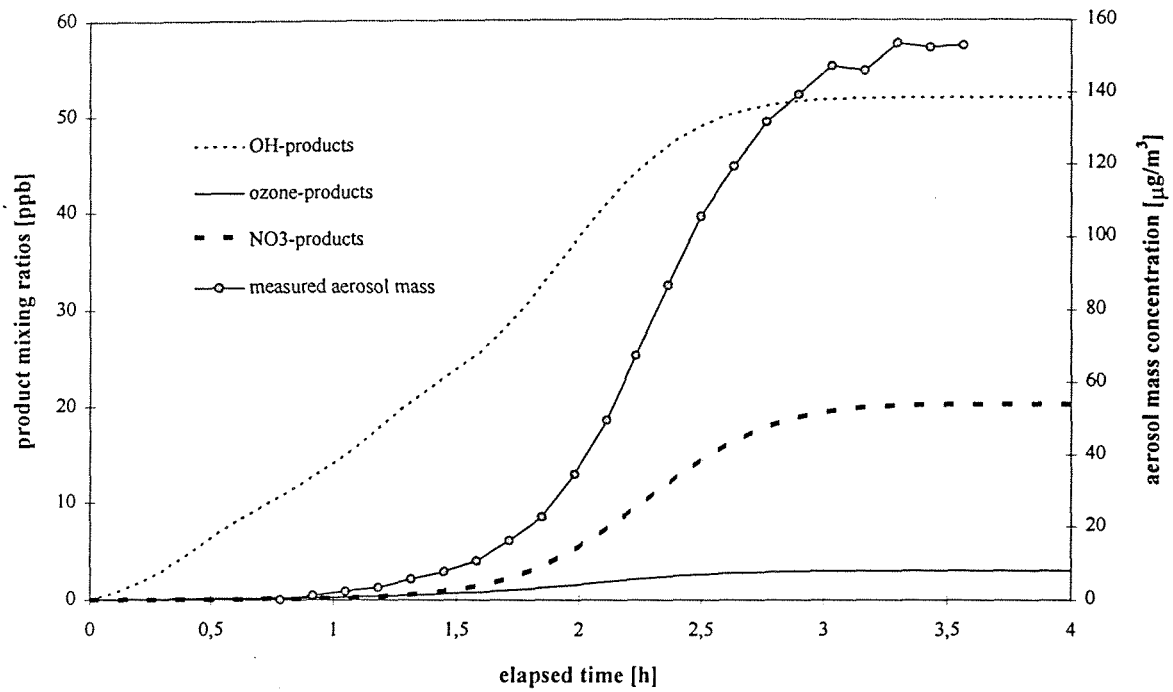
OH-products
ozone-products
NO3-products
measured aerosol mass
product mixing ratios [ppb]
aerosol mass concentration [µg/m³]
elapsed time [h]
0
10
20
30
40
50
60
0
20
40
60
80
100
120
140
160
0
0,5
1
1,5
2
2,5
3
3,5
4

Figure 6.

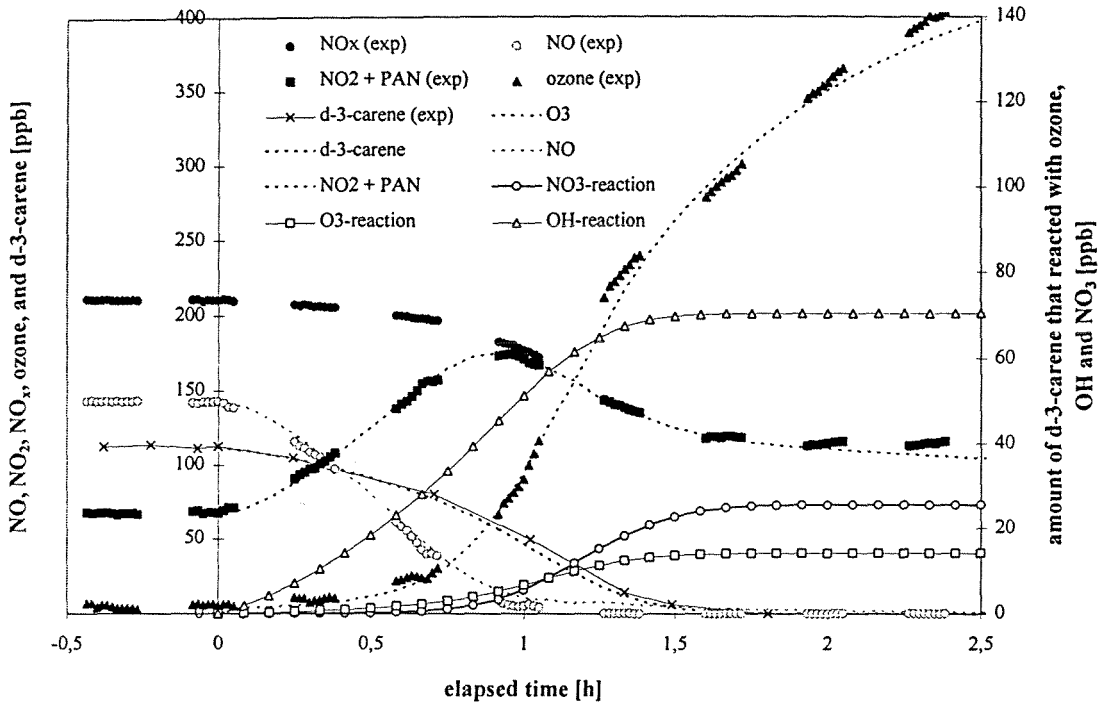
NOx (exp)
NO (exp)
NO2 + PAN (exp)
ozone (exp)
d-3-carene (exp)
O3
d-3-carene
NO
NO2 + PAN
NO3-reaction
O3-reaction
OH-reaction
NO, NO2, NOx, ozone, and d-3-carene [ppb]
amount of d-3-carene that reacted with ozone, OH and NO3 [ppb]
elapsed time [h]
400
350
300
250
200
150
100
50
0
140
120
100
80
60
40
20
0
-0,5
0
0,5
1
1,5
2
2,5

Figure 7.

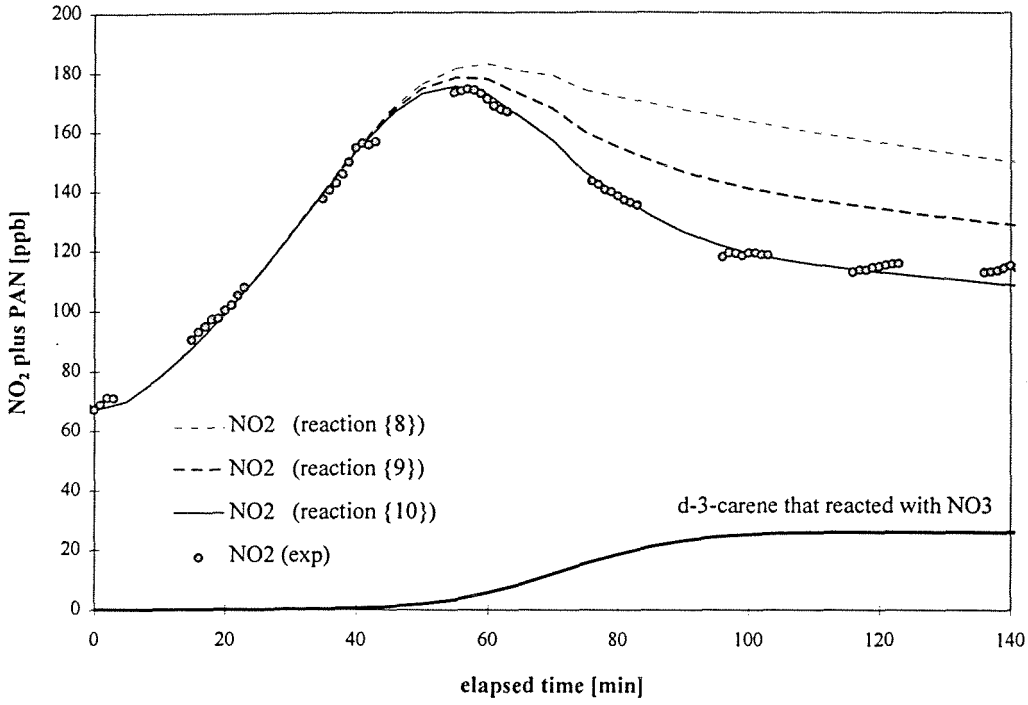
200
180
160
140
120
100
80
60
40
20
0
0
20
40
60
80
100
120
140
NO_2 plus PAN [ppb]
elapsed time [min]
NO2 (reaction {8})
NO2 (reaction {9})
NO2 (reaction {10})
NO2 (exp)
d-3-carene that reacted with NO3

Figure 8.

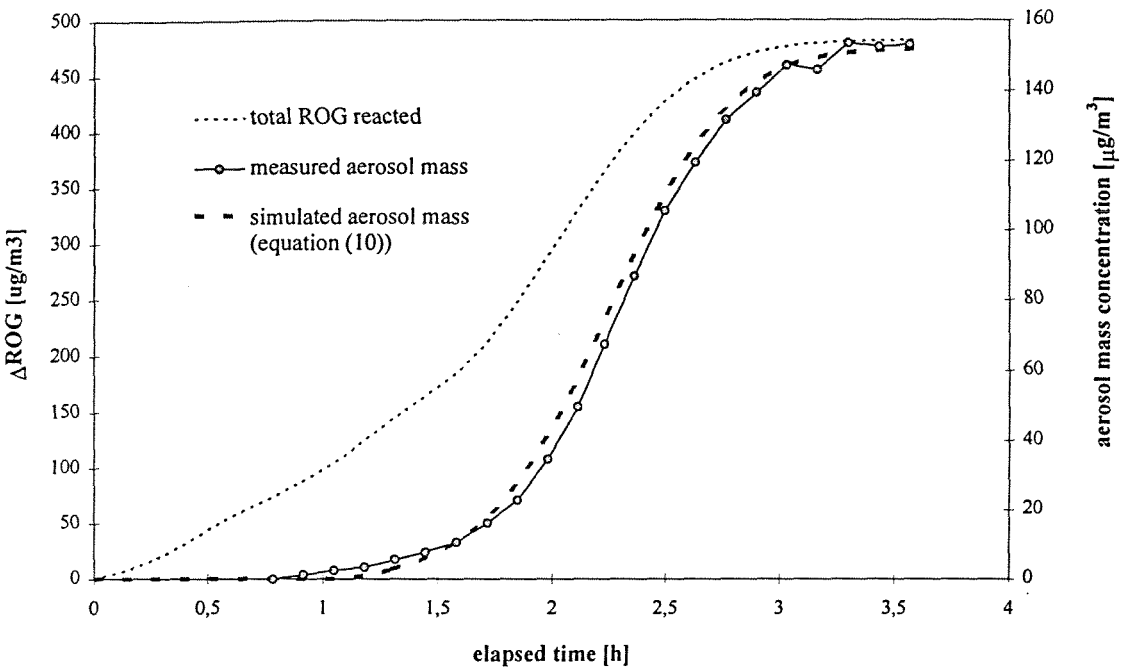
total ROG reacted
measured aerosol mass
simulated aerosol mass (equation (10))
ΔROG [ug/m3]
aerosol mass concentration [μg/m3]
elapsed time [h]
0
50
100
150
200
250
300
350
400
450
500
0
20
40
60
80
100
120
140
160
0
0,5
1
1,5
2
2,5
3
3,5
4

Figure 9.

(a)

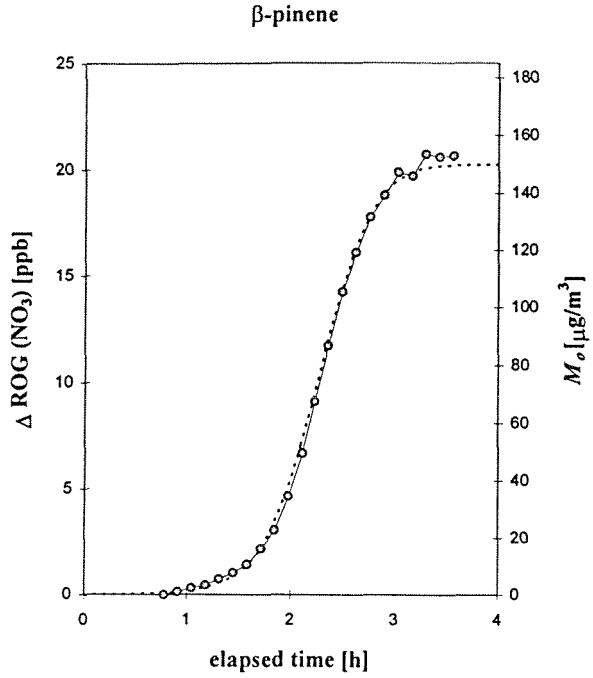
β-pinene
Δ ROG (NO3) [ppb]
Mo [μg/m3]
elapsed time [h]
0
5
10
15
20
25
0
20
40
60
80
100
120
140
160
180
0
1
2
3
4

(b)

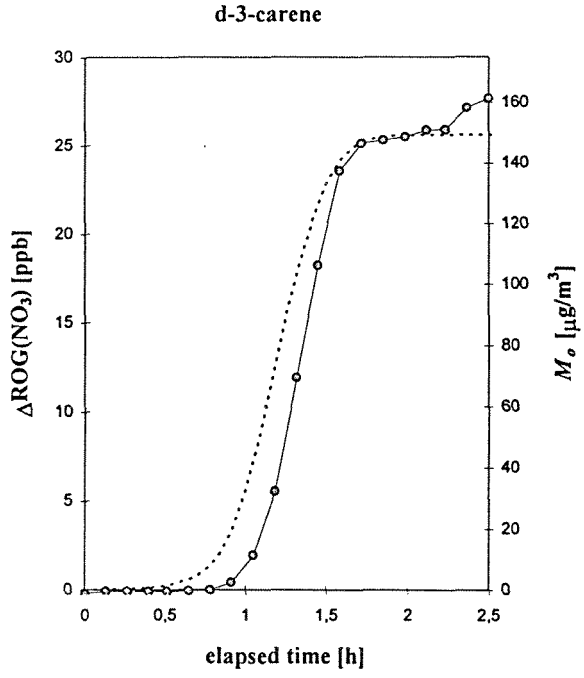
d-3-carene
ΔROG(NO3) [ppb]
Mo [μg/m3]
elapsed time [h]
0
5
10
15
20
25
30
0
20
40
60
80
100
120
140
160
0
0,5
1
1,5
2
2,5

Figure 10.

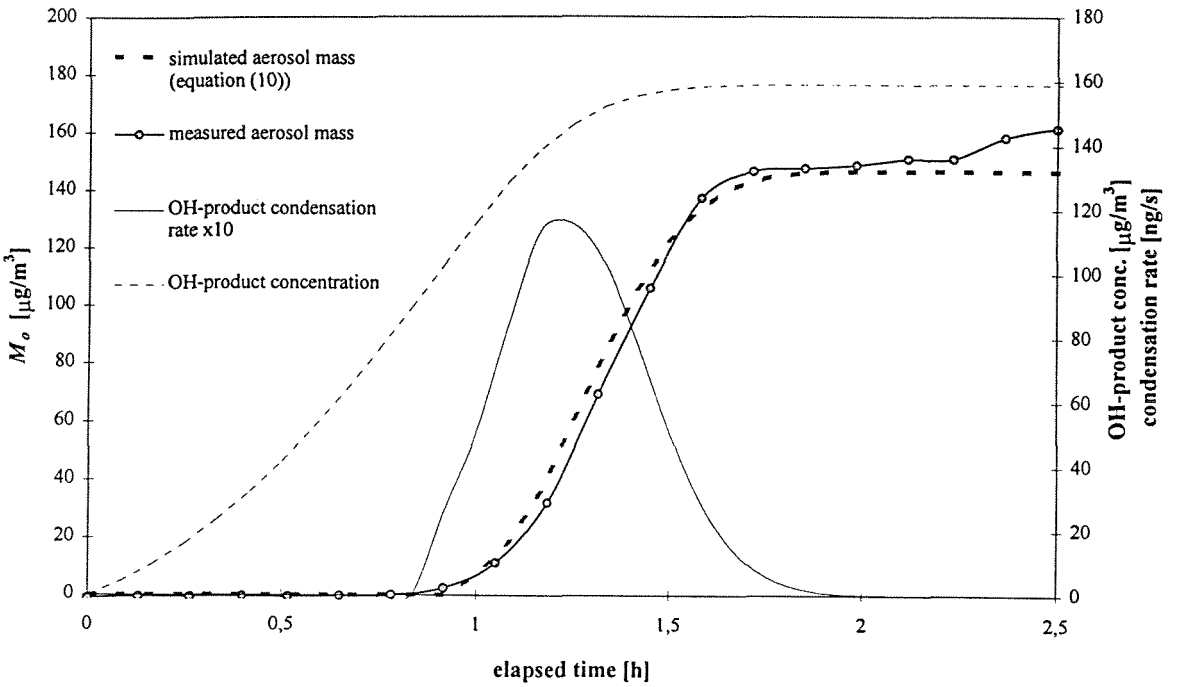
simulated aerosol mass (equation (10))
measured aerosol mass
OH-product condensation rate x10
OH-product concentration
M_o [µg/m^3]
OH-product conc. [µg/m^3] condensation rate [ng/s]
elapsed time [h]
0
20
40
60
80
100
120
140
160
180
200
0,5
1
1,5
2
2,5

Figure 11.

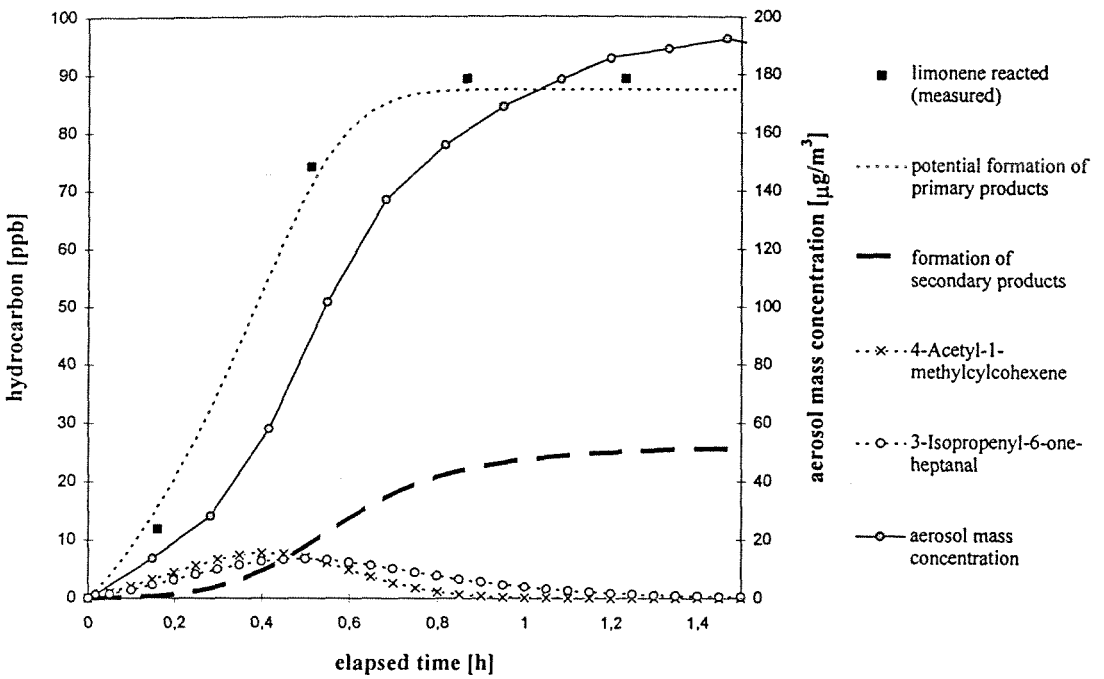
hydrocarbon [ppb]
aerosol mass concentration [µg/m³]
elapsed time [h]
0
10
20
30
40
50
60
70
80
90
100
0
20
40
60
80
100
120
140
160
180
200
0
0,2
0,4
0,6
0,8
1
1,2
1,4
limonene reacted (measured)
potential formation of primary products
formation of secondary products
4-Acetyl-1-methylcylcohexene
3-Isopropenyl-6-one-heptanal
aerosol mass concentration

Figure 12.

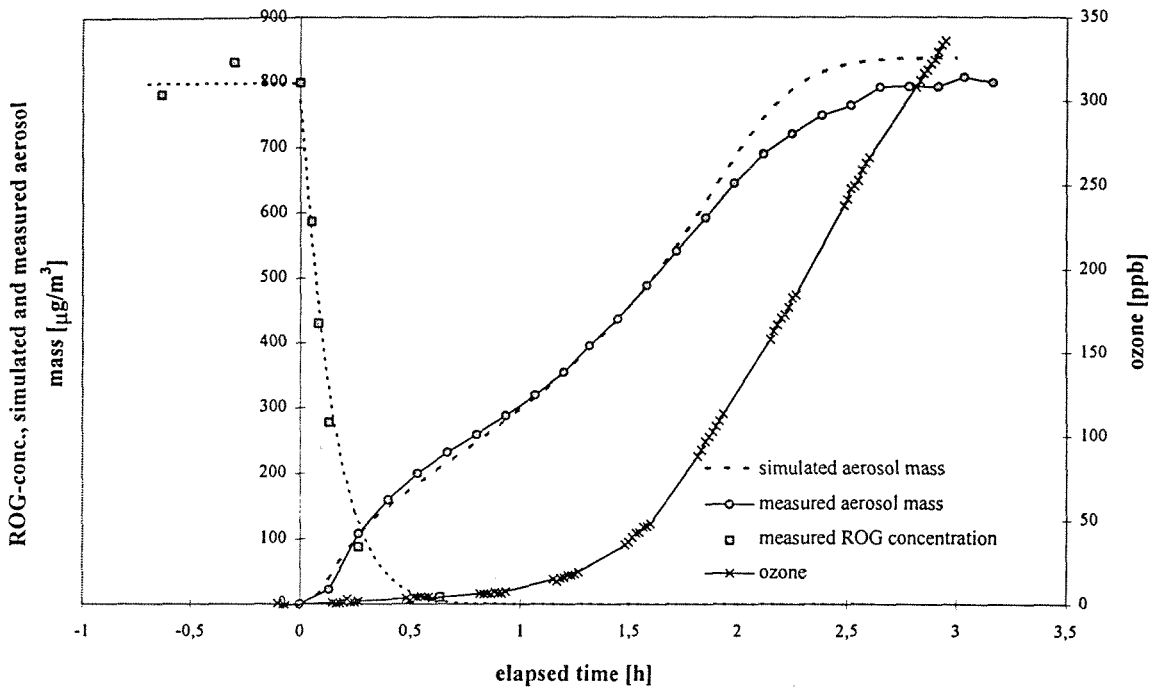
ROG-conc., simulated and measured aerosol mass [µg/m³]
ozone [ppb]
elapsed time [h]
simulated aerosol mass
measured aerosol mass
measured ROG concentration
ozone
900
800
700
600
500
400
300
200
100
0
350
300
250
200
150
100
50
0
-1
-0,5
0
0,5
1
1,5
2
2,5
3
3,5

Figure 13.

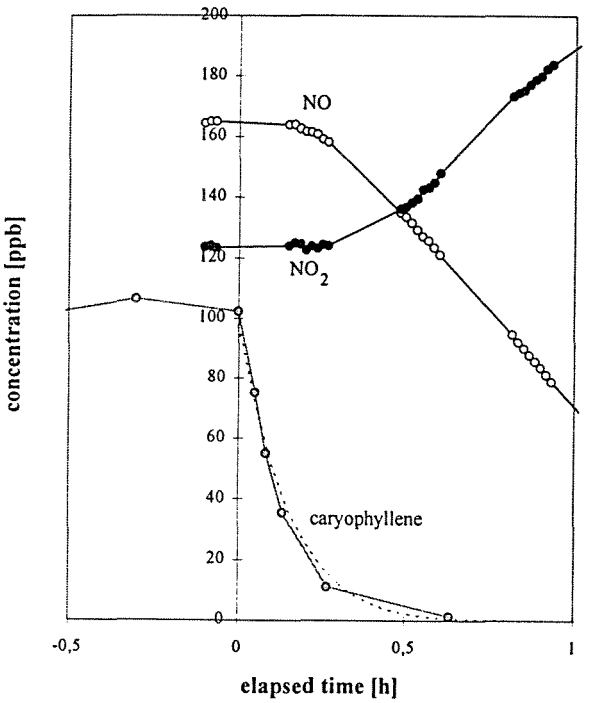
200
180
160
140
120
100
80
60
40
20
0
NO
NO2
caryophyllene
concentration [ppb]
-0,5
0
0,5
1
elapsed time [h]

Figure 14.

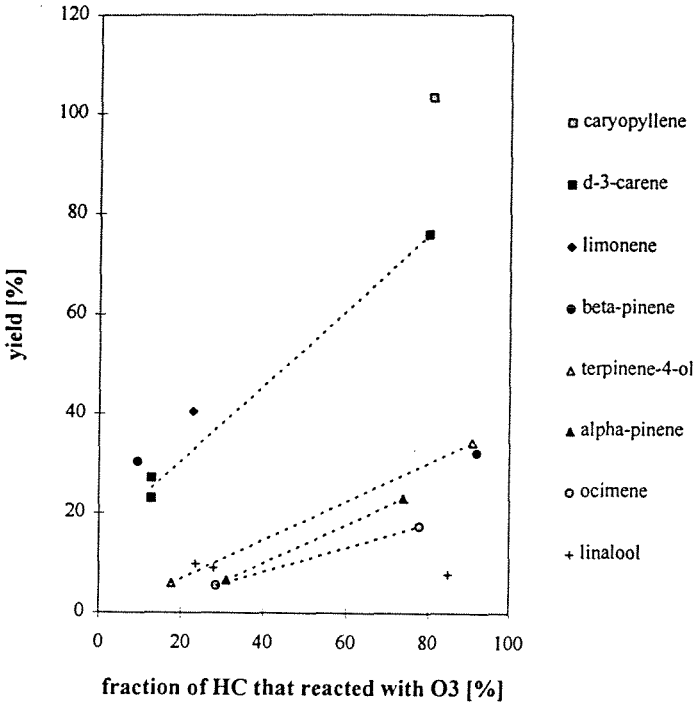
120
100
80
60
40
20
0
yield [%]
0
20
40
60
80
100
fraction of HC that reacted with O3 [%]
caryopyllene
d-3-carene
limonene
beta-pinene
terpinene-4-ol
alpha-pinene
ocimene
linalool

Figure 15.

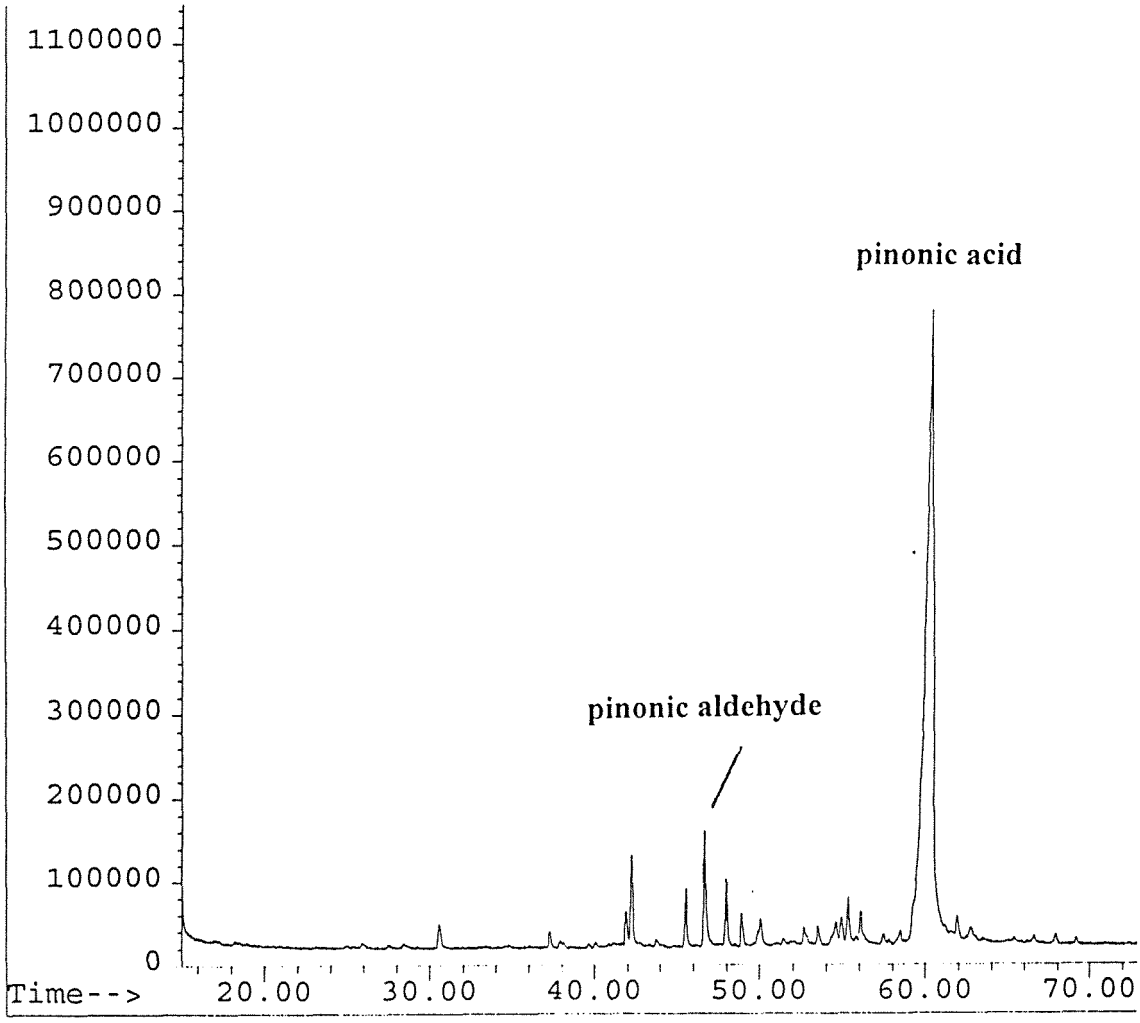
1100000
1000000
900000
800000
700000
600000
500000
400000
300000
200000
100000
0
Time-->
20.00
30.00
40.00
50.00
60.00
70.00
pinonic acid
pinonic aldehyde

CHAPTER 7:

MATHEMATICAL MODEL FOR GAS/PARTICLE PARTITIONING OF SECONDARY ORGANIC AEROSOLS

Submitted to *Atmos. Environ.*

ABSTRACT

A dynamic model is developed for gas-particle absorptive partitioning of semi-volatile organic aerosols. For application to experimental study of secondary organic aerosol formation in smog chambers, the model includes particle wall deposition, and vapor transport to aerosol particles, chamber walls and deposited particles. The model is applied to simulate a pair of *m*-xylene/NO_x outdoor smog chamber experiments. In the presence of an inorganic seed aerosol a threshold for aerosol formation is predicted. An examination of characteristic transport times indicates that gas-particle equilibrium is typically established quite rapidly. Semi-volatile products that are second-generation, rather than first-generation, products of a parent hydrocarbon cause a delay in aerosol formation as a result of the delayed rate at which the second-generation products are formed. The gas/particle accommodation coefficient is the principal transport parameter and is estimated to have a value between 1.0 and 0.1 for the *m*-xylene aerosol.

INTRODUCTION

Secondary organic aerosol formation has been identified as an important process in atmospheres where photochemical ozone formation is substantial. Over the past 20 years smog chamber experiments have been performed to determine secondary aerosol yields for a variety of organic compounds (Grosjean, 1977; Stern *et al.*, 1987; Grosjean and Seinfeld, 1989; Izumi and Fukuyama, 1990; Pandis *et al.*, 1991; Wang *et al.*, 1991*a*; Odum *et al.*, 1996). Data obtained from such experiments have been incorporated into models that seek to predict ambient aerosol concentrations (Wang *et al.*, 1991*b*; Pandis *et al.*, 1992,1993). Pandis *et al.* (1993) simulated changes in aerosol size and composition as primary hydrocarbons react to form condensable organic products assuming gas-phase products condense upon exceeding their saturation vapor pressure. Semi-volatile compounds do partition into the aerosol phase at concentrations below saturation and this phenomenon needs to be accounted for (Pankow, 1994*a*; Odum *et al.*, 1996). In this work we present a model for gas/particle partitioning of secondary organic aerosols that incorporates both equilibrium partitioning and full dynamic transport to simulate aerosol formation and growth.

Our goal is to develop a model of sufficient generality to be used as a component of atmospheric models to predict formation of secondary organic aerosols. The testbed for such a model is the smog chamber, in which virtually all experimental studies of secondary organic aerosol formation have been carried out. We therefore develop the

model to include wall processes that are present in a smog chamber; in atmospheric applications these processes are absent. We seek to address a number of key questions concerning the formation and gas/particle partitioning of secondary organic aerosols: (1) When can the assumption of instantaneous gas/particle equilibrium be invoked? (2) How do observed aerosol yields depend on whether first- or second-generation photooxidation products comprise the condensable species? (3) Under what conditions might homogeneous nucleation of a condensable vapor product be expected to occur? The exact chemical pathways to secondary organic aerosol for most parent hydrocarbons are still uncertain, and because of the large number of compounds identified in those mixtures for which molecular speciation information is available, it is unlikely that all the paths of formation of organic aerosol will be elucidated. The generality of gas/particle partitioning theory, however, offers a framework within which secondary organic aerosol formation can be represented without requiring detailed mechanistic knowledge of the photooxidation paths. It is the properties of that theory that we explore here to address the questions posed above.

CONDENSABLE VAPOR FORMATION

A general representation of the chemical process of organic aerosol formation is that semi-volatile organic gases, S_1, S_2, ..., are formed by the gas-phase reaction of a parent hydrocarbon, HC, with OH radicals,

$$\mathrm{HC} + \mathrm{OH} \xrightarrow{k_{\mathrm{OH}}} \ldots + x_1\,\mathrm{S}_1 + x_2\,\mathrm{S}_2 + \ldots \qquad (1a)$$

where k_{OH} is the reaction rate constant, and x_1, x_2, ... are the stoichiometric product coefficients. If the parent hydrocarbon is an alkene, reactions with O_3 and NO_3 radicals are also possible, providing additional pathways for condensable vapor formation,

$$\mathrm{HC} + \mathrm{O}_3 \xrightarrow{k_{\mathrm{O}_3}} \ldots + x_{1,\mathrm{O}_3}\,\mathrm{S}_{1,\mathrm{O}_3} + x_{2,\mathrm{O}_3}\,\mathrm{S}_{2,\mathrm{O}_3} + \ldots \qquad (1b)$$

$$\mathrm{HC} + \mathrm{NO}_3 \xrightarrow{k_{\mathrm{NO}_3}} \ldots + x_{1,\mathrm{NO}_3}\mathrm{S}_{1,\mathrm{NO}_3} + x_{2,\mathrm{NO}_3}\mathrm{S}_{2,\mathrm{NO}_3} + \ldots \qquad (1c)$$

The first-generation products, S_1, S_2, ... may subsequently undergo reaction themselves creating second-generation condensable products, S_{1a}, S_{1b}, ... and S_{2a}, S_{2b}, ...,

$$\mathrm{S}_1 + \mathrm{OH} \xrightarrow{k_{\mathrm{OH,S_1}}} \ldots + x_{1a}\,\mathrm{S}_{1a} + x_{1b}\,\mathrm{S}_{1b} + \ldots \qquad (2a)$$

$$\mathrm{S}_2 + \mathrm{OH} \xrightarrow{k_{\mathrm{OH,S_2}}} \ldots + x_{2a}\,\mathrm{S}_{2a} + x_{2b}\,\mathrm{S}_{2b} + \ldots \qquad (2b)$$

where $k_{\mathrm{OH,S1}}$ and $k_{\mathrm{OH,S2}}$ are the OH radical reaction rate constants for the products, S_1 and S_2, respectively.

Once semi-volatile products have been formed, partitioning to available surfaces will occur as illustrated in Figure 1. Vapors can condense on suspended aerosol particles, on chamber walls, if the process is occurring in a smog chamber, or on the surface of particles that have deposited on the chamber walls. The distribution of organic species

between the gas phase, aerosol phase, wall, and deposited particles depends on both equilibrium and transport considerations.

GAS-PARTICLE EQUILIBRIUM

Equilibrium gas-particle partitioning of a semi-volatile organic species *i* between the gas phase and an organic phase in the particle can be described using a partitioning coefficient, K_i (m^3 μg^{-1}) (Pankow, 1994*ab*; Odum *et al.*, 1996),

$$K_i = \frac{A_i}{G_i \left(\sum_k A_k + M_{\text{init}} \right)} \tag{3}$$

where A_i (μg m^{-3}) is the aerosol mass concentration of species *i*, G_i (μg m^{-3}) is the gas-phase mass concentration of species *i*, ΣA_k (μg m^{-3}) is the total aerosol mass concentration of all the individual semi-volatile organic species, A_k, and M_{init} represents any initially present absorbing organic mass. Upon rearrangement, (3) can be used to determine the gas-phase concentration of species *i* that exists in equilibrium with the particle surface, G_i^{eq} (μg m^{-3}),

$$G_i^{\text{eq}} = \frac{A_i}{K_i \left(\sum_k A_k + M_{\text{init}} \right)} \tag{4}$$

Thus, given a numerical value for the partitioning coefficient, K_i, and the organic aerosol compositions, A_i, the equilibrium vapor concentration at the particle surface may be calculated.

The absorption partitioning coefficient, K_i ($m^3\ \mu g^{-1}$), has been derived by Pankow (1994*a*),

$$K_i = \left(\frac{RT}{p_i^0 MW}\right)\left(\frac{1}{\zeta_i}\right) 10^{-6} \qquad (5)$$

where R (=6.2x10^{-2} torr m^3 $mol^{-1}K^{-1}$ =8.314 J $mol^{-1}K^{-1}$) is the ideal gas constant, T (K) is temperature, p_i^0 (torr) is the vapor pressure of pure species i at temperature T, MW (g mol^{-1}) is the mean molecular weight of the absorbing organic matter, and ζ_i is the activity coefficient of species i in the organic mixture. The factor 10^{-6} accomplishes the appropriate unit conversions. K_i, therefore, is the inverse of the vapor pressure expressed in mass concentration units ($m^3\ \mu g^{-1}$), modified by an activity coefficient to account for non-ideal mixing.

THRESHOLD CONCENTRATION FOR AEROSOL FORMATION

For atmospheric aerosol some amount of organic material will most likely always be present and $M_{init} > 0$. Under such conditions when a semi-volatile organic product is

formed, it immediately begins to partition into the available organic aerosol. If there is no organic aerosol initially present (M_{init} =0), however, absorption partitioning equilibrium theory predicts that a threshold will exist for aerosol formation. We examine the nature of this threshold considering first the case of a single semi-volatile organic product, and then extend the results to a multicomponent system.

The total concentration of a first-generation semi-volatile product formed when a hydrocarbon reacts is proportional to the amount of hydrocarbon that reacts, ΔHC (μg m^{-3}), and is equal to the sum of the aerosol-phase concentration of species *i* over all particle sizes, A_i^{tot}, and the gas-phase concentration of species *i*,

$$x_i \, \Delta HC = A_i^{tot} + G_i \tag{6}$$

For the case of a single semi-volatile organic product and no initial organic aerosol (M_{init}=0), the equilibrium gas-phase concentration from (4) becomes

$$G_1 = \frac{1}{K_1} \tag{7}$$

which when combined with (5) is

$$G_1 = \frac{p_1^0 \, MW}{RT} 10^6 \tag{8}$$

indicating that the gas-phase concentration will be equal to the saturation vapor pressure as long as a pure component or single component aerosol phase exists. Combining (6)

and (7) the aerosol-phase concentration can be related to the amount of hydrocarbon reacted,

$$A_1^{tot} = x_1 \Delta HC - \frac{1}{K_1} \tag{9}$$

When ΔHC is small, A_1^{tot} will be negative, a physically meaningless result. This situation arises when the gas-phase concentration is below the saturation vapor pressure and no aerosol phase exists. A threshold for aerosol formation, ΔHC^*, can be determined by setting $A_1^{tot}=0$ in the above equation,

$$\Delta HC^* = \frac{1}{x_1 K_1} \tag{10}$$

When $\Delta HC<\Delta HC^*$ all of the semi-volatile organic product formed remains in the gas phase and no aerosol phase is present. When $\Delta HC>\Delta HC^*$ the saturation vapor pressure is reached and organic aerosol forms.

For a multicomponent mixture (4) and (6) can be combined to form an expression for the aerosol-phase concentration of species *i*,

$$A_i^{tot} = \frac{x_i \Delta HC K_i \sum_k A_k^{tot}}{1 + K_i \sum_k A_k^{tot}} \tag{11}$$

Summing (11) over all semi-volatile species *i* we obtain

$$\sum_i A_i^{tot} = \Delta HC \sum_k A_k^{tot} \sum_i \frac{x_i K_i}{1 + K_i \sum_k A_k^{tot}} \quad (12)$$

and since $\Sigma A_i^{tot} = \Sigma A_k^{tot}$, (12) can be simplified and rearranged,

$$\Delta HC = \frac{1}{\sum_i \frac{x_i K_i}{1 + K_i \sum_k A_k^{tot}}} \quad (13)$$

Setting the total aerosol mass to zero we find the threshold for aerosol formation,

$$\Delta HC^* = \frac{1}{\sum_i x_i K_i} \quad (14)$$

For $\Delta HC<\Delta HC^*$, all semi-volatile organics remain in the gas phase; for $\Delta HC>\Delta HC^*$, an aerosol phase exists in equilibrium with the gas phase. Unlike the single component case, however, where the equilibrium gas-phase concentration is a constant, in a multicomponent system gas-particle equilibrium is a function of the organic aerosol concentration, and the equilibrium gas-phase concentrations varies as organic aerosol is formed.

An alternative expression for the aerosol formation threshold, utilizing the gas-phase concentrations of the semi-volatile organics, can be derived by rearranging (4),

$$G_i K_i = \frac{A_i}{\sum_k A_k} \tag{15}$$

summing over all semi-volatile species i,

$$\sum_i G_i K_i = \sum_i \frac{A_i}{\sum_k A_k} \tag{16}$$

and simplifying,

$$\sum_i G_i K_i = 1 \tag{17}$$

The above equation defines the gas-particle equilibrium and is valid whenever gas and aerosol phases coexist, *i.e.*, when the threshold has been exceeded. Below the threshold no aerosol phase will exist and $\Sigma G_i K_i < 1$. Above the threshold, partitioning to the aerosol phase will occur such that $\Sigma G_i K_i$ remains unity. Equation (17) is of a more general nature than (14) and can be applied to semi-volatile species that are formed as secondary products or whose concentrations are otherwise nonlinearly related to the amount of parent hydrocarbon reacted.

It should be emphasized that the existence of a distinct threshold for aerosol formation is predicted only when no absorbing organic material is initially present. This will not be the case for atmospheric aerosol where there is preexisting organic material, but is relevant in smog chamber experiments in which inorganic seed particles are

employed. While the threshold prediction is based on the assumption of purely absorptive partitioning, for inorganic or non-absorbing organic particles it is likely that initially adsorption takes place until a sufficient organic layer can be formed to allow absorption to occur. It can be shown that even when adsorptive partitioning occurs, a threshold for aerosol growth will still exist. (Appendix A)

.

VAPOR-PARTICLE TRANSPORT

Transport of a condensable organic species i from the gas phase to an aerosol particle of diameter D_p (μm) can be described by the flux equation (Wexler and Seinfeld, 1990),

$$J_i = \frac{2\pi D_p \lambda \bar{c}_i \left(G_i - G_i^{eq} \exp\left[\frac{\sigma_i \, MW}{RT \rho D_p} 10^{-3} \right] \right)}{1 + \frac{8\lambda}{\alpha D_p}} \qquad (18)$$

where J_i (μg s^{-1}) is the rate of mass transfer to the particle surface, λ (μm) is the mean free path of air, $\bar{c}_i$ (m s^{-1}) is the mean molecular speed of species i, G_i (μg m^{-3}) is the bulk gas-phase concentration of species i, σ_i (dyne cm^{-1}) is the surface tension of species i, ρ (g cm^{-3}) is liquid-phase density, and α is the accommodation coefficient. The factor 10^{-3}

accomplishes the appropriate unit conversions. The exponential term in (18) accounts for the Kelvin effect at small particle size when surface curvature raises the equilibrium gas concentration. This term is ordinarily negligible; for example, for a 20 nm diameter particle it represents only a 5% correction to the flux. While the overall equilibrium partitioning between gas and aerosol phases is defined by the equilibrium relations, the resulting size distribution of the condensed semi-volatile product cannot be uniquely determined without accounting for size-dependent rates of mass transfer between the gas and aerosol phases.

WALL PROCESSES

Within a smog chamber wall effects are an additional consideration. Particles will deposit to the chamber walls and semi-volatile vapors may condense on the chamber walls or onto previously deposited particles. Conditions within a smog chamber can also arise that lead to nucleation. The equations governing these chamber processes are given in Appendix B.

CHARACTERISTIC TIME SCALES

With the basic equations for gas-particle interaction defined, characteristic times for each of the processes may be defined, as summarized in Table 1. The characteristic time for semi-volatile product formation, τ_F, is the time scale on which the parent hydrocarbon reacts. This time depends on the OH rate constant, k_{OH}, and the OH radical concentration, [OH]. Gas-particle transport is characterized by the time required for vapor diffusion to aerosol particles, τ_{GP}, and is governed by particle number, size, and accommodation coefficient. τ_{GW} and τ_{PW} are characteristic times for transport to the wall for gas and particles, respectively. These times depend on the surface to volume ratio of the chamber (A_c/V_c) and on the mass transfer coefficients, k_{mG} and k_{mP}. The time scale for vapor transport to wall deposited particles, τ_{GD}, is controlled by the surface area of deposited particles, A_p.

Substituting appropriate values for a typical smog chamber experiment allows the relative time scales to be compared. With characteristic times on the order of a few hours, formation of semi-volatile products and particle deposition occur relatively slowly as compared to vapor transport, whereas gas-particle transport occurs on a time scale of order 1 minute. It should be recognized, however, that gas-particle transport times are highly dependent on particle number and diameter. Equilibration between the gas-phase and chamber walls is rapid with a characteristic time of order 30 s. This time scale analysis indicates that equilibrium of a semi-volatile product between the gas phase and

particle surfaces is established within a few minutes. Since condensable vapor formation occurs on a much longer time scale, the gas/particle system will be very near equilibrium at all times. It is appropriate, therefore, to assume instantaneous gas/particle equilibrium when there is sufficient particle surface area to ensure rapid transport.

Exceptions to the assumption of instantaneous equilibrium will arise when there is very little aerosol present or when condensable vapor is formed sufficiently rapidly by a fast-reacting parent hydrocarbon. For example, an aerosol population with number concentration 500 cm^{-3} and mean diameter 50 nm results in a gas/particle transport time on the order of 2 h. A parent hydrocarbon, such as *d*-limonene, with an OH rate constant of $2x10^{-10}$ $cm^3molec^{-1}s^{-1}$, and an OH concentration of $7x10^6$ molec cm^{-3}, results in a characteristic time for semi-volatile product formation, τ_F, of 10 minutes. It should be noted, however, that a prolonged state of non-equilibrium for the semi-volatile product is unlikely. Small particles grow quickly resulting in a greatly increased surface area, more rapid gas/particle transport, and, in extreme cases, nucleation.

Within a smog chamber for typical particle sizes and surface-to-volume ratios, the transport of particles to wall surfaces occurs with a characteristic time of order 5 h, which is sufficiently slow to treat particle deposition separately from the much faster gas transport processes. Partitioning of a semi-volatile product between the gas phase and particles that have deposited on the chamber walls is negligibly slow, occurring on a time scale of several days. Deposited particles and any organic mass that they contain,

therefore, can be considered to be essentially removed from the system with any partitioning occurring once particles reach the chamber wall being neglected.

It should be noted that the time scales for vapor transport indicate the relative rates at which equilibrium will be established, but imply nothing about the equilibrium state that will ultimately be attained. The equilibrium distribution of condensed organic vapor between suspended particles and chamber wall is governed by their respective partitioning coefficients.

MODEL APPLICATION TO SMOG CHAMBER EXPERIMENTS

In the study of secondary organic aerosol formation, typically smog chambers are initially filled with a mixture of NO_x, inorganic seed particles, and an aerosol-producing hydrocarbon. The chamber is then exposed to sunlight, or other UV sources, that initiates photooxidation. As the hydrocarbon reacts it forms semi-volatile products that condense on the seed particles. When transport to the particles is slower than the rate of product formation, the semi-volatile products will accumulate in the gas phase and nucleation may occur.

In our simulation of experiments conducted in the Caltech outdoor smog chamber, the chamber gas-phase chemistry is described by the SAPRC90 chemical mechanism (Carter, 1990) and employs the Carter mechanism preparation software (Carter, 1988) to

define the set of differential equations associated with the gas-phase reactions. The mechanism predicts OH concentrations within the chamber and the resulting OH-reaction rate of the hydrocarbon and its products. Time, date, and location allow one to determine the corresponding actinic flux. Other input variables for the mechanism include temperature, pressure, relative humidity, and a radiation scaling factor.

Reaction mechanisms for individual hydrocarbons have been modified to include one or more products that are designated as semi-volatile species. These first-generation products may themselves undergo reaction to form second-generation gas-phase products that can also condense. For each condensable product, partitioning coefficients for absorption to particles and adsorption to walls are specified, along with estimated surface tensions. For simplicity in presenting results, all semi-volatile organics are assumed to have a similar molecular weight, density, and accommodation coefficient. Wall transport parameters include a size-dependent particle loss coefficient, gas-wall mass transfer coefficient, wall accommodation coefficient, and chamber surface area/volume ratio, which is assumed constant throughout the experiment.

The size variation of the aerosol population is represented using discrete size sections. All particles within each section are assumed to have the same chemical composition which is an excellent assumption for a smog chamber. As particles grow, size changes are calculated using the moving section technique (Gelbard, 1990; Kim and Seinfeld, 1990). Specifically, the total change in the aerosol-phase concentration of

species i, in section j, A_{ij} (μg m^{-3} s^{-1}), is calculated by combining the flux equation (18) with the particle number concentration in section j, N_j (m^{-3}),

$$\frac{dA_{ij}}{dt} = \frac{N_j \, 2\pi D_{p_j} \, \lambda \, \bar{c}_i \left(G_i - G_{ij}^{eq}\right)}{1 + \frac{8\lambda}{\alpha D_{p_j}}} \tag{19}$$

The equilibrium concentration at the particle surface, G_{ij}^{eq} (μg m^{-3}), is size-dependent and is calculated by

$$G_{ij}^{eq} = \frac{A_{ij}}{K_i \left(\sum_k A_{kj} + M_{initj} \right)} \exp\left[\frac{\sigma_i \, MW}{RT \rho \, D_p} 10^{-3} \right] \tag{20}$$

when

$$\sum_i G_i \, K_i \, \exp\left[-\frac{\sigma_i \, MW}{RT \rho \, D_p} 10^{-3} \right] \geq 1 \tag{21}$$

If the aerosol formation threshold has not been reached, *i.e.*,

$$\sum_i G_i \, K_i \, \exp\left[-\frac{\sigma_i \, MW}{RT \rho \, D_p} 10^{-3} \right] < 1 \text{ and } \quad \sum_k A_{kj} + M_{initj} = 0 \tag{22}$$

then the equilibrium gas-phase concentration is identical with the actual gas-phase concentration,

$$G_{ij}^{eq} = G_i \tag{23}$$

The change in the gas-phase concentration of semi-volatile species i, is governed by

$$\frac{dG_i}{dt} = P_i - \sum_j \frac{dA_{ij}}{dt} \tag{24}$$

where P_i ($\mu g\ m^{-3}\ s^{-1}$) is the rate of production of species i from chemical reaction. Taken together, (19) and (24) comprise the set of differential equations that define gas-to-particle conversion.

When a vapor concentration exceeds its equilibrium vapor pressure, nucleation may occur. The nucleation rate is calculated with (B8). If the nucleation rate exceeds an arbitrary threshold level of $10^{-3}\ cm^{-3}\ s^{-1}$, the nucleated particles are assigned to a new size section. The diameter of particles in the nucleation section is that of the critical nucleus size, g^*. These particles subsequently grow along with the initially present seed particles.

SIMULATION OF SMOG CHAMBER EXPERIMENTS

The performance of the model can be demonstrated by using it to simulate a set of smog chamber experiments. This will not only show that the model is capable of reproducing observed experimental results, but also illustrates the general behavior and physics involved with aerosol growth and provides a realistic scenario for examining the

influence of the various equilibrium and transport parameters. We will simulate a pair of experiments performed on August 4, 1995, in the Caltech outdoor smog chamber.* The chamber was divided into two 20 m^3 sides that were both filled with $(NH_4)_2SO_4$ seed particles and mixtures of *m*-xylene, propene, NO and NO_2. Initial conditions for both sides of the chamber are listed in Table 2. One side contained 510 ppb of *m*-xylene and 820 ppb NO_x, while the other contained 1008 ppb *m*-xylene and 1643 ppb NO_x. Both sides had similar propene concentrations, aerosol populations and VOC/NO_x ratios, so that the key difference between the two chambers was the *m*-xylene concentrations.

In the photooxidation of *m*-xylene, the semi-volatile vapor species are expected to be second-generation products of the *m*-xylene. One compound that has been observed as a component of the organic aerosol from *m*-xylene is *m*-toluic acid (Forstner *et al.*, 1996), which is the product of reaction of a first-generation reaction product. The *m*-xylene-OH reaction is assumed to produce a first-generation product, S_1, that reacts with OH to form two semi-volatile second-generation products, S_{1a} and S_{1b}.

The condensable vapors, S_{1a} and S_{1b}, are not intended to represent any specific products of the *m*-xylene photooxidation, and the parameters used in the simulation are those found to best fit the experimental data. The products are generated with stoichiometric coefficients, x_{1a} and x_{1b}, of 0.03 and 0.14, respectively. Absorption

* As presently configured, the model includes 74 gas-phase species, with up to 6 condensable organic species that partition between the gas and aerosol phases. The aerosol population is represented by 39 size sections with 23 for initially present seed particles, 14 for nucleation size sections, 1 section for wall condensate and 1 section to track aerosol mass deposited to the chamber walls.

partitioning coefficients, K_{1a} and K_{1b} for S_{1a} and S_{1b}, were set at 0.06 $m^3\ \mu g^{-1}$ and 0.002 $m^3\ \mu g^{-1}$. These values for the stoichiometric and partitioning coefficients are close to those estimated by Odum *et al.* (1996) from a series of *m*-xylene experiments. Adsorption to the Teflon chamber walls is expected to be much less favorable than absorption into organic matter (Storey *et al.*, 1995) and the wall adsorption partitioning coefficients, K_{1a}^{w} and K_{1b}^{w}, were set at 10^{-4} of the absorption values.

Molecular weight, *MW*, of 150, density, ρ, of 1.5 g cm^{-3}, and surface tension, σ, of 25 dyne cm^{-1} were assumed for both semi-volatile products as representative of typical aromatic products. Accommodation coefficients for both particles and chamber walls were set at 0.2 to fit the experimental observations. The size dependence of the particle deposition loss coefficient, $\beta_P(D_p)$, was based on theoretical predictions for Teflon-walled chambers (McMurry and Rader, 1985) with the absolute value scaled to match observed particle losses. By correlation to experimental deposition rates for small particles, where losses are due primarily to diffusion, the mass transfer coefficient for vapor diffusion to the chamber walls, k_{mG}, was estimated at 1.0 m min^{-1}. A summary of the parameters used to simulate the two experiments is given in Table 3.

Figure 2 compares the simulation results for aerosol growth with experimental observations for Side A. In Figure 2*a* the simulated particle number concentration steadily declines as particles are lost to the chamber walls; this behavior matches that observed since the particle wall deposition rate was adjusted to fit the data. More importantly, the predicted aerosol volume matches the experimental observations. For

the first hour no noticeable aerosol growth occurs and aerosol volume decreases due to deposition. During the next two hours aerosol volume increases from approximately 30 to 250 $\mu m^3 cm^{-3}$ as semi-volatile product deposits on the seed particles. After 3 hours aerosol volume levels off and begins to decrease as growth slows while deposition continues.

The evolving aerosol size distribution is simulated closely (Figure 2*b*). Initially, when growth is small, the distribution moves only slightly to larger particle diameters and the peak height decreases as a result of deposition. As growth begins, the size distribution shifts to larger diameters, the peak height increases, and the distribution exhibits the characteristic narrowing as small particles grow faster than larger particles. Near the end of the experiment when growth slows, the peak height of the distribution decreases again due to deposition.

Similar results for the Side B experiment are shown in Figure 3. As with the Side A experiment, total aerosol volume (Figure 3*a*) initially decreases, then undergoes a period of growth, achieves a maximum value and ultimately decreases. The size distributions in Figure 3*b* also exhibit these periods dominated by particle deposition and aerosol growth. Maximum aerosol growth for the 1008 ppb side, 220 $\mu m^3 cm^{-3}$, is about a factor of 4 higher than that for the 510 ppb side, 50 $\mu m^3 cm^{-3}$, as a result of the larger production of semi-volatile products and the shift in the gas/particle partitioning equilibrium as more organic aerosol is formed. Model predictions fit the observed experimental data quite well.

In both the 510 and 1008 ppb *m*-xylene simulations, the same set of equilibrium and transport parameters was used. These parameters should not be interpreted as unique for all *m*-xylene systems. Different combinations of the parameters can generate similar results. Additionally, under different reaction conditions, i.e., temperature, reactant concentrations, VOC/NO_x ratio, etc., the system chemistry and equilibrium will vary. The influence of these equilibrium and transport parameters will be explored in the following section.

QUALITATIVE NATURE OF DYNAMIC GAS/PARTICLE PARTITIONING

The sensitivity of the model to the various equilibrium and transport parameters will be determined by varying the values of these parameters. In so doing we seek to examine the qualitative nature of gas/particle partitioning and answer the following questions: (1) How do the absorption partitioning coefficients influence the equilibrium aerosol yield? (2) What changes in the timing of aerosol growth and overall aerosol yield are expected when the semi-volatile organics are secondary, instead of primary, products? (3) Which parameters most directly control the rate of mass transfer between the gas and aerosol phases? (4) Within a smog chamber, is partitioning to the chamber walls a significant process? (5) Under what conditions can equilibrium be assumed and when is nucleation expected to occur?

Reaction conditions and parameters from the 1008 ppb *m*-xylene experiment (see Tables 2 and 3) are used with a few modifications as a base case scenario. In order to distinguish between transport and equilibrium related delays in aerosol growth, the condensing organic compounds used in the base case, S_1 and S_2, are first-generation, as opposed to second-generation, photooxidation products of *m*-xylene. Second-generation products cause a delay in aerosol growth which is in addition to those associated with slow mass transfer and the predicted equilibrium threshold. First-generation products, therefore, are used in the base case, eliminating kinetic related delays. Accommodation coefficients for both particles and wall, α and α_w, are unity to ensure equilibrium conditions for the base case. Finally, the particle loss coefficient, $\beta_P(D_p)$, is zero to remove the effect of particle deposition and thereby represent ambient atmospheric conditions more clearly.

Concentrations of the two semi-volatile products, S_1 and S_2, in both the gas-phase, G_1 and G_2, and the aerosol phase, A_1 and A_2, are shown in Figure 4, for the base case simulation. S_1 is the less volatile of the two products with an absorption partitioning coefficient of 0.06 $m^3\mu g^{-1}$, compared to 0.002 $m^3\mu g^{-1}$ for S_2. S_2, however, is produced in greater abundance than S_1 with stoichiometric production rates of 0.03 and 0.14 for S_1 and S_2, respectively. Initially the gas-phase concentrations, G_1 and G_2, increase linearly, with no aerosol partitioning. Then after approximately 0.08 ppm of hydrocarbon has reacted, aerosol growth ensues, dominated at first by the lower volatility product, S_1, and later by the more volatile and more abundant S_2. When aerosol growth begins, the vapor

concentration, G_1, of the lower volatility product S_1 reaches a maximum and slowly declines to a steady value, while G_2 continues to increase but eventually also approaches a steady concentration.

Partitioning of the individual semi-volatile products is shown in Figures 5*a* and 5*b*. The heavy solid line in both figures represents the total amount of semi-volatile product formed and increases linearly with a slope equal to the stoichiometric coefficient. The dashed line shows the equilibrium aerosol concentration. The area below this line represents the aerosol phase, while the area above the dashed line represents the gas phase. Below the threshold of 0.08 ppm hydrocarbon reacted, no aerosol phase exists and all of the semi-volatile product is found in the gas phase. Once the threshold is exceeded, aerosol concentrations increase. For the lower volatility product, S_1, partitioning occurs quite readily, and as ΔHC increases most of S_1 is found in the aerosol phase. The more volatile product, S_2, remains in the gas phase longer and only as an aerosol phase, composed primarily of S_1, is built up, does S_2 undergo significant partitioning.

Initially, the inorganic seed aerosol has no organic layer and gas/particle partitioning is inhibited. The threshold for aerosol growth predicted from (14) using the base case parameters (x_1=0.03, x_2=0.14, K_1=0.06 $m^3\mu g^{-1}$, K_2=0.002 $m^3\mu g^{-1}$) is ΔHC^*=0.082 ppm and corresponds to the break in both aerosol and vapor curves in Figure 4. Before the threshold is reached, all of the condensable vapor remains in the gas phase. Then at the point where the threshold is attained, aerosol formation ensues, first for the less volatile product S_1 and then for S_2.

Aerosol formation by a reacting hydrocarbon can be described in terms of an aerosol yield, Y ($\mu g\ m^{-3}\ ppm^{-1}$) (Grosjean and Seinfeld, 1989; Odum *et al.*, 1996),

$$Y = \frac{\sum_i A_i^{tot}}{\Delta HC} = \sum_i \frac{x_i K_i \left(\sum_k A_k + M_{init} \right)}{1 + K_i \left(\sum_k A_k + M_{init} \right)} \qquad (25)$$

where ΣA_i^{tot} ($\mu g\ m^{-3}$) is the total organic mass in the aerosol phase generated from the parent hydrocarbon and ΔHC ($\mu g\ m^{-3}$) is the amount of the parent hydrocarbon that has reacted. The aerosol yield is most meaningful when it represents equilibrium conditions for primary products of the parent hydrocarbon. As was indicated previously, gas/aerosol transport in the base case scenario for the *m*-xylene experiments is sufficiently rapid to assume equilibrium conditions at all times during the smog chamber experiment. Figure 6 shows how the aerosol yield for the base case changes as hydrocarbon continues to react. The yield is dependent on the amount of organic mass present into which semi-volatile gases may be absorbed. When little hydrocarbon has reacted, and little semi-volatile product has been formed, the yield is negligible, but as more hydrocarbon reacts and organic aerosol forms, partitioning equilibrium shifts to the aerosol phase and yields increase.

It is important to distinguish between aerosol yield, Y, and stoichiometric coefficients, x_i. Stoichiometric coefficients are assumed constant and represent the total amount of semi-volatile product formed, in both gas and aerosol phases, per amount of

parent hydrocarbon reacted. The yield, on the other hand, which measures only the semi-volatile product that has partitioned into the aerosol phase, is not constant but will vary depending on the amount of organic mass available as an absorption medium. Stoichiometric coefficients by themselves are not sufficient to predict the amount of aerosol formation. Partitioning coefficients and organic aerosol mass are also required to determine the correct aerosol concentrations and yields.

Effect of Absorption Partitioning Coefficient

The effect of the values of the absorption partitioning coefficients, K_1 and K_2, on the equilibrium aerosol yield is presented in Figure 7. When both K_1 and K_2 are large (10^{-1} m^3 μg^{-1}), the yield curve is composed of two distinct regions. At higher organic mass concentrations, the yield is more or less constant, while at low organic mass the curve appears initially to increase linearly from zero. Large partitioning coefficients are indicative of relatively low volatility products with an equilibrium that favors the aerosol phase. As long as there is organic aerosol mass into which the semi-volatile product may be absorbed, virtually all of it will partition into the aerosol phase. The asymptotic aerosol yield seen at high organic mass values represents the maximum yield based on complete gas-to-particle conversion. At low organic mass concentrations, gas- and aerosol-phase concentrations are comparable and the aerosol yield depends directly on the amount of organic mass available as an absorption medium.

For intermediate volatility products ($K_1=K_2=10^{-2}$ m^3 μg^{-1}), the transition between the two regions is less sharp, and at high organic mass the yield is still increasing. In this case, equilibrium is shifted more to the gas phase relative to the large K case and at equal organic mass concentrations, less of the condensable product is found in the aerosol phase. At higher volatility ($K_1=K_2=10^{-3}$ m^3 μg^{-1}), nearly linear behavior is observed for the organic mass levels shown. Here the gas/particle equilibrium favors the gas phase and most of the condensable product remains as a vapor. When K_1 and K_2 differ ($K_1=10^{-1}$ $m^3\mu g^{-1}$, $K_2=10^{-3}$ $m^3\mu g^{-1}$), the resulting yield curve is simply an additive combination of the individual values, weighted by the stoichiometric coefficients for each species.

Given experimentally determined yield data, partitioning and stoichiometric coefficients for a parent hydrocarbon can be evaluated by fitting the theory to the data (Odum *et al.* 1996). The resulting parameters are, however, strictly valid only when the yield data represent equilibrium conditions. Time-dependent yields may not accurately predict these parameters when gas/aerosol transport is slow or when condensing species are secondary products. For this reason, coefficients should be estimated from yields determined at the conclusion of experimental runs when the parent hydrocarbon has finished reacting, conversion to secondary products is complete, and equilibrium between gas and aerosol phases has been attained. Coefficients determined in such a manner are extremely useful as a simplified approximation of a complex array of condensable organics most likely involved in partitioning, for which individual identification and parameter determination is not feasible.

Effect of Secondary Product Formation

When the semi-volatile organics are not first-generation products, S_1, but second-generation products resulting from OH-reaction of primary products, S_{1a} and S_{1b}, as in reaction (2*a*), the OH rate constant of the primary product, $k_{OH,S1}$, becomes a controlling factor in aerosol growth. Figure 8 shows how the equilibrium aerosol concentration of the secondary products S_{1a} and S_{1b} is affected by varying $k_{OH,S1}$. Gas/particle partitioning and stoichiometric coefficients for the semi-volatiles S_{1a} and S_{1b} are taken as the same as those used in the base case for the first-generation products S_1 and S_2. Compared to the case in which the semi-volatile products are first-generation, when the aerosol concentration results from second-generation products, a time delay of varying magnitude is exhibited, with a greater delay for smaller values of $k_{OH,S1}$. This delay is not a mass transport effect but reflects simply the slower rate at which the second-generation products are formed. Given a sufficiently fast secondary reaction, no difference would be observed in aerosol concentrations from either first- or second-generation semi-volatile products. At sufficiently long time the secondary concentrations approach the primary curve.

Effect of Accommodation Coefficient

The accommodation coefficient for semi-volatile products on the particle surface, α, is the principal transport parameter. Figure 9 demonstrates how aerosol growth is

affected by the value of the accommodation coefficient. As was noted earlier, when there is sufficient initial particle surface area, mass transport from the gas to aerosol phase is rapid and conditions approach equilibrium. For α values exceeding 0.1, equilibrium is essentially achieved instantaneously, but at lower values of α, mass transfer becomes the limiting factor in particle growth. For $\alpha = 0.01$ and 0.003, transport is initially slowed until particle growth leads to sufficient surface area that equilibrium is eventually reached. For the case of $\alpha = 0.001$, mass transfer is sufficiently slow that the vapor concentration of semi-volatile product S_1 reaches supersaturation and nucleation occurs. Upon nucleation a large number of small particles are formed that rapidly increase in surface area as they grow, actually allowing the system to reach equilibrium faster than in the α=0.003 case where nucleation did not occur. This is an unexpected consequence of the effect of the accommodation process.

Effect of Wall Adsorption Partitioning Coefficients

The relative importance of vapor partitioning to the chamber walls is controlled by the ratio between the adsorption partitioning coefficient for the wall, K^w, and K. Figure 10 shows the amount of organic matter that condenses on the chamber walls for various values of K^w/K. When partitioning to walls or particles is equally favorable, organic wall growth is predicted to be quite large, almost completely dominating over particle growth. At lower K^w/K ratios, however, wall growth concentrations increase initially, but soon reach a maximum after which all remaining partitioning is with the

aerosol phase. Storey *et al.* (1995) have shown that partitioning to organic particulate matter exceeds that to an inorganic quartz surface by several orders of magnitude. The Teflon surface of a smog chamber is similarly expected to be a poor adsorption medium such that vapor partitioning to the chamber walls will be negligible.

Effect of Initial Surface Area

As in the case of the accommodation coefficient, initial aerosol surface area, SA_{init}, has a significant effect on the rate of gas-particle partitioning. Figure 11 shows the predicted aerosol growth behavior for different initial aerosol surface areas. At high initial surface area, the system is at equilibrium at all times; for lower initial surface area, mass transport is slower, and if initial surface area is sufficiently small, semi-volatile product concentrations can accumulate to the point where nucleation will occur.

Effect of Surface Tension

Whereas the accommodation coefficient and initial surface area help determine when saturation levels can be reached, the surface tension of the semi-volatile product most directly controls the level of supersaturation at which nucleation will occur and the nature of the resulting nucleation burst. The lower the surface tension, the more facile is nucleation; at higher surface tension values nucleation slows considerably such that further increasing the surface tension has no observable effect. When nucleation does occur, gas/particle equilibrium may actually be reached more quickly because of the

immediate addition of particle surface area, but the effect is much less dramatic than that seen for changes in accommodation coefficient or initial surface area. High surface tensions may also inhibit aerosol growth for small particles, such as those formed by nucleation, due to the Kelvin effect. As particles grow, however, surface curvature becomes unimportant and surface tension has no influence on aerosol growth.

Effect of Molecular Weight and Density

The molecular weight, *MW*, and density, ρ, of the semi-volatile products have no significant effect on aerosol mass concentration. Molecular weight values ranging from 100 to 300 g mol^{-1} and density values between 1 and 3 g cm^{-3} produce almost identical aerosol mass curves. Aerosol volumes and vapor pressures inferred from partitioning coefficients will depend directly on ρ and *MW*, but since partitioning coefficients and aerosol concentrations are both expressed in mass units, model predictions are not sensitive to the exact values used for molecular weight and density.

SUMMARY

A comprehensive model is presented for the dynamic process of gas/particle partitioning of semi-volatile organics generated from the oxidation of atmospheric hydrocarbons. Partitioning of the organic products is governed by gas-particle

equilibrium and transport. Particle deposition, nucleation, and vapor transport to aerosol particles, chamber walls, and deposited particles are accounted for by the model, allowing the aerosol size distribution to be predicted both in the ambient atmosphere and in a laboratory smog chamber. When inorganic seed particles are present, gas-particle partitioning exhibits a threshold for aerosol growth. Until sufficient hydrocarbon reacts to create a concentration of condensable products that will exist in equilibrium with an organic aerosol phase, no aerosol is formed.

Characteristic times for the various transport processes involved in the formation of secondary organic aerosol have been examined. Gas-particle and gas-wall transport (in a smog chamber) are estimated to occur quite rapidly leading to equilibration within a few minutes. Particle wall deposition is a considerably slower process that occurs on a time scale of hours for typical smog chamber surface-to-volume ratios. Partitioning between the gas phase and particles deposited on the chamber walls is of negligible importance as transport times are on the order of several days.

A set of partitioning and transport parameters have been determined that fit observed aerosol yields in two simultaneous outdoor smog chamber experiments with *m*-xylene. Based on the time delay for the onset of aerosol growth and the observed yield curves, the condensing vapor species from *m*-xylene are predicted to be second- rather than first-generation products of the photooxidation. This conclusion is supported in part by some observed products of *m*-xylene oxidation.

An evaluation of the model's sensitivity to the various input parameters allows one to understand the nature of secondary organic aerosol formation and gas-particle partitioning in general. The smog chamber system is predicted to have been at gas/particle equilibrium because of the relatively high particle concentrations. The particle accommodation coefficient may also be estimated to have a value between 1.0 and 0.1. Significantly lower values would have resulted in more gradual aerosol growth, particularly initially, an effect not evident in the experimental data. Non-equilibrium conditions may arise when particle surface areas are not large enough to ensure rapid gas-particle transport (SA<1000 $\mu m^2 cm^{-3}$) or when the aerosol precursor is a fast-reacting hydrocarbon. Such conditions, however, are not typically expected to persist as particle growth or nucleation will increase surface area and accelerate the approach to equilibrium.

ACKNOWLEDGMENT

This work was supported, in part, by U.S. Environmental Protection Agency Center on Airborne Organics (R-819714-01-0), by National Science Foundation grant ATM-9307603, by the Coordinating Research Council (A-5-1), and by the Chevron Corporation. The authors would also like to thank Hali Forstner for insight regarding conditions necessary for nucleation.

REFERENCES

Carter W. P. L. (1988) Documentation for the SAPRC atmospheric photochemical mechanism preparation and emissions processing programs for implementation in airshed models. Final report for the California Air Resources Board, Sacramento, CA.

Carter W. P. L. (1990) A detailed mechanism for the gas-phase atmospheric reactions of organic compounds. *Atmos. Environ.* **24**, 481-518.

Crump J. G. and Seinfeld J. H. (1981) Turbulent deposition and gravitational sedimentation of an aerosol in a vessel of arbitrary shape. *J. Aeros. Sci.* **12**, 405-415.

Forstner H. J. L., Flagan, R. C. and Seinfeld, J. H. (1996) Secondary organic aerosol formation from the photooxidation of aromatic hydrocarbons: II. Molecular composition. *Env. Sci. Technol.* (submitted for publication).

Gelbard F. (1990) Modeling multicomponent aerosol particle growth by vapor condensation. *Aerosol Sci. Technol.* **12**, 399-412.

Grosjean D. (1977) *Aerosols*. Chapter 3, Ozone and other photochemical oxidants, NAS, Washington D.C., 45-125.

Grosjean D. and Seinfeld J. H. (1989) Parameterization of the formation potential of secondary organic aerosols. *Atmos. Environ.* **23**, 1733-1747.

Izumi K. and Fukuyama T. (1990) Photochemical aerosol formation from aromatic hydrocarbons in the presence of NO_x. *Atmos. Environ.* **24**, 1433-1441.

Kim Y. P. and Seinfeld J. H. (1990) Simulation of multicomponent aerosol condensation by the moving sectional method. *J. Colloid Interf. Sci.* **135**, 185-199.

McMurry P. H. and Rader D. J. (1985) Aerosol wall losses in electrically charged chambers. *Aerosol Sci. Technol.* **4**, 249-268.

Odum J. R., Hoffmann T., Bowman F., Collins D., Flagan R. C. and Seinfeld J. H. (1996) Gas/particle partitioning and secondary organic yields. *Env. Sci. Technol.* **30**, 2580-2585.

Oxtoby D. W. (1992) Homogeneous nucleation - theory and experiment. *J. Physics Condensed Matter* **38**, 7627-7650.

Pandian M. D. and Friedlander S. K. (1988) Particle deposition to smooth and rough walls of stirred chambers. *Physicochemical Hydrodynamics* **10**, 639-645.

Pandis S. N., Paulson S. E., Seinfeld J. H. and Flagan R. C. (1991) Aerosol formation in the photooxidation of isoprene and beta-pinene. *Atmos. Environ.* **25**, 997-1008.

Pandis S. N., Harley R. A., Cass G. R. and Seinfeld J. H. (1992) Secondary organic aerosol formation and transport. *Atmos. Environ.* **26**, 2269-2282.

Pandis S. N., Wexler A. S. and Seinfeld J. H. (1993) Secondary organic aerosol formation and transport - II. Predicting the ambient secondary organic aerosol size distribution. *Atmos. Environ.* **27**, 2403-2416.

Pankow J. F. (1994*a*) An absorption model of gas/particle partitioning of organic compounds in the atmosphere. *Atmos. Environ.* **28**, 185-188.

Pankow J. F. (1994*b*) An absorption model of gas/aerosol partitioning involved in the formation of secondary organic aerosol. *Atmos. Environ.* **28**, 189-193.

Pankow J. F. and Bidleman T. F. (1991) Effects of temperature, TSP and percent non-exchangeable material in determining the gas-particle partitioning of organic compounds. *Atmos. Environ.* **25**, 2241-2249.

Storey J. M. E., Luo W., Isabelle L. M. and Pankow J. F. (1995) Gas-solid partitioning of semi-volatile organic compounds to model atmospheric solid surfaces as a function of relative humidity 1. Clean quartz. *Environ. Sci. Technol.* **29**, 2420-2428.

Wang S. C., Paulson S. E., Grosjean D., Flagan R. C. and Seinfeld J. H. (1991*a*) Aerosol formation and growth in atmospheric organic/NO_x systems - I. Outdoor smog chamber studies of C_7- and C_8-hydrocarbons. *Atmos. Environ.* **26**, 403-420.

Wang S. C., Flagan R. C. and Seinfeld J. H. (1991*b*) Aerosol formation and growth in atmospheric organic/NO_x systems - II. Aerosol dynamics. *Atmos. Environ.* **26**, 421-434.

Wexler A. S. and Seinfeld J. H. (1990) The distribution of ammonium salts among a size and composition dispersed aerosol. *Atmos. Environ.* **24**, 1231-1246.

APPENDIX A. ADSORPTION PARTITIONING THRESHOLD

Adsorption, as opposed to absorption, is the expected partitioning process for inorganic particles with no absorbing organic material and for smog chamber walls. Adsorption partitioning is dependent on the surface coverage of organic on the particle or wall. A dimensionless surface coverage, θ, can be defined as

$$\theta = \frac{\sum_i A_i}{\gamma} \tag{A1}$$

where γ ($\mu g\ m^{-3}$) is the mass concentration of an organic monolayer on the particle surface. When there is much less than a monolayer coverage of organic, i.e., $\theta << 1$, the partitioning coefficient is given by

$$K_i = \frac{A_i}{G_i\ \gamma} \qquad \text{for } \theta << 1 \tag{A2}$$

If there is much more than a monolayer coverage, $\theta >> 1$, the partitioning coefficient takes the same form as that for absorption,

$$K_i = \frac{A_i}{G_i \sum_k A_k} \qquad \text{for } \theta >> 1 \tag{A3}$$

At near a monolayer coverage, $\theta \approx 1$, the partitioning coefficient definition will be described by the specific adsorption isotherm involved. For simplicity the two limiting case definitions, (A2) and (A3), can be applied to intermediate coverages with an intersection occurring at $\theta = 1$,

$$K_i = \begin{cases} \dfrac{A_i}{G_i \sum_k A_k}\theta & \text{for } \theta < 1 \\ \dfrac{A_i}{G_i \sum_k A_k} & \text{for } \theta > 1 \end{cases} \qquad \text{(A4)}$$

This definition assumes that a complete monolayer is formed before any additional layers are initiated. While simplistic, such a definition is adequate to develop a threshold theory for adsorption partitioning.

For a single semi-volatile product, the mass balance relationship will be

$$x_1 \, \Delta HC = A_1^{tot} + G_1 \qquad \text{(A5)}$$

where A_1^{tot} ($\mu g \, m^{-3}$) represents the total aerosol-phase mass concentration for all particle sizes. Equation (A4) can be combined with (A5) to yield an expression for the total aerosol concentration,

$$A_1^{tot} = \begin{cases} x_1 \dfrac{K_1 \gamma^{tot}}{1 + K_1 \gamma^{tot}} \Delta HC & \text{for } \theta < 1 \\ x_1 \Delta HC - \dfrac{1}{K_1} & \text{for } \theta > 1 \end{cases} \qquad \text{(A6)}$$

where γ^{tot} ($\mu g\ m^{-3}$) represents the total organic mass required to form a monolayer on all particles in the entire aerosol population. For a single component system aerosol concentration is linearly related to ΔHC for all values of θ, but the slope, or rate of aerosol formation, changes at $\theta=1$. When $\theta>1$, the slope is equal to x_1, but for $\theta<1$ the slope will be less then x_1. A monolayer surface coverage, therefore, represents the threshold for aerosol formation, as aerosol formation accelerates when $\theta>1$. Solving (A6) for ΔHC when $A_1^{tot}=\gamma^{tot}$ gives the threshold concentration based on adsorption, ΔHC^{**},

$$\Delta HC^{**} = \frac{1 + K_1 \gamma^{tot}}{x_1 K_1} \qquad \text{(A7)}$$

which will be somewhat larger than the absorption threshold, ΔHC^{*},

$$\Delta HC^{*} = \frac{1}{x_1 K_1} \qquad \text{(A8)}$$

depending on the value of $K_1\gamma^{tot}$. Semi-volatile compounds have values of K that range from 10^2 to 10^{-3} ($m^3\mu g^{-1}$) (Pankow and Bidleman, 1991). For a typical urban aerosol with

surface area of 10^2 $\mu m^2 cm^{-3}$, the total mass of a monolayer, γ^{tot}, will be of order 10^{-1} μg m^{-3}. In many instances, therefore, $K\gamma^{tot} << 1$ and $\Delta HC^{**} \approx \Delta HC^{*}$. When $K\gamma^{tot} << 1$ the rate of aerosol formation will be very near zero for $\theta < 1$. At larger values of $K\gamma^{tot}$, the aerosol formation rate will be much higher and the relative values of the two thresholds will differ. However, if K is large and γ^{tot} is small, the total amount of aerosol formation before reaching the threshold will be small and the absolute values of both ΔHC^{*} and ΔHC^{**} will be near zero. Thus, only when γ^{tot} is large do absorption and adsorption theory predict significantly different threshold behavior.

APPENDIX B. SMOG CHAMBER TRANSPORT EQUATIONS

Particle-Wall Transport

Particle deposition to the wall of a smog chamber is the net result of turbulent and Brownian diffusion and gravitational sedimentation, and is a function of particle size. Particle wall losses can be described as a first-order process with a particle loss coefficient, $\beta_p(D_p)$ (s^{-1}),

$$\frac{dN(D_p)}{dt} = -\beta_p(D_p)\,N(D_p) \qquad \text{(B1)}$$

where $N(D_p)$ (m^{-3}) is the number concentration of particles (assumed to be well mixed in the chamber) with diameter D_p, and $\beta_P(D_p)$ is the loss coefficient for particles with diameter D_p. β_P can be determined theoretically (Crump and Seinfeld, 1981; McMurry and Rader, 1985) or directly from experimental measurements. The particle loss coefficient, β_P, is directly related to the particle-wall mass transfer coefficient, k_{mP} (m s^{-1}),

$$\beta_P = \frac{A_c}{V_c} k_{mP} \qquad \text{(B2)}$$

where A_c (m^2) is the chamber wall surface area and V_c (m^3) is the chamber volume. It is assumed that once a particle encounters the wall it sticks with unit probability.

Vapor-Wall Transport

Transport of organic vapor to the wall of a chamber can be represented in a manner similar to that of particles,

$$\frac{dG_i}{dt} = -\beta_G \left(G_i - G_i^{eq}\right) \quad \text{(B3)}$$

$$\beta_G = \alpha_w \frac{A_c}{V_c} k_{mG} \quad \text{(B4)}$$

where β_G (s^{-1}) is the vapor loss coefficient, α_w is the wall accommodation coefficient, and k_{mG} ($m\ s^{-1}$) is the gas-wall mass transfer coefficient. The wall surface equilibrium concentration, G_i^{eq}, is as defined in (A3) and will depend on the partitioning coefficient for organic adsorption to the chamber wall, K_i^w ($m^3\ \mu g^{-1}$), which generally will be different from the absorption partitioning coefficient, K_i ($m^3\ \mu g^{-1}$).

Within a chamber, the mass transfer coefficient, k_m ($m\ s^{-1}$), can be related to the molecular diffusivity, D ($m^2\ s^{-1}$), according to the mass transfer correlation (Pandian and Friedlander, 1988),

$$Sh = 0.63\ Re^{2/3}\ Sc^{1/3} \quad \text{(B5)}$$

where $Sh = k_m l/D$ is the Sherwood number, l (m) is a characteristic length of the chamber, Re is the Reynolds number describing the degree of mixing in the chamber, $Sc = \nu/D$ is the Schmidt number, and ν ($m^2\ s^{-1}$) is the kinematic viscosity of air. Equation (B5) was developed from experimental data for particle losses (D_p<0.1μm) within a turbulently

mixed, smooth-walled, cylindrical container and should apply to diffusion of gases as well as small particles. Using (B5), the gas and particle mass transfer coefficients, k_{mG} and k_{mP}, can be related to their molecular and Brownian diffusivities, D_G and D_P, as follows:

$$\frac{k_{mG}}{k_{mP}} = \left(\frac{D_G}{D_P}\right)^{2/3} \tag{B6}$$

Thus, by measuring the particle-wall mass transfer coefficient, k_{mP}, at small particle sizes where losses are diffusional, the gas-wall mass transfer coefficient, k_{mG}, for the same chamber can be determined from (B6).

Vapor Transport to Deposited Particles

Transport between the gas-phase and particles that have been deposited on the chamber walls follows (B3), but the surface equilibrium concentration used is that for particles, and the vapor loss coefficient is dependent on the surface area of deposited particles, A_p (m^2),

$$\beta_G = \alpha \frac{A_p}{V_c} k_{mG} \tag{B7}$$

Nucleation

When vapor transport rates are slow, gas-phase concentrations will increase as semi-volatile compounds build up in the gas phase. If the gas-phase concentration exceeds the saturation vapor pressure, gas to aerosol conversion can occur directly through nucleation. Classical nucleation theory (Oxtoby, 1992) predicts a nucleation rate, J_{nucl} ($cm^{-3}s^{-1}$),

$$J^{nucl} = \left(\frac{2\,\sigma\,N_A}{\pi\,MW}\right)^{1/2} \frac{N_A\,MW\left(p^0\right)^2\,S}{\rho\,(RT)^2} \exp\left(-\frac{16x10^{-21}\pi\,N_A}{3}\left(\frac{MW}{\rho}\right)^2\left(\frac{\sigma}{RT}\right)^3\left(\frac{1}{\ln S}\right)^2\right) \tag{B8}$$

where σ (dyne cm^{-1}) is surface tension, N_A (=$6.02x10^{23}$ $mole^{-1}$) is Avogadro's number, MW (g $mole^{-1}$) is molecular weight, p^0 (torr) is the equilibrium vapor pressure, S is the saturation ratio, ρ (g cm^{-3}) is liquid density, R (=8.314 J $mole^{-1}$ K^{-1} = $6.2x10^4$ torr cm^3 $mole^{-1}$ K^{-1}) is the ideal gas constant, and T (K) is temperature. The factor 10^{-21} accomplishes the appropriate unit conversions. The critical cluster size for nucleation, g^*, is given by

$$g^* = \frac{32x10^{-21}\,\pi\,N_A}{3}\left(\frac{MW}{\rho}\right)^2\left(\frac{\sigma}{RT\ln S}\right)^3 \tag{B9}$$

Table 1. Characteristic times of gas-particle interactions.

	Characteristic Time	Typical Value [a]
Formation of condensable organic gas	$\tau_F = \frac{1}{k_{OH}[OH]}$	2 h
Gas-particle transport	$\tau_{GP} = \frac{1+8\lambda/\alpha D_p}{2\pi N D_p \lambda \bar{c}}$	1 min
Gas-wall transport	$\tau_{GW} = \frac{1}{\alpha_w (A_c/V_c) k_{mG}}$	30 s
Particle-wall transport	$\tau_{PW} = \frac{1}{(A_c/V_c) k_{mP}}$	5 h
Gas-deposited particle transport	$\tau_{GD} = \frac{1}{\alpha (A_p/V_c) k_{mG}}$	3 days

[a] $k_{OH}=2\times10^{-11}$ cm^{3}molecule^{-1}s^{-1}

$[OH]=7\times10^6$ molecule cm^{-3}

$N=5\times10^4$ cm^{-3}

$D_p=100$ nm

$\alpha=1.0$

$\alpha_w=1.0$

$(A_c/V_c)=1.0$ m^{-1}

$k_{mG}=1.0$ m min^{-1}

$k_{mP}=1.5\times10^{-3}$ m min^{-1}

$(A_p/V_c)=2.6\times10^{-4}$ m^{-1}

Table 2. Initial conditions for *m*-xylene smog chamber experiments carried out in Los Angeles, CA, on August 4, 1995.[a]

	Side A	Side B
m-xylene	1008 ppb	510 ppb
propene	200 ppb	200 ppb
NO	957 ppb	450 ppb
NO2	686 ppb	370 ppb
N_0	9.7×10^3 cm^{-3}	8.3×10^3 cm^{-3}
$\overline{D}_p$	0.1 μm	0.1 μm

[a]Start time 9:00 am (PDT)

Temperature 40±5 ^{0}C

Table 3. Partitioning and transport parameters for *m*-xylene smog chamber simulations.

x_1	0.03 [a]
x_2	0.14 [a]
K_1	0.06 $m^3\mu g^{-1}$ [a]
K_2	0.002 $m^3\mu g^{-1}$ [a]
K^w/K	10^{-4} [b]
MW	150 [c]
ρ	1.5 g cm^{-3} [c]
σ	25 dyne cm^{-1} [c]
α	0.2 [b]
α_w	0.2 [b]
k_{mG}	1.0 m min^{-1} [d]

[a]Based on estimates for m-xylene (Odum *et al.*, 1996)

[b]Adjusted to fit experimental results

[c]Assumed values for organic aerosol

[d]Based on correlation with particle deposition rates

LIST OF FIGURES

Figure 8. Predicted secondary product formation rate as compared with equilibrium aerosol concentration for various values of $k_{OH,S1}$ ($cm^3 molecule^{-1} s^{-1}$).

Figure 9. Predicted aerosol concentrations as a function of accommodation coefficient of semi-volatile product on particle surface, α.

Figure 10. Predicted effect of the wall adsorption partitioning coefficient to absorption partitioning coefficient ratio, K^w/K, on organic wall condensate ($\mu g\ m^{-3}$).

Figure 11. Simulated organic aerosol concentrations for different initial particle surface areas, SA_{init} ($\mu m^2 cm^{-3}$).

Figure 1.

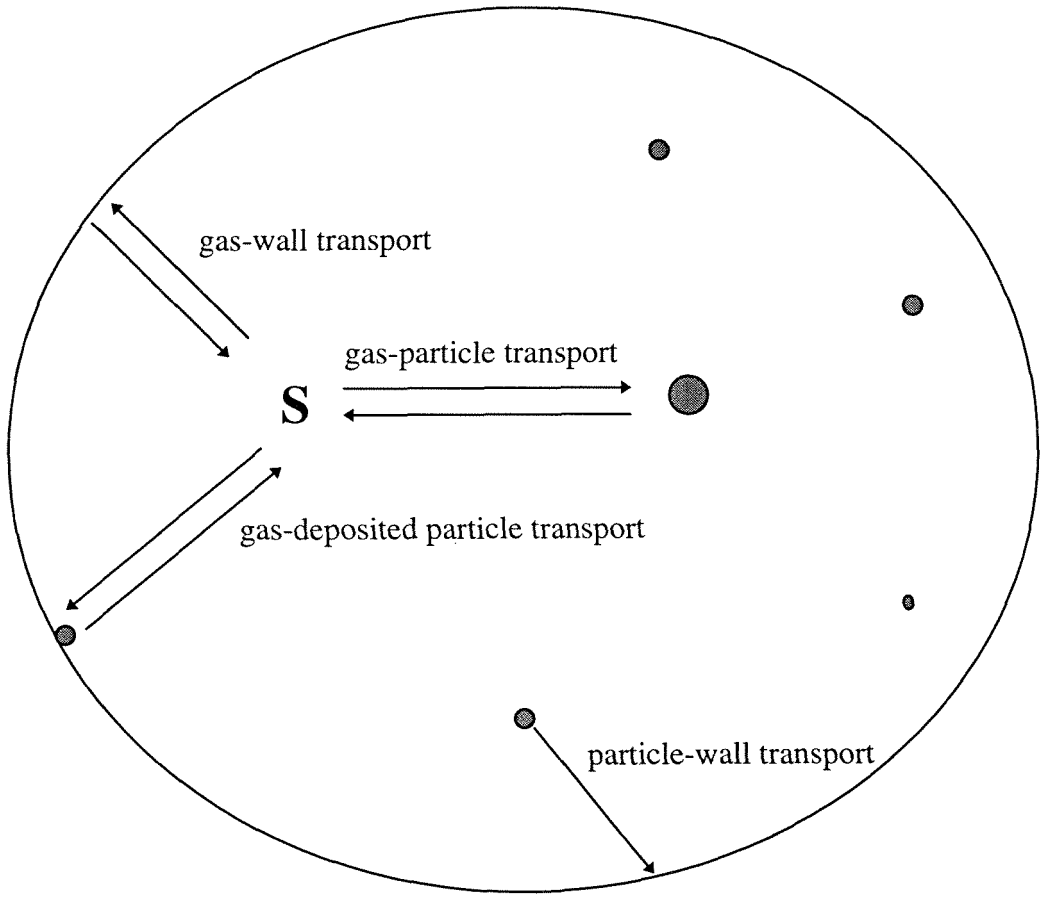
gas-wall transport
gas-particle transport
S
gas-deposited particle transport
particle-wall transport

Figure 2.

(a)

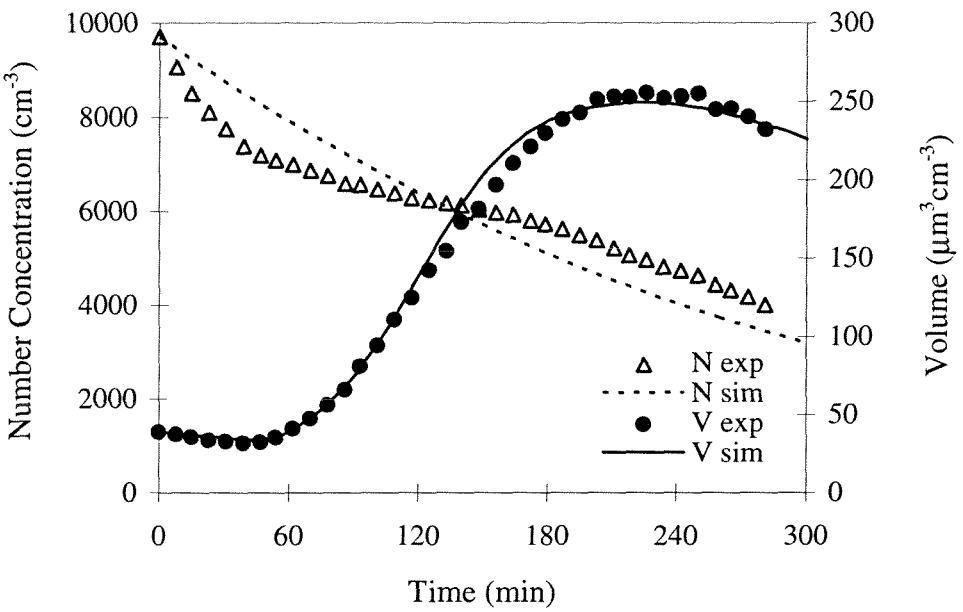
Number Concentration (cm^{-3})
Volume (μm^{3}cm^{-3})
Time (min)
N exp
N sim
V exp
V sim
10000
8000
6000
4000
2000
0
300
250
200
150
100
50
0
0
60
120
180
240
300

(b)

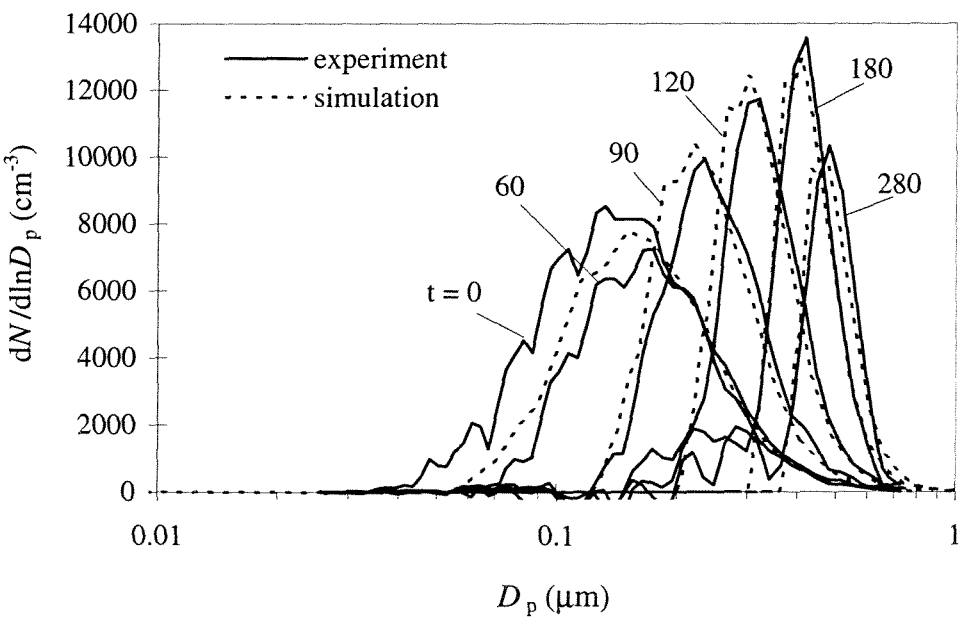
experiment
simulation
t = 0
60
90
120
180
280
dN/dlnD$_p$ (cm^{-3})
D$_p$ (μm)
14000
12000
10000
8000
6000
4000
2000
0
0.01
0.1
1

Figure 3.

(a)

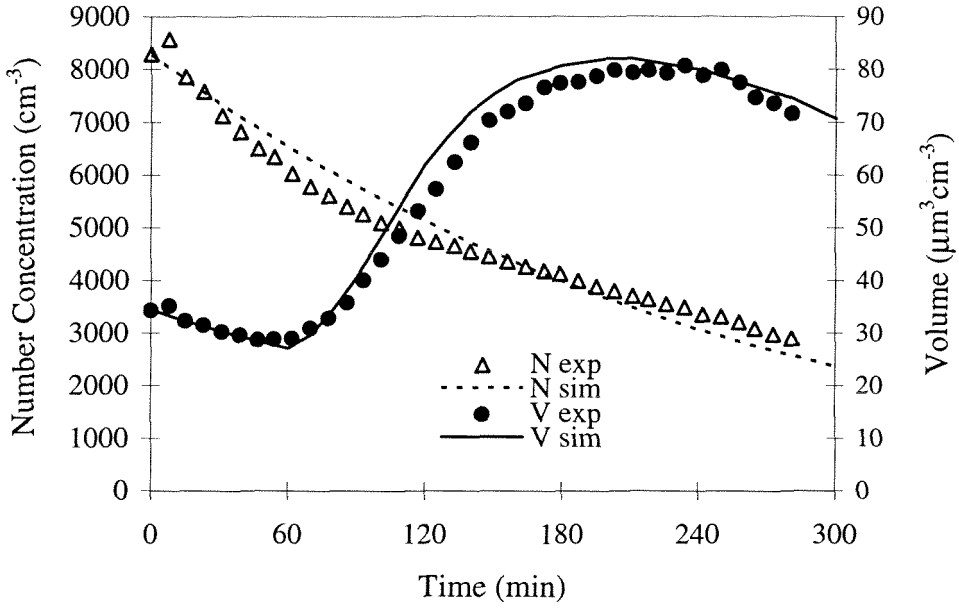
Number Concentration (cm-3)
Volume (μm3cm-3)
Time (min)
N exp
N sim
V exp
V sim
0
1000
2000
3000
4000
5000
6000
7000
8000
9000
0
10
20
30
40
50
60
70
80
90
0
60
120
180
240
300

(b)

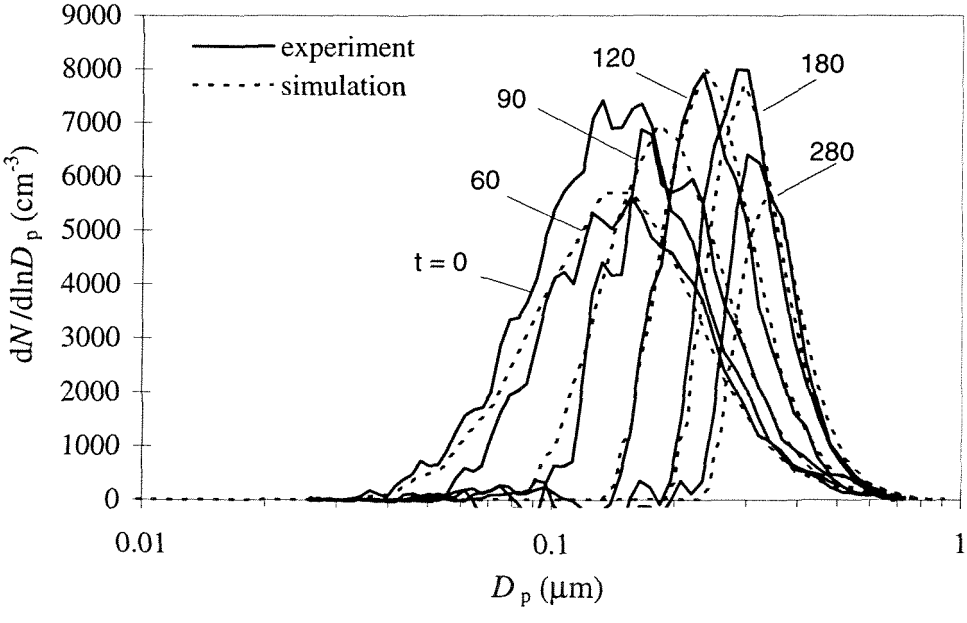
experiment
simulation
t = 0
60
90
120
180
280
dN/dlnDp (cm-3)
Dp (μm)
0
1000
2000
3000
4000
5000
6000
7000
8000
9000
0.01
0.1
1

Figure 4.

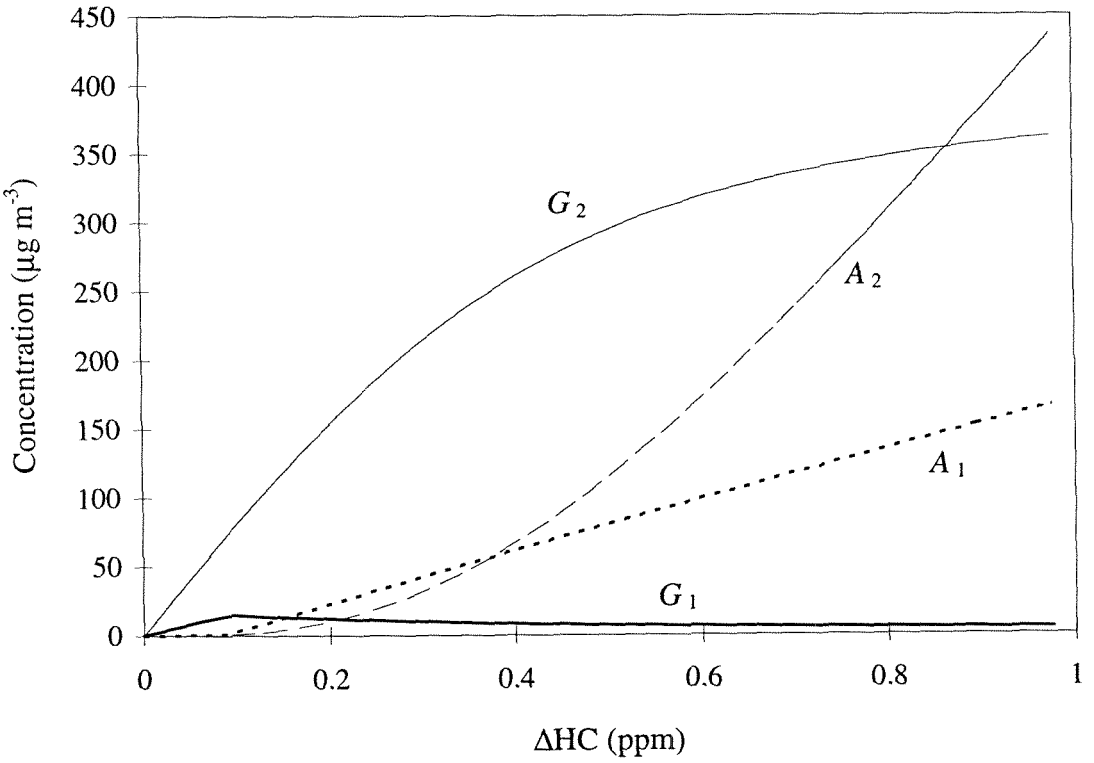
450
400
350
300
250
200
150
100
50
0
Concentration (µg m-3)
0
0.2
0.4
0.6
0.8
1
ΔHC (ppm)
G2
A2
A1
G1

Figure 5.

(a)

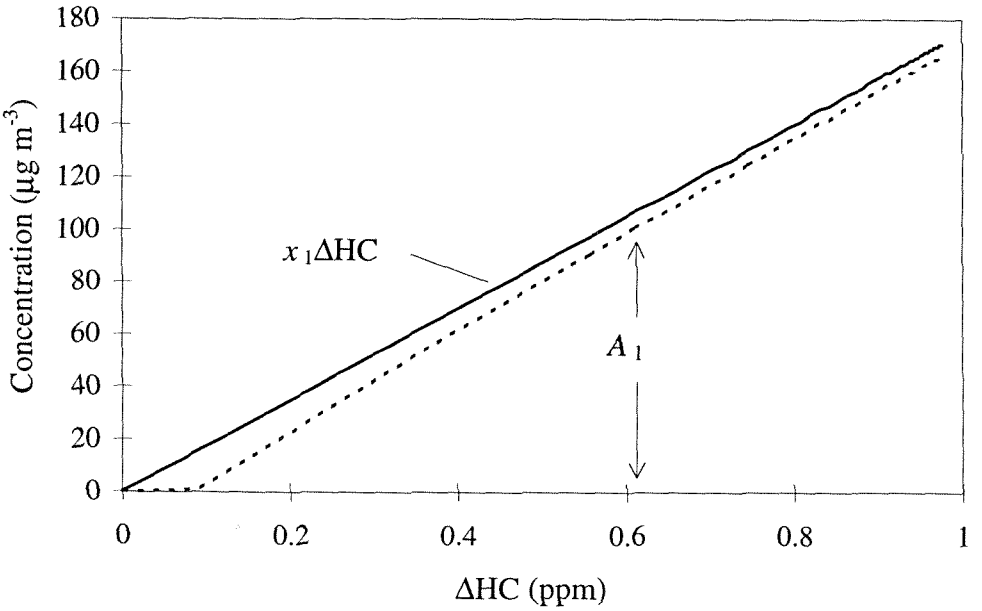
180
160
140
120
100
80
60
40
20
0
Concentration (μg m-3)
x 1ΔHC
A 1
0
0.2
0.4
0.6
0.8
1
ΔHC (ppm)

(b)

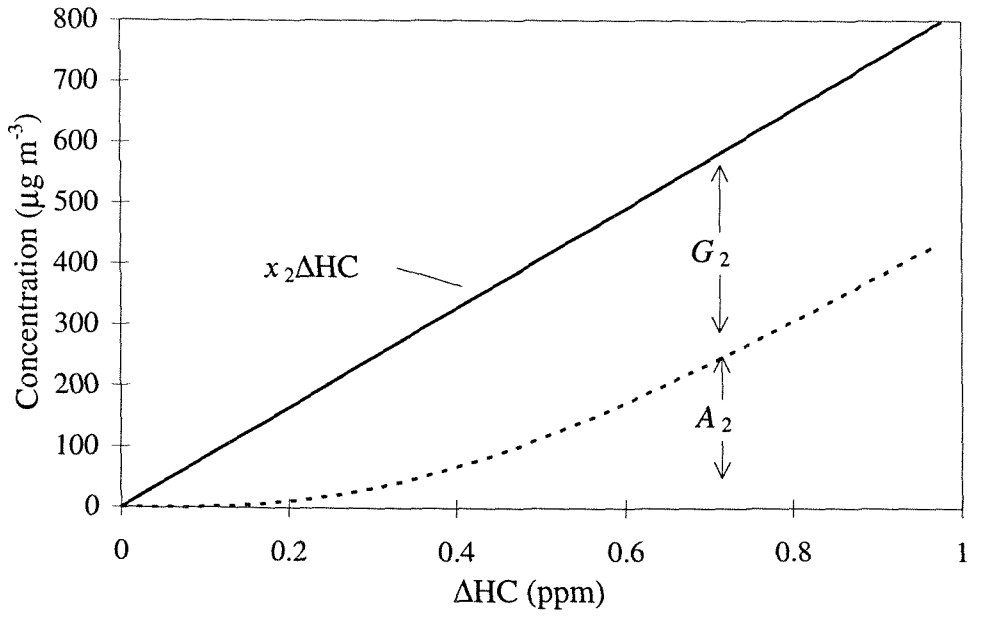
800
700
600
500
400
300
200
100
0
Concentration (μg m-3)
x 2ΔHC
G 2
A 2
0
0.2
0.4
0.6
0.8
1
ΔHC (ppm)

Figure 6.

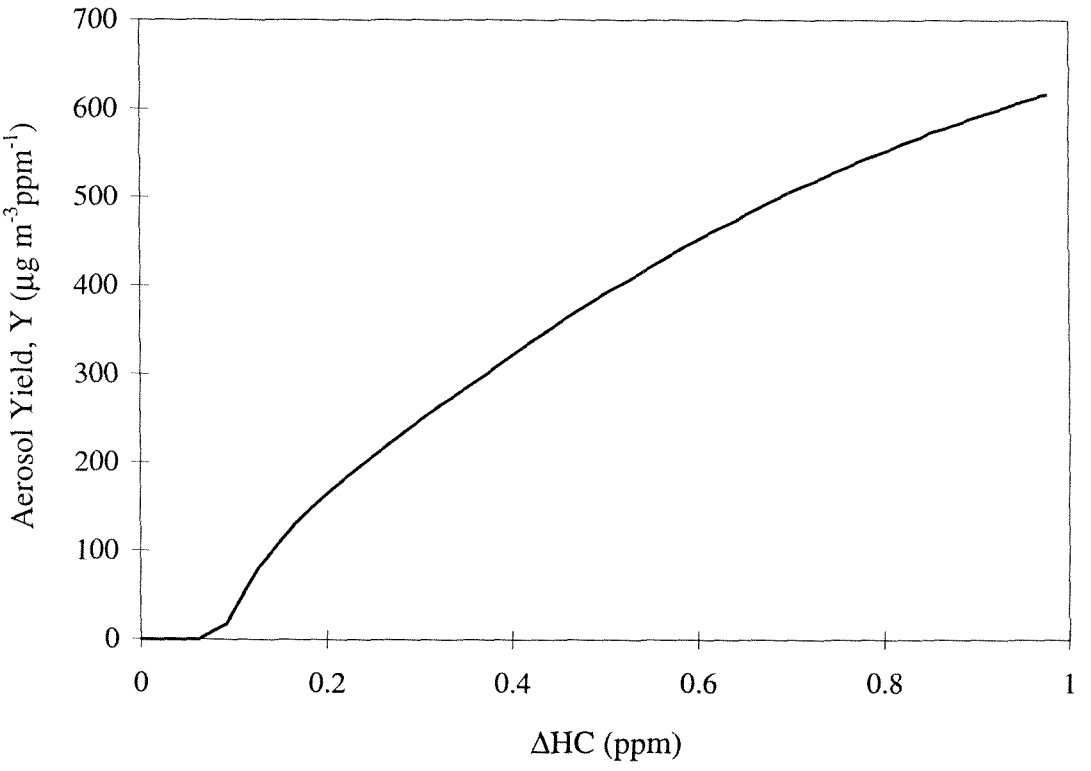
700
600
500
400
300
200
100
0
0
0.2
0.4
0.6
0.8
1
Aerosol Yield, Y (µg m-3ppm-1)
ΔHC (ppm)

Figure 7.

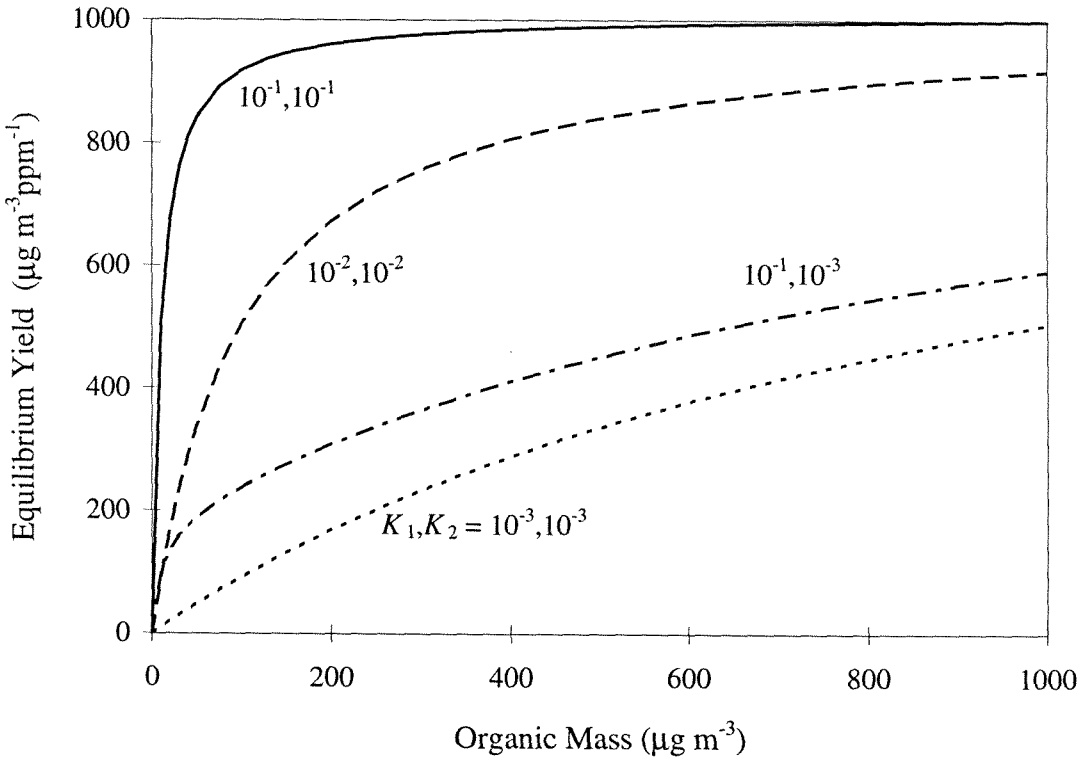
1000
800
600
400
200
0
0
200
400
600
800
1000
Equilibrium Yield (µg m-3ppm-1)
Organic Mass (µg m-3)
10-1,10-1
10-2,10-2
10-1,10-3
K1,K2 = 10-3,10-3

Figure 8.

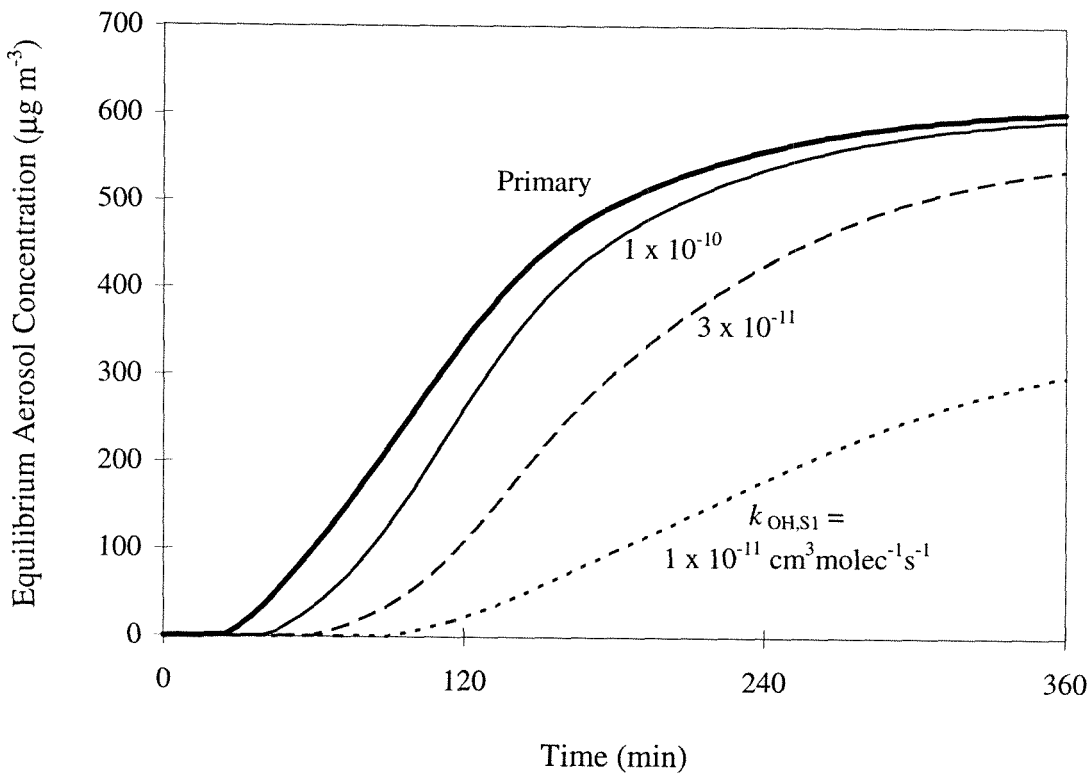
Equilibrium Aerosol Concentration (μg m-3)
700
600
500
400
300
200
100
0
0
120
240
360
Time (min)
Primary
1 x 10-10
3 x 10-11
kOH,S1 =
1 x 10-11 cm3molec-1s-1

Figure 9.

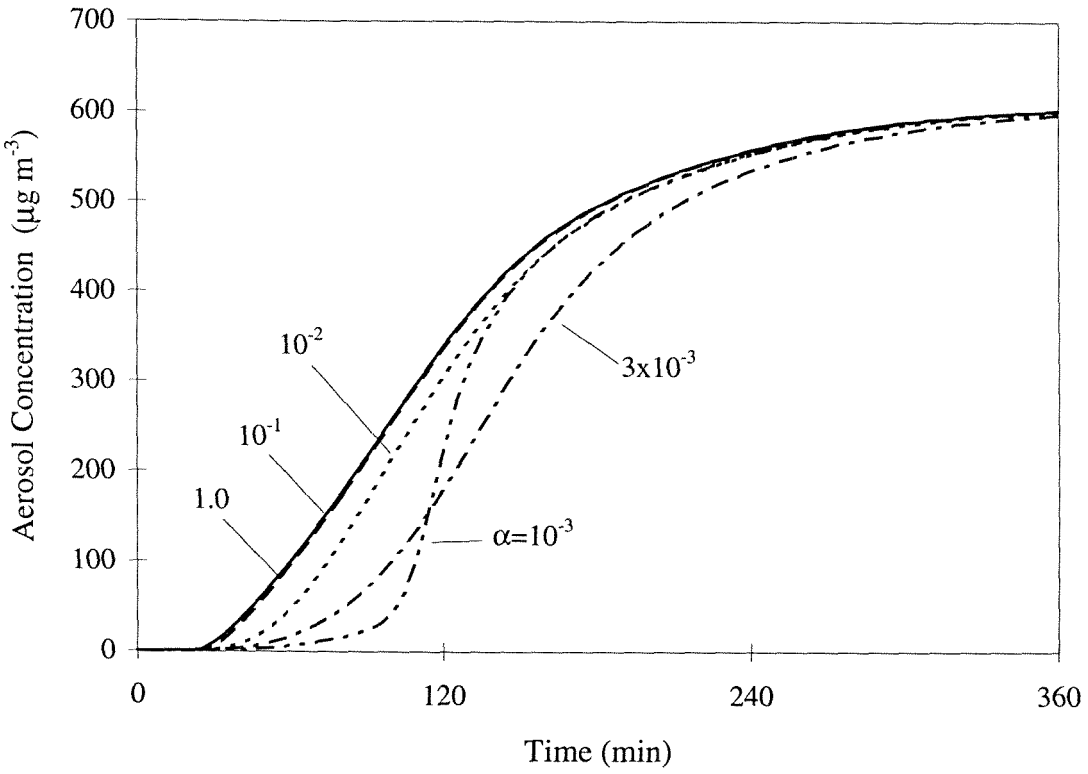
700
600
500
400
300
200
100
0
Aerosol Concentration (μg m-3)
0
120
240
360
Time (min)
1.0
10-1
10-2
α=10-3
3x10-3

Figure 10.

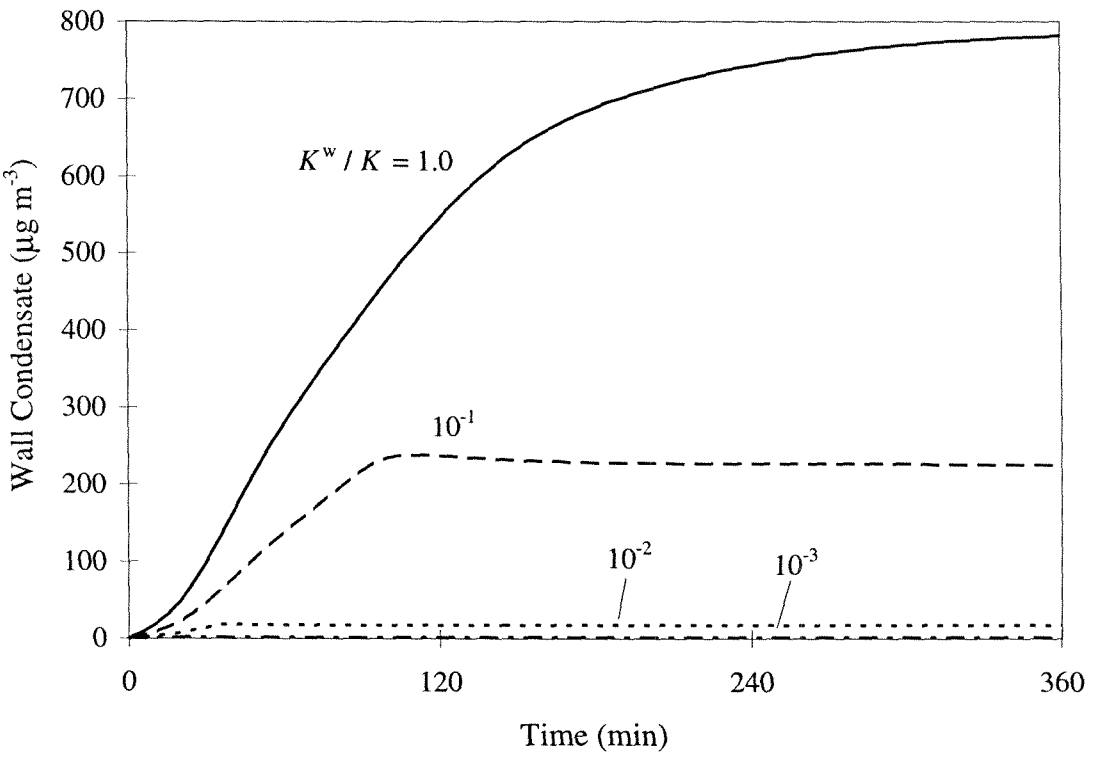
800
700
600
500
400
300
200
100
0
Wall Condensate (µg m-3)
Kw / K = 1.0
10-1
10-2
10-3
0
120
240
360
Time (min)

Figure 11.

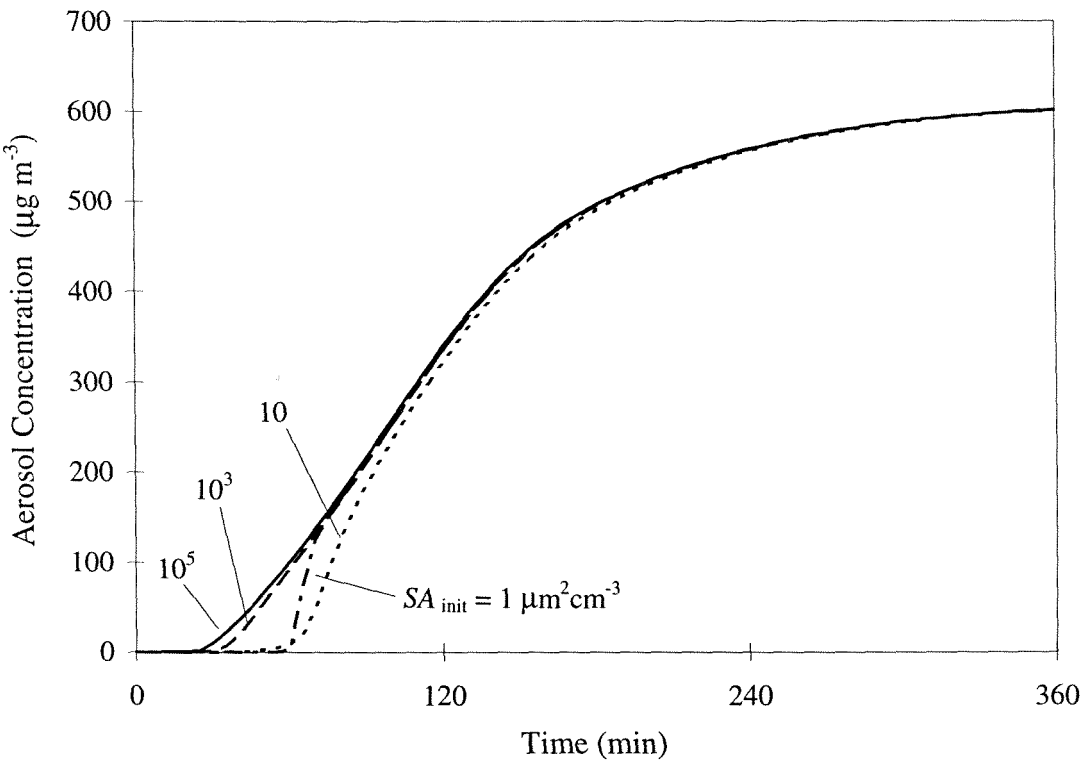
700
600
500
400
300
200
100
0
Aerosol Concentration (μg m-3)
0
120
240
360
Time (min)
10
10^3
10^5
SA init = 1 μm2cm-3

CONCLUSIONS

The underlying principle of this research has been that by understanding the characteristics of individual components in an organic mixture, the resulting behavior of the overall mixture may be better understood. The assignment method was developed to investigate the reaction pathways of complex VOC/NO_x chemical mechanisms. By following the reaction pathways of a mechanism and tracing the ozone formed back to the original organic precursors, the assignment method provides a window on the inner workings of the mechanism and helps explain how and why ozone is formed. The reactivity measure associated with the assignment method is termed productivity and describes the relative amount of ozone produced by an individual organic species.

In modeling studies using the SAPRC chemical mechanism with conditions representative of summertime Los Angeles, it was demonstrated that a wide variety of organic species contribute to ozone formation in the urban atmosphere. In general, the most productive organics were determined to be aldehydes, alkenes and higher aromatics. The abundance in the atmosphere of species such as CO and the alkanes results in large contributions to ozone from these relatively unproductive species. The same species that are most productive with respect to ozone formation were also shown to be effective precursors of PAN, HNO_3 and secondary organic aerosol.

There appear to be four major factors that help determine how much of a contribution a given organic species will make to the total amount of ozone (or other

secondary product) formed. First, is the abundance of an organic in the atmosphere. Though considered unreactive, CO is typically present in such high concentrations that it is a significant contributor to ozone formation. Other organics may be emitted at such small concentrations that on an individual basis they have essentially no influence on total ozone levels. Second, is the rate at which an organic reacts. At equal concentrations, the fast-reacting aldehydes will have a much greater effect on ozone than the slower reacting alkanes. Third, is the efficiency with which an organic molecule produces ozone upon reacting. Some organics will form unreactive products or very few ozone-producing peroxy radicals as they react, while others may create multiple radicals that lead to ozone as they degrade in the atmosphere. Fourth, is the influence an individual organic has on the remainder of the VOC/NO_x reaction mixture. Through changes to the radical pool, an organic may alter both the rate at which other species react and the efficiency with which they produce ozone. The incremental reactivity of a specific organic compound is influenced by each of these factors, particularly the effect on other species in the organic mixture.

In studying eight fuel oxygenates it was determined that these compounds have relatively low incremental reactivities with values similar to those of the alkanes. This low reactivity is due both to their slow reaction rates and to the formation of relatively unreactive formate and acetate compounds as products. The more reactive of the fuel oxygenates were found to be those containing ethyl groups which react faster than their counterparts containing only methyl and *tert*-butyl groups.

As with ozone formation, the generation of secondary organic aerosol is the result of interactions between organic precursors. A model was developed to simulate the dynamic process of gas/particle partitioning of semi-volatile organic products. This partitioning was shown to depend on both equilibrium and transport considerations. Gas-particle equilibrium is a function of the volatility of individual products as well as the total absorbing organic mass present. When no organic mass is initially present, a threshold for aerosol growth will exist that prevents an aerosol phase from forming until sufficient hydrocarbon has reacted to create equilibrium gas-phase concentrations. Gas-particle transport times are estimated to be quite short indicating rapid equilibration under typical atmospheric conditions. Non-equilibrium conditions may arise, however, when particle surface areas are small or when aerosol precursors are fast-reacting hydrocarbons. The ability to fit smog chamber data for the photooxidation of *m*-xylene supports the absorption partitioning theory used by the model.

Much remains to be understood regarding the impact of hydrocarbon precursors on ozone and secondary organic aerosol formation. The number of distinct hydrocarbon species that react in the atmosphere to form ozone and that exist together as secondary organic aerosol is tremendous. Characterization of the chemical and physical properties of each individual species is, therefore, impractical. Even when an organic species is well understood, a universal measure of its ozone- or aerosol-generating capability is unavailable. The formation of these pollutants will vary with organic mixture composition, VOC/NO_x ratio, temperature, emissions patterns and a whole host of other

variables. It is hoped that the research presented here will serve to increase our understanding of and provide a basis for further investigation of ozone and secondary organic aerosol formation.

APPENDIX A:

GAS/PARTICLE PARTITIONING AND SECONDARY ORGANIC AEROSOL YIELDS

Published in *Environ. Sci. Technol.*, **30**, 2580-2585 (1996)

Gas/Particle Partitioning and Secondary Organic Aerosol Yields

JAY R. ODUM,[†]
THORSTEN HOFFMANN,[‡]
FRANK BOWMAN,[§] DON COLLINS,[†]
RICHARD C. FLAGAN,[§] AND
JOHN H. SEINFELD*,[§]

Department of Environmental Engineering Science and Department of Chemical Engineering, California Institute of Technology, Pasadena, California 91125

Secondary organic aerosol (SOA) formation is considered in the framework of the gas/particle partitioning absorption model outlined by Pankow (*1*, *2*). Expressions for the fractional SOA yield (Y) are developed within this framework and shown to be a function of the organic aerosol mass concentration, M_o. These expressions are applied to over 30 individual reactive organic gas (ROG) photooxidation smog chamber experiments. Analysis of the data from these experiments clearly shows that Y is a strong function of M_o and that secondary organic aerosol formation is best described by a gas/particle partitioning absorption model. In addition to the 30 individual ROG experiments, three experiments were performed with ROG mixtures. The expressions developed for Y in terms of M_o, used in conjunction with the overall yield data from the individual ROG experiments, are able to account for the M_o generated in the ROG mixture experiments. This observation not only suggests that SOA yields for individual ROGs are additive but that smog chamber SOA yield data may be confidently extrapolated to the atmosphere in order to determine the important ambient sources of SOA in the environment.

Introduction

It is now well recognized that secondary organic matter can significantly contribute to the particulate burden in urban atmospheres. However, because of the enormous complexity of the chemical matrix of organic aerosol and the lack of direct chemical analysis methods for a majority of the compounds comprising the organic aerosol fraction, estimates of secondary organic aerosol (SOA) contributions in the urban environment have been restricted to indirect methods of determination. For example, Turpin and Huntzicker used correlations between measured organic carbon (OC) and elemental carbon (EC) to estimate SOA contributions in Los Angeles during the summer Southern California Air Quality Study (SCAQS) in 1987 (*3*). The study showed that as much as 70% of the organic aerosol can be of secondary origin under peak photochemical conditions. Other estimates, based on chemical mass balance methods, suggest that on a yearly average, 20–30% of the fine organic particulate matter in the South Coast Air Basin may be secondary (*4*).

Efforts to represent SOA formation in ambient models have primarily been based on using experimentally determined fractional aerosol yields (*5–7*). The fractional aerosol yield (Y), defined as the fraction of a reactive organic gas (ROG) that is converted to aerosol, is calculated by

$$Y = \frac{\Delta M_o}{\Delta \mathrm{ROG}} \tag{1}$$

where ΔM_o is the organic aerosol mass concentration ($\mu g\ m^{-3}$) produced for a given amount of ROG reacted, ΔROG ($\mu g\ m^{-3}$). Aerosol yields have been estimated from smog chamber data for a variety of ROGs by various researchers over the last 20 years (*8–15*). In general, measured yields for a single compound have shown a wide degree of variation both between and within laboratories. For example, observed SOA yields for α-pinene range from less than 10% to greater than 50% (*5*, *16*). Several factors likely contribute to this dramatic variability, but the major factor may be the way that SOA formation has been represented.

Secondary aerosols are formed by reaction of an ROG to produce both semivolatile and nonvolatile products. Previously, it has been assumed that the vapor-phase products begin to condense onto existing seed particles (or to homogeneously nucleate) only after a product exceeds its saturation concentration and that the amount of a product that condenses is the quantity in excess of its saturation concentration. For the initial condensation process and certainly for the initial nucleation process, this may be the case. However, Pankow has suggested that, once organics have begun to condense and an organic layer has formed on the particles, even products whose gas-phase concentrations are below their saturation concentrations will partition a portion of their mass into this condensed organic phase (*2*). For each compound that partitions into the absorbing organic material (om) phase, Pankow has defined an absorption equilibrium constant ($K_{p,i}$) as

$$K_{p,i} = \frac{F_{i,\mathrm{om}}}{A_i \mathrm{TSP}} = \frac{760 RT f_{\mathrm{om}}}{\mathrm{MW}_{\mathrm{om}} 10^6 \zeta_i p_{L,i}^{\circ}} \tag{2}$$

where A_i is the gas phase concentration (ng m^{-3}) of compound i, $F_{i,\mathrm{om}}$ is the concentration of compound i (ng m^{-3}) in the absorbing om phase, TSP is the total suspended particulate concentration ($\mu g\ m^{-3}$), R is the ideal gas constant (8.206×10^{-5} m^3 atm mol^{-1} K^{-1}), T is temperature (K), f_{om} is the mass fraction of the TSP that is the absorbing om phase, $\mathrm{MW}_{\mathrm{om}}$ is the mean molecular weight of the absorbing om (g mol^{-1}), ζ_i is the activity coefficient of compound i in the om phase, and $p_{L,i}^{\circ}$ is the vapor pressure

* To whom correspondence should be addressed; e-mail address: april@macpost.caltech.edu.
† Department of Environmental Engineering Science.
‡ Present address: Institute fur Spektrochemie und Angewandte Spektroscopie D-44139, Dortmund, Germany.
§ Department of Chemical Engineering.

S0013-936X(95)00943-6 CCC: $12.00

(Torr) of the absorbing compound as a liquid (subcooled, if necessary).

Considering only the mass of the om phase, one can similarly define a partitioning coefficient for species i ($K_{om,i}$) in terms of the organic mass concentration

$$K_{om,i} = \frac{F_{i,om}}{A_i M_o} = K_{p,i}/f_{om} \quad (3)$$

where like K_p, K_{om} has units of (m^3 μg^{-1}), and M_o is the absorbing organic mass concentration (μg m^{-3}). This equilibrium partitioning coefficient suggests that, for $K_{om,i}$ to be constant for a given compound, the fraction of a compound's total mass residing in the particulate phase will increase with increasing organic mass concentrations. This behavior for the semivolatile products involved in SOA formation would lead to the high variability found for published values of SOA yields for a given ROG, since the fractional aerosol yields will be dependent on the organic aerosol mass concentration.

Pandis et al. state that two of the three major uncertainties in predictions of ambient SOA are the discrepancies in experimentally determined SOA yields and in the partitioning of the condensable vapors between the gas and aerosol phases (*6*). In this paper, both of these factors will be addressed. We shall use the partitioning theory of Pankow (*1*, *2*) to develop expressions for the fractional secondary aerosol yield (Y) in terms of organic mass concentration. These expressions are then applied to over 30 SOA smog chamber experiments conducted in the summer of 1995. This analysis is used to show how SOA smog chamber data can be used to identify the important sources of SOA in the urban environment.

Experimental Description

Experiments were performed in a 60-m^3 sealed collapsible Teflon bag that has been described in detail previously (*8*, *9*). Most of these experiments were conducted in a dual-chamber mode, in which the bag was divided in the center with a clamped PVC pipe, so that two different experiments could be conducted under identical environmental (i.e., sunlight intensity, temperature, etc.) conditions. The two resulting chambers had volumes of approximately 20 m^3. The gas-phase instrumentation and aerosol data acquisition system are housed in a laboratory adjacent to the chamber. All aerosol sampling equipment was housed in a cart adjacent to the chamber that was maintained at a constant temperature of 25 °C. Prior to every experiment, the chamber was continuously flushed with purified laboratory compressed air for at least 38 h and baked in sunlight for at least 1 day. The compressed air was processed through three consecutive packed-bed scrubbers containing, in order, Purafil, Drierite and 13× molecular sieves, and activated charcoal. After purification, the air was rehumidified to a relative humidity of approximately 10% with distilled/dionized water before entering the chamber. The resulting air contained no detectable reactive hydrocarbons, no particles, and less than 5 ppb NO_x.

Hydrocarbon measurements were made using a Hewlett Packard (Palo Alto, CA) 5890 gas chromatograph (GC) that was equipped with a DB-5 column (J&W Scientific, Davis, CA) and a flame ionization detector (FID). The GC temperature program was as follows: −60 °C for 1 min, −60 to 100 °C at 40 °C min^{-1}, and hold at 100 °C for 1 min. Hydrocarbon calibrations were performed prior to each experiment either using certified gas mixtures or by vaporizing microliter volumes of a calibration solution of the pure hydrocarbon in CH_2Cl_2 into a 60-L Teflon bag filled with a measured volume of Ultra Zero (Air Liquid America Corp., Houston, TX) compressed air.

The calibrations were generally followed by injection of $(NH_4)_2SO_4$ seed particles to obtain particle concentrations of 5000−10 000 particles cm^{-3} with a number mean diameter of approximately 100 nm. The particles were generated by atomizing an aqueous solution of $(NH_4)_2SO_4$ using a stainless steel, constant rate atomizer. The aerosol was passed through heated copper tubing into a diffusional dryer, followed by a ^{85}Kr charge neutralizer before entering the chamber.

After obtaining the desired initial seed particle concentration, propene, hydrocarbons, NO_x, and hexafluorobenzene (C_6F_6) were injected (approximately 1 h prior to the start of the experiment) through Teflon lines into the chamber, which was completely shrouded from sunlight with a black polyethylene tarpaulin. Propene, NO, and NO_2 were injected using certified cylinders containing approximately 500 ppm of the gas in nitrogen. Hydrocarbons and C_6F_6 were introduced into the chamber by injecting microliter quantities of the pure liquid compound into a glass bulb that was gently heated while being diluted with purified compressed lab air that went directly to the chamber. Propene was used at mixing ratios of 250−350 ppb to generate OH radicals in sufficient concentrations for the inception of the experiment. C_6F_6 was used as an internal standard for hydrocarbon gas chromatographic (GC) samples in order to normalize for injection variations of the six-port stainless steel injection valve (Valco, Houston, TX), equipped with a heated (100 °C) 2-mL Teflon sampling loop. The half-life of C_6F_6 in the chamber was of the order of several days ($k_{OH} = 1.72 \times 10^{-13}$ cm^3 $molecule^{-1}$ s^{-1}), and so its concentrations were stable for times much longer than the typical experiment, allowing it to serve as an excellent internal standard. The use of the internal standard yielded estimated uncertainties in the hydrocarbon measurements of less than ±2% for most experiments.

After injection of the gases and seed aerosol, but before uncovering the chamber, initial measurements of hydrocarbons, NO_x, O_3, and aerosol concentrations and size distributions were made to obtain initial values and to ensure that the contents were well mixed. Generally, three to five initial hydrocarbon measurements, using the HP 5890 GC described above, were made for each side of the bag. A Thermo Environmental Instruments (Franklin, MA) Model 42 chemiluminescence NO_x monitor was used to measure NO, NO_2, and NO_x. Prior to the start of each experiment, a zero/span calibration was performed on the NO_x monitor using certified cylinders of NO and NO_2. In addition, a complete calibration of the NO_x monitor was performed on approximately a weekly basis. A Dasibi Environmental Corp. (Glendale, CA) Model 1008-PC O_3 analyzer was used to monitor O_3 concentrations. The NO_x and O_3 measurements were made at 10-min intervals between alternating sides of the chamber. The estimated uncertainties in the NO and NO_2 measurements are approximately ±4% and ±7%, respectively. The ozone instrument has an estimated uncertainty of ±4% in its initial calibration and was seen to drift only a few percent over the period of several months.

Complete number and size distribution measurements were recorded for both sides of the chamber with a 1-min

frequency throughout an experiment. The aerosol instrumentation consisted of one radial scanning electrical mobility spectrometer (*17*) and one TSI Model 3071 cylindrical scanning electrical mobility spectrometer for each side of the divided chamber. All four scanning electrical mobility spectrometers (SEMS) were equipped with either a model 3760 or model 3025 TSI condensation nuclei counter (CNC) to count transmitted particles. SEMS voltages were scanned from 40 to 8500V with a 1-min ramp. The radial SEMS were operated with sheath and excess flows of 15 L min^{-1} and inlet and classified aerosol flows of 1.5 L min^{-1} to allow for measurement of particle size distributions over the range of 5–80 nm. The cylindrical SEMS were operated with sheath and excess flows of 2.5 L min^{-1} and inlet and classified aerosol flows of 0.25 L min^{-1} to allow for measurement of particle size distributions in the range of 30–850 nm. A more complete description of the SEMS scanning cycle and operation has been published previously (*9*). Particle losses in the SEMS, SEMS response functions, particle charging efficiencies, CNC counting efficiency, and particle deposition in the chamber have been taken into account in the analysis of the aerosol data (*9*). The estimated uncertainty in the SEMS size and concentration measurements are approximately ±10%.

After making initial measurements prior to the start of the experiment, the black tarpaulin (chamber cover) was removed to begin the photooxidation experiment. Hydrocarbon measurements were made for both sides of the chamber every 8–10 min throughout the experiment. NO, NO_2, NO_x, and O_3, were continuously monitored during 10-min intervals alternating between the two sides of the chamber. Temperature, total solar radiation, and UV were continuously monitored over the course of the experiment.

Results and Discussion

Expressions for SOA Yields. In the presence of absorption partitioning of secondary organic aerosol species, fractional aerosol yields should be dependent on the total organic aerosol mass concentration. In order to derive the functional form of this dependence, let us begin by assuming that the concentrations of the dozens of individual products that result from the photooxidation of an ROG are proportional to the amount of ROG that reacts (ΔROG) such that

$$1000\alpha_i\,\Delta\mathrm{ROG} = C_i \qquad (4)$$

where α_i is the proportionality constant relating the concentration of ROG that reacts to the total concentration of product i (C_i) that is formed. The total concentration of a product that is formed is simply the concentration of the product that is in the gas phase (A_i) plus the concentration of the product that is in the aerosol phase (F_i). The factor of 1000 in eq 4 is needed because the units of ΔROG are $\mu g\ m^{-3}$ and the units of C_i are ng m^{-3}. Since the parent ROG and the products have different molecular weights, α_i is actually the product of the stoichiometric factor for the reaction forming product i and the ratio of the molecular weight of product i to the molecular weight of the parent ROG.

The desired property of the aerosol yield (Y) is that it possess a value that, when multiplied by the total mass of an ROG that reacts, gives the total mass of products that end up in the aerosol phase

$$Y(1000V_c\Delta\mathrm{ROG}) = \sum_i (F_i V_c) \qquad (5)$$

where V_c is the volume in which the reaction takes place, and once again a factor of 1000 is needed due to the difference in units for ΔROG and F_i. Combining eqs 3–5 and using the mass balance constraint (i.e., $C_i = A_i + F_i$) gives the following expression for the yield of an individual product (Y_i):

$$Y_i = M_o\left(\frac{\alpha_i K_{om,i}}{1 + K_{om,i} M_o}\right) \qquad (6)$$

Similarly, the expression for the overall SOA yield (Y) is given by

$$Y = \sum_i Y_i = M_o \sum_i \left(\frac{\alpha_i K_{om,i}}{1 + K_{om,i} M_o}\right) \qquad (7)$$

Equations 6 and 7 have several interesting features. First, they suggest that for low organic mass concentrations and for products that have relatively small partitioning coefficients, the SOA yield will be directly proportional to the total aerosol organic mass concentration, M_o. Secondly, for very nonvolatile products and/or for large organic mass concentrations, the individual product yields will be independent of the organic mass concentration and will be equal to α_i. Finally, they suggest that the individual yields for the more volatile products will be sensitive to temperature since $K_{om,i}$ is inversely proportional to the vapor pressure of the species (see eqs 2 and 3). If the semivolatile products involved in SOA formation exhibit the type of partitioning behavior indicated in eqs 6 and 7, then it is highly unlikely that a particular ROG will have a unique fractional aerosol yield. Instead, it will exhibit a range of yields over a range of organic mass concentrations.

Experimentally Determined SOA Yields. A list of the SOA experiments that are discussed in this paper are summarized in Table 1. Over 30 experiments were performed with *m*-xylene, 1,2,4-trimethylbenzene, and α-pinene. Table 1 lists the date on which the experiment was performed, the initial ROG concentrations (ROG_o), the total amount of ROG consumed in each experiment (ΔROG), the total organic aerosol mass that was produced (M_o), the initial NO_x concentration, the initial propene concentration (C_3H_6), the ratio of consumed hydrocarbon to initial NO_x (ΔHC/NO_x), and the overall SOA yield (Y). Total organic aerosol mass concentration was calculated from the observed total organic aerosol volume, assuming a density of 1 g cm^{-3}.

SOA Yields of Aromatics. The functional form of eq 7 suggests that fractional aerosol yields should be a function of organic aerosol mass concentrations. For example, fractional aerosol yields (Y) versus organic aerosol mass concentrations (M_o) for *m*-xylene and 1,2,4-trimethylbenzene are shown in Figures 1 and 2. As is evident from the figures, Y is a strong function of the value of M_o. It can be seen that for small M_o, the yield increases rapidly with increasing M_o and becomes a weaker function of M_o at higher concentrations, in accord with the behavior predicted by eq 7. The lines through the data in Figures 1 and 2 have been generated from eq 7 assuming that there are two products that partition to the absorbing om phase to a measurable degree for each ROG. Values for α_1, α_2, $K_{om,1}$, and $K_{om,2}$ are chosen to fit the data for each ROG by

TABLE 1

Outdoor Smog Chamber Experiment Summary

	date	ROG_o ($\mu g\ m^{-3}$)	ΔROG ($\mu g\ m^{-3}$)	M_o ($\mu g\ m^{-3}$)	NO_x (ppb)	C_3H_6 (ppb)	$\Delta HC/NO_x$ (ppb of C/ppb)	Y (%)
m-xylene	07/27A	2264	2114	101	629	300	7.8	4.78
m-xylene	07/27B	399	362	1.7	342	300	4.6	0.47
m-xylene	07/31A	1423	1219	20.1	521	235	6.0	1.64
m-xylene	07/31B	1494	1290	38.1	528	245	6.1	2.95
m-xylene	08/04A	4194	3953	396	1697	300	4.9	10.0
m-xylene	08/04B	2160	2018	106	933	300	4.9	5.25
m-xylene	08/09B	1049	795	18.8	1077	325	2.4	2.36
m-xylene	08/11A	1136	728	26.5	130	265	16.9	3.64
m-xylene	08/11B	1203	945	23.0	235	263	11.1	2.43
m-xylene	09/11A	1215	861	32.0	146	421	20.2	3.72
m-xylene	09/11B	1248	1032	35.5	279	421	11.8	3.44
m-xylene	09/13A	1211	1028	21.4	231	294	12.4	2.08
m-xylene	09/13B	1252	774	1.5	1609	294	1.3	0.19
m-xylene + α-pinene	09/15A	1394 + 278	1207 + 278	80.3	503	300	7.4	
m-xylene + α-pinene	09/19A	1132 + 342	936 + 342	82.2	409	300	8.1	
m-xylene	10/17A	2331	1945	188	998	300	4.5	9.67
1,2,4-Tmb	10/17B	2391	1996	113	975	300	4.7	5.66
1,2,4-Tmb	11/02A	3367	2282	155	1178	300	4.3	6.79
1,2,4-Tmb	11/02B	1607	1198	43.0	490	300	6.3	3.59
1,2,4-Tmb	11/07A	1932	1533	78.0	590	300	6.3	5.09
1,2,4-Tmb	11/07B	1237	1020	26.5	359	300	7.7	2.60
1,2,4-Tmb	11/09B	1745	1309	53.0	528	300	6.2	4.05
1,2,4-Tmb + *m*-xylene	11/09A	1633 + 1538	1270 + 979	195	1048	300	4.8	
α-pinene	08/14A	726	726	87.0	240	300	9.8	12.0
α-pinene	08/14B	769	769	96.0	240	300	10.2	12.5
α-pinene	08/17A	384	384	22.7	203	300	8.0	5.91
α-pinene	08/17B	104	104	1.3	113	300	9.7	1.25
α-pinene	09/15B	283	283	8.0	206	300	6.9	2.83
α-pinene	09/22A	505	505	33.0	135	300	13.7	6.53
α-pinene	09/22B	467	467	38.2	125	300	14.5	8.18
α-pinene	09/25A	510	510	39.3	124	300	14.9	7.71
α-pinene	09/25B	505	505	34.2	122	300	15.1	6.77

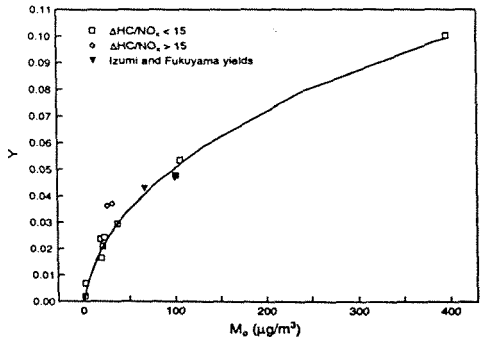

FIGURE 1. SOA yields for *m*-xylene as a function of M_o. Values used to generate the two-product model line are 0.03, 0.167, 0.032, and 0.0019 for α_1, α_2, $K_{om,1}$, and $K_{om,2}$, respectively.

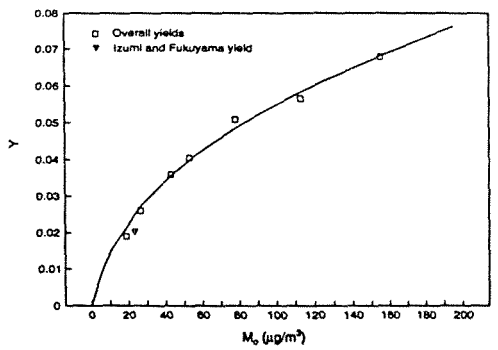

FIGURE 2. SOA yields for 1,2,4-trimethylbenzene as a function of M_o. Values used to generate the two-product model line are 0.0324, 0.166, 0.053, and 0.002 for α_1, α_2, $K_{om,1}$, and $K_{om,2}$, respectively.

minimizing the square of the residuals. Two products are the minimum number needed to fit the behavior of the system. A one-product model is insufficient to represent the shape of the curve, and three or more products are superfluous. Since it is known that there are dozens of products in the particle phase from the reactions of these two aromatics, the four constants that were chosen to fit the data for each ROG have no actual physical meaning, other than perhaps as an average of all the α and K_{om} values. However, the degree of fit to the data does suggest that the functional form of eq 7 captures the dependence of Y on M_o and that fractional aerosol yields do indeed depend on organic aerosol mass concentrations. This dependence also offers an explanation for observed increasing yields for increasing amounts of ROG reacted (*8*, *16*); as more ROG reacts, more condensed organic mass is produced, leading to a higher observed yield.

The data points in Figure 1 come from data obtained from 12 experiments that cover a range of initial hydrocarbon concentrations from 399 to 4194 $\mu g\ m^{-3}$ (96–1008 ppb) and a range of $\Delta HC/NO_x$ ratios from 1.3 to 20.2 ppb of C/ppb (Table 1). The model line through the data was chosen to fit the data points that were obtained from the experiments with $\Delta HC/NO_x$ ratios less than 15. As can be seen in the figure, the two points with a $\Delta HC/NO_x$ ratio greater than 15 have yields that are slightly higher than those with ratios less than 15. So it appears that the fractional aerosol yield for *m*-xylene is slightly dependent upon $\Delta HC/NO_x$. This is not surprising considering that

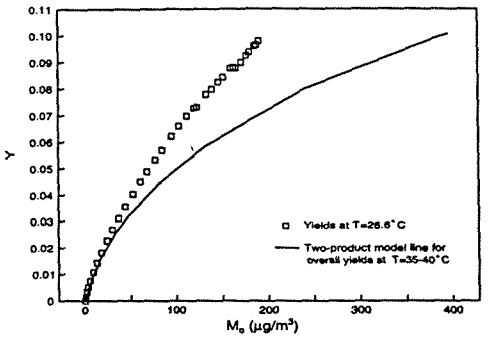

FIGURE 3. Comparison of temperature dependence of *m*-xylene SOA yields. Two-product model line is from data in Figure 1, which corresponds to experiments conducted at 35–40 °C. Data points correspond to yields for experiment 10/17A, which was conducted at 26.6 ± 1 °C.

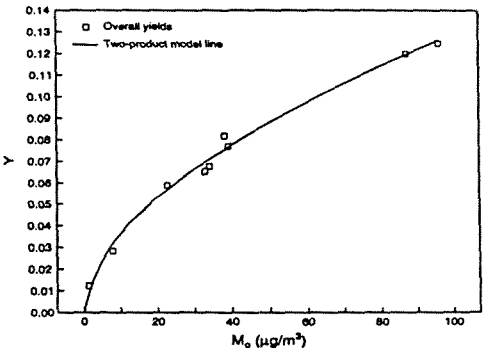

FIGURE 4. SOA yields for α-pinene as a function of M_o. Values used to generate the two-product model line are 0.038, 0.326, 0.171, and 0.004 for α_1, α_2, $K_{om,1}$, and $K_{om,2}$, respectively.

the photooxidation product distributions will depend on $\Delta HC/NO_x$. However, the data suggest that the effect on the yield is minimal.

The yields in Figure 1 and 2 were calculated using eq 1, where ΔM_o is the total organic aerosol mass concentration that was produced and ΔROG is the total amount of ROG that reacted over the course of an experiment. Most of the data in Figures 1 and 2 are from the experiments that were conducted in our laboratory in the summer and fall of 1995 (Table 1). However, two of the data in Figure 1 and one datum in Figure 2 are those of Izumi and Fukuyama (*11*). The points from the data of Izumi and Fukuyama agree quite well with the Caltech measurements and further demonstrate the generality of the dependence of Y on M_o.

The temperature dependence of Y is illustrated in Figure 3. The line in the figure is the two-product model line used to fit the data in Figure 1, which corresponds to experiments that were conducted in the temperature range of 35–40 °C. The data points in Figure 3 correspond to yield data that were obtained from an experiment (10/17A) that was conducted at 26.6 ± 1 °C. As eqs 2 and 7 suggest, Y seems to be a strong function of temperature. Since K_{om} is inversely proportional to the pure component vapor pressure, the yield is higher at lower temperatures for a given M_o. The yield values from Izumi and Fukuyama (*11*) agree better with the higher temperature yields from this group even though they were generated at a temperature closer to the lower temperature run from this group. The most likely cause for this discrepancy is that Izumi and Fukuyama (*11*) did not take aerosol deposition losses into account in estimating their yields and, therefore, probably slightly underestimated the yield values for the temperature at which they were obtained. However, it is still remarkable that the values obtained by Izumi and Fukuyama agree so well with the Caltech data when viewed in terms of organic aerosol mass concentrations.

The SOA yields for 1,2,4-trimethylbenzene that are shown in Figure 2 are from experiments that were conducted at temperatures from 22 to 26 °C. The yield values are very similar to those for both the lower and higher temperature *m*-xylene data at organic mass concentrations below 60 μg m^{-3}. At organic mass concentrations above 60 μg m^{-3}, the yields for 1,2,4-trimethylbenzene are higher than those for the higher temperature *m*-xylene data and lower than those for the lower temperature *m*-xylene data. Thus, for most atmospherically relevant M_o values (i.e., 60 μg m^{-3} or less), 1,2,4-trimethylbenzene has a similar yield to *m*-xylene for a given organic mass concentration. This is not all that surprising considering that the types of products that are formed from the oxidation of these two aromatic species are quite similar.

SOA Yields of α-Pinene. SOA smog chamber experiments were also conducted with α-pinene. The overall yields (Y) for α-pinene versus M_o are shown in Figure 4. As for *m*-xylene and trimethylbenzene, the line through the data is generated using a two-product model, where α_1, α_2, $K_{om,1}$, and $K_{om,2}$ were chosen to fit the data by minimizing the square of the residuals. Yields for α-pinene follow the same trend with M_o as do those for the aromatics but are considerably higher for a given M_o. For example, the yield for α-pinene at an M_o of 50 μg m^{-3} is 8.85% while that for *m*-xylene is 3.3%. As with the majority of the experiments for *m*-xylene, the experiments for α-pinene were conducted at 35–40 °C. The yields are expected to be even higher for lower temperatures. Also the yield experiments for α-pinene were conducted over a range of $\Delta HC/NO_x$ ratios of 6.9–15.1. There was little observed dependence of the yield on the ratio.

SOA Yields for ROG Mixtures. In addition to the individual ROG experiments, three multiple ROG experiments were also conducted. Two experiments were performed with a mixture of *m*-xylene and α-pinene, and one experiment was conducted with a mixture of *m*-xylene and 1,2,4-trimethylbenzene. These experiments were used to further test the hypothesis that Y is a function of organic aerosol mass concentrations. In both cases, selected concentrations of the two ROGs were placed in the chamber together with NO_x and irradiated with sunlight. The initial ROG concentrations, $\Delta HC/NO_x$ ratios, and the final M_o values are listed in Table 1. The two experiments with *m*-xylene and α-pinene were conducted at temperatures between 35 and 40 °C.

In experiment 09/15A, a maximum organic aerosol mass concentration of 80.3 μg m^{-3} was generated by the end of the experiment. Using the model generated lines in Figures 1 and 4, an M_o of 80.3 μg m^{-3} corresponds to a yield of 4.4% for *m*-xylene and a yield of 11.5% for α-pinene. Multiplying the value for *m*-xylene by the amount of *m*-xylene that reacted (1207 μg m^{-3}) gives an M_o of 53.1 μg m^{-3}. Multiplying the value for α-pinene by its amount reacted (278 μg m^{-3}) gives an M_o of 32.0 μg m^{-3}. The sum of these two values is 85.1 μg m^{-3}, which is extremely close to the overall observed organic aerosol mass concentration of 80.3

$\mu g\ m^{-3}$ that was generated from the mixture of the two ROGs. This observation lends strong support to the idea that eq 7 correctly describes the dependence of SOA yields on organic aerosol mass concentrations.

A second multiple ROG experiment (09/19A) was conducted with *m*-xylene and α-pinene, and the final M_o that was generated from the combined oxidation of these two ROGs was 82.2 $\mu g\ m^{-3}$. If one goes through the same procedure as above, using Figures 1 and 4 to obtain the appropriate yield values that correspond to an M_o of 82.2 $\mu g\ m^{-3}$, the combined single M_o values add up to 81.2 $\mu g\ m^{-3}$. Once again the yields for the individual hydrocarbons, when used in conjunction with eq 7, are capable of accounting for the total organic aerosol mass concentrations that are produced from the oxidation of the ROG mixture.

A multiple ROG experiment with *m*-xylene and 1,2,4-trimethylbenzene was also conducted. The experiment was performed at a temperature of 25.5 ± 2 °C, and the final organic aerosol mass concentration was 195 $\mu g\ m^{-3}$. Since the experiment was conducted at 25.5 ± 2 °C, the two product model line for *m*-xylene in Figure 1 that applies at 35–40 °C cannot be used. However the data points for experiment 10/17A in Figure 3 were obtained at 26.6 ± 1 °C. Using these points to generate a two-product model line gives a yield of 9.94% for *m*-xylene at an M_o of 195 $\mu g\ m^{-3}$ and a temperature of 26.6 °C. Using the model line for 1,2,4-trimethylbenzene in Figure 2, the yield is 7.61% at an M_o of 195 $\mu g\ m^{-3}$. Multiplying these yields for each of the ROGs by the amount that each ROG reacted gives M_o values of 97.3 $\mu g\ m^{-3}$ for *m*-xylene and 97.6 $\mu g\ m^{-3}$ for 1,2,4-trimethylbenzene. The sum of these is 194.9 $\mu g\ m^{-3}$, which is virtually identical to the M_o of 195 $\mu g\ m^{-3}$ that was generated from the mixture. That the single ROG yields used in conjunction with eq 7 account for the organic aerosol mass concentrations generated in the multiple ROG experiments clearly shows that an absorption model appears to correctly represent SOA formation.

Ambient SOA Yields. Ambient SOA yields cannot be represented by a unique value for a given ROG, because they are dependent on organic aerosol mass concentration and temperature. Examination of eqs 2,3, and 7 suggests that the only differences between the yields obtained from smog chamber studies and those in the ambient environment, for a given M_o and temperature, will be due to differences in the mean molecular weight of the absorbing om phase and in the activity coefficients of the absorbing products in the om phase. In smog chamber studies, the om phase is generated from the products of oxidation of a single ROG; in the ambient environment, the om phase is comprised of a mixture of condensed primary and secondary species. Even though there will be differences in the mean molecular weight of the om phase and in the activity coefficients between smog chamber SOA and ambient atmospheric aerosol, it seems unlikely that these differences will be large.

The mean molecular weight of the om phase is most likely in the range of 150–250 $g\ mol^{-1}$ both in smog chamber studies and in the ambient environment. On days when SOA formation in the atmosphere is important and oxidation products comprise a significant fraction of the om phase, activity coefficients for SOA products in the ambient om phase will likely be similar to those for SOA products in smog chamber-generated secondary organic aerosol. This hypothesis is supported by the fact that the individual ROG yield data were able to so accurately account for the organic aerosol mass that was generated in the ROG mixture experiments. For example, if the products of α-pinene and *m*-xylene oxidation had significantly different polarities, then the activity coefficients of the products from *m*-xylene oxidation would be different if those products were partitioned into an organic aerosol layer comprised entirely of *m*-xylene oxidation products as opposed to an organic aerosol layer that was comprised of the oxidation products of both *m*-xylene and α-pinene. This would mean that the yield for *m*-xylene would be different, for a given organic aerosol mass concentration, depending on whether it was measured from an experiment in which only *m*-xylene was used or whether a mixture of *m*-xylene and some other ROG was used. If this were the case, then the organic aerosol mass concentrations in the ROG mixture experiments would not be so accurately accounted for by the individual yield data. This is rather significant because it suggests that SOA yield data obtained from smog chamber studies may likely account for the yield of individual ROGs when applied to the ambient atmosphere and could thus be used in conjunction with ambient models to determine the important sources of secondary organic aerosol in an urban airshed.

Acknowledgments

This work was supported by the U.S. Environmental Protection Agency Exploratory Environmental Research Center on Airborne Organics (R-819714-01-0), the National Science Foundation Grant ATM-9307603, the Coordinating Research Council (A-5-1), and the Chevron Corporation.

Literature Cited

(1) Pankow, J. F. *Atmos. Environ.* **1994**, *28A*, 185–188.
(2) Pankow J. F. *Atmos. Environ.* **1994**, *28A*, 189–193.
(3) Turpin, B. J.; Huntzicker, J. J. *Atmos. Environ.* **1995**, *29B*, 3527–3544.
(4) Schauer, J. J.; Rogge, W. F.; Hildermann, L. M.; Mazurek, M. A.; Simoneit, B. R.; Cass, G. R. *Atmos. Environ.*, in press.
(5) Grosjean, D.; Seinfeld, J. H. *Atmos. Environ.* **1989**, *23*, 1733–1747.
(6) Pandis, S. N.; Harley, R. A.; Cass, G. R.; Seinfeld, J. H. *Atmos. Environ.* **1992**, *26A*, 2269–2282.
(7) Pandis, S. N.; Wexler, A. S.; Seinfeld, J. H. *Atmos. Environ.* **1993**, *27A*, 2403–2416.
(8) Pandis, S. N.; Paulson, S. E.; Seinfeld, J. H. Flagan, R. C. *Atmos. Environ.* **1991**, *25A*, 997–1008.
(9) Wang, S. C.; Paulson, S. E.; Grosjean, D.; Flagan, R. C.; Seinfeld, J. H. *Atmos. Environ.* **1992**, *26A*, 403–420.
(10) Hatakeyama, S.; Izumi, K.; Fukuyama, T.; Akimoto, H.; Washida, N. *J. Geophys. Res.* **1991**, *96*, 947–958.
(11) Izumi, K.; Fukuyama, T. *Atmos. Environ.* **1990**, *24A*, 1433–1441.
(12) Stern, J. E.; Flagan, R. C.; Grosjean, D.; Seinfeld, J. H. *Environ. Sci. Technol.* **1987**, *21*, 1224–1231.
(13) Gery, M. W.; Fox, D. L.; Jeffries, H. E. *Int. J. Chem. Kinet.* **1985**, *17*, 931–955.
(14) Leone, J. A.; Flagan, R. C.; Grosjean, D.; Seinfeld, J. H. *Int. J. Chem. Kinet.* **1985**, *17*, 177–216.
(15) Grosjean D. Aerosols. In *Ozone and Other Photochemical Oxidants*; National Academy of Sciences: Washington, DC, 1977; Chapter 3, pp 45–125.
(16) Zhang, S.; Shaw, M.; Seinfeld, J. H.; Flagan, R. C. *J. Geophys. Res.* **1992**, *97*, 20,717–20,729.
(17) Zhang, S.; Akutsu, Y.; Russell, L. M.; Flagan, R. C.; Seinfeld, J. H. *Aerosol Sci. Technol.* **1995**, *23*, 357–372.
(18) Atkinson, R. *J. Phys. Chem. Ref. Data* **1989**, *Monograph 1*, 1.
(19) Atkinson, R.; Aschmann, S. M.; Arey, J. *Int. J. Chem. Kinet.* **1991**, *23*, 77–97.
(20) Grosjean, D. *Sci. Total Environ.* **1991**, *100*, 367–414.

Received for review December 18, 1995. Revised manuscript received April 17, 1996. Accepted April 19, 1996.•
ES950943+

• Abstract published in *Advance ACS Abstracts*, June 15, 1996.